| | |
|---|---|
| **Titre:** Title: | Modeling of Thermal Mass Energy Storage in Buildings with Phase Change Materials |
| **Auteur:** Author: | Benoit Delcroix |
| **Date:** | 2015 |
| **Type:** | Mémoire ou thèse / Dissertation or Thesis |
| **Référence:** Citation: | Delcroix, B. (2015). Modeling of Thermal Mass Energy Storage in Buildings with Phase Change Materials [Thèse de doctorat, École Polytechnique de Montréal]. PolyPublie. https://publications.polymtl.ca/1820/ |

UNIVERSITÉ DE MONTRÉAL

# MODELING OF THERMAL MASS ENERGY STORAGE IN BUILDINGS WITH PHASE CHANGE MATERIALS

BENOIT DELCROIX

DÉPARTEMENT DE GÉNIE MÉCANIQUE

ÉCOLE POLYTECHNIQUE DE MONTRÉAL

THÈSE PRÉSENTÉE EN VUE DE L'OBTENTION

DU DIPLÔME DE PHILOSOPHIAE DOCTOR

(GÉNIE MÉCANIQUE)

AOÛT 2015

UNIVERSITÉ DE MONTRÉAL

ÉCOLE POLYTECHNIQUE DE MONTRÉAL

Cette thèse intitulée :

# MODELING OF THERMAL MASS ENERGY STORAGE IN BUILDINGS WITH PHASE CHANGE MATERIALS

présentée par : DELCROIX Benoit

en vue de l'obtention du diplôme de : Philosophiae Doctor

a été dûment acceptée par le jury d'examen constitué de :

M. TRÉPANIER Jean-Yves, Ph. D., président

M. KUMMERT Michaël, Doctorat, membre et directeur de recherche

M. DAOUD Ahmed, Ph. D., membre et codirecteur de recherche

M. SAVADOGO Oumarou, D. d'état, membre

M. GROULX Dominic, Ph. D., membre externe

# DEDICATION

*To a better world*

# ACKNOWLEDGEMENTS

This Ph. D. thesis represents a complex work which would have been difficult to realize without the help and the support of people I have met during these four years of Ph. D. studies.

First, I am very grateful to my research director, Professor *Michaël Kummert*, for his support and trust that he has placed in me during my Ph. D. studies. His friendly guidance, constant questioning and experience have been priceless to me. I will always remember his precious advices during my whole career.

I would like to thank *Ahmed Daoud*, my co-director and supervisor at Laboratoire des Technologies de l'Énergie (LTE), who have taken over my supervision in the lab and have brought to me his experience and constructive advices. Likewise, I want to thank *Jonathan Bouchard*, who have been to me an extra co-supervisor in the lab.

I would like to thank all the research group BEE (Bâtiment et Efficacité Énergétique) from the department of Mechanical Engineering, with who I have had wonderful moments at École Polytechnique de Montréal : *Aurélie Verstraete*, *Katherine D'Avignon*, *Narges Roofigari*, *Behzad Barzegar*, *Corentin Lecomte*, *Humberto Quintana*, *Kun Zhang*, *Massimo Cimmino*, *Mathieu Lévesque*, *Romain Jost*, *Samuel Letellier-Duchesne*, *Simon Maltais Larouche*, and Professor *Michel Bernier*. I wish to thank in particular *Katherine*, with who I have "struggled" during long hours about thorny questions related to phase change materials.

I also thank Professor *Philippe Pasquier* to have let us carry out thermal conductivity tests using their lab equipment.

I am grateful to all the LTE staff, who has warmly welcomed me during three years. In particular, I would like to thank *Michel Dostie*, *Jocelyn Millette* and *Éric* Dumont, who have made it possible. I also really enjoyed our serious and less serious discussions with *Brice Le Lostec*, *Hervé Nouanegue* and the numerous interns present in the lab.

I wish to thank *Marion Hiller*, of Transsolar in Stuttgart, for providing us the needed computer tools and for her related help.

I would like to thank professors *Jean-Yves Trépanier*, *Oumarou Savadogo* and *Dominic Groulx* for having accepted being part of my thesis committee.

The project have been financially supported by Fonds de Recherche du Québec en Nature et Technologies (FRQNT), Natural Sciences and Engineering Research Council of Canada (NSERC) and Hydro-Québec.

Last but not least, I would like to deeply thank my friends and family who support me continuously, just by being themselves.

Thanks to everyone,

Benoit Delcroix

Montreal, August 2015

# RÉSUMÉ

La masse thermique d'un bâtiment est un paramètre-clé qui détermine la capacité d'un bâtiment à atténuer les variations de température en son sein et d'assurer ainsi un meilleur confort thermique aux occupants. Afin d'augmenter l'inertie thermique de bâtiments à structure légère, des matériaux à changement de phase (MCP) peuvent être utilisés. Ces matériaux offrent en effet une haute capacité de stockage d'énergie (notamment sous forme latente) et un changement de phase à température quasiment constante. Ils s'intègrent aussi parfaitement dans des projets de bâtiments à consommation énergétique nette nulle. L'intérêt actuel pour ceux-ci et pour de meilleures stratégies de gestion de l'appel de puissance requiert des outils capables de simuler des bâtiments hautement isolés possédant une masse thermique importante avec des pas de temps courts (inférieur ou égal à 5 minutes). Ceci représente un défi majeur pour les programmes actuels de simulation énergétique des bâtiments qui ont été développé initialement pour réaliser des calculs horaires. Le modèle de bâtiment utilisé dans le programme TRNSYS présente notamment certains problèmes dans ces circonstances. L'origine de ces problèmes provient de la méthode utilisée pour modéliser la conduction thermique dans les murs. Il s'agit de la méthode des fonctions de transfert. Pour un mur hautement isolé et lourd, la méthode est incapable de générer, pour un pas de temps court, les coefficients supposés représenter la réponse thermique du mur en question. De plus, cette méthode ne permet pas de définir des couches avec des propriétés thermophysiques variables, tels qu'affichés par des MCP. La modélisation de ces MCP est en outre limitée par les informations rendues disponibles par les manufacturiers, qui sont souvent incomplètes ou erronées. Finalement, les modèles actuels simulant des MCP dans les murs ne permettent pas de représenter toute leur complexité. Ceux-ci différencient rarement les processus de fusion et de solidification (hystérèse), prennent en compte occasionnellement la conductivité thermique variable et ne modélisent jamais le sous-refroidissement. Toutes ces problématiques sont soulevées dans cette thèse et des solutions sont proposées.

La première partie (chapitre 4) traite de l'amélioration de la méthode des fonctions de transfert dans TRNSYS grâce à l'utilisation d'un modèle d'état qui permet de diminuer significativement les pas de temps utilisés. La résolution entière de cette problématique est ensuite atteinte en couplant dans TRNSYS un modèle de mur utilisant la méthode aux différences finies à la méthode des fonctions de transfert (chapitre 5).

La deuxième partie (chapitre 6) s'attelle à caractériser les propriétés thermophysiques d'un MCP utilisé dans divers bancs d'essais, i.e. la densité (annexe A), la conductivité thermique (annexe B) et la capacité thermique. La variété des configurations (MCP en échantillons ou encapsulés dans un film plastique placé dans un mur) et des taux de transfert de chaleur (0.01 à 0.8 °C/min) permet de plus de mettre en évidence l'influence des conditions expérimentales sur le comportement du MCP. La caractérisation est complétée dans le chapitre 7 par une étude du comportement du MCP lors d'interruption de changement de phase (fusion et solidification).

La dernière partie (chapitres 8 et 9) se concentre sur le développement et la validation d'un nouveau modèle permettant de simuler un mur intégrant un ou des MCP (ou plus généralement des couches aux propriétés variables). Le modèle est basé sur une méthode explicite aux différences finies couplée avec une méthode enthalpique pour représenter le comportement du/des MCP. Ce modèle est apte à simuler un MCP avec, à la fois, une hystérèse, un sous-refroidissement et une conductivité thermique variable. Une description détaillée de la méthode et de l'algorithme est donnée. Le modèle est d'abord validé numériquement par comparaison avec des modèles de référence sur 9 cas de murs différents proposés par l'Agence Internationale de l'Énergie. Cette méthode est ensuite comparée à un modèle à capacité thermique effective. Sur 2 aspects (détection du changement de phase et respect de la conservation de l'énergie), la méthode enthalpique développée s'est montrée plus performante que l'autre méthode. Le modèle développé est finalement validé expérimentalement avec des données provenant d'un banc d'essai à échelle réelle.

# ABSTRACT

Building thermal mass is a key parameter defining the ability of a building to mitigate inside temperature variations and to maintain a better thermal comfort. Increasing the thermal mass of a lightweight building can be achieved by using Phase Change Materials (PCMs). These materials offer a high energy storage capacity (using latent energy) and a nearly constant temperature phase change. They can be integrated conveniently in net-zero energy buildings. The current interest for these buildings and for better power demand management strategies requires accurate transient simulation of heavy and highly insulated slabs or walls with short time-steps (lower than or equal to 5 minutes). This represents a challenge for codes that were mainly developed for yearly energy load calculations with a time-step of 1 hour. It is the case of the TRNSYS building model (called Type 56) which presents limitations when modeling heavy and highly insulated slabs with short time-steps. These limitations come from the method used by TRNSYS for modeling conduction heat transfer through walls which is known as the Conduction Transfer Function (CTF) method. In particular, problems have been identified in the generation of CTF coefficients used to model the walls thermal response. This method is also unable to define layers with variable thermophysical properties, as displayed by PCMs. PCM modeling is further hindered by the limited information provided by manufacturers: physical properties are often incomplete or incorrect. Finally, current models are unable to represent the whole complexity of PCM thermal behavior: they rarely include different properties for melting and solidification (hysteresis); they sometimes take into account variable thermal conductivity; but they never model subcooling effects. All these challenges are tackled in this thesis and solutions are proposed.

The first part (chapter 4) focuses on improving the CTF method in TRNSYS through state-space modeling, significantly decreasing the achievable time-steps. A complete solution to this issue can be reached by implementing in TRNSYS a wall model using a finite-difference method and coupling it with the CTF method in Type 56 (chapter 5).

The second part (chapter 6) proposes an in-depth characterization of thermophysical properties of a PCM used in different test-benches, i.e. the density (Appendix A), the thermal conductivity (Appendix B) and the thermal capacity. This section also highlights the influence of the experimental conditions on the PCM thermal behavior: the impact of different configurations (PCM samples or plastic films with encapsulated PCMs located in walls) and different heat transfer

rates (0.01 to 0.8 °C/min) is discussed. The PCM characterization is completed with a study dedicated to define the PCM thermal behavior when phase change (melting or solidification) is interrupted (chapter 7).

The last part (chapters 8 and 9) focuses on the development and validation of a new model for walls with PCMs, or more generally layers with variable thermal properties. The developed model is based on an explicit finite-difference method coupled with an enthalpy method to model the PCM thermal behavior. This model is able to simulate a PCM with hysteresis, subcooling and temperature-dependent thermal conductivity. A detailed description of the method and the algorithm is given. This model is numerically validated, using comparisons with reference models simulating wall test cases proposed by the International Energy Agency. The developed model is also compared to a reference effective heat capacity model. On two specific aspects (phase change detection and energy conservation principle), the developed enthalpy method is more effective than the other method. Finally, the developed model is experimentally validated using data from a full-scale test-bench.

# TABLE OF CONTENTS

# LIST OF TABLES

# LIST OF FIGURES

# LIST OF SYMBOLS AND ABBREVIATIONS

| | |
|---|---|
| $A$ | Area [m²] |
| $a, b, c, d$ | Conduction transfer function coefficients |
| Bi | Biot number [-] |
| $C$ | Capacitance [J/m²-K] |
| $C_p$ | Specific heat [J/g-K] |
| Fo | Fourier number [-] |
| $H$ | Enthalpy [J/kg] |
| $h$ | Coefficient of convection [W/m²-K] |
| $h_g$ | Global heat transfer coefficient [W/m²-K] |
| $k$ | Thermal conductivity [W/m-K] |
| $L$ | Latent heat [J/kg] |
| $L_c$ | Characteristic length [m] |
| $l_f$ | Liquid fraction [-] |
| $n_a, n_b, n_c, n_d$ | Number of coefficients $a$, $b$, $c$ and $d$ |
| $\mathcal{O}$ | Truncation error |
| $Q$ | Energy [J] |
| $\dot{q}$ | Heat flow [W] |
| $R$ | Thermal resistance [m²-K/W] |
| St | Stefan number [-] |
| $s$ | Laplace variable |
| $T$ | Temperature [°C] |
| $t$ | Time [s] |
| $U$ | Heat transfer coefficient [W/m²-K] |

| | |
|---|---|
| $x$ | Position [m] |
| $\Delta t$ | Time-step [s] |
| $\Delta t_b$ | Timebase (CTF time-step) [s] |

**Greek symbols**

| | |
|---|---|
| $\alpha$ | Thermal diffusivity [m²/s] |
| $\rho$ | Density [kg/m³] |
| $\tau$ | Time constant [s] |

**Subscripts**

| | |
|---|---|
| $abs$ | Absorbed |
| $CL$ | Convective parts of internal loads |
| $cond$ | Conductive |
| $conv$ | Convective |
| $eq$ | Equipment |
| $i$ | Inside |
| $IV$ | Infiltration and/or ventilation |
| $j$ | Iteration level |
| $l$ | Liquid |
| $LWR$ | Long-wave radiation |
| $n$ | Node |
| $o$ | Outside |
| $pc$ | Phase change |
| $rad$ | Radiative |
| $s$ | Surface or solid |
| $sol$ | Solar |

| | |
|---|---|
| $SW$ | Short-wave radiation |
| $sys$ | System |

**Abbreviations**

| | |
|---|---|
| 1-D | One-dimensional |
| 3-D | Three-dimensional |
| BPS | Building performance simulation |
| BTCS | Backward time and central space |
| C-N | Crank-Nicolson |
| CTF | Conduction transfer function |
| DLL | Dynamic-link library |
| DRF | Direct-root finding |
| DSC | Differential scanning calorimetry |
| FD | Finite-difference |
| FTCS | Forward time and central space |
| LTI | Linear time-invariant |
| PCM(s) | Phase change material(s) |
| RMSD | Root mean square deviation |
| SS | State-space |

# LIST OF APPENDICES

# CHAPTER 1 INTRODUCTION

Building thermal mass is a key parameter to mitigate inside temperature variations. Used with an optimized control strategy, a thermal mass increase is a solution to maintain a better thermal comfort, to stabilize heating and cooling loads and to mitigate peak power demand. In Québec, more than two thirds of households live in all-electric houses and are therefore partially responsible for the electric grid peaks, especially during winter (Leduc, Daoud, & Le Bel, 2011). The share of all-electric houses is expected to rise even higher in the future, mainly because of the fluctuations in oil and gas prices compared to the stable – and low – electricity prices in the province. Québec is almost entirely (more than 90 %) supplied by hydroelectric installations (Ministère des Ressources naturelles et de la Faune, 2010). In winter, the maximum power peak demand can reach up to approximately 40 GW (Leduc et al., 2011), which represents 103 % of the capacity managed by Hydro-Québec, 90 % of the capacity installed in Québec, or 80 % of the capacity available in Québec (including Churchill falls installations in the province of Newfoundland) (Ministère des Ressources naturelles et de la Faune, 2010). An increasing number of all-electric buildings will require additional power capacity in order to guarantee the future electric supply, unless effective peak load management strategies are implemented.

Figure 1-1 presents the prediction of the average power demand in Québec in January and July 2007 performed by Hydro-Québec in 2006. Clear seasonal and hourly differences are observed.

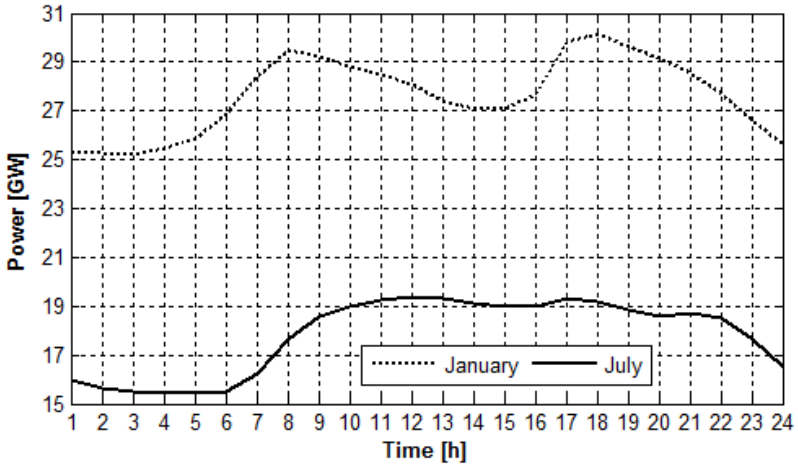


Figure 1-1: Prediction of the average hourly power demand in the province of Québec in January and July 2007 (Hydro-Québec, 2006)

A higher power demand is observed during winter, caused mainly by buildings heating loads. Two peaks are distinguished during winter in the morning and the evening, corresponding to the beginning and the end of regular working days. During summer, the power demand is mainly driven by the daily schedule of most human activities, and the impact of building cooling loads is comparatively lower than the impact of heating loads.

Strong variations of the peak power demand are a source of instability for the electrical network in Québec. Increasing buildings thermal mass can contribute to mitigate these variations by spreading out the energy consumption over time. An interesting option to achieve this goal is the addition of phase change materials (PCMs) to building walls, floors and ceilings. Their latent energy storage capacity coupled with their nearly isothermal phase change temperature are significant assets. Compared to heavy materials such as concrete, PCMs have the advantage of storing more energy in more compact and lighter materials. Currently, PCMs are mainly used for cooling applications in countries with warmer climates. But PCMs also have a potential in colder climates for heating applications.

However using PCMs in the building envelope remains marginal and only few commercial products are available. Companies such as Phase Change Energy Solutions (2014) and DuPont (2012) have developed and commercialized products which can be easily implemented directly in building walls.

As with any other energy conservation or peak power reduction measure, the impact of adding PCMs to the building envelope must be assessed through a detailed analysis involving Building Performance Simulation (BPS) programs such as TRNSYS, EnergyPlus or ESP-r. Assessing peak power demand management strategies requires accurate transient simulations of highly insulated and heavy walls with short time-steps (< 5 minutes). This represents a challenge for most BPS tools, which are primarily dedicated to yearly energy performance analysis with an hourly time-step. This is for example the case in TRNSYS, where the building model (known as Type 56) presents some limitations in this particular context. These limitations come from the method used to model 1-D thermal conduction through walls, which is known as the Conduction Transfer Function (CTF) method. Moreover, the CTF method is not designed to simulate building materials with temperature-dependent properties, such as experienced by PCMs. A finite-difference method is then preferably used in order to overcome these limitations. The PCM temperature-dependent

thermal capacity is generally modeled with enthalpy-temperature or specific-heat-temperature curves. Unfortunately, most models do not include the whole complexity of PCMs thermal behavior. A differentiation between heating and cooling processes is rarely modeled while subcooling is almost never taken into account.

Modeling a PCM requires to know its thermophysical properties, i.e. density, thermal conductivity and capacity. Manufacturers document most of the time these main properties. However, these data are generally incomplete or not representative. For example, the definition of the thermal conductivity is often given with only one value, while PCM thermal conductivity is actually variable, depending on its temperature and state (liquid or solid). Likewise, the PCM thermal capacity values provided by manufacturers are often incomplete and do not always represent the actual final product. Few data sheets provided by manufacturers include enthalpy-temperature or specific heat-temperature curves for heating and cooling processes. If provided, these curves are most often obtained using Differential Scanning Calorimetry (DSC) tests. This method uses small samples (a few milligrams) and imposes high heat fluxes to the sample, which is not representative of PCMs implemented in building walls (large quantity of PCMs, relatively low heat fluxes and temperature variations).

The three main objectives of this thesis result from the above-mentioned issues and two of them are composed of several more specific goals:

- Improvement of the CTF method in TRNSYS to allow accurate low-time-step simulations of buildings with highly resistive and heavy walls.
- Accurate and representative characterization of a selected PCM:
    - Evaluation of the density and thermal conductivity through experimentations.
    - Evaluation of the temperature-dependent thermal capacity based on inverse methodology and analysis of the impacts of different configurations (PCM samples of a few grams or walls equipped with PCMs) and varying heating / cooling rates on this property.
    - In the case of a PCM with 2 enthalpy-temperature curves (heating and cooling): identification of the PCM thermal behavior when phase change is interrupted.
- Accurate modeling of a wall with PCMs, considering all aspects of the PCM thermal behavior complexity:

- Development of a model of wall including PCM(s) or layer(s) with temperature-dependent properties.
- Numerical validation of the developed model through a comparison with reference models for several wall test cases.
- Experimental validation of the developed model using experimental data from a full-scale test-bench.

**Preliminary notes and clarifications:**

a) In the present thesis, it is indicated that DSC tests should not be used to determine the $H(T)$ curves because they are not representative of the way how PCMs are used in the building envelope. DSC tests are intended to obtain the latent heat and the melting temperature of a PCM, but they are often used by practitioners and researchers in building sciences to obtain the $H(T)$ curve of a PCM. The work in this thesis shows that the $H(T)$ curves obtained through this method are not applicable to the PCM encapsulation techniques and thermal solicitations typically found in buildings. Rather than the DSC tests, it is the extrapolated $H(T)$ curves that cannot be used.

b) In this thesis, the term "subcooling" is used to denote the phenomenon observed when a PCM is cooled below its solidification temperature, which is followed by a sudden temperature increase (after a perturbation) leading to solidification. This phenomenon is more properly denoted by supercooling.

c) The experimental results presented in this thesis aim to show that phase change differs depending on the experimental conditions, especially the phase change temperature range during melting and solidification. In this thesis, phase change temperature range denotes the temperature "plateau" observed in graphs showing PCM temperature evolutions and defined between two temperatures, often interpreted as the "onset" and "offset" of fusion or solidification. Below the lower temperature, the PCM is assumed solid. On the other hand, the PCM is supposed liquid if the measured temperature is beyond the upper temperature. These interpretations are often found in the scientific literature but may not be strictly accurate from the chemical point of view.

d) Temperature measurements during all experimentations presented in this thesis are performed using T-type thermocouples, having a measurement uncertainty of ± 0.5 °C.

# CHAPTER 2 LITERATURE REVIEW

This literature review first discusses heat transfer modeling in Building Performance Simulation (BPS) tools (section 2.1), focusing on transient conduction through walls (section 2.2). The modeling of transient conduction heat transfer with the presence of PCMs is then presented in section 2.3.

## 2.1 Heat transfer modeling in buildings

Most BPS programs such as TRNSYS (Klein et al., 2012), EnergyPlus (Crawley et al., 2001) and ESP-r (Energy Systems Research Unit, 1998) are based on the heat balance methodology for modeling the whole heat transfer in buildings. This method is illustrated in Figure 2-1 (ASHRAE, 2013).

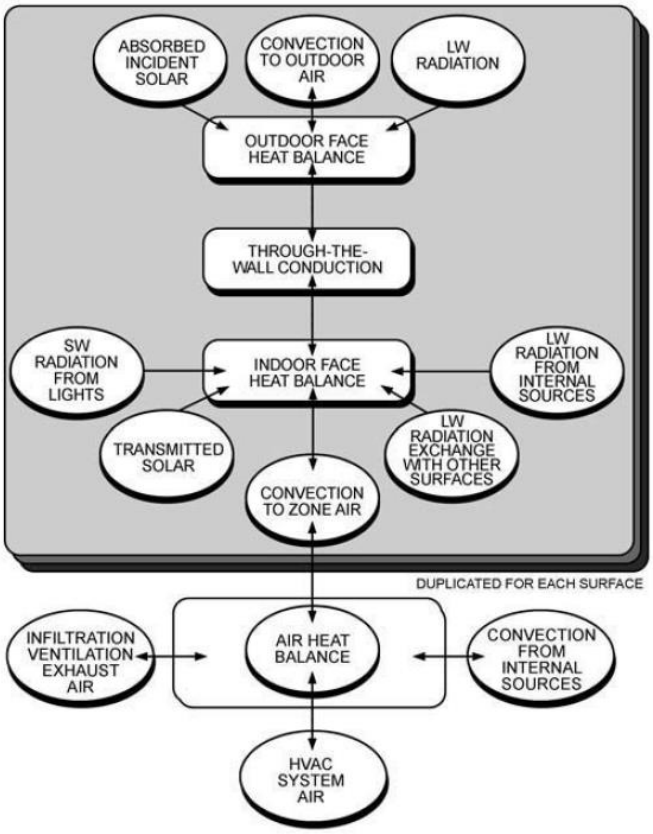


Figure 2-1: Heat balance method (ASHRAE, 2013)

The heat balance method can be viewed as four distinct processes (as suggested in Figure 2-1):

a) Outdoor face heat balance

For each surface, the heat balance on the outdoor face depends on the absorbed solar radiation $\dot{q}_{abs,sol}$, the net long-wave radiation exchange $\dot{q}_{LWR}$ with the sky and the surroundings, the convective exchange $\dot{q}_{conv}$ with the outside air and the conductive heat transfer into the wall $\dot{q}_{cond,o}$. It can be formulated as follows:

$$\dot{q}_{abs,sol} + \dot{q}_{LWR} + \dot{q}_{conv,o} - \dot{q}_{cond,o} = 0 \qquad (2.1)$$

The first three terms of Equation ( 2.1 ) are positive for net heat flows to the outdoor face. The conductive term is considered positive from outdoors to inside the wall.

b) Heat conduction through walls

Many methods have been developed for modeling heat conduction through walls. They are based on time series methods, transform methods or numerical methods. This problem, which is at the core of this thesis, is discussed further in section 2.2 for methods used to model heat conduction through walls with constant properties and in section 2.3 for walls including PCMs or layer(s) with variable properties.

c) Indoor face heat balance

As for the outdoor face, the heat balance on the indoor face involves all heat transfer modes (conduction, convection and radiation) and is composed of:

- The net long-wave radiative exchange between zone surfaces $\dot{q}_{LWR,s}$.
- The long-wave radiation from equipment $\dot{q}_{LWR,eq}$.
- The short-wave radiation from lights to surface $\dot{q}_{SW}$.
- The conductive heat transfer through wall (outside to inside) $\dot{q}_{cond,i}$.
- The transmitted solar radiation absorbed at surface $\dot{q}_{sol}$.
- The convective heat transfer to zone air $\dot{q}_{conv,i}$.

The indoor face heat balance is therefore formulated such as:

$$\dot{q}_{LWR,s} + \dot{q}_{LWR,eq} + \dot{q}_{SW} + \dot{q}_{cond,i} + \dot{q}_{sol} - \dot{q}_{conv,i} = 0 \qquad (2.2)$$

d) Air heat balance

The last balance to be performed is on the zone air. It is formulated as follows:

$$\dot{q}_{IV} + \dot{q}_{CE} + \dot{q}_{sys} + \dot{q}_{conv,i} = 0 \qquad (2.3)$$

Where:

- $\dot{q}_{IV}$ is the sensible load caused by infiltration and ventilation.
- $\dot{q}_{CE}$ is the convective gains of internal loads (e.g. heat released by occupants).
- $\dot{q}_{sys}$ is the heat transfer to/from HVAC system.
- $\dot{q}_{conv,i}$ is the convection from all surfaces.

The three first elements a) to c) are duplicated for each surface while the last (air heat balance) is carried out for each air node.

## 2.2 1-D conduction heat transfer modeling through walls

Transient heat conduction in BPS programs is mainly modeled using two methods. First, the Conduction Transfer Function (CTF) method is an analytical method and is for example used in TRNSYS and EnergyPlus. Secondly, finite-difference methods are numerical methods and are used in ESP-r and optionally in EnergyPlus. Prior to reviewing these methods, a brief reminder on the Fourier law and two important dimensionless numbers is presented.

### 2.2.1 Fourier law and dimensionless numbers

Conduction heat transfer was experimentally defined by Fourier (1822), who formulated the following relationship:

$$\frac{dQ}{dt} = -k\,A\,\frac{dT}{dx} \qquad (2.4)$$

Equation ( 2.4 ) indicates that the heat flow is proportional to the heat exchange surface $A$, the thermal conductivity $k$ and the temperature gradient between 2 points.

In order to characterize transient conduction problems, two dimensionless numbers are of interest: Fourier and Biot numbers.

Named after Fourier, this number Fo is the ratio of the heat conduction rate to the rate of thermal energy storage in a solid (Bergman, Lavine, Incropera, & Dewitt, 2011). It is sometimes defined as dimensionless time. It is formulated as follows:

$$\mathrm{Fo} = \frac{\alpha\, \Delta t}{L_c^2} \qquad (2.5)$$

Where $L_c$ is the characteristic length and the thermal diffusivity $\alpha$ depends on the thermal conductivity $k$, on the density $\rho$ and on the specific heat $C_p$ and is computed such as:

$$\alpha = \frac{k}{\rho\, C_p} \qquad (2.6)$$

Physically a lower Fourier number means a lower heat transmission rate. It also means that the thermal mass increases.

The second dimensionless number is the Biot number. It is defined as the ratio of the internal thermal resistance of a solid to the boundary layer thermal resistance (Bergman et al., 2011). This number is mathematically expressed as follows:

$$\mathrm{Bi} = \frac{h\, L_c}{k} \qquad (2.7)$$

Where $h$ is the convective heat transfer coefficient.

A Biot number with a value higher than 1 means that the heat transmission rate is lower inside the material than at its surface. It also indicates a significant temperature gradient inside the material. This temperature gradient is theoretically assumed negligible if the Biot number is equal to or lower than 0.1. Computing the Biot number is also a way to validate the conformity of using a lumped capacitance model.

### 2.2.2 Conduction transfer function method

CTF method is used in BPS programs like TRNSYS to model 1-D transient heat conduction through building walls with constant thermophysical properties. This method was primarily developed by Stephenson and Mitalas (1971) and consists in computing the Conduction Transfer Functions by solving the heat conduction equation with the Laplace and Z transforms theory. Later,

Mitalas and Arseneault (1972) developed an algorithm to compute the CTF coefficients, based upon the method of Stephenson and Mitalas.

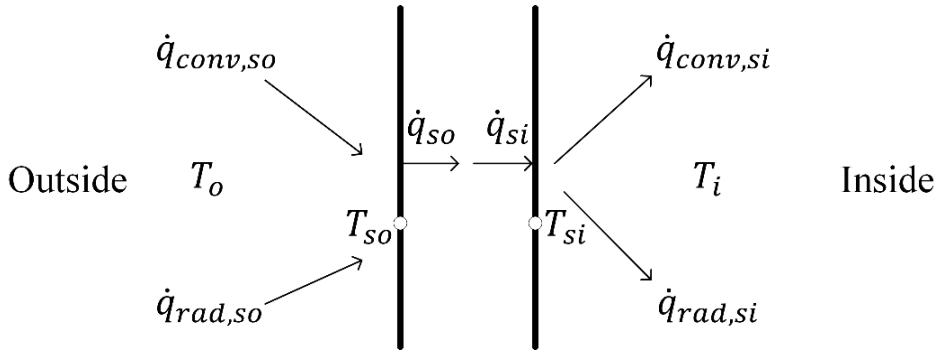


Figure 2-2: CTF method

Conduction Transfer Functions solve linear time invariant (LTI) systems from time series composed of current and past inputs and past outputs. In TRNSYS, the CTF method computes the inside and outside surface heat flows $\dot{q}_{si}$ and $\dot{q}_{so}$ from current and past values of the inside and outside surface temperatures $T_{si}$ and $T_{so}$ and from the past outputs values ($\dot{q}_{si}$ and $\dot{q}_{so}$) (Figure 2-2):

$$\dot{q}_{si,t} = \sum_{i=0}^{n_b} b_{t-i\Delta t_b}\, T_{so,t-i\Delta t_b} - \sum_{i=0}^{n_c} c_{t-i\Delta t_b}\, T_{si,t-i\Delta t_b} - \sum_{i=1}^{n_d} d_{t-i\Delta t_b}\, \dot{q}_{si,t-i\Delta t_b} \qquad (2.8)$$

$$\dot{q}_{so,t} = \sum_{i=0}^{n_a} a_{t-i\Delta t_b}\, T_{so,t-i\Delta t_b} - \sum_{i=0}^{n_b} b_{t-i\Delta t_b}\, T_{si,t-i\Delta t_b} - \sum_{i=1}^{n_d} d_{t-i\Delta t_b}\, \dot{q}_{so,t-i\Delta t_b} \qquad (2.9)$$

Where the coefficients $a$, $b$, $c$ and $d$ must meet the following requirement:

$$\frac{\sum_{i=0}^{n_a} a_{t-i\Delta t_b}}{\sum_{i=0}^{n_d} d_{t-i\Delta t_b}} = \frac{\sum_{i=0}^{n_b} b_{t-i\Delta t_b}}{\sum_{i=0}^{n_d} d_{t-i\Delta t_b}} = \frac{\sum_{i=0}^{n_c} c_{t-i\Delta t_b}}{\sum_{i=0}^{n_d} d_{t-i\Delta t_b}} = U \qquad (2.10)$$

$\Delta t_b$ is named the timebase and is the CTF time-step. It must be equal to or an integer multiple of the simulation time-step. If $i$ equals 0 in Equations ( 2.8 ) to ( 2.10 ), it means the current time-step. If $i$ equals 1, it then means the previous time-step. And so on until it reaches the number of coefficients.

Equations ( 2.8 ) and ( 2.9 ) depend on the current surface temperatures $T_{si}$ and $T_{so}$, which are unknown. Surface temperatures depend on net convective and radiative heat gains with the surroundings but also on the heat conduction through the wall. Surface heat balance is solved using an iterative procedure, as explained and suggested by Mitalas (1968).

Coefficients $a$, $b$, $c$ and $d$ characterize the thermal behavior of a wall and can be generated using several methods, which were for example compared by Li et al. (2009). The mainly used two methods are the Direct Root Finding (DRF) and State-Space (SS) methods. The first was developed by Mitalas, Stephenson and Arseneault (Mitalas & Arseneault, 1972; Stephenson & Mitalas, 1971) and is used in TRNSYS. On the other hand, the latter was developed by Ceylan, Myers and Seem (Ceylan & Myers, 1980; Seem, 1987) and is implemented in EnergyPlus.

#### 2.2.2.1 Direct Root Finding method

This method is based on Pipe's method (1957) for computing heat flows through walls, which is also documented by Carslaw and Jaeger (1959). Pipe shows that the Laplace transforms of the heat flow and temperature at inside and outside wall surfaces are related by the following matrix expression:

$$\begin{bmatrix} T_{so}(s) \\ \dot{q}_{so}(s) \end{bmatrix} = \begin{bmatrix} A(s) & B(s) \\ C(s) & D(s) \end{bmatrix} \begin{bmatrix} T_{si}(s) \\ \dot{q}_{si}(s) \end{bmatrix} \quad (2.11)$$

Where $s$ is the Laplace variable, and:

$$A(s) = D(s) = \cosh\left(L\sqrt{\frac{s}{\alpha}}\right) \quad (2.12)$$

$$B(s) = -\frac{\mathrm{R}\sinh\left(L\sqrt{\frac{s}{\alpha}}\right)}{L\sqrt{\frac{s}{\alpha}}} \quad (2.13)$$

$$C(s) = -\frac{L\sqrt{\frac{s}{\alpha}}\sinh\left(L\sqrt{\frac{s}{\alpha}}\right)}{R} \quad (2.14)$$

Where $L$ is the thickness and $R$ is the thermal resistance.

The square matrix in Equation ( 2.11 ) is called transmission matrix and is further shortened conveniently as $[M]$. For a multilayer wall, the transmission matrix is the product of matrices of each layer. For a n-layer wall, the transmission matrix is therefore:

$$[M] = [M_1][M_2] \dots [M_n] \qquad (2.15)$$

If one of the layer is purely resistive (no thermal mass), the transmission matrix is as follows: $\begin{bmatrix} 1 & -R \\ 0 & 1 \end{bmatrix}$.

The determinant of all transmission matrices is one. Equation ( 2.11 ) can then be rearranged in order to relate the inputs ($T_{si}$ and $T_{so}$) to the outputs ($\dot{q}_{si}$ and $\dot{q}_{so}$), as needed in Equations ( 2.8 ) and ( 2.9 ). The following expression is obtained:

$$\begin{bmatrix} \dot{q}_{so}(s) \\ \dot{q}_{si}(s) \end{bmatrix} = \begin{bmatrix} \frac{D(s)}{B(s)} & -\frac{1}{B(s)} \\ \frac{1}{B(s)} & -\frac{A(s)}{B(s)} \end{bmatrix} \begin{bmatrix} T_{so}(s) \\ T_{si}(s) \end{bmatrix} \qquad (2.16)$$

The transmission matrix is composed of four transfer functions which relate each input to each output. Equation ( 2.16 ) is a continuous expression and has to be discretized with a sampling interval equivalent to the timebase $\Delta t_b$ using Z-transform theory in order to compute the CTF coefficients. This stage requires computing the roots of $B(s)$ with a numerical root-finding procedure. For highly resistive and heavy walls, the root-finding procedure can miss several roots and can therefore be unable to generate the CTF coefficients. Hittle and Bishop (1983) discussed this issue and developed an improved root-finding procedure.

Once the roots of $B(s)$ obtained, the CTF coefficients are computed, as explained by Stephenson and Mitalas (1971) or more recently by Giaconia and Orioli (2000).

#### 2.2.2.2 State-Space method

The State-Space (SS) method is used in EnergyPlus for generating CTF coefficients. It was initially developed by Ceylan and Myers (1980) to model multidimensional heat transfer with transfer functions generated from a set of first order differential equations. Seem (1987) improved this method by generating only significant coefficients and therefore decreasing their numbers.

Myers (1971) showed that a heat transfer problem can be modeled with a state-space representation, using finite-difference method to spatially discretize the problem. Heat transfer problems can then be presented such as LTI systems with $n_s$ states, $n_i$ inputs and $n_o$ outputs:

$$\frac{d\begin{bmatrix} T_1 \\ \dots \\ T_n \end{bmatrix}}{dt} = [A]\begin{bmatrix} T_1 \\ \dots \\ T_n \end{bmatrix} + [B]\begin{bmatrix} T_i \\ T_o \end{bmatrix} \quad (2.17)$$

$$\begin{bmatrix} \dot{q}_i \\ \dot{q}_o \end{bmatrix} = [C]\begin{bmatrix} T_1 \\ \dots \\ T_n \end{bmatrix} + [D]\begin{bmatrix} T_i \\ T_o \end{bmatrix} \quad (2.18)$$

Where $A$, $B$, $C$ and $D$ are matrices with constant coefficients. Their sizes are respectively ($n_s$,$n_s$), ($n_s$,$n_i$), ($n_o$,$n_s$) and ($n_o$,$n_i$). Temperatures $T_i$ and $T_o$ are inputs. Heat flows $\dot{q}_i$ and $\dot{q}_o$ are outputs. The vector including temperatures $T_1$ to $T_n$ is the state vector.

Figure 2-3 presents a practical example of a homogeneous wall modeled with 2 nodes at the outside and inside surfaces, using the electrical (Resistor – Capacitor) analogy.

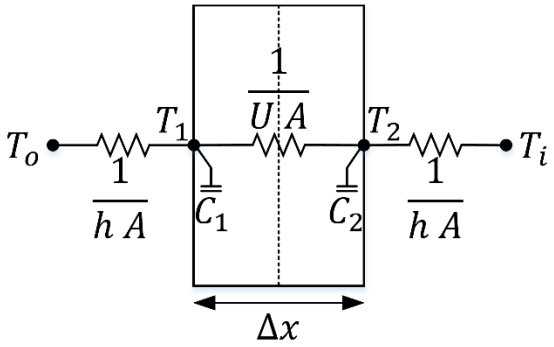


Figure 2-3: 1-D two-node model of a wall

The following equations can be written for the example illustrated in Figure 2-3:

$$C_1 \frac{dT_1}{dt} = h\ A\ (T_o - T_1) + U\ A\ (T_2 - T_1) \quad (2.19)$$

$$C_2 \frac{dT_2}{dt} = h\ A\ (T_i - T_2) + U\ A\ (T_1 - T_2) \quad (2.20)$$

$$\dot{q}_i = h\,A\,(T_i - T_2) \qquad (2.21)$$

$$\dot{q}_o = h\,A\,(T_1 - T_o) \qquad (2.22)$$

Where:

$$C_1 = C_2 = \frac{\rho\,C_p\,A\,\Delta x}{2} \qquad (2.23)$$

Equations ( 2.19 ) to ( 2.22 ) can be rewritten in a matrix form:

$$\frac{d\begin{bmatrix}T_1\\T_2\end{bmatrix}}{dt} = \begin{bmatrix}-\frac{U\,A}{C_1} - \frac{h\,A}{C_1} & \frac{U\,A}{C_1} \\ \frac{U\,A}{C_2} & -\frac{U\,A}{C_2} - \frac{h\,A}{C_2}\end{bmatrix}\begin{bmatrix}T_1\\T_2\end{bmatrix} + \begin{bmatrix}\frac{h\,A}{C_1} & 0 \\ 0 & \frac{h\,A}{C_2}\end{bmatrix}\begin{bmatrix}T_o\\T_i\end{bmatrix} \qquad (2.24)$$

$$\begin{bmatrix}\dot{q}_o\\\dot{q}_i\end{bmatrix} = \begin{bmatrix}h\,A & 0\\0 & -h\,A\end{bmatrix}\begin{bmatrix}T_1\\T_2\end{bmatrix} + \begin{bmatrix}-h\,A & 0\\0 & h\,A\end{bmatrix}\begin{bmatrix}T_o\\T_i\end{bmatrix} \qquad (2.25)$$

Through matrix computations, a state-space representation can be converted in a transfer function representation in order to relate outputs and inputs without using the state vector. Unlike the DRF method, the SS method avoids the numerical pitfalls of the root-finding procedure.

### 2.2.3 Finite-difference method

Finite-difference methods are numerical methods and consist in replacing partial differential equations by discrete approximations. Numerical solutions are given for a defined number of points called nodes. All nodes constitute a mesh defined by the user. This principle is illustrated in Figure 2-4. Horizontally, each node is spatially separated to the previous or following one by a regular interval $\Delta x$. The y-axis is the time, divided in even periods called time-steps $\Delta t$.

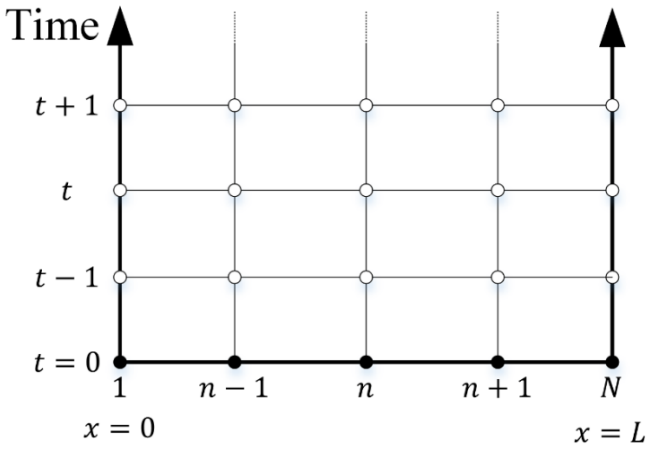


Figure 2-4: 1-D finite-difference grid

The core idea of finite-difference methods is to replace derivatives by discrete approximations. For example, the time derivative of the temperature of node $n$ can be approximated as follows:

$$\frac{dT_n}{dt} = \frac{T_n^{t+1} - T_n^t}{\Delta t} + \mathcal{O}(\Delta t) \qquad (2.26)$$

Where $\mathcal{O}(\Delta t)$ is the truncation error caused by the approximation, which is proportional to the used time-step $\Delta t$.

The 1-D heat equation is formulated in the following form:

$$\frac{dT}{dt} = \alpha \frac{d^2T}{dx^2} \qquad (2.27)$$

Equation (2.27) is composed of a first order time derivative and a second order space derivative. When approximated, the accuracy of the numerical solution depends on the time-step $\Delta t$ and on the space interval $\Delta x$. The more they approach zero, the more the computed solution approaches the ideal solution and the more the model is time-consuming. The combination of nodes used to compute the solution determines the type of finite-difference method. Numerical solutions to heat transfer problems have been documented by several authors, such as Ames (1992), Cooper (1998), Morton and Mayers (1994). Fletcher (1988) also discussed for some methods their implementation in Fortran.

Prior to discussing further different finite-difference methods (explicit, implicit and Crank-Nicolson), a brief review of methods for selecting the number of nodes to spatially discretize a wall is presented.

#### 2.2.3.1 Spatial discretization

The definition of a criteria in order to choose the number of nodes and the manner to distribute them in multilayer walls in finite-difference models has been discussed by Waters and Wright (1985) and in the engineering reference of EnergyPlus (2014).

For the number of nodes, both references have different approaches. Waters and Wright suggest to compare each layer to the others. For each layer, a value called $\beta$ is computed as follows:

$$\beta = \frac{\alpha}{L^2} \qquad (2.28)$$

Where $\alpha$ is the thermal diffusivity and $L$ is the thickness. Higher $\beta$ values result from lower thermal resistances and capacitances, and a lower number of nodes is then attributed to the layer. The number of nodes $n$ per layer is calculated such as:

$$n = n_{min}\sqrt{\frac{\beta_{max}}{\beta_i}} \qquad (2.29)$$

Where $n_{min}$ is the minimum number of nodes, $\beta_{max}$ is the maximum $\beta$ value among all layers and $\beta_i$ is the $\beta$ value of the layer for which the number of nodes is computed. The layer with the highest $\beta$ value (i.e. $\beta_{max}$) obtains the minimum number of nodes.

On the other hand, the method implemented in EnergyPlus is based on the Fourier number, expressed through its inverse ($C_d = 1/Fo$), to choose the number of nodes per layer. A space interval between 2 nodes is computed for each layer such as:

$$\Delta x = \sqrt{C_d\ \alpha\ \Delta t} \qquad (2.30)$$

In EnergyPlus, $C_d$ is fixed at 3 by default, which corresponds to a Fourier number of $\frac{1}{3}$, i.e. a value which satisfies the stability condition of the forward time and central space (FTCS) finite-

difference method (Bergman et al., 2011). Unlike the method proposed by Waters and Wright, this method takes into account the time-step $\Delta t$.

Both methods distribute the nodes using the same methodology. They locate nodes on the limits of boundary conditions, on each layer interface and inside each layer. Nodes on the limits of boundary conditions and on each layer interface are considered as half-nodes while nodes inside each layer are considered as whole nodes. For resistive layers, only one node is needed at the interface between the previous layer and the resistive layer.

#### 2.2.3.2 Explicit method

The explicit method uses current values (time $t$) to compute the future value for node $n$ (time $t+1$). Figure 2-5 illustrates this method, which is also called forward time and central space method.

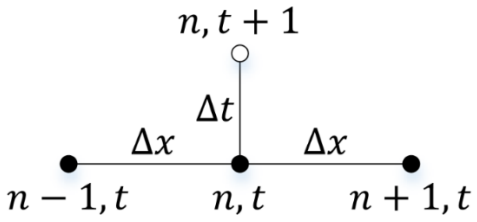


Figure 2-5: Explicit scheme

As shown in (Recktenwald, 2011), the first order time derivative and the second order space derivative in Equation ( 2.27 ) can be approximated as follows:

$$\frac{dT_n}{dt} = \frac{T_n^{t+1} - T_n^t}{\Delta t} + \mathcal{O}(\Delta t) \qquad (2.31)$$

$$\frac{d^2T_n}{dx^2} = \frac{T_{n-1}^t - 2T_n^t + T_{n+1}^t}{\Delta x^2} + \mathcal{O}(\Delta x^2) \qquad (2.32)$$

Where $\mathcal{O}$ is the truncation error related to the approximations. This error depends on the time-step $\Delta t$ and on the square of the space interval $\Delta x$.

The terms of Equation ( 2.27 ) can be substituted by the approximations given in Equations ( 2.31 ) and ( 2.32 ):

$$\frac{T_n^{t+1} - T_n^t}{\Delta t} = \alpha \frac{T_{n-1}^t - 2T_n^t + T_{n+1}^t}{\Delta x^2} + \mathcal{O}(\Delta t) + \mathcal{O}(\Delta x^2) \quad (2.33)$$

Future value $T_n^{t+1}$ can then be expressed as a function of the current values while neglecting the truncation errors:

$$T_n^{t+1} = T_n^t + \frac{\alpha \, \Delta t}{\Delta x^2} (T_{n-1}^t - 2T_n^t + T_{n+1}^t) \quad (2.34)$$

The Fourier number Fo appears in Equation ( 2.34 ) since $\text{Fo} = \frac{\alpha \, \Delta t}{\Delta x^2}$. As documented by Bergman et al. (2011), the explicit method is subject to stability conditions, in which the Fourier number is involved. For internal nodes, the stability condition is the following:

$$\text{Fo} = \frac{\alpha \, \Delta t}{\Delta x^2} \leq \frac{1}{2} \quad (2.35)$$

For surface nodes (subject to boundary conditions), the stability conditions is more restrictive and involves the Biot number:

$$\text{Fo}\,(1 + \text{Bi}) = \frac{\alpha \, \Delta t}{\Delta x^2}\left(1 + \frac{h_g \, \Delta x}{k}\right) \leq \frac{1}{2} \quad (2.36)$$

Where $h_g$ is the global heat transfer coefficient (including convective and radiative heat transfer).

#### 2.2.3.3 Implicit method

The implicit method uses future values and the current value of node $n$ to compute future values (time $t + 1$). Figure 2-6 illustrates this method, which can also be called backward time and central space method.

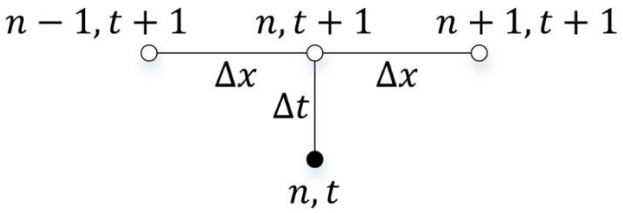


Figure 2-6: Implicit scheme

The approximations of the first order time derivative and the second order space derivative are as follows (Recktenwald, 2011):

$$\frac{dT_n}{dt} = \frac{T_n^{t+1} - T_n^t}{\Delta t} + \mathcal{O}(\Delta t) \qquad (2.37)$$

$$\frac{d^2T_n}{dx^2} = \frac{T_{n-1}^{t+1} - 2T_n^{t+1} + T_{n+1}^{t+1}}{\Delta x^2} + \mathcal{O}(\Delta x^2) \qquad (2.38)$$

Substituting the terms of Equation ( 2.27 ) by those of Equations ( 2.31 ) and ( 2.32 ), the following equations is obtained:

$$\frac{T_n^{t+1} - T_n^t}{\Delta t} = \alpha \frac{T_{n-1}^{t+1} - 2T_n^{t+1} + T_{n+1}^{t+1}}{\Delta x^2} + \mathcal{O}(\Delta t) + \mathcal{O}(\Delta x^2) \qquad (2.39)$$

The truncation errors are similar to the explicit method. However, Equation ( 2.39 ) is composed of several unknowns. To be solved, this equation must be part of a system of equations where the number of unknowns is equal to the number of equations. Doing so requires additional CPU time. Unlike the explicit method, the implicit method is unconditionally stable, which is a significant advantage.

#### 2.2.3.4 Crank-Nicolson method

The Crank-Nicolson method uses current and future values to compute future values (time $t + 1$), as illustrated in Figure 2-7.

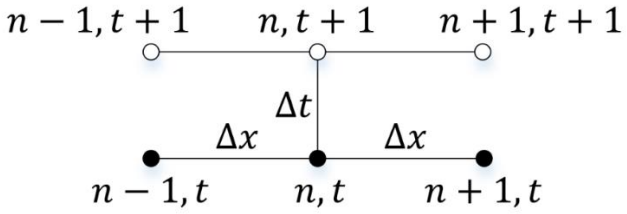


Figure 2-7: Crank-Nicolson scheme

The Crank-Nicolson method uses the same approximation of the first order time derivative as the explicit and implicit methods. The second order space derivative is approximated using the average of the approximations of the explicit and implicit methods. The following expression is then obtained (Recktenwald, 2011):

$$\frac{T_n^{t+1} - T_n^t}{\Delta t} = \frac{\alpha}{2}\left(\frac{T_{n-1}^{t+1} - 2T_n^{t+1} + T_{n+1}^{t+1}}{\Delta x^2} + \frac{T_{n-1}^{t} - 2T_n^{t} + T_{n+1}^{t}}{\Delta x^2}\right) + \mathcal{O}(\Delta t^2) + \mathcal{O}(\Delta x^2) \quad (2.40)$$

Like the implicit method, the discretized equation is composed of several unknowns and must be solved as part of a system of equations. The Crank-Nicolson method is also considered unconditionally stable. A significant advantage of this method is the better temporal truncation error, which is proportional to the square of the time-step $\Delta t$ (instead of $\mathcal{O}(\Delta t)$ for both explicit and implicit schemes).

## 2.3 Conduction heat transfer modeling with PCM

Modeling conduction heat transfer through a PCM layer involves solving a set of non-linear equations. This non-linearity comes from variable PCM properties, which depend on the PCM temperature and state. The properties of interest are the thermal conductivity, the density and the thermal capacity. All of them can be variable. A first discussed prerequisite is therefore the determination of these properties. Then, 1-D modeling methods used to simulate the PCM thermal behavior in building walls are reviewed. The last issue discussed in this section is modeling approaches for specific thermal behaviors which can be observed when using PCMs.

### 2.3.1 PCM classification and thermophysical properties

As noted by Zalba et al. (2003), Sharma et al. (2009) and Baetens et al. (2010), PCMs are generally classified in three categories, i.e. organics (e.g. paraffins, alcohols or fatty acids), inorganics (e.g. salt hydrates) and eutectics. Eutectics are mixtures of organics and / or inorganics. According to Sharma et al. (2009), inorganics have in general approximately twice more volumetric latent heat storage capacity than organics. These review papers also present large lists of available PCMs with their main properties.

These properties are measured using proven methods. The German Institute for Quality Assurance and Certification (2013) have documented a list of possible methods used to measure the thermal conductivity and capacity of PCMs.

The standard method for measuring PCM thermal conductivity is the hot-wire method (Alvarado, Marín, Juárez, Calderón, & Ivanov, 2012; ASTM International, 2000). The hot-wire equipment is

composed of a data acquisition system and a needle which includes a heating wire and a temperature probe. During measurements, the needle is immersed into a large PCM sample and is considered as a linear heat source. The heat flow going across the sample is assumed radial. The temperature evolution recorded by the probe defines the thermal conductivity. Lower measured temperature increases lead to higher thermal conductivities.

In order to measure PCM temperature-dependent thermal capacity, the German Institute for Quality Assurance and Certification (2013) suggests to use Differential Scanning Calorimetry (DSC) or T-history methods. DSC technique was primarily developed by Watson et al. (1964). Its principle is based on a comparative analysis of a PCM sample to a reference. The test consists in recording the energy necessary over time flowing in (heating) or out (cooling) the sample and the reference to maintain both at nearly the same temperature. The temperature-dependent specific heat is then derived from the DSC results. Many authors point out several limitations when using DSC method. As highlighted by Zhang et al. (1999) and Cheng et al. (2013), DSC tests are applied on very small samples (1-10 mg). A careful sampling is consequently required to obtain a representative property. A second limitation presented by Zhang et al. (1999) is the significant cost of DSC tests.

The T-history method is also based on a comparison between a PCM sample and a reference. Initially, Zhang et al. (1999) proposed this method as an alternative to DSC tests. Unlike DSC method, the sample size is higher (a few grams) and the test is less expensive to perform. During T-history experimentations, the PCM sample and the reference (e.g. water) undergo a similar cooling (or heating as suggested by Günther et al. (2006)). A comparison of temperature evolutions between the PCM sample and the reference allows obtaining specific heat (solid and liquid) and latent heat values of the PCM. Several authors have improved the T-history method, following different approaches. Kravvaritis et al. (2010) proposed the “thermal delay method” (Figure 2-8 (a)), which consists in comparing the temperature variation of the PCM sample and the reference during the same time range. On the other hand, Marín et al. (2003) suggested another approach called “time delay method”. The goal is to compare the time durations passed on a defined temperature range between the PCM sample and the reference (Figure 2-8 (b)). The temperature-dependent specific heat is then obtained through these two approaches. An extensive review of the T-history method is for example documented by Solé et al. (2013).

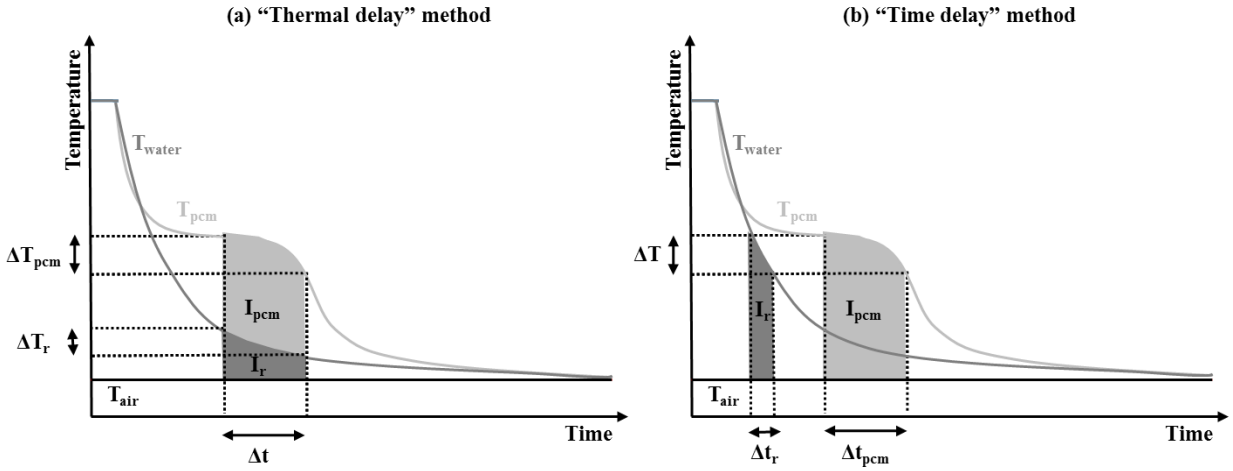


Figure 2-8: Two different approaches of T-history tests

Two limitations of the T-history method are discussed by Cheng et al. (2013). First, the sample temperature must be considered uniform. Mathematically, it means that the Biot number must be equal to or lower than 0.1 (Bergman et al., 2011). Second, a T-history method is not suited to materials for which it is difficult to obtain a small uniform sample, e.g. PCM-concrete bricks as studied by Cheng et al. (2013).

Other alternatives to measure the temperature-dependent specific-heat are also available. A method based on a dynamic Heat Flow Meter Apparatus ("HFMA method") was proposed by Kosny et al. (2010). It can be applied to a large amount of PCM encapsulated in a plastic film, i.e. in conditions closer to the actual use in buildings envelope. Coupling a detailed 3-D model of the plastic film including PCM encapsulations and experimental data generated with the heat flow meter apparatus allows obtaining the temperature-dependent specific heat of the PCM. Their presented results also indicate that the latent heat calculated with the HFMA method is around 30 % lower than the value obtained with the DSC test. This methodology is close to inverse modeling techniques. These latter were already used to identify thermophysical properties of a material. Using experimental data and a 1-D finite-element model coupled with an optimization algorithm based on least squares method, Atchonouglo et al. (2008) identified the constant thermal capacity and conductivity of polymers. Using the same methodology but with an optimization algorithm based on the conjugate gradient method, Huang and Jan-Yuan (1995) determined simultaneously the temperature-dependent thermal capacity and conductivity of a material. Cheng et al. (2013) also applied an inverse technic for only obtaining the temperature-dependent specific-heat of PCM-concrete bricks. Several

optimization algorithms based on genetic algorithm, particle swarm optimization algorithm and sequential quadratic programming method were coupled with a 1-D finite-difference model to define this property and to determine the most effective algorithm. The results show that all algorithms generate nearly the same optimized temperature-dependent specific-heat. They also show that the sequential quadratic programming method is the most time-effective.

### 2.3.2 Modeling methods

Conduction heat transfer in PCMs is a moving boundary problem (Crank, 1987) or a Stefan problem, named after the Slovene physicist who introduced this class of problem for ice formation. An important dimensionless number named after Stefan is useful to analyze phase change problems. It is defined as the ratio of sensible heat to latent heat and is formulated as:

$$\mathrm{St} = \frac{C_p \left(T_{fusion} - T_{sys}\right)}{L} \qquad (2.41)$$

Moving boundary problem involves to deal with non-linear phenomena which change with time and space. In the basic case of water solidification, this process involves the presence of liquid and solid phases separated by a moving boundary which should be tracked. Few analytical solutions exist for phase change problems and are among others formulated by Crank (1987), Alexiades and Solomon (1992). Stefan was the first to propose analytical solutions to phase change problems, which are documented, among others, by Hu and Argyropoulos (1996). Numerical methods are nevertheless preferred since they are easily adapted to different cases. Numerical solutions are classified into two main categories:

- Deforming grid or front-tracking methods (or strong solutions): the space grid is deformed during calculations, depending on the position of the solidification / melting front. These methods are for example described by Voller (1996). However they require time-consuming calculations.
- Fixed grid methods (or weak solutions): the space grid remains fixed during calculations and the solidification / melting front is tracked using an auxiliary function. These solutions are widespread methods and some review papers document them (Al-Saadi & Zhai, 2013; Voller, Swaminathan, & Thomas, 1990).

In the following sections, only fixed grid methods are discussed since they are the most suited for 1-D modeling of a wall with PCMs. Among these methods, two are mainly used in the literature: the heat capacity and enthalpy methods, which are discussed below. Less often-used methods such as the temperature transforming (Cao & Faghri, 1990) or heat source (for example reviewed by Al-Saadi and Zhai (2013)) are not covered in this discussion.

#### 2.3.2.1 Heat capacity method

The heat capacity method (Goodrich, 1978; Yao & Chait, 1993) consists in adapting the PCM specific heat depending on its temperature and/or state. Until recently, two approaches, named the apparent and effective heat capacity, were used to define this property. Their differences were in particular discussed by Poirier (1986). For both terminologies, the apparent or effective specific-heat combines sensible and latent heat. Today, both terminologies are interchangeably used.

The governing 1-D heat equation (Equation ( 2.27 )) can be rewritten as follows:

$$\rho \; C_p(T) \; \frac{dT}{dt} = \frac{d\left(k \frac{dT}{dx}\right)}{dx} \qquad (2.42)$$

Where the specific heat $C_p$ is temperature-dependent (Figure 2-9 (a)). The core idea of this method is then to approximate correctly this property for each location and time-step.

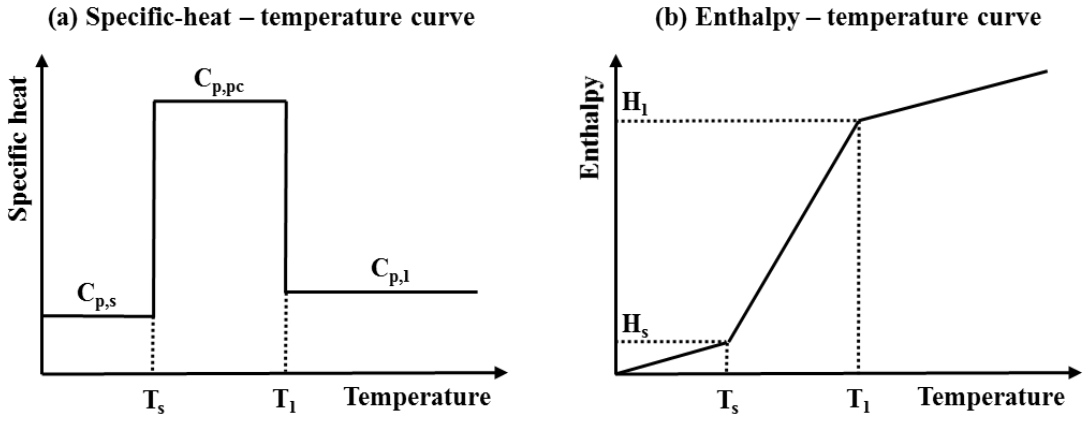


Figure 2-9: (a) Specific-heat – temperature and (b) enthalpy – temperature curves of a PCM with a phase change temperature range $[T_s, T_l]$

Mathematically, the temperature-dependent specific-heat of a PCM with a solidification / melting range can be computed such as (Voller, 1996):

$$C_p = \begin{cases} C_{p,s}, & T < T_s \\ \dfrac{L}{T_l - T_s}, & T_s \leq T \leq T_l \\ C_{p,l}, & T > T_l \end{cases} \quad (2.43)$$

Like the specific-heat, the thermal conductivity can be temperature-dependent and is determined such as:

$$k = \begin{cases} k_s, & T < T_s \\ (1 - l_f)\, k_s + l_f\, k_l, & T_s \leq T \leq T_l \\ k_l, & T > T_l \end{cases} \quad (2.44)$$

Where the liquid fraction $l_f$ is:

$$l_f = \frac{T - T_s}{T_l - T_s} \; or \; l_f = \frac{H - H_s}{H_l - H_s} \quad (2.45)$$

Equation ( 2.42 ) can be solved explicitly (Voller, 1996), using a forward time and central space scheme such as (for node $n$):

$$T_n^{t+1} = T_n^t + \frac{\alpha\, \Delta t}{\Delta x^2} \left(T_{n-1}^t - 2T_n^t + T_{n+1}^t\right) \quad (2.46)$$

Where the thermal diffusivity $\alpha$ depends on the temperature-dependent specific-heat and thermal conductivity. The stability condition for this fully explicit scheme becomes:

$$Max(Fo_s, Fo_l) = Max\left(\frac{\alpha_s\, \Delta t}{\Delta x^2}, \frac{\alpha_l\, \Delta t}{\Delta x^2}\right) \leq \frac{1}{2} \quad (2.47)$$

If a fully implicit or Crank-Nicolson scheme is applied, iterative calculations are required since the specific-heat and thermal conductivity at time $t + 1$ are unknown. Solving the equations system requires using common linear solvers such as a Gauss-Seidel algorithm (Morgan, Lewis, & Zienkiewicz, 1978) or a tridiagonal matrix algorithm (TDMA) (Pasupathy & Velraj, 2006). For each iteration, the specific-heat must be updated such as proposed by Morgan et al. (1978):

$$C_p = \frac{\Delta H}{\Delta T} = \frac{H^{j+1} - H^j}{T^{j+1} - T^j} \quad (2.48)$$

Where $H$ is the enthalpy and $j$ is the iteration level. This calculation is possible only if the enthalpy – temperature curve is known (Figure 2-9 (b)). Unlike Morgan et al., Lemmon (1981) proposed to approximate the specific-heat based on the space average (instead of the time average for Morgan et al.).

Convergence is reached as soon as temperature variation between two iterations becomes negligible. If the time-step is too large and / or the phase change temperature range is too small, the phase change can be undetected and / or convergence issues can occur. Solutions to these limitations were proposed in the literature (Gong & Mujumdar, 1997; Yao & Chait, 1993).

#### 2.3.2.2 Enthalpy method

The governing 1-D heat equation (Equation ( 2.27 )) can be formulated using an enthalpy term including sensible and latent heat:

$$\rho \frac{dH}{dt} = \frac{d\left(k \frac{dT}{dx}\right)}{dx} \qquad (2.49)$$

As suggested by Klimes et al. (2012), Equation ( 2.49 ) can be solved with an explicit finite-difference method (for node $n$):

$$H_n^{t+1} = H_n^t + \frac{k\,\Delta t}{\rho\,\Delta x^2}\left(T_{n-1}^t - 2T_n^t + T_{n+1}^t\right) \qquad (2.50)$$

The temperature values $T^{t+1}$ can then be calculated using the enthalpy – temperature curve (as illustrated in Figure 2-9 (b)). The same stability condition as formulated in Equation ( 2.47 ) is required.

If a fully implicit method is used, the future enthalpy $H_n^{t+1}$ of node $n$ depends on future temperatures $T_{n-1}^{t+1}$, $T_n^{t+1}$ and $T_{n+1}^{t+1}$ such as:

$$H_n^{t+1} = H_n^t + \frac{k\,\Delta t}{\rho\,\Delta x^2}\left(T_{n-1}^{t+1} - 2T_n^{t+1} + T_{n+1}^{t+1}\right) \qquad (2.51)$$

The equations system (for all nodes) have therefore more unknowns than equations, which make the resolution impossible.

The most used approach to solve Equation ( 2.51 ) consists in linearizing the enthalpy term $H_n^{t+1}$ using a technique proposed by Patankar (1980). At the iterative level, this term can be written as follows:

$$H_n^{t+1,j+1} = H_n^{t+1,j} + C_p(T)^{t+1,j}\left(T_n^{t+1,j+1} - T_n^{t+1,j}\right) \quad (2.52)$$

Equation ( 2.52 ) is substituted into Equation ( 2.51 ), which yields the following linear discretized equation:

$$-\frac{k\,\Delta t}{\rho\,\Delta x^2}\,T_{n-1}^{t+1,j+1} + \left(C_p(T)^{t+1,j} + \frac{2\,k\,\Delta t}{\rho\,\Delta x^2}\right)T_n^{t+1,j+1} - \frac{k\,\Delta t}{\rho\,\Delta x^2}\,T_{n+1}^{t+1,j+1} = H_n^t - H_n^{t+1,j} + C_p(T)^{t+1,j}T_n^{t+1,j} \quad (2.53)$$

Equation ( 2.53 ) can be formulated in a simplified matrix form:

$$[A]^{t+1,j} \times [T]^{t+1,j+1} = [B]^{t+1,j} \quad (2.54)$$

Equation ( 2.54 ) is then solved iteratively using a Gauss-Seidel algorithm (Shamsundar & Rooz, 1988; Shamsundar & Sparrow, 1975) or a tridiagonal matrix algorithm (TDMA) (Swaminathan & Voller, 1993; Voller, 1996). Convergence is reached as soon as temperature variation between two iterations become negligible.

In order to reduce computation time, a non-iterative method was also proposed by Pham (1985). It consists in solving Equations ( 2.54 ) using a TDMA algorithm to obtain the temperature field. Enthalpies are computed using Equation ( 2.52 ) and the temperature field is then corrected based on the new enthalpies. Unfortunately, Voller (1996) showed that this method might not conserve energy at every time-step.

#### 2.3.2.3 Reported problems of iterative methods

Using implicit or semi-implicit finite-difference methods is advantageous since no restriction on time-stepping is required. On the other hand, this kind of methods involves iterative calculations when dealing with non-linear equations. Tavakoli and Davami (2007) showed that the product of the number of time-steps by the number of iterations when using an implicit method might be higher than the number of time-steps when using an explicit method. They took cases presented by

Swaminathan and Voller (1992) and compared their results generated with an implicit method to results generated with a fully explicit method. The comparison indicated that explicit methods might be more efficient than implicit methods since the number of iterations (including time-steps and inner iterations) is less numerous for explicit schemes.

Another drawback is the difficulty to apply implicit methods for modeling PCMs with complex thermal behaviors such as hysteresis and subcooling (presented in the following section). The implicit methods presented previously were all adapted to cases with constant-temperature phase change or phase change over a certain temperature range. None of them was applied on PCM with subcooling and different thermal behavior during heating and cooling processes.

### 2.3.3 Specific PCM thermal behaviors

Most models do not take into account two specific PCM thermal behaviors: hysteresis and subcooling. The first is highlighted by a different PCM thermal behavior during heating (melting) and cooling (solidification) processes, as illustrated in Figure 2-10. Both melting and solidification occur over different temperature ranges, which has an impact on the enthalpy – temperature curves. Subcooling is experienced when the liquid state is cooled down below its assumed solidification temperature (Figure 2-11). This is followed by a steep temperature increase caused by an abrupt latent heat release, leading to solidification. Kuznik and Virgone (2009) and Günther et al. (2007) suggest that the hysteresis and the subcooling can have a significant impact on PCM performance, respectively. Günther et al. (2007) also present a manner to model subcooling in PCMs.

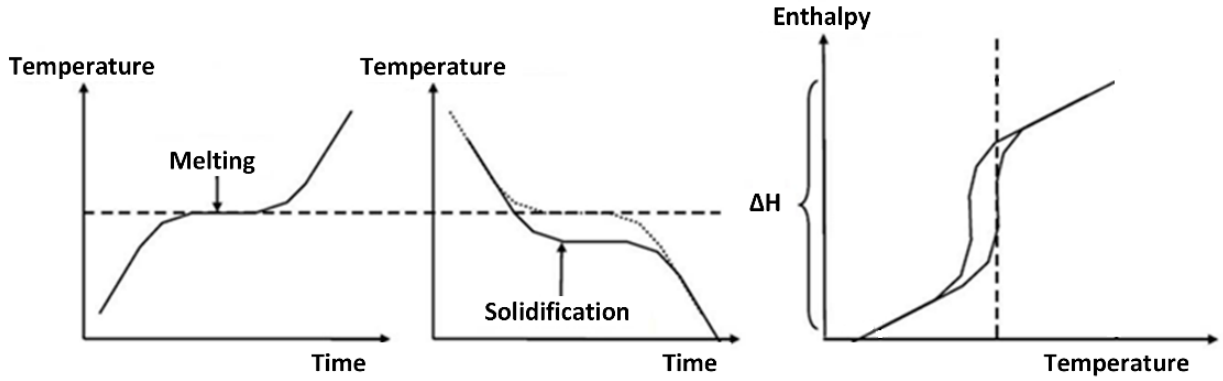


Figure 2-10: PCM hysteresis

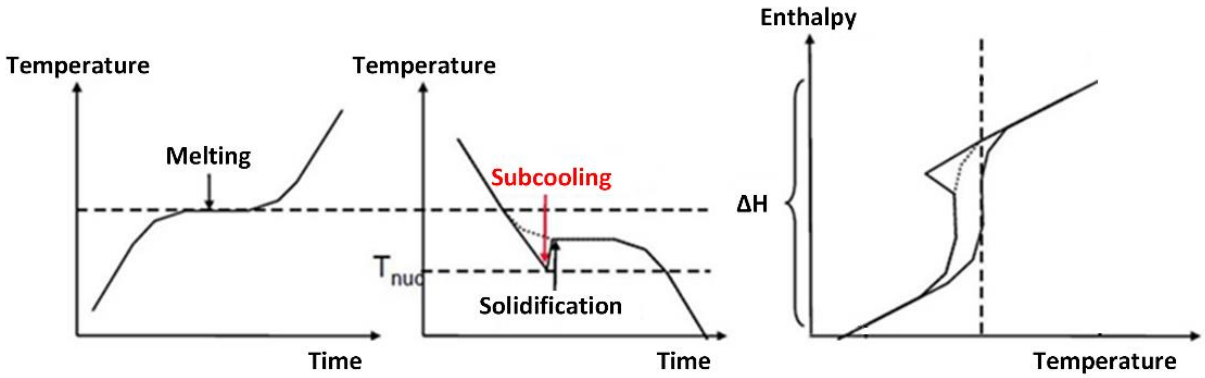


Figure 2-11: PCM subcooling

The presence of hysteresis in a PCM requires to model the transition between heating and cooling enthalpy – temperature curves during phase change. Three scenarios are documented in the literature. Bony and Citherlet (2007) propose to switch between curves using a slope equivalent to the specific-heat in the liquid or solid state ("wT" in Figure 2-12). Another option suggested by Chandrasekharan et al. (2013) consists in staying on the same curve ("noT" in Figure 2-12). The last scenario proposed by Rose et al. (2009) is applied in the BPS program BSim (Danish Building Energy Institute, 2013) and consists in instantaneous switches between heating and cooling curves.

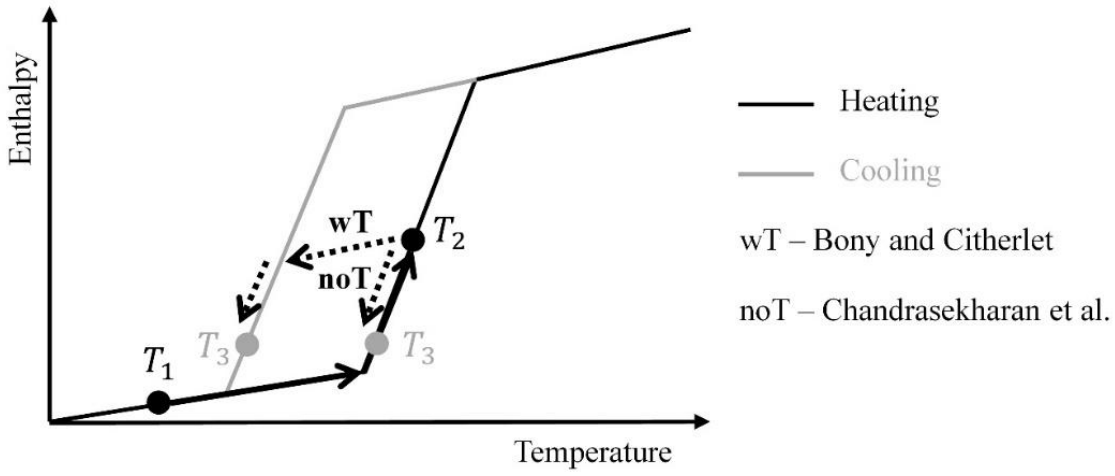


Figure 2-12: Possible behavior of a PCM cooled down after partial melting

### 2.3.4 Existing models of a wall with PCMs

Several models of a wall including PCM layer(s) are available in well-known BPS programs such as TRNSYS, EnergyPlus and ESP-r. ESP-r and EnergyPlus possess a PCM model which is directly

implemented in the building model. ESP-r uses a PCM model based on the effective heat capacity method and solved with a finite-difference method (Heim & Clarke, 2004). The thermal conductivity can be defined for liquid and solid states. On the other hand, subcooling and hysteresis cannot be modeled. However Geissler (2008) recently implemented in ESP-r a development version of a subroutine based on the work of Hoffman (2006) allowing to model hysteresis. EnergyPlus does use an enthalpy method coupled with an iterative finite-difference method using a fully implicit or Crank-Nicolson (C-N) scheme (Pedersen, 2007). This model was validated in multiple studies (Shrestha et al., 2011; Tabares-Velasco, Christensen, Bianchi, & Booten, 2012; Tabares-Velasco, Christensen, & Bianchi, 2012). Like ESP-r, the model implemented in EnergyPlus is unable to define subcooling and hysteresis while a temperature-dependent thermal conductivity can be modeled. It should be noted that EnergyPlus used to model heat conduction through walls only with the CTF method. Barbour and Hittle (2005) have studied the possibility to adapt the CTF method to PCM modeling in a development version of EnergyPlus. They proposed to generate multiple sets of CTF coefficients, depending on the PCM state and temperature. A switching mechanism deals with the selection of the right sets of CTF coefficients during the simulation. To our knowledge this method has never been implemented in the release version of EnergyPlus.

In TRNSYS, different models exist to simulate PCM in building walls. These models are encapsulated in components called “Types” and must be coupled with the multizone building model, known as Type 56. The first PCM models developed in TRNSYS were simulated as an active layer. This approach was used in Type 222 (Ibánez, Lázaro, Zalba, & Cabeza, 2005) and Type 232 (Castell, Medrano, Castellón, & Cabeza, 2009). However, this methodology has been superseded because it did not represent the actual physical phenomena. From this moment, all TRNSYS PCM models were developed based on finite-difference (FD) methods. Type 1270 developed by TESS (Thermal Energy Systems Specialists, 2012) is a very simple PCM model which considers a constant-temperature phase change and a spatially uniform temperature inside the PCM layer. Multiple TRNSYS models such as Type 204 (Poulad, Fung, & Naylor, 2011), Type 260 (Kuznik, Virgone, & Johannes, 2010) and Type 399 (Dentel & Stephan, 2010a; Dentel & Stephan, 2013) use the effective heat capacity method to model PCMs in walls. On the other hand, the literature documents two models using an enthalpy method to simulate PCM in walls, i.e. Type 241 (Schranzhofer, Puschnig, Heinz, & Streicher, 2006) and Type 285 (Al-Saadi & Zhai, 2014).

Table 2-1 presents the most recent and documented PCM models for building walls available in TRNSYS. It focuses on the main capabilities of each model. It also shows that:

- None of these models are able to model subcooling.
- Only one model (Type 399) is able to model PCM hysteresis.
- Temperature-dependent thermal conductivity can be defined in only one model.

Table 2-1: Most recent and documented PCM models for building walls in TRNSYS

| Characteristics | Type 1270 | Type 285 | Type 260 | Type 399 |
|---|---|---|---|---|
| PCM modeling method | Constant-temperature phase change | Enthalpy method | Effective heat capacity method | |
| Numerical method | Lumped capacitance model | Iterative implicit FD method | Implicit FD method | Semi-implicit FD method (C-N) |
| Hysteresis | No | | | Yes |
| Subcooling | No | | | |
| Transition between heating and cooling curves | Not possible (one-curve model) | | | Instantaneous switch between $C_p(T)$ curves. |
| Variable thermal conductivity | No | | Yes | No |

# CHAPTER 3 OBJECTIVES AND THESIS ORGANIZATION

The literature review highlights current limitations when building walls including PCMs have to be simulated in common BPS programs. No current BPS program is capable of modeling a wall with PCMs including temperature-dependent thermal conductivity, hysteresis and subcooling. In particular, TRNSYS is not adapted for this purpose since conduction heat transfer through walls is modeled using the CTF method. This method is moreover not appropriate for low-time-step simulations (< 5 minutes) of buildings with highly resistive and heavy walls.

The literature review also highlights the complexity of measuring PCM thermophysical properties, and in particular the heat capacity. Measurement techniques can lead to different test results, depending on the experimental conditions.

These limitations underlie the objectives formulated in the following section.

## 3.1 Objectives

The three main objectives of this thesis result from the above-mentioned issues and two of them are composed of several more specific goals:

- **Objective 1 – Improvement of the CTF method in TRNSYS to allow accurate low-time-step simulations of buildings with highly resistive and heavy walls.**
- **Objective 2 – Accurate and representative characterization of thermophysical properties of a selected PCM.**
    - Evaluation of the density and thermal conductivity through experimentations.
    - Evaluation of the temperature-dependent thermal capacity based on inverse method and analysis of the impacts of different configurations (PCM samples of a few grams or PCM-equipped walls) and varying heating / cooling rates on this property.
    - In the case of a PCM with 2 enthalpy-temperature curves (heating and cooling): identification of the PCM thermal behavior when phase change is interrupted.
- **Objective 3 – Development and validation of a 1-D finite-difference PCM wall model implemented in TRNSYS.**

- Development of a model of wall including PCM(s) (potentially with hysteresis and subcooling) or layer(s) with temperature-dependent properties.
- Numerical validation of the developed model through a comparison with reference models for several wall test cases.
- Experimental validation of the developed model using experimental data from a full-scale test-bench.

## 3.2 Thesis organization

This thesis is composed of eleven chapters (including the introduction and the conclusion) and is submitted as a thesis by articles. The literature review presented in Chapter 2 discusses the modeling methods used to simulate conduction heat transfer through building walls without and with PCMs. Chapter 3 presents the objectives and the organization of this thesis.

Chapter 4 presents the first article titled “Improved conduction transfer function coefficients generation in TRNSYS multizone building model”. This paper discusses the limitations of the CTF method implemented in TRNSYS and proposes a new algorithm based on the state-space method for generating the CTF coefficients. This topic is also discussed in Chapter 5, highlighting the benefit of coupling the CTF method with a finite-difference method. Both Chapter 4 and Chapter 5 address the first objective of this thesis dedicated to the improvement of the CTF method in TRNSYS to allow short-time-step simulations of buildings with highly resistive and heavy walls (required e.g. for simulating improved power demand management strategies).

Chapter 6 presents the second paper entitled “Influence of experimental conditions on measured thermal properties used to model phase change materials” and published in Building Simulation: An International Journal. This chapter focuses on the definition of the PCM temperature-dependent heat capacity. Experimentations with PCM samples are performed and processed using an inverse method in order to obtain $C_p(T)$ and $H(T)$ curves for both heating and cooling processes. The density and thermal conductivity of the tested PCM are defined through additional experimentations presented in Appendices A and B. Experimentations with PCMs included in building walls are also presented. Since the PCM layer is also composed of air and plastic film, this layer must be considered as an equivalent layer. $C_p(T)$ and $H(T)$ curves of this equivalent layer are computed using an inverse method and the influence of the heating / cooling rates on the

$H(T)$ curves are studied. The equivalent thermal conductivity is determined using THERM (Lawrence Berkeley National Laboratory, 2013), as explained in Appendix C. Chapter 7 complements Chapter 6 by identifying the PCM thermal behavior when phase change is interrupted. Both Chapter 6 and Chapter 7 address the second objective of this thesis, i.e. the definition of thermophysical properties of the tested PCM.

Chapter 8 presents the fourth article entitled "Modeling of a wall with phase change materials. Part I: Development and numerical validation". This chapter describes in details a newly developed PCM wall 1-D model based on an explicit finite-difference method and coupled with an enthalpy method for PCM modeling. This model is named Type 3258 and is able to simulate a wall including PCMs with temperature-dependent thermal conductivity, hysteresis and subcooling. A numerical validation of the presented model is performed using wall test cases proposed by the International Energy Agency. Part II of this paper (Chapter 9) completes this topic with an experimental validation and with a discussion about the coupling methods used to link the multizone building model to the PCM wall model in TRNSYS. The developed model (Type 3258) is also described in details in Appendix D. Both Chapter 8 and Chapter 9 address the third objective of this thesis about the development and validation of a new PCM wall model able to simulate PCMs with temperature-dependent thermal conductivities, hysteresis and subcooling.

A general discussion presented in Chapter 10 highlights the main contributions of this thesis while the conclusion and recommendations for further research are presented in Chapter 11.

# CHAPTER 4 ARTICLE 1: IMPROVED CONDUCTION TRANSFER FUNCTION COEFFICIENTS GENERATION IN TRNSYS MULTIZONE BUILDING MODEL

Delcroix, B., Kummert, M., Daoud, A., Hiller, M., (2013). Improved conduction transfer function coefficients generation in TRNSYS multizone building model. 13th Conference of International Building Performance Simulation Association. Chambéry, France, pp. 2667 – 2674.

## Abstract

Many building energy performance simulation programs (including TRNSYS) use the Conduction Transfer Function (CTF) method to compute 1-D transient heat conduction through multi-layer slabs. Problems have been reported with the current CTF implementation in the TRNSYS multizone building model, especially during the CTF coefficients generation. These problems are related to heavy and highly insulated slabs and short time-step simulations (less than 15-minute time-step). This paper describes the implementation of a new CTF coefficients generation method in the TRNSYS building preprocessor (TRNBuild). The efficiency and the limitations of this method are also discussed.

## 4.1 Introduction

Transient conduction heat transfer through building slabs is a key aspect of cooling and heating loads calculation. These calculations can be performed by several Building Performance Simulation (BPS) programs such as EnergyPlus (EnergyPlus, 2014), ESP-r (Energy Systems Research Unit, 1998) and TRNSYS (TRANSSOLAR Energietechnik Gmbh, 2012). The current interest for net-zero energy buildings and for better power demand management strategies requires accurate transient simulation of heavy and highly insulated slabs with short time-steps (lower than 15 minutes). It then represents a challenge for codes that were mainly developed for yearly energy load calculations with a time-step of 1 hour. It is the case of the TRNSYS building model (called Type 56) which is known to have limitations with heavy and highly insulated slabs and with short time-steps. These limitations come from the method used by TRNSYS for modeling conduction heat transfer through slabs which is known as the Conduction Transfer Function (CTF) method. In particular, problems have been identified in the generation of CTF coefficients, and a solution has

been proposed (Delcroix, Kummert, Daoud, & Hiller, 2012). This paper reports on the implementation of a new method of CTF coefficients generation in the TRNSYS building preprocessor, known as TRNBuild. The method is explained, and a simple example is provided. Results obtained using the improved version of TRNBuild for different wall types that cause problems are presented and discussed, including a full house model for a net-zero energy renovation project.

## 4.2 State of the art

The CTF method has been implemented in many BPS programs (including TRNSYS and EnergyPlus) to model 1-D transient conduction heat transfer through building slabs. It was introduced by Mitalas and Stephenson (1971) and consists in time series which allow to compute the inside and outside surface heat flows ($\dot{q}_{si}$and $\dot{q}_{so}$) from current and past values of surface temperatures ($T_{si}$ and $T_{so}$) and past values of heat flows themselves:

$$\dot{q}_{si,t} = \sum_{k=0}^{n_b} b_{t-k\Delta t_b} T_{so,t-k\Delta t_b} - \sum_{k=0}^{n_c} c_{t-k\Delta t_b} \; T_{si,t-k\Delta t_b} - \sum_{k=1}^{n_d} d_{t-k\Delta t_b} \; \dot{q}_{si,t-k\Delta t_b} \qquad (4.1)$$

$$\dot{q}_{so,t} = \sum_{k=0}^{n_a} a_{t-k\Delta t_b} \; T_{so,t-k\Delta t_b} - \sum_{k=0}^{n_b} b_{t-k\Delta t_b} T_{si,t-k\Delta t_b} - \sum_{k=1}^{n_d} d_{t-k\Delta t_b} \; \dot{q}_{so,t-k\Delta t_b} \qquad (4.2)$$

Where:

$$\frac{\sum_{k=0}^{n_a} a_{t-k\Delta t_b}}{\sum_{k=0}^{n_d} d_{t-k\Delta t_b}} = \frac{\sum_{k=0}^{n_b} b_{t-k\Delta t_b}}{\sum_{k=0}^{n_d} d_{t-k\Delta t_b}} = \frac{\sum_{k=0}^{n_c} c_{t-k\Delta t_b}}{\sum_{k=0}^{n_d} d_{t-k\Delta t_b}} = U \qquad (4.3)$$

The coefficients *a*, *b*, *c* and *d* are known as the CTF coefficients. These coefficients allow characterizing the dynamic behavior of a slab. They are generated only once before the simulation for a certain timebase value $\Delta t_b$ which is the CTF time-step. The timebase must be distinguished from the simulation time-step. TRNSYS simulations can run with a time-step that is shorter than the timebase, as long as the latter is an integer multiple of the former. The ideal case is to have equivalent values, but this cannot always be achieved for heavy and highly insulated slabs, which require longer timebase values (sometimes several hours) to be simulated in TRNSYS. A difference

between timebase and time-step creates a stair-step effect which becomes more pronounced as the difference increases.

Several methods exist for generating the CTF coefficients. Spitler et al. made a comparison between the different available methods (Li et al., 2009). The two methods most often used in practice are the Direct-Root Finding (DRF) and the State-Space (SS) methods. The first one was developed by Mitalas and Arseneault (1972) and is used in TRNSYS. The SS method is for example described by Seem (1987) and is currently used in EnergyPlus. Several papers (including (Li et al., 2009)) demonstrated that the SS method is more efficient because it allows generating the CTF coefficients for a lower timebase value.

With the stair-step effect, there is a second drawback with the CTF method which is the difficulty to take into account time-variant properties, since the coefficients are generated only once before the simulation (pre-processing). This is generally not an issue with conventional walls but it is an obstacle to modeling phase change materials (PCMs) embedded in walls and slabs.

## 4.3 Mathematical description

The method to generate CTF coefficients presented in this section is adapted from Seem (1987). The principle is to obtain a state-space (SS) representation of a slab and to convert that model into a transfer function representation.

Generating the CTF coefficients requires 5 steps:

- Selection of the number of nodes and their positioning.
- Construction of the SS model.
- Discretization of the SS model.
- Calculation of the CTF coefficients.
- Check of the generated CTF coefficients.

### 4.3.1 Selection of the number of nodes and their positioning

The first step consists in spatially discretizing each layer of the slab by nodes. The number of nodes is chosen according to layers characteristics, and more especially the Fourier number Fo which is

computed as shown in equation ( 4.4 ). This method is adapted from the one used in EnergyPlus (EnergyPlus, 2014).

$$\mathrm{Fo} = \frac{\alpha\, \Delta t_b}{L^2} \qquad (4.4)$$

Where the thermal diffusivity $\alpha$ is defined as:

$$\alpha = \frac{k}{\rho\, C_p} \qquad (4.5)$$

The principle is now to define an optimal spacing between the nodes, named $\Delta x$ (equation ( 4.6 )). A high Fourier number will give more accuracy (more nodes) but a higher computational time. A value of 200 was selected after initial testing.

$$\Delta x = \sqrt{\frac{\alpha\, \Delta t_b}{\mathrm{Fo}}} \quad (where\ \mathrm{Fo} = 200) \qquad (4.6)$$

With the value of $\Delta x$, it is possible to define the number of nodes by dividing the layer thickness by $\Delta x$. Then the largest following integer is chosen.

A maximum number of nodes for a slab was also defined to avoid excessively long calculation times. The limit was fixed at 400 (calculation time per slab of approximately 4 seconds). In the current implementation, if the number of nodes reaches that value, an error message prompts the user to adapt (increase) the timebase.

Nodes are distributed equally, with half-nodes located at each interface between layers. The surface nodes do not take into account inside and outside convection coefficients, which are handled separately.

### 4.3.2 Construction of the SS model

An SS model of a linear time-invariant (LTI) system with $n$ nodes, 2 inputs ($T_{si}$ and $T_{so}$) and 2 outputs ($\dot{q}_{si}$and $\dot{q}_{so}$) can be expressed as following (Myers, 1971):

$$\frac{d\begin{bmatrix} T_1 \\ \dots \\ T_n \end{bmatrix}}{dt} = [A]\begin{bmatrix} T_1 \\ \dots \\ T_n \end{bmatrix} + [B]\begin{bmatrix} T_{si} \\ T_{so} \end{bmatrix} \quad (4.7)$$

$$\begin{bmatrix} \dot{q}_{si} \\ \dot{q}_{so} \end{bmatrix} = [C]\begin{bmatrix} T_1 \\ \dots \\ T_n \end{bmatrix} + [D]\begin{bmatrix} T_{si} \\ T_{so} \end{bmatrix} \quad (4.8)$$

The variables $T_i \dots T_n$ are the temperatures at each node and are known as the state variables. *A*, *B*, *C* and *D* are constant coefficients matrices with a size of respectively (*n*,*n*), (*n*,2), (2,*n*) and (2,2). These matrices characterize the system and can be determined if the nodes properties are known.

Equations ( 4.7 ) and ( 4.8 ) can be rewritten as equations ( 4.9 ) and ( 4.10 ), where $U_l$ and $U_r$ are respectively the heat transfer coefficients to the left and the right of the node *i*.

$$C_i \frac{dT_i}{dt} = U_l(T_{i-1} - T_i) + U_r(T_{i+1} - T_i) \quad (4.9)$$

$$\dot{q}_s = U(T_s - T_i) \quad (4.10)$$

### 4.3.3 Discretization of the SS model

The third step is the discretization of the SS model. It means that we have to discretize the matrices *A*, *B*, *C* and *D* with relation to time (the discretization time-step is the timebase). The discretization method used is the First-Order Hold method which assumes a linear interpolation between the discretized data, to be consistent with TRNSYS conventions to pass average values over the time-steps between components.

First, a new matrix *M* is built, including matrices *A* and *B*. It also includes an identity matrix *I* with the size (2,2) which is divided by the timebase. The matrix *M* can be presented as follows:

$$M = \begin{bmatrix} A(nx,nx) & B(nx,nu) & zeros(nx,nu) \\ zeros(nu,nx) & zeros(nu,nu) & \frac{I(nu)}{\Delta t_b} \\ zeros(nu,nx) & zeros(nu,nu) & zeros(nu,nu) \end{bmatrix} \quad (4.11)$$

We can now compute the matrix exponential of *M*, which is named *Φ*:

$$\Phi = e^{M\Delta t_b} \quad (4.12)$$

Numerous methods exist to compute a matrix exponential (see e.g. Moler and Van Loan (2003) for a comparative review of 19 methods). The Padé approximation method implemented in "DGPADM" routine (Sidje, 1998) was selected.

$\Phi$ allows defining 2 intermediate matrices (*F1* and *F2*) and the discretized matrix $A_d$:

$$F1 = \Phi(1{:}nx, nx+1{:}nx+nu) \quad (4.13)$$

$$F2 = \Phi(1{:}nx, nx+nu+1{:}nx+2\,nu) \quad (4.14)$$

$$A_d = \Phi(1{:}nx, 1{:}nx) \quad (4.15)$$

*F1*, *F2* and $A_d$ then give the discretized matrices $B_d$, $C_d$ and $D_d$:

$$B_d = F1 + A_d\,F2 - F2 \quad (4.16)$$

$$C_d = C \quad (4.17)$$

$$D_d = D + C_d\,F2 \quad (4.18)$$

### 4.3.4 Calculation of the CTF coefficients

CTF coefficients are computed from the discretized matrices. This step consists in the conversion of the SS model in a transfer function representation. The computation process is for example documented in the Matlab documentation (The MathWorks Inc., 2010).

First, the *d* coefficients are calculated using the eigenvalues of the matrix $A_d$. In FORTRAN, the eigenvalues of a matrix are computed with a routine named "DGEEVX" which is included in the LAPACK package (2011).

The 3 other coefficients (*a*, *b* and *c*) are then computed from the *d* coefficients and several sets of eigenvalues calculated for different matrices involving the matrices $A_d$, $B_d$, $C_d$ and $D_d$.

The *d* coefficients are dimensionless but *a*, *b* and *c* express the ratio between heat transfer rate and a temperature so care must be taken to comply with the non-standard TRNSYS units (kJ/h-K).

### 4.3.5 Check of the generated CTF coefficients

The validity of the computed CTF coefficients is checked using Equation ( 4.3 ): the calculated U-values must be within 0.001% of the "actual" value (i.e. computed from the layers description).

## 4.4 Example

This section illustrates the CTF coefficients generation by a simple example of a slab with 3 nodes. The example (Figure 4-1) is a concrete slab with a thickness $L$ of 0.3 m, a density $\rho$ of 2200 kg/m³, a specific heat $C_p$ of 0.84 kJ/kg-K and a thermal conductivity $k$ of 1.7 W/m-K. The inside and outside film coefficients $h_i$ and $h_o$ have a value of respectively 8.3 and 34.5 W/m²-K (in TRNSYS, these coefficients would be handled in a different part of the program and would not be included in the CTF coefficients).

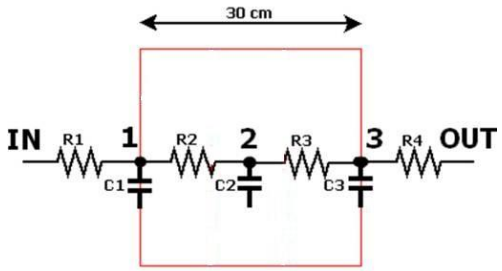


Figure 4-1: Scheme of a three-node example

Once the nodes are defined, the *A*, *B*, *C* and *D* matrices of the SS model can be calculated. The thermal capacity and resistance (or U-value) for each node are presented in equations ( 4.19 ) to ( 4.24 ):

$$C_w = \rho\, C_p\, L = 2200 \times 840 \times 0.3 = 554400 \frac{J}{m^2 K} \qquad (4.19)$$

$$C1 = C3 = \frac{554400}{4} = 138600\ \frac{J}{m^2 K} \qquad (4.20)$$

$$C2 = \frac{554400}{2} = 277200 \frac{J}{m^2 K} \qquad (4.21)$$

$$U1 = \frac{1}{R1} = h_i = 8.3 \frac{W}{m^2 K} \qquad (4.22)$$

$$U2 = U3 = \frac{1}{R2} = \frac{k}{\frac{L}{2}} = \frac{1.7}{0.15} = 11.33\frac{W}{m^2K} \quad (4.23)$$

$$U4 = \frac{1}{R4} = h_o = 34.5\frac{W}{m^2K} \quad (4.24)$$

Differential equations similar to equation ( 4.9 ) can then be written for each node:

$$\frac{dT_1}{dt} = \frac{U1}{C1}(T_i - T_1) + \frac{U2}{C1}(T_2 - T_1) = \frac{8.3}{138600}(T_i - T_1) + \frac{11.33}{138600}(T_2 - T_1) \quad (4.25)$$

$$\frac{dT_2}{dt} = \frac{U2}{C2}(T_1 - T_2) + \frac{U3}{C2}(T_3 - T_2) = \frac{11.33}{277200}(T_1 - T_2) + \frac{11.33}{277200}(T_3 - T_2) \quad (4.26)$$

$$\frac{dT_3}{dt} = \frac{U3}{C3}(T_2 - T_3) + \frac{U4}{C3}(T_o - T_3) = \frac{11.33}{138600}(T_2 - T_3) + \frac{34.5}{138600}(T_o - T_3) \quad (4.27)$$

Equations ( 4.25 ) to ( 4.27 ) can be written in a matrix form, where the 3-by-3 matrix is *A* and the 3-by-2 matrix is *B* in the SS model:

$$\frac{d}{dt}\begin{bmatrix} T_1 \\ T_2 \\ T_3 \end{bmatrix} = \begin{bmatrix} -\frac{19.63}{138600} & \frac{11.33}{138600} & 0 \\ \frac{11.33}{277200} & -\frac{22.66}{277200} & \frac{11.33}{277200} \\ 0 & \frac{11.33}{138600} & -\frac{45.83}{138600} \end{bmatrix}\begin{bmatrix} T_1 \\ T_2 \\ T_3 \end{bmatrix} + \begin{bmatrix} \frac{8.3}{138600} & 0 \\ 0 & 0 \\ 0 & \frac{34.5}{138600} \end{bmatrix}\begin{bmatrix} T_i \\ T_o \end{bmatrix} \quad (4.28)$$

Heat flows are computed from the first and last nodes and boundary conditions:

$$\dot{q}_{si} = h_i(T_i - T_1) = 8.3\,(T_i - T_1) \quad (4.29)$$

$$\dot{q}_{so} = h_o(T_o - T_3) = 34.5\,(T_o - T_3) \quad (4.30)$$

Or, in a matrix form:

$$\begin{bmatrix}\dot{q}_{si}\\ \dot{q}_{so}\end{bmatrix} = \begin{bmatrix}-8.3 & 0 & 0\\ 0 & 0 & -34.5\end{bmatrix}\begin{bmatrix}T_1\\ T_2\\ T_3\end{bmatrix} + \begin{bmatrix}8.3 & 0\\ 0 & 34.5\end{bmatrix}\begin{bmatrix}T_i\\ T_o\end{bmatrix} \quad (4.31)$$

The 2-by-3 and 2-by-2 matrices in equation ( 4.31 ) are respectively *C* and *D* in the SS model.

The four matrices are discretized for a time-step of 1 hour (3600 seconds):

$$A_d = \begin{bmatrix}0.6147 & 0.1999 & 0.01142\\ 0.09994 & 0.7725 & 0.07353\\ 0.01142 & 0.1471 & 0.3133\end{bmatrix} \quad (4.32)$$

$$B_d = \begin{bmatrix}0.1355 & 0.01029\\ 0.02049 & 0.06137\\ 0.002475 & 0.3142\end{bmatrix} \quad (4.33)$$

$$C_d = \begin{bmatrix}-8.3 & 0 & 0\\ 0 & 0 & -34.5\end{bmatrix} \quad (4.34)$$

$$D_d = \begin{bmatrix}7.537 & -0.009171\\ -0.009171 & 23.68\end{bmatrix} \quad (4.35)$$

The CTF coefficients are calculated from the discretized matrices as explained previously. Table 4-1 shows the results:

Table 4-1: Values of the CTF coefficients

| | **a** | **b** | **c** | **d** |
|---|---|---|---|---|
| 1 | 85.2408 | 0.033 | 27.1343 | 1.0000 |
| 2 | -183.9657 | 0.2512 | -50.1883 | -1.7004 |
| 3 | 127.8714 | 0.169 | 28.1085 | 0.8785 |
| 4 | -28.6833 | 0.01 | -4.5913 | -0.1361 |
| Sum | 0.4632 | 0.4632 | 0.4632 | 0.042 |
| U-value [kJ/h-m²-K] | 11.0286 | 11.0286 | 11.0286 | / |

The actual U-value (including the film coefficients) of the concrete slab is 11.045 kJ/h-m²-K while the U-value calculated with the coefficients is 11.029 kJ/h-m²-K. The observed error is 0.15 % which is greater than the limit of 0.001 %. So the coefficients should be considered as non-reliable.

This result is normal because the number of nodes (3) is not sufficient for that type of heavy wall. Equation ( 4.6 ) would require 74 nodes for this concrete slab.

## 4.5 Implementation in TRNSYS

The developed SS method has been implemented in a development version of TRNSYS 17.

CTF coefficients used in the multizone building model (Type 56) are generated by routines called by TRNBuild, the building preprocessor. They are implemented in a DLL called GenTRN, which is coded in FORTRAN. Several subroutines are included in this program. Figure 4-2 below presents a general scheme of the GenTRN new structure when the SS method is implemented as an alternative to the current method.

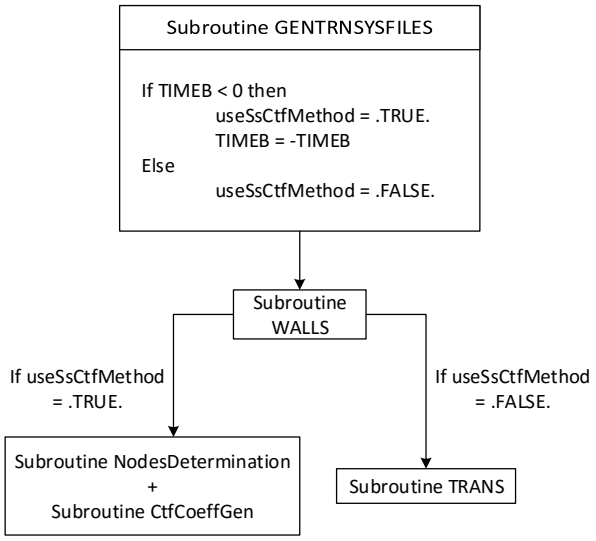


Figure 4-2: Scheme of the implementation of the SS method in TRNSYS

The subroutine “GENTRNSYSFILES” is the main entry point into the DLL, which is called by TRNBuild and calls all the other subroutines in the DLL. The main routine receives all the building description data from TRNBuild (walls, layers,…). In the current test version, the user selects the new CTF coefficients generation method by specifying a negative timebase value. This choice is caught by the main routine and passed to the WALLS subroutine which calls the appropriate CTF coefficients generation routine according to the user choice.

## 4.6 Wall tests in TRNSYS

Extensive tests were performed to debug and quality-check the new CTF coefficients generation method. This paper reports on 2 wall types: an insulated concrete form (ICF) wall and a plain wooden wall. The characteristics of each slab are presented in the following table (from inside to outside).

Table 4-2: Description of the presented walls

| Slabs | L [m] | k [W/(m-K)] | ρ [kg/m³] | $C_p$ [kJ/(kg-K)] | R [m²-K/W] |
|---|---|---|---|---|---|
| **ICF** | Wall-only U-value: 0.188 W/(m²-K) | | | | |
| G01 - Gypsum board | 0.016 | 0.16 | 800 | 1.09 | 0.100 |
| I03 - EPS (expanded polystyrene) board | 0.076 | 0.03 | 43 | 1.21 | 2.533 |
| M15 - Heavyweight concrete | 0.203 | 1.95 | 2240 | 0.9 | 0.104 |
| I03 - EPS board | 0.076 | 0.03 | 43 | 1.21 | 2.533 |
| F07 - Stucco | 0.025 | 0.72 | 1856 | 0.84 | 0.035 |
| **Wood wall** | Wall-only U-value: 0.260 W/(m²-K) | | | | |
| Wood | 0.500 | 0.130 | 600 | 1.88 | 3.846 |

The plain 50-cm wooden wall is an extreme case that illustrated the limits of the CTF method (as currently implemented and with the new coefficients generation method).

The scenario that we have tested is the one presented in the Figure 4-3. It represents a typical set-back scenario.

The outside temperature is kept constant at 0°C. No radiative heat flows are considered. The heating system power is initially set to maintain a steady-state indoor temperature of 20°C. The heating system is then stopped for 4 hours, and restarted with a heating power equal to 1.5 times the initial value.

The simulation time-step is one minute and the inside and outside convection coefficients have a value of 8.3 and 34.5 W/m²-K, respectively.

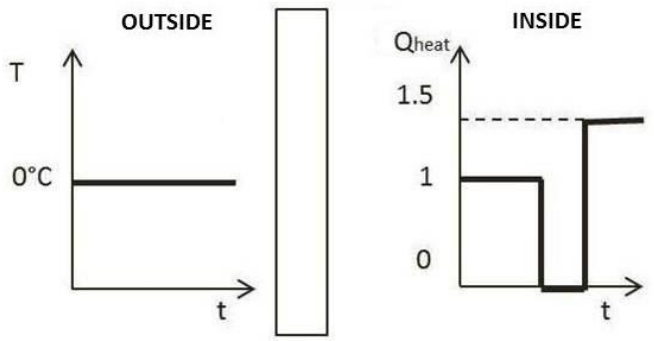


Figure 4-3: Description of the presented scenario

In the following four graphs, three kind of results are presented: firstly, in dotted lines, the results coming from the current version of TRNSYS; secondly, in dashed lines, the results performed by using the SS method for generating the CTF coefficients; thirdly, in solid lines, a reference solution implemented in Matlab (The MathWorks Inc., 2010) by simulating a discretized wall model with a large number of nodes. All graphs present the evolution of the inside surface temperature according to time.

The first two graphs (Figure 4-4 and Figure 4-5) concern the ICF wall (Figure 4-5 is a zoom into Figure 4-4 to highlight the differences between the curves). The results show that the original and modified versions of TRNSYS match the reference solution at the end of each timebase but the presence of a stair-step effect is influenced by that timebase. The minimum timebase value that can be reached with the new method is 12 minutes, while it was 1 hour with the DRF method.

The next two graphs are about the plain wooden wall with a thickness of 0.5 m, the second one being a zoom where the minimum temperature is reached. This wall is not typical from walls encountered in real buildings but it allows highlighting problems with the CTF method. These problems appear clearly in the graphs. The results generated by the current and modified versions of TRNSYS are affected by a stair-step effect. That effect is more pronounced for the current TRNSYS version (minimum timebase value = 3 hours, vs. 1 hour for the new method). During the temperature drop, the modified version behaves better while it is the opposite during the temperature increase. It is not clear at this stage why the new CTF coefficient generation shows an offset in addition to the stair-step effect. This will be investigated in the future.

Figure 4-7 shows that both curves present a negative peak that is not present in the reference solution. Again, future work will aim at clarifying why the response of the wooden wall is incorrect.

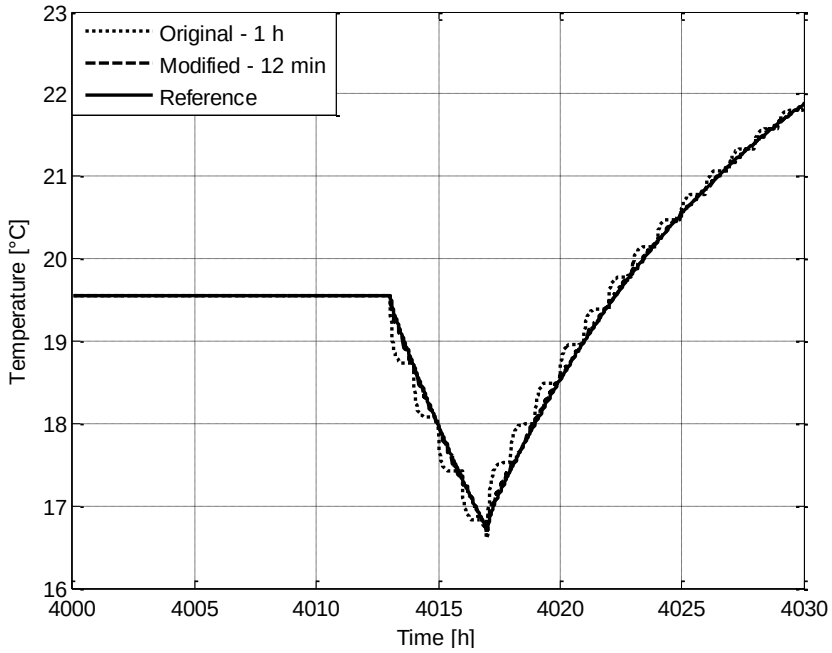


Figure 4-4: Evolution of the inside surface temperature for an ICF wall

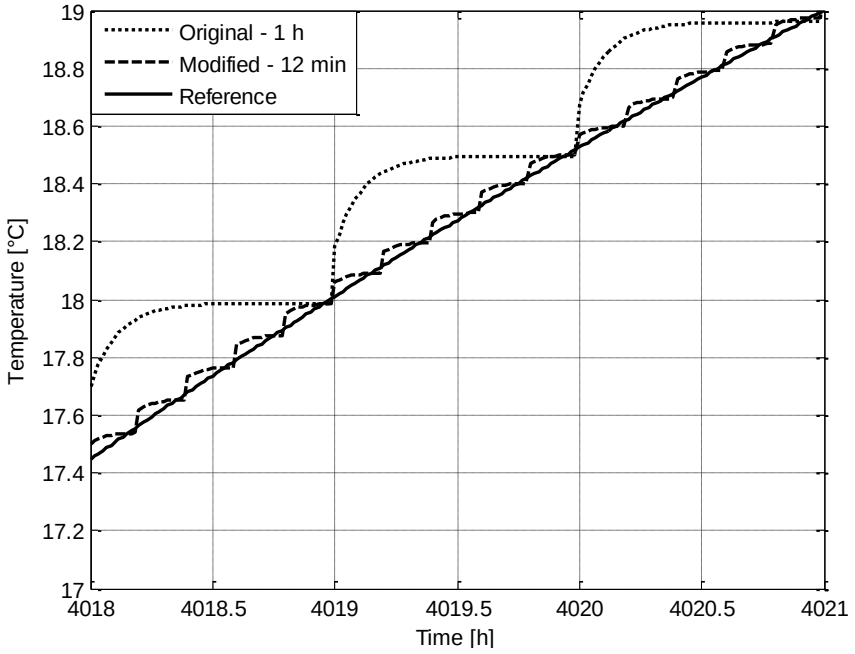


Figure 4-5: Evolution of the inside surface temperature for an ICF wall (zoom)

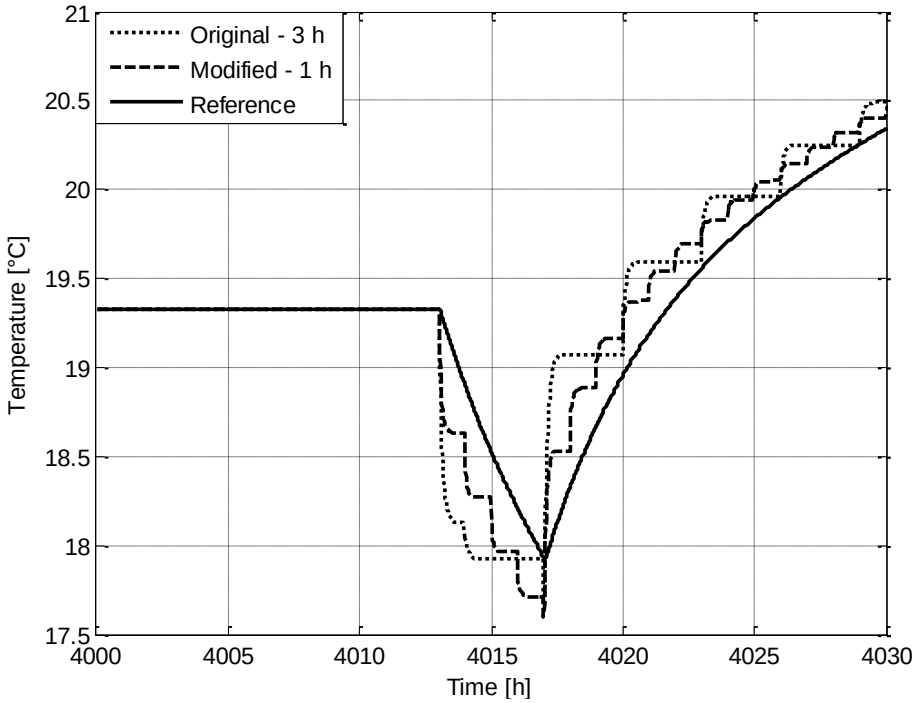


Figure 4-6: Evolution of the inside surface temperature for a wooden wall

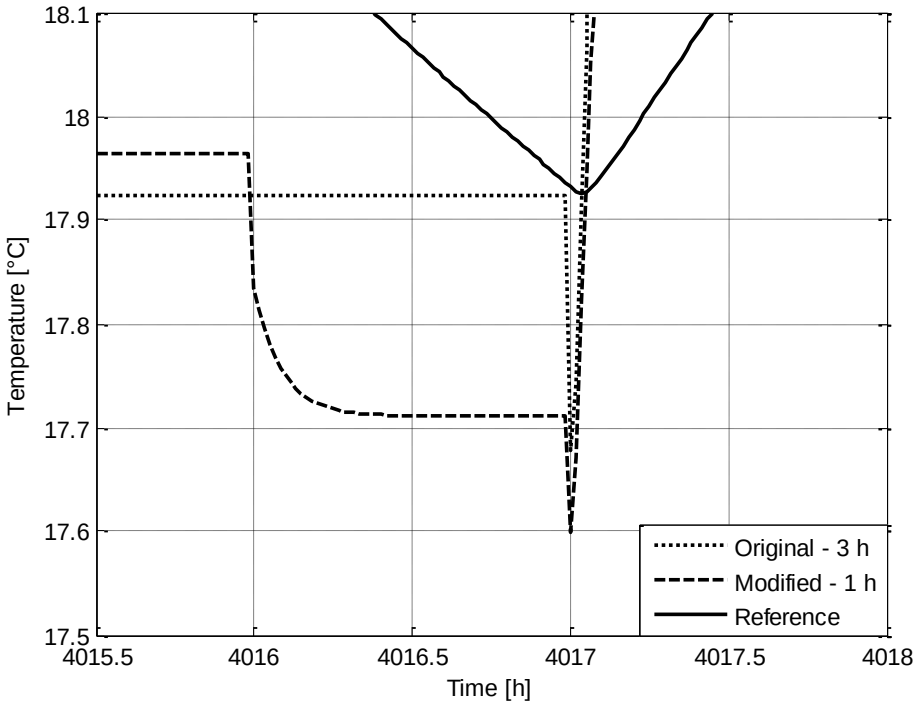


Figure 4-7: Evolution of the inside surface temperature for a wooden wall (zoom)

CTF coefficients are generated once per simulation, in the building pre-processing stage. Computational time is imperceptible with the current method. The SS method takes much longer,

and the computational time depends on the number of nodes for each wall and the timebase. Table 4-3 sums up the results obtained for various tests on 6 wall types. The ICF and wooden slabs were described above. The 4 others are a double stud wall with brick veneer (DST), a structural insulated panel (SIPS), a concrete slab (0.5 m thick) and an insulation slab (0.5 m thick) .

Table 4-3: Comparison of the minimum timebase value and the calculation time between the DRF and SS methods

| | Original timebase (DRF method) | New timebase (SS method) | Number of nodes (SS method) | Calculation time (SS method) |
|---|---|---|---|---|
| | [h] | [h] | [-] | [s] |
| ICF | 1 | 0.2 | 255 | 2 |
| DST | 0.25 | 0.1 | 323 | 3.4 |
| SIPS | 0.15 | 0.05 | 350 | 3.7 |
| Concrete | 0.25 | 0.2 | 268 | 2.2 |
| Insulation | 0.5 | 0.1 | 333 | 3.4 |
| Wood | 3 | 1 | 347 | 3.5 |

The table shows that the SS method allows decreasing the timebase values (three times in average). This improvement decreases the inaccuracies related to the stair-step effect. The maximum cost of this improvement in terms of calculation time per slab is 4 seconds (once per simulation).

## 4.7 Full building test in TRNSYS

In this section, results coming from the original and modified versions of TRNSYS on a complete house model are presented.

The test was realized in the context of a renovation project, called Zero Energy House Renovation and located in Oud-Heverlee, Belgium (Peeters & Mols, 2012). The building (Figure 4-8) is an old house built in 1931 and composed of 3 floors (basement, ground floor and 1$^{st}$ floor). The project consists in renovating this house by trying to make it a smart nearly zero energy building. This example is typical of cases encountered by TRNSYS users where the limitations in the current CTF method become apparent, and sometimes make it difficult to obtain meaningful results for short-term analyses (e.g. regarding demand-side management strategies or transients in heating / cooling system controls).

Figure 4-8: Picture of the house in project ZEHR (Zero Energy House Renovation) (Peeters & Mols, 2012)

The presented results focus on the evolution of the operative temperature in the kitchen, as shown in Figure 4-9.

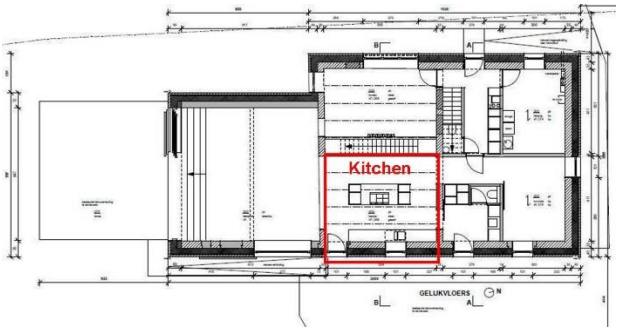


Figure 4-9: Plan of the house's ground floor (Peeters & Mols, 2012)

Table 4 below describes the external wall of the kitchen, which is a highly insulated (U = 0.115 W/m²-K) and heavy slab.

Table 4-4: Description of the external wall in the kitchen (Peeters & Mols, 2012)

| | L [m] | k [W/m-K] | ρ [kg/m³] | $C_p$ [kJ/kg-K] | R [m²-K/W] |
|---|---|---|---|---|---|
| Cavity | / | / | / | / | 0.140 |
| Foamglass | 0.300 | 0.038 | 130 | 0.840 | 7.895 |
| Brick | 0.330 | 0.500 | 1500 | 0.840 | 0.660 |
| Plaster | 0.010 | 0.700 | 1400 | 0.840 | 0.014 |

The setback scenario presented above is extended to this case. The outside temperature is fixed at 0°C. There are no solar gains. The only room to be heated is the kitchen (convective heater). The heating system stops during 4 hours before a restart with more power (1.5 times the initial power).

The simulation has been carried out twice: firstly, with the original version of TRNSYS (DRF method – Timebase = 5 hours, the minimum achievable) and secondly, with the modified version of TRNSYS (SS method – Timebase = 1.5 hours, the minimum achievable).

Figure 4-10 below shows the evolution of the operative temperature in the kitchen according to time. The results present a clear difference between the 2 methods (DRF and SS) for generating the CTF coefficients. The SS method allows reducing the stair-step effect, as shown in the single-wall examples. The observed maximum and mean temperature differences between the 2 methods are respectively 0.49 and 0.16 °C.

Another important parameter to take into account is the impact of the method on the computational time during the simulation (and not during the CTF coefficients generation). For a 168-day simulation with a time-step of 1 minute, the computational times for the original and modified versions of TRNSYS are respectively 21 and 23 minutes.

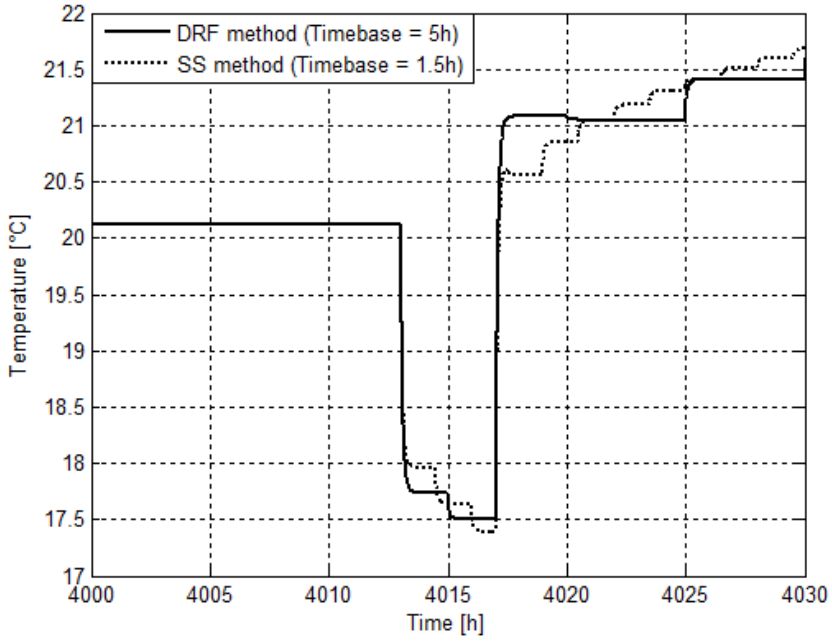


Figure 4-10: Evolution of the operative temperature in the kitchen [corrected after publication]

## 4.8 Discussion and conclusions

This paper describes the implementation of a new CTF coefficients generation method in TRNSYS. The method was successfully implemented in a development version of the TRNSYS building pre-processor (TRNBuild). This work is intended to respond to problems faced by TRNSYS users who

simulate heavy, highly insulated walls and want to perform short term analyses to study demand-side management strategies or transients in heating and cooling system controls.

The proposed method alleviates the stair-step effect that occurs in these circumstances, allowing to reduce the minimum timebase by a factor of 3 in average. It provides very satisfactory results in some cases for time-steps down to the order of one minute. Some walls present more difficulties such as the extreme 50-cm thick plain wooden slab selected for our test. In these cases, the new method delivers some improvements regarding the stair-step effects but does not compare favorably with a reference solution. Further work will aim at better understanding the limitations of the CTF method while the new method is released to more TRNSYS users.

The impact on computational time to generate the CTF coefficients is significant, but this operation only takes place once per simulation and the cost amounts to a few seconds per wall type. The impact on simulation time in a realistic case is acceptable (10% increase).

# Nomenclature

| | |
|---|---|
| *A, B, C and D* | State-space matrices |
| *a, b, c and d* | CTF coefficients |
| *C* | Thermal capacity [J/m²-K] |
| $C_p$ | Specific heat [J/kg-K] |
| Fo | Fourier number |
| *h* | Convection coefficient [W/m²-K] |
| *k* | Thermal conductivity [W/m-K] |
| *L* | Thickness [m] |
| *n* | Number of coefficients or nodes |
| *nx* | Nodes number |
| *nu* | Inputs number (= 2) |
| $\dot{q}$ | Heat flow [W or kJ/h] |
| *R* | Thermal resistance [m²-K/W] |

| | |
|---|---|
| $T$ | Temperature [°C or K] |
| $t$ | Time [s] |
| $U$ | Heat transfer coefficient [W/m²-K] |
| $x$ | Position [m] |
| $\Delta t_b$ | Timebase [s] |

*Greek symbols*

| | |
|---|---|
| $\alpha$ | Thermal diffusivity [m²/s] |
| $\Delta$ | Difference |
| $\rho$ | Density [kg/m³] |

*Subscript*

| | |
|---|---|
| $d$ | Discretized |
| $i$ | Inside or i-node |
| $k$ | Number of CTF coefficient |
| $l$ | Left |
| $o$ | Outside |
| $r$ | Right |
| $s$ | Surface |
| $w$ | Wall |

# Acknowledgements

The research work presented in this paper is financially supported by a grant of Hydro-Québec, FRQNT (Fonds de Recherche du Québec de Recherche en Nature et Technologies) and NSERC (Natural Sciences and Engineering Research Council of Canada). Moreover the presentation of the full building test in this paper has been possible thanks to the cooperation of Leen Peeters who works on the “Zero Energy House Renovation” project.

# References

Delcroix, B., Kummert, M., Daoud, A., & Hiller, M. (2012). Conduction transfer functions in TRNSYS multizone building model: current implementation, limitations and possible improvements. SimBuild (p. 8). Madison, Wisconsin.

Energy Systems Research Unit. (1998). ESP-r User Guide: The ESP-r System for Building Energy Simulation. Glasgow.

EnergyPlus Documentation. (2012). Engineering Reference (p. 1247).

LAPACK. (2011). DGEEVX: computation of the eigenvalues of a general matrix. Retrieved from http://www.netlib.org/lapack/individualroutines.html

Li, X. Q., Chen, Y., Spitler, J. D., & Fisher, D. (2009). Applicability of calculation methods for conduction transfer function of building constructions. International Journal of Thermal Sciences, 48(7), 1441–1451. doi:10.1016/j.ijthermalsci.2008.11.006

Mitalas, G. P., & Arseneault, J. G. (1972). Fortran IV program to calculate z-transfer functions for the calculation of transient heat transfer through walls and roofs. Division of Building research, National Research Council Canada. Retrieved from http://nparc.cisti-icist.nrc-cnrc.gc.ca/npsi/ctrl?action=shwart&index=an&req=5752842

Moler, C., & Van Loan, C. (2003). Nineteen Dubious Ways to Compute the Exponential of a Matrix, Twenty-Five Years Later. SIAM Review, 45(1), 3–49.

Myers, G. E. (1971). Analytical methods in conduction heat transfer (McGraw-Hil.). New-York.

Peeters, L., & Mols, R. (2012). Zero Energy House Renovation. Retrieved February 8, 2013, from http://www.zehr.be

Seem, J. E. (1987). Modeling of heat transfer in buildings. University of Wisconsin, Madison.

Sidje, R. B. (1998). Expokit: a software package for computing matrix exponentials. ACM Transactions on Mathematical Software, 24(1), 130–156.

Stephenson, D. G., & Mitalas, G. P. (1971). Calculation of heat conduction transfer functions for multi-layer slabs. ASHRAE Transactions, 77(2), 117–126. Retrieved from http://nparc.cisti-icist.nrc-cnrc.gc.ca/npsi/ctrl?action=shwart&index=an&req=5757086&lang=en

The MathWorks Inc. (2010). Matlab help. Natick, MA, USA.

TRANSSOLAR Energietechnik Gmbh. (2011). TRNSYS 17 - Multizone building modeling with Type 56 and TRNBuild (p. 258). Stuttgart.

# CHAPTER 5 ADDITIONAL COMMENTS ON ARTICLE 1

This chapter presents additional details about the conditions in which the CTF method yields accurate results. These conditions are compared to the stability conditions for finite-difference methods, to illustrate the complementarity between the two approaches.

In TRNSYS, the validity of the CTF method is assessed by a simple condition: the sum of each coefficients set (*a*, *b* and *c*) must be higher than or equal to 0.0005 such as:

$$\sum_{k=0}^{n_a} a_{t-k\Delta t_b} \geq 0.0005 \; ; \; \sum_{k=0}^{n_b} b_{t-k\Delta t_b} \geq 0.0005 \; ; \; \sum_{k=0}^{n_c} c_{t-k\Delta t_b} \geq 0.0005 \qquad (5.1)$$

If this condition is not met, the CTF coefficients are not generated and an error window (see Figure 5-1) prompts the user to adapt the timebase value. As shown in Chapter 4, these three sums must have the same value.

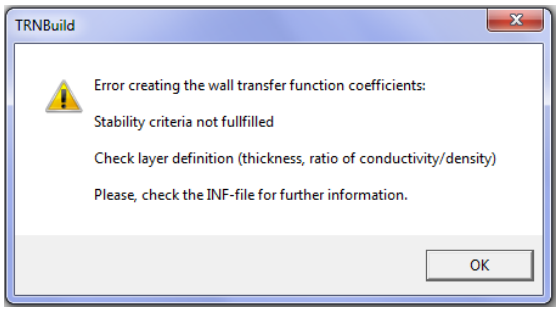


Figure 5-1: Error window when TRNBuild fails to generate transfer function coefficients

The sum of each coefficients set is directly proportional to the Fourier number. For example, Table 5-1 presents the evolution of the sum of a set of CTF coefficients and the Fourier number as a function of the timebase for a wall case presented in section 4.6, i.e. the plain wooden wall.

Table 5-1: Evolution of the sum of a set of CTF coefficients and the Fourier number as a function of the timebase for the plain wooden wall

| Timebase [h] | Sum of a set of CTF coefficients | Fourier number |
|---|---|---|
| 3 | 0.0008 | 0.0050 |
| 4 | 0.0028 | 0.0066 |
| 5 | 0.0064 | 0.0083 |

This condition avoids therefore generating CTF coefficients as soon as the wall becomes too insulated and / or thermally heavy, i.e. a wall with a low Fourier number. Maestre et al. (2014)

propose a solution, which consists in subdividing a wall into thinner parts. A set of CTF coefficients is then generated for each subdivision. Unfortunately, this solution introduces further iterative computations and possible convergence issues, which must be considered.

On the other hand, BPS tools using finite-difference methods to model transient conduction through walls are not affected by these problems. With these methods, lower Fourier numbers lead to more stable solutions. In the case of an explicit method, the stability condition requires that the Fourier number should be lower than 0.5. An implicit scheme is moreover assumed to be unconditionally stable. However, the opposite problem can occur with finite-difference methods, since high Fourier numbers (> 0.5) cause instable solutions. Even with an implicit method, a condition is generally required to guarantee accurate and stable results. For example, in EnergyPlus, when using the finite-difference method with a fully implicit scheme, an error occurs when a thin air layer is included in a wall (in a simulation with a 3-minute time-step):

> ** Severe ** InitialInitHeatBalFiniteDiff: Found Material that is too thin and/or too highly conductive, material name = AIR
>
> ** ~~~ ** High conductivity Material layers are not well supported by Conduction Finite Difference, material conductivity = 2.600E-002 [W/m-K]
>
> ** ~~~ ** Material thermal diffusivity = 2.158E-005 [m2/s]
>
> ** ~~~ ** Material with this thermal diffusivity should have thickness > 0.10795 [m]

In summary, finite-difference methods are well adapted to low Fourier numbers, while the CTF method is well adapted to high Fourier numbers. Figure 5-2 illustrates this fact. The limit of use of the CTF method is around a Fourier number of 0.005 (the value calculated for the wooden wall with a timebase of 3 hours). That limit is not defined precisely as it depends on the method used to generate CTF coefficients and on the walls properties. On the other hand, the limit of 0.5 for the finite-difference method corresponds to the stability condition of the explicit method for 1-D model.

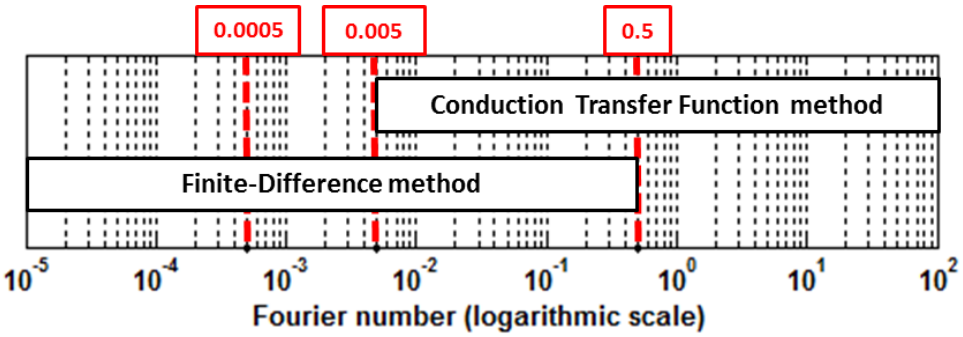


Figure 5-2: Complementarity of the CTF method and the finite-difference methods

Figure 5-2 also highlights the complementarity of both methods. This complementarity can be exploited in TRNSYS, where an external type modeling a wall with a finite-difference method can be linked to two boundary walls modeled with the CTF method in Type 56 ("Multizone building model").

This method has been applied on the example presented in section 4.7 to show the merits of using an external type to model a highly resistive and heavy wall. Peeters and Mols (2012) presented a renovation project called "Zero Energy House Renovation" and located in Oud-Heverlee in Belgium. The building is an old house composed of 3 floors, including a basement. The renovation works required to add insulation to the existing building. In particular, the roof poses a challenge to the CTF method, and requires using a timebase greater than or equal to 5 hours for the simulation, because of its very low thermal diffusivity. Table 5-2 presents the composition of this wall from outside to inside.

Table 5-2: Composition of the roof of the studied case (from outside to inside)

| Material | Thickness [m] | Thermal conductivity [W/m-K] | Density [kg/m³] | Specific heat [kJ/kg-K] |
|---|---|---|---|---|
| Cellulosic insulation | 0.380 | 0.040 | 350 | 2.150 |
| Wood fiber panel (Celit 4D) | 0.020 | 0.055 | 270 | 2.068 |
| Plaster | 0.010 | 0.700 | 1400 | 0.840 |

The test case to evaluate the efficiency of the proposed method is illustrated in Figure 5-3. The inside temperature is kept constant at 20 °C and the outside temperature changes by steps.

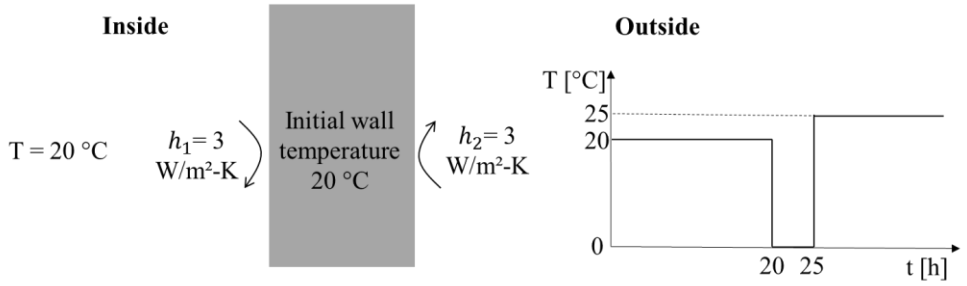


Figure 5-3: Test case with temperature step-changes

Two simulation configurations are tested. For all simulations, a time-step of 6 minutes is used. First, the entire wall is modeled in Type 56 using the CTF method with a timebase of 5 hours (which is the minimum achievable). Secondly, a small part of the wall (1 cm of cellulosic insulation and the 1-cm plaster layer) is modeled using the CTF method while the other part (37 cm of cellulosic insulation and the wood fiber panel) is modeled in an external type using a finite-difference method. The last configuration allows using a timebase of 6 minutes, i.e. equivalent to the simulation time-step.

Results are presented for the outside surface temperature in Figure 5-4. Discrepancies appears with the CTF method where the gap between the timebase (5 hours) and the time-step (6 minutes) causes a strong stair-step effect. Figure 5-4 (b) focuses on the corrections performed by the CTF method at the 30$^{th}$, 35$^{th}$ and 40$^{th}$ hours, i.e. every 5 hours. On the other hand, using an external type for modeling the wall with a finite-difference method allows producing correct results without stair-step effects.

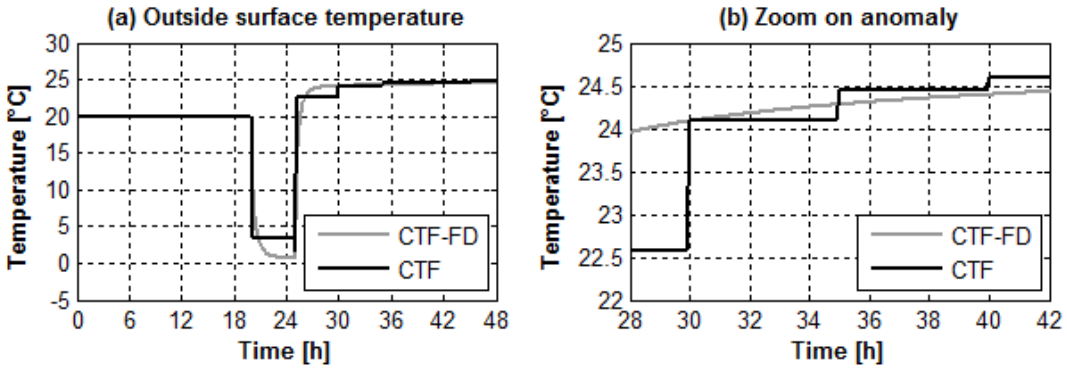


Figure 5-4: Results comparison between both configurations

# CHAPTER 6 ARTICLE 2: INFLUENCE OF EXPERIMENTAL CONDITIONS ON MEASURED THERMAL PROPERTIES USED TO MODEL PHASE CHANGE MATERIALS

Delcroix, B., Kummert, M., Daoud, A., Bouchard, J., (2015). Influence of experimental conditions on measured thermal properties used to model phase change materials. Building Simulation: An International Journal. doi:10.1007/s12273-015-0241-8

## Abstract

Modeling phase change materials (PCMs) thermal behavior requires solving a system of non-linear equations to account for temperature-dependent thermal capacity and thermal conductivity. These properties depend on the PCM temperature and state (solid, liquid or mushy). Most models rely on enthalpy-temperature or specific heat-temperature curves to consider the variable thermal capacity during heating and cooling processes. These curves are generally obtained through experimental methods such as a Differential Scanning Calorimetry (DSC) test or the T-history method. Significant differences can be observed between the results of these methods, due to different experimental conditions. In order to clarify the influence of experimental conditions, experimentations on a bio-based PCM are performed with varying heat transfer rates and different configurations (PCM samples and PCM-equipped walls). Enthalpy-temperature or specific heat-temperature curves are computed for each case using an inverse method. A comparison between the results obtained with different methods and different heat transfer rates shows significant differences. The phase change temperature range obtained with the inverse method applied to the PCM samples is larger than the range obtained with the DSC test. The tests on the PCM-equipped walls show that varying heat transfer rates have a significant impact on the phase change temperature range and the hysteresis between heating and cooling curves. Higher rates increase the hysteresis and shift the phase change temperature range towards colder temperatures. Given the observed differences between properties obtained from different experimental conditions, it is recommended to carefully select the method used to define PCM enthalpy-temperature curves, taking into account the modeling application (PCM configuration and expected heating / cooling rates).

**Keywords:** Phase change material (PCM); Latent heat storage capacity; Enthalpy-temperature curve; Differential Scanning Calorimetry (DSC); Inverse modeling method

# Nomenclature

| | |
|---|---|
| $A$ | Heat-exchange surface [m²] |
| Bi | Biot number [-] |
| $C$ | Capacitance [J/m²-K] |
| $C_p$ | Specific heat [J/g-K] |
| $h$ | Enthalpy [J/g] |
| $h_g$ | Global heat transfer coefficient [W/m²-K] |
| $k$ | Thermal conductivity [W/m-K] |
| $L_c$ | Characteristic length [m] |
| $m$ | Mass [g] |
| $R$ | Thermal resistance [m².K/W] |
| $r$ | Radius [m] |
| S | Surface |
| $T$ | Temperature [°C] |
| $t$ | Time [s] |
| $U$ | Heat transfer coefficient [W/m²-K] |
| $\Delta h$ | Enthalpy variation [J/g] |
| $\Delta x$ | Node interval [m] |
| $\rho$ | Density [kg/m³] |

*Subscripts*

| | |
|---|---|
| $c$ | Cooling |
| $exp$ | Experimental |

| | |
|---|---|
| $f$ | Final |
| $h$ | Heating |
| $i$ | Initial |
| $in$ | Center or inside |
| $l$ | Left or liquid |
| $n$ | Node |
| $out$ | Outside |
| $pcm$ | Phase change material |
| $r$ | Right |
| $s$ | Sample or solid |
| $si$ | Inside surface |
| $sim$ | Simulated |
| $so$ | Outside surface |
| $w$ | Water |

## 6.1 Introduction

Latent heat storage systems using Phase Change Materials (PCMs) are increasingly used and studied for building applications. PCMs offer a high energy storage capacity and a nearly isothermal phase change, which help reducing peaks in space heating and cooling loads and maintaining thermal comfort. Several authors have documented PCM properties and possible applications. Reviews presented by Zalba et al. (2003), Sharma et al. (2009) and Baetens et al. (2010) document PCM classifications and a wide range of PCMs with their most important properties. Zalba et al. (2003) provide a large overview of possible applications, while Sharma et al. (2009) and Baetens et al. (2010) focus on solar and building applications. Mehling and Cabeza (2008) also offer an in-depth description of the theoretical aspects and multiple applications related to PCM.

The effective heat capacity (Goodrich, 1978; Yao & Chait, 1993) and enthalpy (Voller & Cross, 1981) methods are often used to model the PCM non-linear thermal behavior in buildings. Building energy performance simulation programs such as ESP-r (Energy Systems Research Unit, 1998), EnergyPlus (Crawley et al., 2001) and TRNSYS (Klein et al., 2012) use these methods. The effective thermal capacity method is integrated into the ESP-r building model (Heim & Clarke, 2004), while the enthalpy method is implemented into EnergyPlus (Pedersen, 2007; Shrestha et al., 2011; Tabares-Velasco, Christensen, & Bianchi, 2012). Several component models (known as "Types") using both methods have been implemented in TRNSYS (Castell et al., 2009; A Dentel & Stephan, 2010; Ibánez et al., 2005; Kuznik et al., 2010; Poulad et al., 2011; Schranzhofer et al., 2006). Few models are able to represent specific PCM effects such as hysteresis and subcooling. Figure 6-1 illustrates these characteristics on schematic temperature-enthalpy curves. Hysteresis consists in a temperature difference between heating and cooling curves during phase change. Subcooling is experienced when a liquid is cooled down below its solidification temperature. This is followed by a nucleation process (Günther et al., 2007) coupled with a steep temperature increase, leading to solidification. Kuznik and Virgone (2009) and Günther et al. (2007) show respectively that hysteresis and subcooling can have a significant impact on PCM performance.

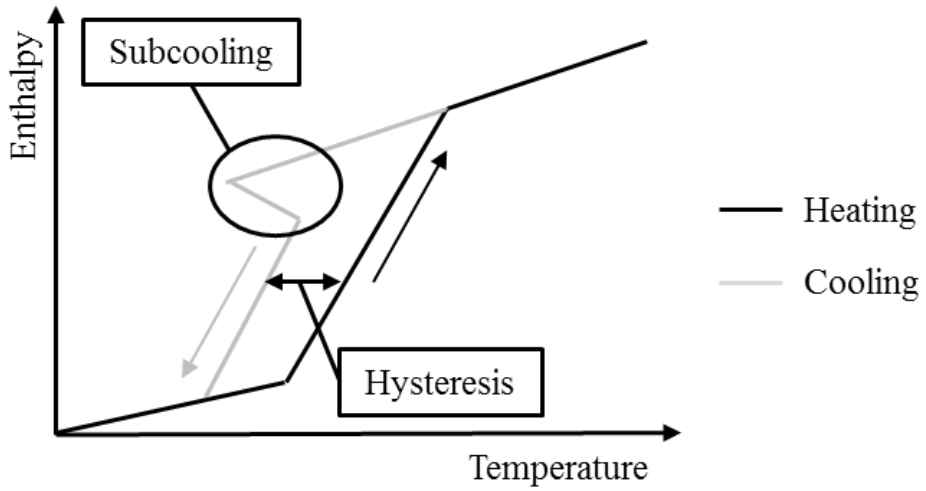


Figure 6-1: Schematic representation of the hysteresis and subcooling effects

Modeling PCM requires to obtain their thermo-physical properties, i.e. density, thermal conductivity and specific heat. The latter is the most important property since it exhibits strong variation with temperature ($C_p(T)$ curve). The enthalpy-temperature $h(T)$ curve is obtained by

integration of the $C_p(T)$ curve since the enthalpy variation $\Delta h$ between an initial and final temperatures $T_i$ and $T_f$ is formulated as follows:

$$\Delta h = \int_{T_i}^{T_f} C_p \, dT \qquad (6.1)$$

Several methods exist to obtain the PCM specific heat $C_p(T)$, including the Differential Scanning Calorimetry (DSC) test and the T-history method (German Institute for Quality Assurance and Certification, 2009; Günther, Hiebler, Mehling, & Redlich, 2009). Solé et al. (2013) present an extensive review of the T-history method. Both methods aim at obtaining the PCM specific heat $C_p(T)$ by applying high heating and cooling rates to small PCM samples, from a few milligrams for a DSC test to a few grams for the T-history method. These experimental conditions are not representative of the application in the building envelope. Günther et al. (2009) showed that test results vary depending on test methods and conditions. This is also highlighted by Kosny et al. (2010), who investigated a bio-based PCM provided in plastic pouches and compared results obtained from DSC tests with an alternative method based on a dynamic Heat Flow Meter Apparatus ("HFMA method"). This HFMA method is applied to a relatively large amount of PCM encapsulated in plastic pouches, i.e. in conditions closer to the actual use of the product in buildings. Their results show that the measured latent heat calculated with the HFMA method is around 30 % lower than the value obtained with the DSC test, potentially impacting on simulations results.

Inverse modeling methods were also used in the literature, at the building scale and to identify material properties. Braun and Chaturvedi (2002) used an inverse model in order to identify parameters of a state-space model for transient building load prediction. Coupling a 1-D finite-element model with an optimization algorithm (least squares method), Atchonouglo et al. (2008) identified the thermal conductivity and capacity of polymers. Huang and Jan-Yuan (1995) performed an inverse analysis to determine the temperature-dependent thermal conductivity and capacity of a material, using an optimization algorithm based on the conjugate gradient method. Cheng et al. (2013) also applied inverse modeling to obtain the temperature-dependent specific-heat of PCM-concrete brick. A 1-D finite-difference model was coupled with different optimization algorithms (based on sequential quadratic programming method, genetic algorithm or particle

swarm optimization algorithm) in order to determine the property of interest and the most effective algorithm. All algorithms generated the same optimized specific heat distribution with temperature but the sequential quadratic programming method led to the shortest computing time.

## 6.2 Objectives and methodology

The main objective of this paper is the evaluation and comparison of enthalpy-temperature $h(T)$ or specific heat-temperature $C_p(T)$ curves for the same PCM through different methods and test conditions presented in Table 6-1. Results with PCM samples are not directly comparable to those with the PCM-equipped wall since the layer containing the PCM is also composed of air and plastic film (see Figure 6-11). Properties of each component are then combined to yield the properties of an assumed equivalent layer. This step is necessary because most building energy performance simulation programs approximate the heat conduction through walls as 1-D.

An inverse modeling method is applied to each set of experimental data to obtain the $h(T)$ or $C_p(T)$ curves for both heating and cooling processes in each application. The $h(T)$ curves generated for the PCM-equipped walls and PCM samples are compared to the manufacturer DSC test. Results for the PCM-equipped walls are then used to observe the influence of varying heat transfer rate on the PCM thermal behavior during phase change.

Table 6-1: Summary of the experimental data

| Test method | PCM configuration | Heat transfer rate | Reference |
|---|---|---|---|
| DSC test | PCM sample of a few milligrams | 2 °C/min | Manufacturer (Phase change energy solutions, 2008) |
| Inverse method | PCM sample of around 10 grams | 0.8 °C/min | Experimental (dual-temperature chamber) |
| | PCM-equipped wall (1.465 kg PCM/m²) | 0.04 - 0.18 °C/min | Experimental (dual-temperature chamber) |
| | PCM-equipped wall (1.465 kg PCM/m²) | 0.01 - 0.03 °C/min | Experimental (full-scale test-cell) |

## 6.3 Paper organization

Section 6.4 presents the tested PCM and its encapsulation. The next main sections present the experimental results obtained on small PCM samples (section 6.5) and on PCM-equipped walls (section 6.6). Section 6.5 is organized in 3 main parts: experimental setup (section 6.5.1), inverse method used for the analysis (section 6.5.2), and results presentation and analysis (section 6.5.3). The tests performed on the PCM-equipped walls comprise heating/cooling step-changes applied to a 1 m² wall section in a dual-temperature chamber and a full-scale experimentation in a test-cell exposed to ambient conditions. The experimental setups for these two phases are respectively presented in sections 6.6.1.1 and 6.6.1.2. Section 6.6.2 discusses the inverse modeling method used to analyze the results obtained with the PCM-equipped wall. Section 6.6.3 then presents the results and their analysis. Section 6.7 presents our conclusions and recommendations.

## 6.4 Description of the PCM

The selected PCM for this study is a mixture of a bio-based PCM composed of soybean and palm oil. Two additives are also added to the mixture: a gelling agent and a fire retardant. It is commercially available as a plastic film with PCM pouches, as shown in Figure 6-2. The mass fractions of the additives are unknown. Table 6-2 presents the relevant properties obtained from the manufacturer and other references. Most properties are provided for the PCM without the additives. Only three properties (right side in Table 6-2) are provided for the complete product as commercially available. The density and thermal conductivity of the PCM with additives have been obtained through additional experiments. When implemented in the building envelope, the plastic film with PCM pouches is intended to be placed on the backside of wall boards as close as possible to the inside space.

Figure 6-2: Plastic film with PCM pouches

Table 6-2: PCM properties

| Without additives | | With additives | |
|---|---|---|---|
| Phase change temperature | 23 °C | Phase change temperature | 23 °C |
| Latent heat storage capacity | 203 J/g | Latent heat storage capacity | 165-200 J/g |
| Density | 830 kg/m³ | | |
| Specific heat (solid) | 1.84 J/g-K | Weight per unit surface | 1.465 kg/m² |
| Specific heat (liquid) | 1.99 J/g-K | Density | 883 kg/m³ * |
| Thermal conductivity (solid) | 0.207 W/m-K | Thermal conductivity (solid and liquid) | 0.212 W/m-K ^ |
| Thermal conductivity (liquid) | 0.171 W/m-K | | |
| * Experimental measurements (standard deviation: ± 15 kg/m³) – not from manufacturer<br>^ Experimental measurements (standard deviation: ± 0.022 W/m-K) – not from manufacturer | | | |

Figure 6-3 presents the manufacturer DSC test results of the PCM including the additives (Phase change energy solutions, 2008). The left-side graph shows the heat flow evolution as a function of the temperature. Negative and positive values correspond respectively to heat absorption (heating process) or release (cooling process). It also indicates that the solidification and the fusion occur over different temperature ranges: from ≃ 15 °C to ≃ 20 °C for the former and from ≃ 18.5 °C to ≃ 25 °C for the latter. The right-side graph presents the resulting enthalpy-temperature curves. The specific heat values for solid and liquid phases and the latent heat are respectively estimated as 1.9 J/g-K, 2 J/g-K and 200 J/g. Those values agree with the properties in Table 6-2. A hysteresis of 4 °C to 5 °C is observed between the cooling and heating curves, while no subcooling is apparent.

In previous work, Delcroix et al. (2014) implemented the properties presented above in a building simulation model. A comparison between experimental and simulated data highlighted that the enthalpy-temperature curves obtained with the DSC test do not allow to simulate the PCM thermal behavior accurately.

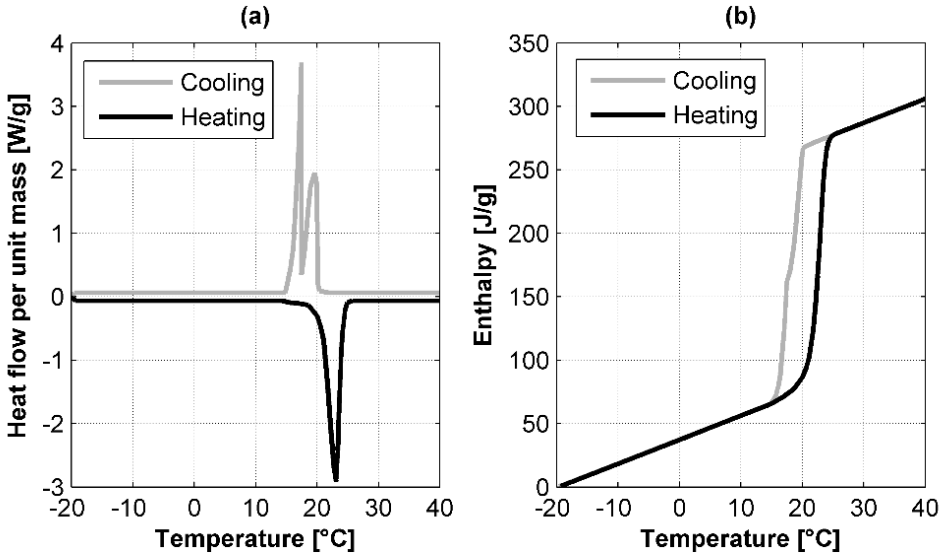


Figure 6-3: (a) Differential Scanning Calorimetry test (2 °C/min) and (b) resulting enthalpy-temperature curves (adapted from (Phase change energy solutions, 2008))

## 6.5 Experimental results obtained with PCM samples

This section presents the experimental setup, the inverse method and the main results related to PCM samples.

### 6.5.1 Experimental setup

Experimentations are carried out according to the T-history methodology (Solé et al., 2013) with PCM and water (as reference) samples going from cold to hot environments, and conversely. The experimental setup is composed of 12 PCM samples (≃ 10 grams per sample) and 2 water samples (≃ 11.5 grams per sample) contained in test tubes instrumented with thermocouples having a measurement accuracy of ± 0.5 °C. The cold and hot environments are respectively a cold chamber maintained between 2 and 3 °C and an oven maintained around 60 °C. Three cooling-heating cycles are performed and the measurement time-step is 10 seconds. The experimentations follow the steps illustrated in Figure 6-4.

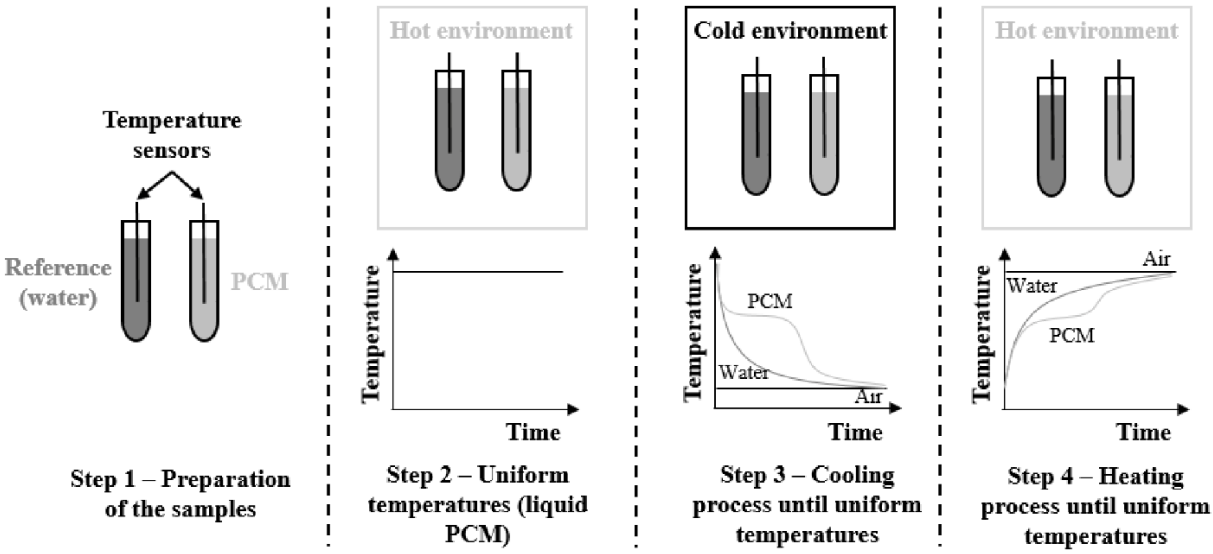


Figure 6-4: Principle of the T-history experimentation

The mass-weighted mean temperature evolutions for the PCM and the reference material (water) during the final cooling-heating cycle are presented in Figure 6-5. The air temperature fluctuation in the cold environment is due to the cooling system on/off control. During the cooling process, a slight subcooling effect is observed during the phase change. It divides the phase change into 2 distinct periods. This phenomenon is not observed during the heating process.

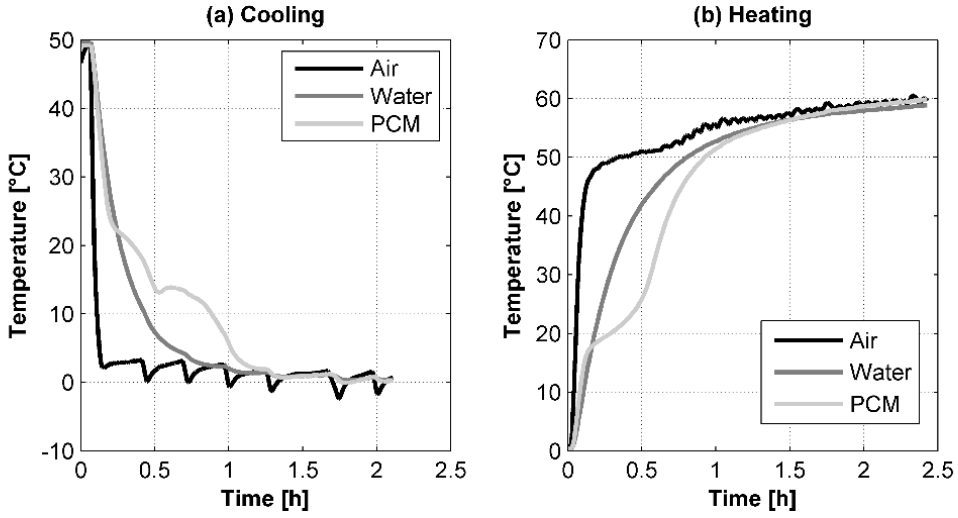


Figure 6-5: Temperature evolutions of the air, water and PCM during (a) cooling and (b) heating processes

Experimental data presented in Figure 6-5 could have been processed with a T-history method (Solé et al., 2013). However, this method assumes a uniform temperature in the sample, which is mathematically assessed by the Biot number. Values equal to or lower than 0.1 are generally required to assume a uniform temperature. In this case, the calculated Biot numbers are higher, as shown in section 6.5.2.1.

### 6.5.2 Inverse method applied to PCM samples experimentations

The principle of the inverse modeling method consists in using experimental data to identify model parameters. In the present case, this method is carried out in 2 steps. First the studied system is modeled while setting the known parameters. In a second step, the unknown parameters are identified using a genetic algorithm-based optimization program (The MathWorks Inc., 2014) in order to minimize the Root Mean Square Deviation ($RMSD$) between simulated and experimental data. The objective function is formulated as follows (for $n$ time-steps):

$$Minimize\ RMSD = \sqrt{\frac{\sum_{j=1}^{n}\left(T_{exp,j} - T_{sim,j}\right)^2}{n}} \qquad (6.2)$$

The studied systems are water and PCM samples in test tubes where the measured temperature is assumed to be located in the center and the heat transfer is assumed to be radial. As illustrated in Figure 6-6 and Figure 6-7, the water and PCM samples are simplified as R-C (resistance-capacitance) models. The thermal mass of the thermocouple is neglected. The water sample is modeled using a single node since the sample temperature is considered uniform (high thermal conductivity and convection). On the other hand, the PCM sample is modeled using 3 nodes. Each node represents a section (one-third of the radius) of the sample. The temperature of the central section ($T_1$) is assumed to be the measured temperature. The thermal resistances $R_1$, $R_2$ and $R_3$ are calculated for radial systems (Bergman et al., 2011) and corresponding heat-exchange surfaces are defined ($A_1$, $A_2$ and $A_3$). $R_{out}$ is determined when the inverse method is applied to the water sample and is equal to $\frac{1}{h_g}$.

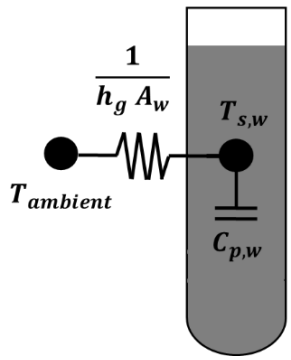


Figure 6-6: R-C model for the water sample

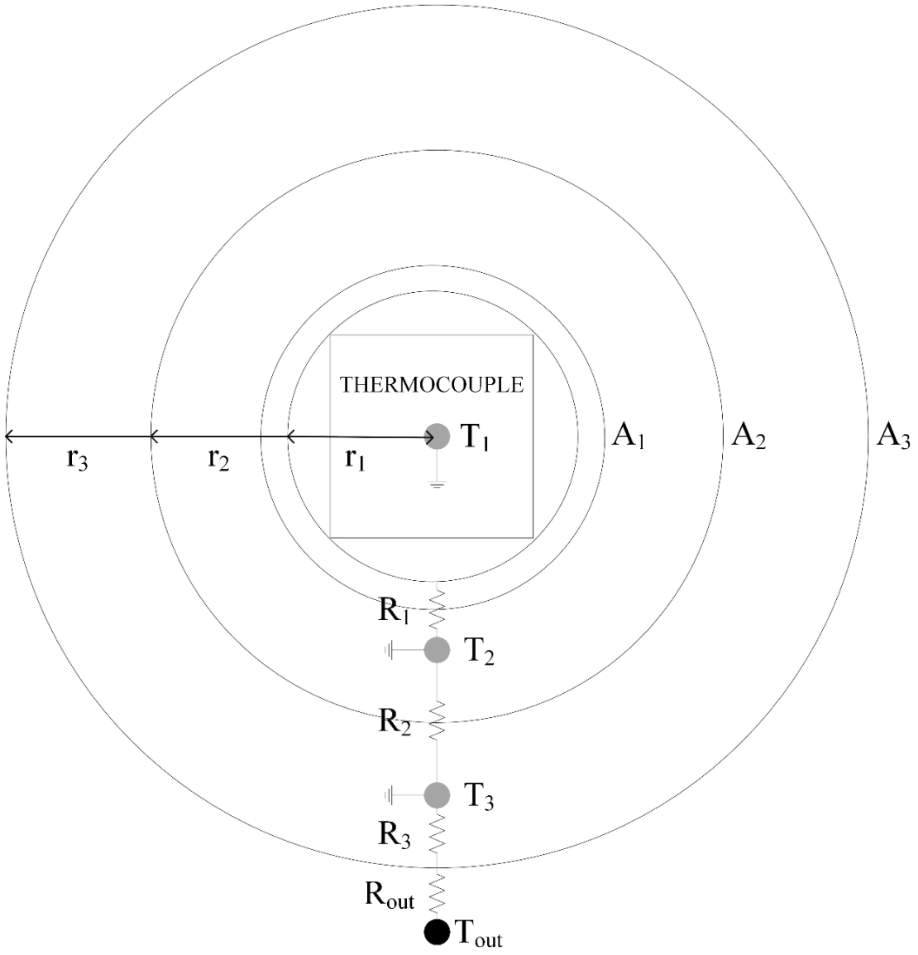


Figure 6-7: R-C model for the PCM sample (top-view)

The water sample model can be mathematically expressed with the following differential equation:

$$\frac{dT_{s,w}}{dt} = \frac{h_g\ A_w}{C_{p,w}\ m_w}(T_{ambient} - T_{s,w}) \qquad (6.3)$$

The PCM sample model is mathematically expressed using the three following differential equations:

$$\frac{dT_1}{dt} = \frac{A_1}{R_1 \times C_{p,pcm}(T) \times m_1}(T_2 - T_1) \quad (6.4)$$

$$\frac{dT_2}{dt} = \frac{A_1}{R_1 \times C_{p,pcm}(T) \times m_2}(T_1 - T_2) + \frac{A_2}{R_2 \times C_{p,pcm}(T) \times m_2}(T_3 - T_2) \quad (6.5)$$

$$\frac{dT_3}{dt} = \frac{A_2}{R_2 \times C_{p,pcm}(T) \times m_3}(T_2 - T_3) + \frac{A_3}{(R_3 + R_{out}) \times C_{p,pcm}(T) \times m_3}(T_{out} - T_3) \quad (6.6)$$

Equation ( 6.3 ) and the system of Equations ( 6.4 ) to ( 6.6 ) are solved with a forward time finite-difference method (Recktenwald, 2011) with a time-step of 10 seconds. The resulting stability condition which requires that the Fourier number is below 0.5 is satisfied (Bergman et al., 2011).

In order to assess the $h(T)$ curves for the PCM sample, two major steps must be performed:

- Calculate the global heat transfer coefficient $h_g$ from the water sample.
- Calculate the optimized $C_p(T)$ curves for both heating and cooling processes.

#### 6.5.2.1 Computation of the global heat transfer coefficient

When applied to the water sample, the only unknown in Equation ( 6.3 ) is the global heat transfer coefficient $h_g$ between the sample and the external condition. This parameter is found by error minimization using the objective function given in Equation ( 6.2 ) and the genetic algorithm-based optimization program. Simulated and measured water data are compared in Figure 6-8, which shows a good agreement. The $h_g\ A_w$ values estimated for the cooling and heating processes are respectively 0.075 W/K and 0.060 W/K. The cold environment has a higher internal ventilation rate, which explains the larger heat transfer. The $RMSD$ values are below 0.5 °C, which is considered to be acceptable as it is lower than the accuracy of the thermocouples.

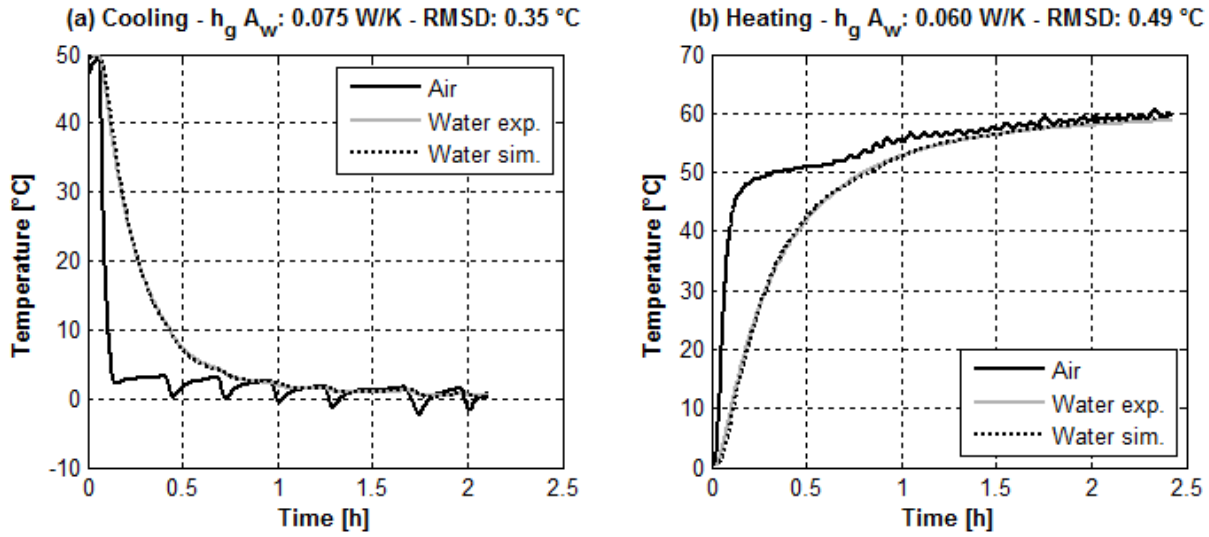


Figure 6-8: Comparison between simulated and measured data for the water sample during (a) cooling and (b) heating processes

The resulting global heat transfer coefficients $h_g$ in Figure 6-8 for cooling and heating processes are respectively 21.9 and 17.6 W/m²-K. The Biot number $Bi$ of the PCM sample can now be calculated such as:

$$\mathrm{Bi} = \frac{h_g \, L_c}{k_{pcm}} \qquad (6.7)$$

Where $L_c$ is the characteristic length and is equal to the test tube radius $r$ (0.007 m) (Kula & Yovanovich, 1991) and $k_{pcm}$ is the PCM thermal conductivity (0.212 W/m-K).

The Biot number is 0.72 for cooling and 0.58 for heating. These values are significantly higher than 0.1. The PCM sample cannot be considered thermally uniform.

#### 6.5.2.2 Computation of the PCM specific heat

The temperature evolution inside the PCM sample is formulated with a system of differential equations (see Equation ( 6.4 ) to ( 6.6 )). This system of equations is solved using the same finite-difference method as previously. In the PCM case, the only unknown in this system is the PCM specific heat which should be characterized by a $C_p(T)$ curve. The same optimization algorithm as previously is used to determine the curve that minimizes the $RMSD$ between simulated and experimental data. The $C_p(T)$ curve is discretized with a certain number of points defined by their

values of specific heat and temperature. Temperature values are fixed while $C_p$ values are variable. After several optimizations, nine and seven points were defined for the cooling and heating processes, respectively. The cooling process needs more points due to the more complex temperature evolution (see Figure 6-5 and Figure 6-9). Figure 6-9 presents the comparison between simulated and experimental temperature evolutions for both processes. In the presented case, $RMSD$ values of 0.31 °C and 0.35 °C are obtained for the cooling and heating processes, respectively. The simulation cannot reproduce the subcooling effect during cooling because a negative $C_p$ value is not physical.

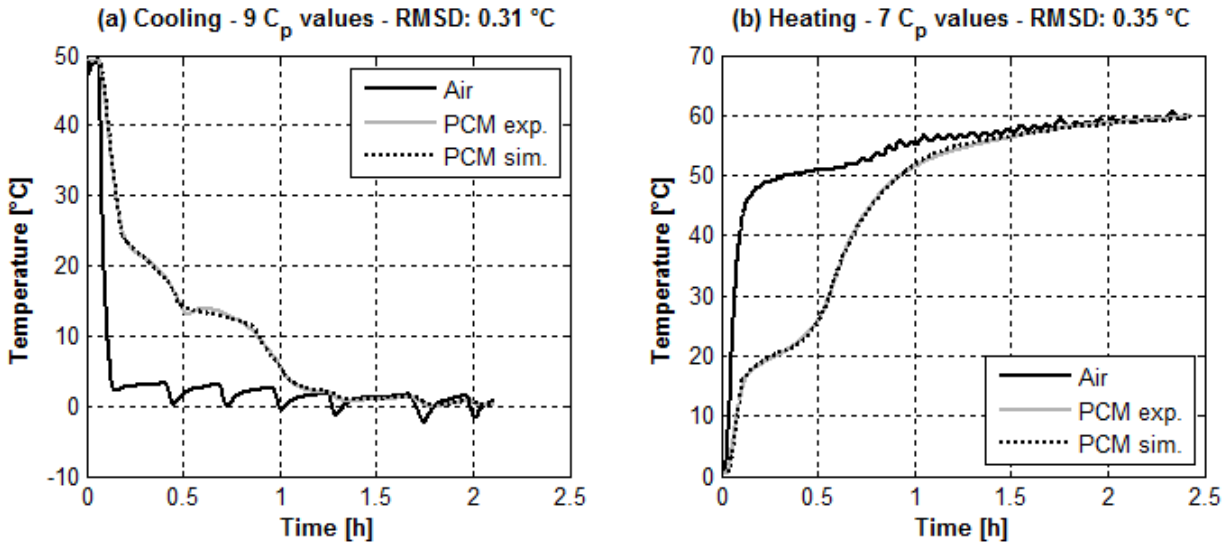


Figure 6-9: Comparison between experimental and simulated temperature evolution of the PCM sample during (a) cooling and (b) heating processes

### 6.5.3 PCM samples results

From the optimized $C_p$ values obtained for cooling and heating processes of the PCM sample, a pair of enthalpy-temperature curves is obtained and presented in Figure 6-10. These curves are compared to the ones generated from the manufacturer DSC test. In order to match heating and cooling curves, post-processing is applied to the specific heat values generated by the inverse method. Three modifications are performed:

- The specific heat value used for solid state is the one from the heating process since it is certain that the PCM is initially solid.

- The specific heat value used for liquid state is the one from the cooling process since it is certain that the PCM is initially liquid.
- The latent heat value used is the average of both cooling and heating processes.

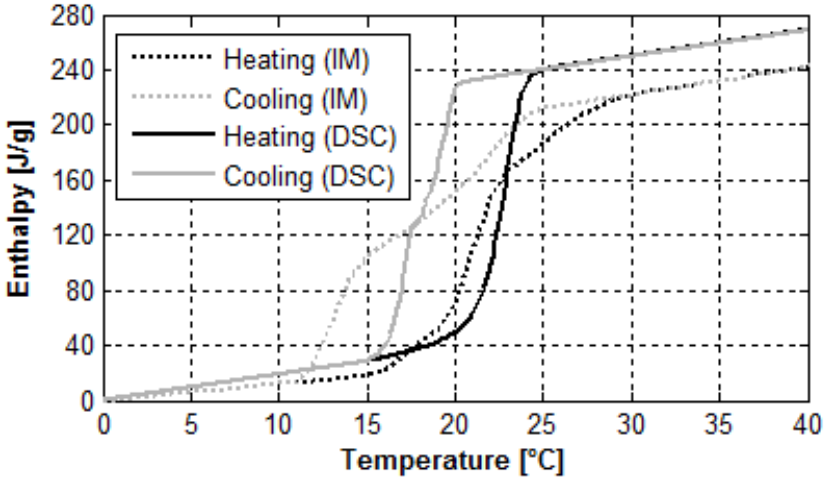


Figure 6-10: Comparison between the enthalpy-temperature curves of the inverse method (IM) and the DSC test

Figure 6-10 shows that the thermal capacity computed with the inverse method (IM) presented in dotted lines is slightly lower. The latent heat obtained with the inverse method is nearly equivalent to the value given by the DSC test (around 200 J/g). The curve slope during the solid state is slightly lower with the inverse method, meaning that the specific heat (solid) has a lower value. On the other hand, the specific heat for the liquid state shows no significant difference with the DSC value.

The inverse method shows a larger phase-change temperature range than the DSC test (especially for cooling). This larger range is also observable on the temperature profiles shown in Figure 6-5. These discrepancies can be attributed to different test conditions such as the applied heating and cooling rates but also to sample size. The DSC tests have a rate of 2 °C/min and samples of a few milligrams while the inverse method has a rate of around 0.8 °C/min and samples of approximately 10 grams.

## 6.6 Experimental results obtained with PCM-equipped walls

This section presents the experimental setup, the inverse method and the main results related to the PCM-equipped walls.

### 6.6.1 Experimental setup

The tested PCM-equipped wall consists of a double layer of plastic film with PCM pouches placed between 2 plywood panels. The PCM-equipped walls are instrumented with 6 thermocouples such as illustrated in Figure 6-11. Two kinds of experimentations are performed. In the first test, a PCM-equipped wall is submitted to large temperature variations by being located successively in stabilized warm and cold rooms (in a dual-temperature chamber). As shown in Figure 6-11, the wall perimeter is insulated to avoid side-effects. The second test is in a full-scale test-cell where PCM-equipped walls are added to internal walls. In this case, there is no insulation on the sides of the PCM-equipped walls.

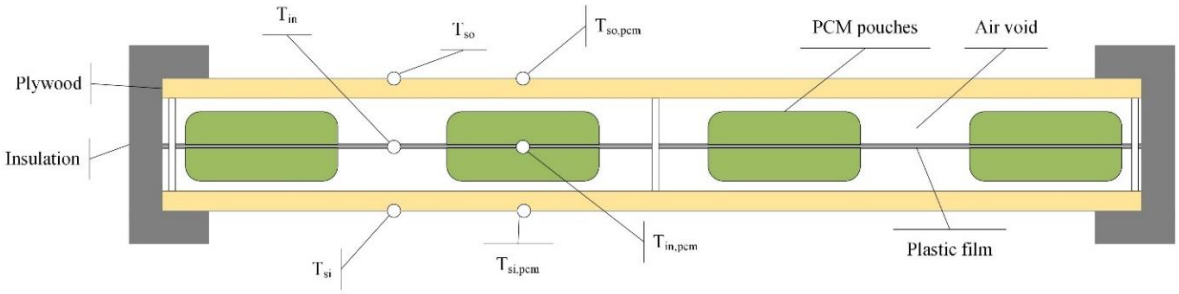


Figure 6-11: Schematic of the instrumented PCM-equipped walls

A previous study (Delcroix et al., 2014) has shown that the wall center temperature is significantly different depending on the position of the thermocouple between 2 PCM pouches or in the air void ($T_{in} \neq T_{in,pcm}$). The study also shows that the non-uniformity is limited within the PCM layer, and that the surface temperatures can be considered uniform ($T_{so} = T_{so,pcm}$ ; $T_{si} = T_{si,pcm}$). When experimental and simulated results are compared, the equivalent temperature in the center of the wall is used and is an average value of both measurements ($T_{in}$ and $T_{in,pcm}$) weighted by the mass of each material in the equivalent layer (PCM (76 %) and others (24 %)).

#### 6.6.1.1 Experimentations in the dual-temperature chamber

In these experiments, the insulated PCM-equipped wall is placed vertically successively in controlled warm and cold rooms. The temperature inside both rooms does not change and the PCM-equipped wall is transferred quickly from one room to the other by a small opening so that the room temperature is not affected. The wall is left in the room until it reaches a thermal equilibrium with the room. Eight heating-cooling cycles are performed. The data acquisition period is 10 seconds.

Figure 6-12 presents results for a cooling-heating cycle. Solid lines with circles show the temperature evolutions of the PCM ($T_{in,pcm}$ in Figure 6-11) and in the air void ($T_{in}$ in Figure 6-11). Solid lines (S1 and S2) are surface temperatures. The dotted lines in grey and black present the temperature evolutions for the air room and the equivalent layer (mass-weighted average of the temperatures presented by solid lines with circles), respectively.

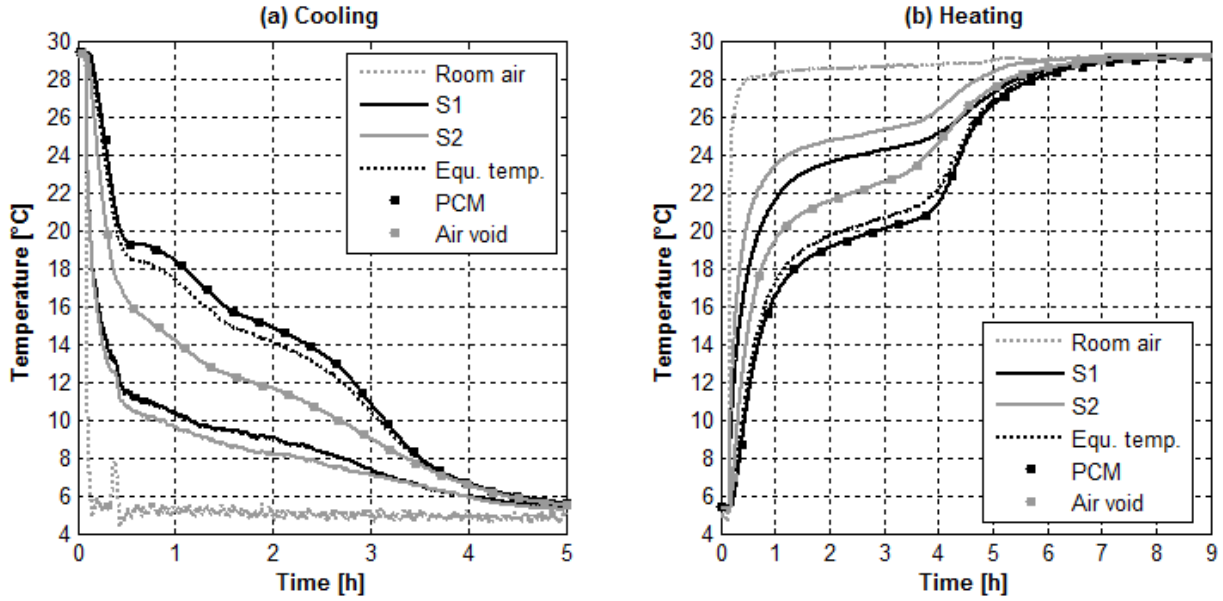


Figure 6-12: Experimental data for a cooling-heating cycle in the dual temperature chamber

Both graphs show that the phase change temperature range during cooling and heating is different. The range is between 13 °C and 19 °C during cooling and between 17 °C and 21 °C during heating if the black solid lines with circles are considered. It means that there is an important hysteresis effect in these test conditions. If the average phase change temperatures are considered for cooling (16 °C) and heating (19 °C), the hysteresis is around 3 °C. These graphs also show that cooling is faster than heating. This can be explained by the higher convection coefficient in the cold zone of the dual-temperature chamber, which has a higher ventilation rate.

#### 6.6.1.2 Experimentations in the test-cell

The full-scale test-cell is fitted with instrumented PCM-equipped walls, which are added on the inside surface of the north-west and south-west external walls (see Figure 6-13). Results are presented for an extreme set-back scenario with a temperature set-point changing from 5 to 30 °C

every day (Figure 6-14). This scenario was applied during 21 days during April 2013. The average ambient temperature was around 8 °C and the data acquisition period is 60 seconds.

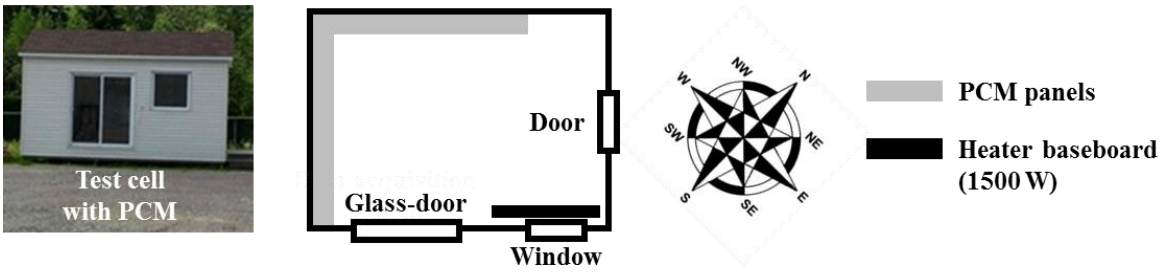


Figure 6-13: Picture and top-view of the test cell with PCM-equipped walls

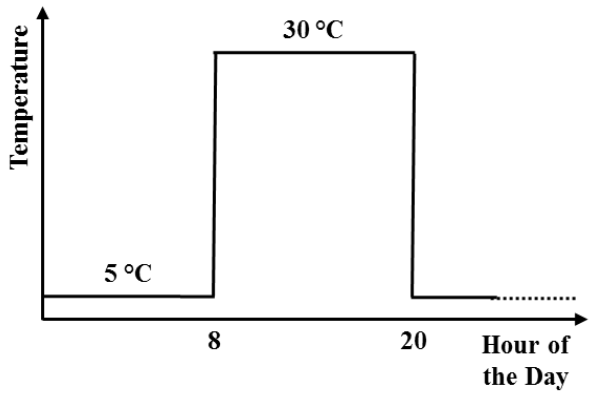


Figure 6-14: Graph explaining the extreme set-back scenario

Figure 6-15 is similar to Figure 6-12: it shows the temperature evolution for a cooling and heating period inside the PCM-equipped wall, at both surfaces and in the room. In these experiments, the heating and cooling rates are lower. For example, it takes about 16 hours for the PCM temperature to cool down from 28 °C to 15 °C instead of 5 hours to cool down from 29 °C to 6 °C in Figure 6-12. The cooling or heating rate seems to have an impact on the PCM behavior. In Figure 6-15, the phase change during cooling and heating occurs approximatively in the same temperature range, i.e. from 19 °C to 23 °C. In Figure 6-12, where the cooling and heating rates are higher, the phase change occurs over significantly different temperature ranges, as previously observed.

Graphs in Figure 6-15 show that the heating is faster than the cooling because it is driven by electric baseboard heating while the cooling is due to heat losses after a set-point drop.

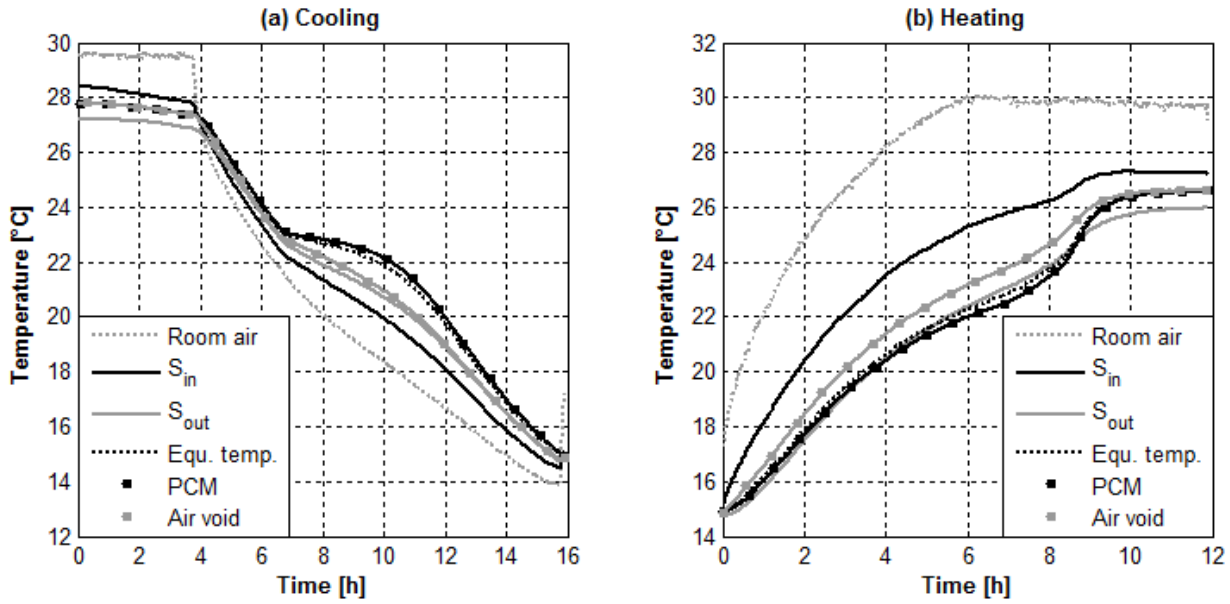


Figure 6-15: Experimental data for a cooling-heating cycle in the test-cell

### 6.6.2 Inverse method applied to PCM-equipped walls experimentations

The PCM-equipped wall is represented as an R-C model (Figure 6-16) with 30 nodes whose boundary conditions are the surface temperatures. The properties (Table 6-3) of the central equivalent layer consist in combined properties of each material, i.e. PCM, plastic film and air. The density is the volumetric average of the densities. The equivalent thermal conductivity is estimated using THERM (Lawrence Berkeley National Laboratory, 2013). The air thermal resistance was determined by assuming a thermal conductivity of 0.026 W/m-K and a radiative heat transfer computed from Kirchhoff's law (Spakovszki, 2014). As the air layer is very thin, the convective heat transfer is assumed to be negligible. The equivalent specific heat $C_p(T)$ is determined through the inverse method. First, the equivalent values of latent heat and specific heat for solid and liquid states (Table 6-4) can be calculated from known thermal capacity values and the mass fraction of each material in the equivalent layer. Then the phase change temperature range is determined by the inverse method. The central node inside the equivalent layer is the one used to match simulated and experimental data. The objective function shown in Equation ( 6.2 ) is used.

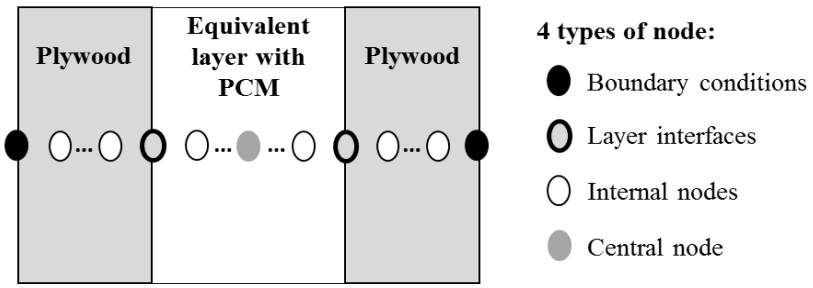


Figure 6-16: Modeling of the PCM-equipped wall

Table 6-3: Properties of the model for the PCM-equipped wall

| Layer | Thickness [m] | Thermal conductivity [W/m-K] | Density [kg/m³] | Specific heat [J/g-K] |
|---|---|---|---|---|
| Plywood | 0.006 | 0.084 | 850 | 1.25 |
| Equivalent layer | 0.017 | 0.042 | 223 | N/A |

Table 6-4: Thermal capacity definition of the equivalent layer

| Material | Mass share [%] | Specific heat [J/g-K] | Specific heat (solid) [J/g-K] | Specific heat (liquid) [J/g-K] | Latent heat [J/g] |
|---|---|---|---|---|---|
| Air | 0.4 | 1 | N/A | N/A | N/A |
| Plastic film | 23.5 | 1.5 | N/A | N/A | N/A |
| PCM | 76.1 | N/A | 1.84 | 1.99 | 200 |
| Equivalent layer | N/A | N/A | 1.76 | 1.87 | 150 |

For each node presented in Figure 6-16, the temperature variation over time is computed as follows:

$$\frac{dT_n}{dt} = \frac{U_{l,n}}{C_n}\,(T_{n-1} - T_n) + \frac{U_{r,n}}{C_n}\,(T_{n+1} - T_n) \qquad (6.8)$$

Equation ( 6.8 ) is solved with a forward time and central space finite-difference method with a time-step of 10 and 60 seconds, respectively for the dual-temperature chamber and test-cell experimentations. The corresponding stability condition based on the Fourier number is met (Bergman et al., 2011). In Equation ( 6.8 ), the only parameter that has to be determined for the equivalent layer is the node capacitance $C_n$, which is equal to:

$$C_n = \rho_n\, C_{p,n}\, \Delta x_n \qquad (6.9)$$

The density $\rho$ and the node interval $\Delta x$ are constant. Only the temperature-dependent specific heat $C_p(T)$ is to be optimized and is defined using 2 variables (Figure 6-17). Two temperatures defining the beginning ($T_{on}$) and the end ($T_{off}$) of the phase change are optimized. The three specific heat values for solid ($C_{p,s}$), mushy ($C_{p,pc}$) and liquid ($C_{p,l}$) states are set to the values in Table 6-4.

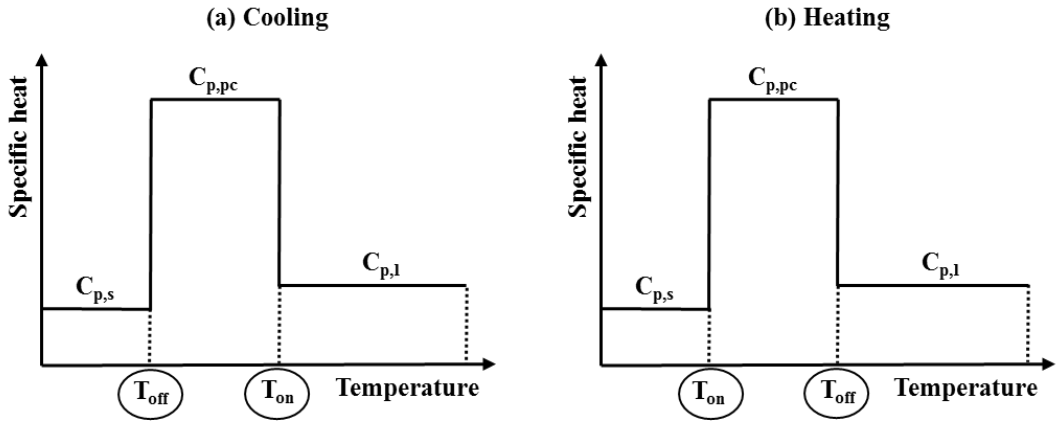


Figure 6-17: Graphs explaining the variables to be optimized during (a) cooling and (b) heating processes

Optimizations are separately applied to 50 cooling cases (42 in the test-cell and 8 in the dual-temperature chamber) and 48 heating cases (40 in the test-cell and 8 in the dual-temperature chamber), which display varying degree of heating and cooling rates.

A case for both tests and processes is shown in Figure 6-18 and Figure 6-19, where simulated and experimental results are in good agreement.

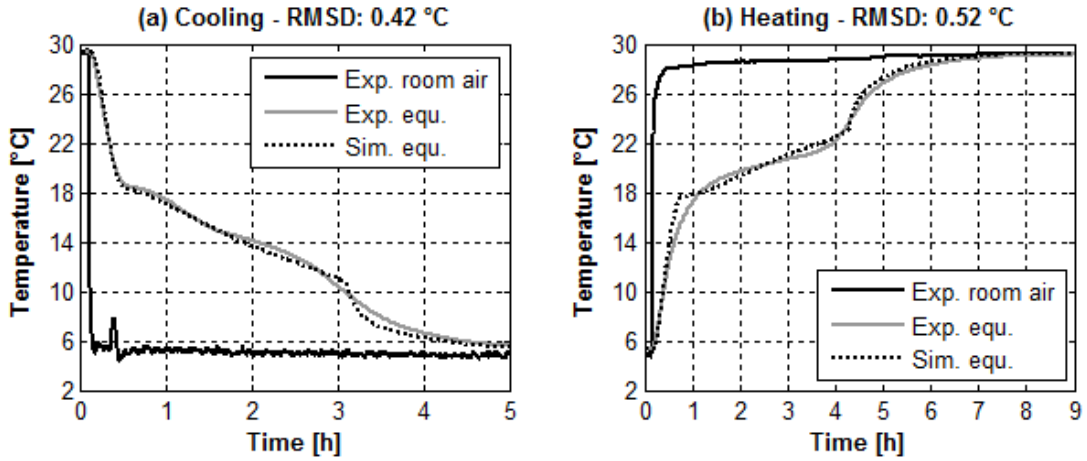


Figure 6-18: Comparison between experimental and simulated temperature evolution for wall experimentations during (a) cooling and (b) heating processes

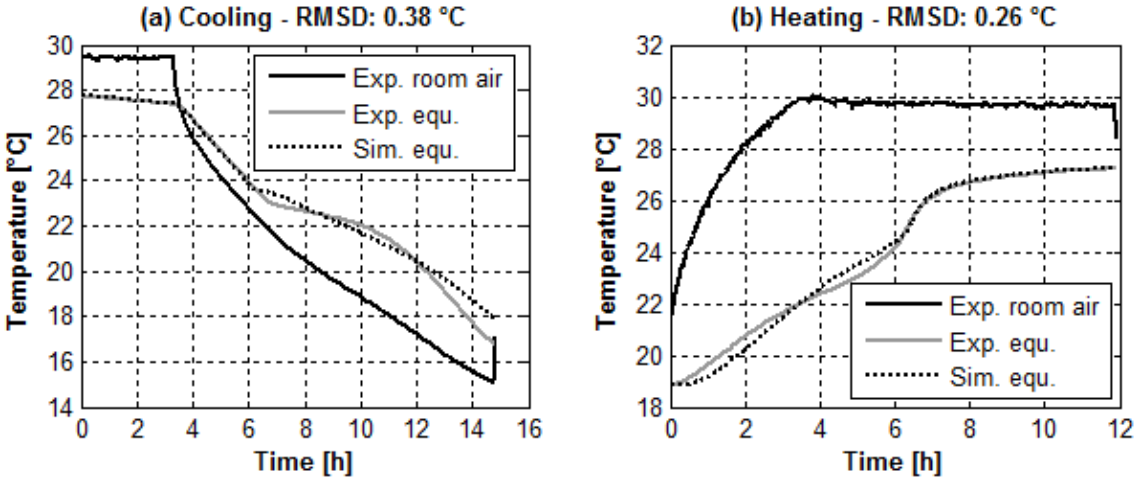


Figure 6-19: Comparison between experimental and simulated temperature evolution for test-cell experimentations during (a) cooling and (b) heating processes

## 6.6.3 PCM-equipped walls results

### 6.6.3.1 Variation of the phase change temperature range

The phase change temperature range is influenced by the cooling and heating rates. Figure 6-20 shows that the temperature differences between the beginning ($T_{on}$) and the end ($T_{off}$) of the phase change are stable around 8 °C for cooling and around 6 °C for heating. $T_{on}$ cannot be estimated accurately from the heating processes in the test-cell because the PCM is in a mushy state (i.e. not fully solidified) when heating in the test-cell begins. A decrease of both $T_{on}$ and $T_{off}$ is observed when heat transfer rates rise.

Red marks indicate the average values for three categories of cooling and heating rates:

- Low cooling and heating rates in the test-cell with average rates of 0.014 °C/min and 0.019 °C/min, respectively.
- Medium cooling and heating rates in the dual-temperature chamber with average rates of 0.072 °C/min and 0.048 °C/min, respectively.
- High cooling and heating rates in the dual-temperature chamber with average rates of 0.179 °C/min and 0.073 °C/min, respectively.

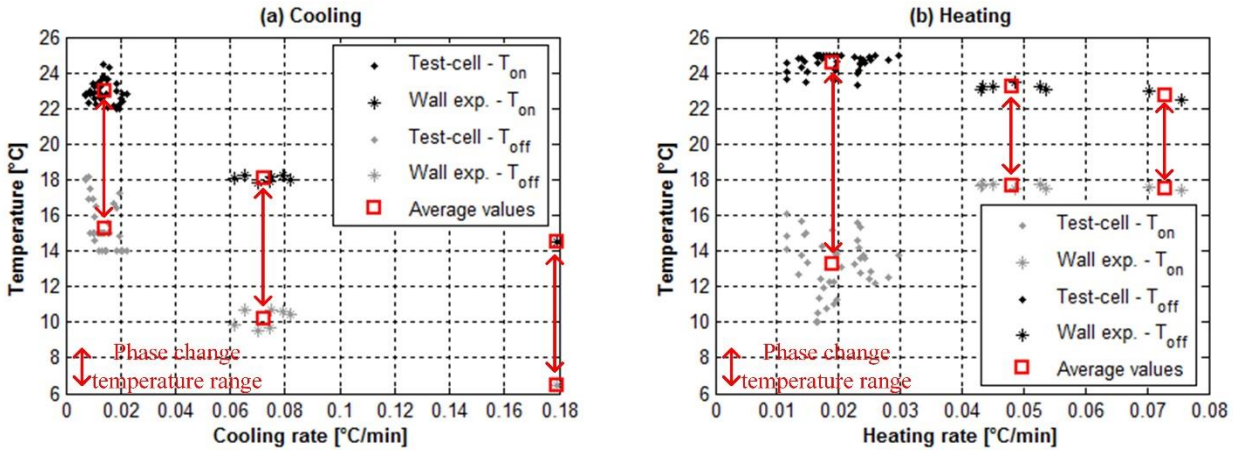


Figure 6-20: Variation of the phase change temperature range as a function of the (a) cooling and (b) heating rates

### 6.6.3.2 Variation of the hysteresis effect

The hysteresis effect is described as the temperature difference between the heating and cooling $C_p(T)$ or $h(T)$ curves. From the experiments in the dual-temperature chamber and the test-cell, the hysteresis is analyzed as a function of the cooling and heating rates. Figure 6-21 presents the variation of the hysteresis at two levels (see Figure 6-17 for references to notations) : first (a), between the temperatures at the beginning of the phase change during the cooling ($T_{on,c}$) and at the end of the phase change during the heating ($T_{off,h}$); secondly (b), between the temperatures at the end of the phase change during the cooling ($T_{off,c}$) and at the beginning of the phase change during the heating ($T_{on,h}$).

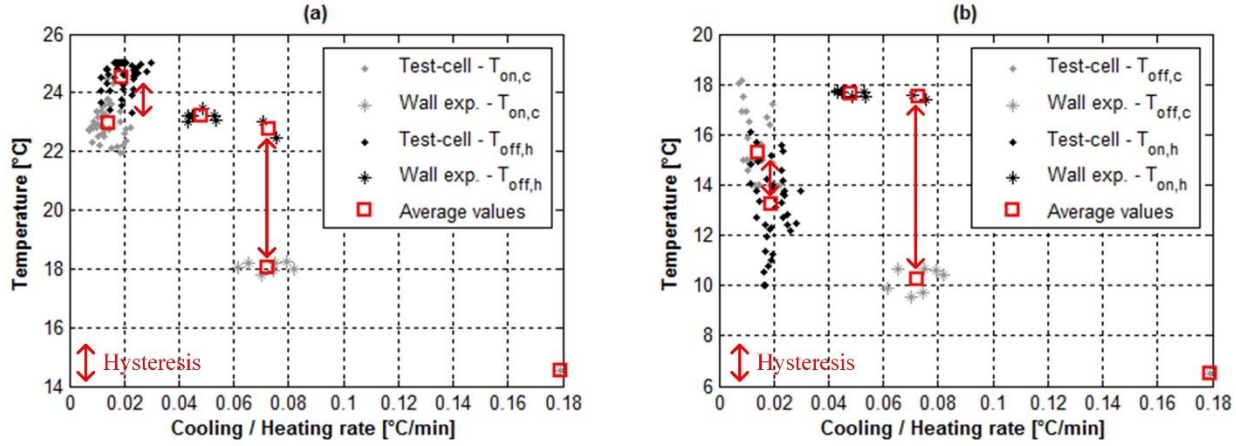


Figure 6-21: Variation of the hysteresis effect as a function of the cooling / heating rates

Again, the values of $T_{on}$ cannot be estimated accurately during heating, because the PCM is not fully solidified at the start of the process. The other results show that the hysteresis is low (around 1 °C) at low cooling and heating rates, while it can reach up to around 7-8 °C at higher rates. As in Figure 6-20, the temperature values decrease when rates increase.

#### 6.6.3.3 Variation of $h(T)$ curves

For each category defined in Figure 6-20 and Figure 6-21 (average values) and using PCM properties defined in Table 6-4, average $h(T)$ curves were defined for both cooling and heating processes (Figure 6-22). Results from the DSC test and the inverse method applied on PCM samples are also presented for comparison.

Figure 6-22 shows that the discrepancies are more apparent for cooling processes. Phase change temperature ranges during heating are similar for each configuration, except in the test-cell. This latter issue has already been discussed in the previous sections 6.6.3.1 and 6.6.3.2. Cooling $h(T)$ curves are more sensitive to heat transfer rates. A rate increase leads to a hysteresis rise. This figure also shows that the $h(T)$ curve shape depends significantly on configurations (sample or wall), methods (DSC or inverse method) and test conditions (heat transfer rates).

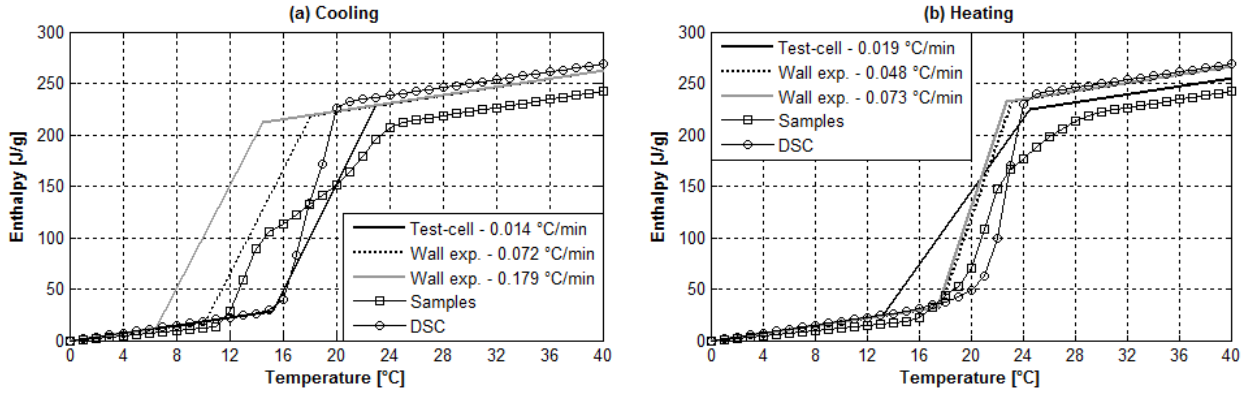


Figure 6-22: Comparison of $h(T)$ curves for both (a) cooling and (b) heating processes

## 6.7 Conclusions and recommendations

This paper compares the thermal behavior of a commercially available bio-based PCM subjected to four types of experimental conditions: the manufacturer DSC test realized on a PCM sample of a few milligrams; temperature step-change tests (as suggested by the T-history methodology) on PCM samples of a few grams; temperature step-change heating and cooling tests on a PCM-

equipped wall; tests in a full-scale test-cell equipped with PCM submitted to an extreme set-back scenario. An inverse modeling technique is proposed and used to process the experimental data and compute $h(T)$ curves for both heating and cooling processes in each test (excluding the DSC test).

The proposed inverse method for PCM samples tests allows to overcome the T-history limitation which requires that the PCM sample must be thermally uniform ($Bi \leq 0.1$). A comparison between the DSC test and the inverse method for PCM samples tests shows a clear difference in terms of phase change temperature range, which can be attributed to different test conditions (different sample sizes and heat transfer rates). Latent heat and specific heat values obtained with the inverse method are close to the ones obtained with the DSC test. Our results shows that the proposed inverse method can be successfully applied and replace a DSC test (if too expensive) or the T-history method (if not applicable).

This paper also proposes a methodology to obtain the equivalent properties of a layer composed of PCM, air and plastic film. Once the equivalent density and thermal conductivity have been calculated through proven methods, an inverse method is applied to identify the $h(T)$ curves. Results obtained with the PCM-equipped wall highlight that the PCM thermal behavior is affected by the heat transfer rates: higher rates lead to higher hysteresis. The phase change temperature range is shifted towards colder temperatures, while its amplitude (difference between the temperature levels at which the phase change starts and ends) remains constant. The results variability highlighted in this paper shows that the analysis of different test methods leads to different PCM properties. The test method should be carefully chosen to represent heating and cooling rates found in the application. In the case of PCM embedded in building walls for residential or commercial applications, our recommendation is that DSC test results and T-history results obtained from small samples (a few milligrams to a few grams) subject to high heating and cooling rates (0.8 °C/min to 2 °C/min in our cases) are not directly applicable. Other experimental tests should be used, such as the ones presented here for a PCM-equipped wall and a full-scale test cell experiment, or potentially the HFMA method documented by Kosny et al. (2010).

## Acknowledgements

The research work presented in this paper is financially supported by Hydro-Québec, FRQNT (Fonds de Recherche du Québec en Nature et Technologies) and NSERC (Natural Sciences and Engineering Research Council of Canada).

## References

Atchonouglo, K., Banna, M., Vallée, C., & Dupré, J.-C. (2008). Inverse transient heat conduction problems and identification of thermal parameters. Heat and Mass Transfer, 45(1), 23–29. doi:10.1007/s00231-008-0383-7

Baetens, R., Jelle, B. P., & Gustavsen, A. (2010). Phase change materials for building applications: A state-of-the-art review. Energy and Buildings, 42(9), 1361–1368. doi:http://dx.doi.org/10.1016/j.enbuild.2010.03.026

Bergman, T. L., Lavine, A. S., Incropera, F. P., & Dewitt, D. P. (2011). Fundamentals of heat and mass transfer. Wiley.

Braun, J. E., & Chaturvedi, N. (2002). An Inverse Gray-Box Model for Transient Building Load Prediction. HVAC&R Research, 8(1), 73–99. Retrieved from http://www.tandfonline.com/doi/abs/10.1080/10789669.2002.10391290

Castell, A., Medrano, M., Castellón, C., & Cabeza, L. F. (2009). Analysis of the simulation models for the use of PCM in buildings. In Effstock: Thermal Energy Storage for Efficiency and Sustainability. Stockholm.

Cheng, R., Pomianowski, M., Wang, X., Heiselberg, P., & Zhang, Y. (2013). A new method to determine thermophysical properties of PCM-concrete brick. Applied Energy, 112, 988–998. doi:10.1016/j.apenergy.2013.01.046

Crawley, D. B., Lawrie, L. K., Winkelmann, F. C., Buhl, W. F., Huang, Y. J., Pedersen, C. O., Strand, R. K., Liesen, R. J., Fischer, D. E., Witte, M. J., Glazer, J. (2001). EnergyPlus:

creating a new-generation building energy simulation program. Energy and Buildings, 33(4), 319–331. doi:http://dx.doi.org/10.1016/S0378-7788(00)00114-6

Delcroix, B., Kummert, M., Daoud, A., & Bouchard, J. (2014). Experimental assessment of a phase change material in walls for heating and cooling applications. In eSim (pp. 1 – 13). Ottawa, ON, Canada.

Dentel, A., & Stephan, W. (2010). Thermal Comfort in Rooms with active PCM Constructions. In 8th International Conference on System Simulation in Buildings (pp. 1–16). Liège, Belgium.

Energy Systems Research Unit. (1998). ESP-r User Guide: The ESP-r System for Building Energy Simulation. Glasgow.

German Institute for Quality Assurance and Certification. (2009). Phase change material. Berlin, Germany.

Goodrich, L. E. (1978). Efficient numerical technique for one-dimensional thermal problems with phase-change. International Journal of Heat and Mass Transfer, 21(5), 615.

Günther, E., Hiebler, S., Mehling, H., & Redlich, R. (2009). Enthalpy of Phase Change Materials as a Function of Temperature: Required Accuracy and Suitable Measurement Methods. International Journal of Thermophysics, 30(4), 1257.

Günther, E., Mehling, H., & Hiebler, S. (2007). Modeling of subcooling and solidification of phase change materials. Modelling and Simulation in Materials Science and Engineering, 15, 879–892. doi:10.1088/0965-0393/15/8/005

Heim, D., & Clarke, J. A. (2004). Numerical modelling and thermal simulation of PCM–gypsum composites with ESP-r. Energy and Buildings, 36, 795–805. doi:10.1016/j.enbuild.2004.01.004

Huang, C.-H., & Jan-Yuan, Y. (1995). An inverse problem in simultaneously measuring temperature-dependent thermal conductivity and heat capacity. International Journal of Heat and Mass Transfer, 38(18), 3433–3441. doi:10.1016/0017-9310(95)00059-I

Ibánez, M., Lázaro, A., Zalba, B., & Cabeza, L. F. (2005). An approach to the simulation of PCMs in building applications using TRNSYS. Applied Thermal Engineering, 25, 1796–1807.

Klein, S. A., Beckman, W. A., Mitchell, J. W., Duffie, J. A., Duffie, N. A., & Freeman, T. L. (2012). TRNSYS 17: A Transient System Simulation Program. Madison, USA: Solar Energy Laboratory, University of Wisconsin. Retrieved from http://sel.me.wisc.edu/trnsys

Kosny, J., Stovall, T., Shrestha, S., & Yarbrough, D. (2010). Theoretical and Experimental Thermal Performance Analysis of Complex Thermal Storage Membrane Containing Bio-Based Phase-Change Material (PCM). In Building XI (p. 11).

Kula, L. W., & Yovanovich, M. M. (1991). Characteristic length of complex bodies for transient conduction. ASME Thermal Engineering Proceedings, 1, 259–267.

Kuznik, F., & Virgone, J. (2009). Experimental investigation of wallboard containing phase change material: Data for validation of numerical modeling. Energy and Buildings, 41(5), 561–570. doi:10.1016/j.enbuild.2008.11.022

Kuznik, F., Virgone, J., & Johannes, K. (2010). Development and validation of a new TRNSYS type for the simulation of external building walls containing PCM. Energy and Buildings, 42, 1004–1009.

Lawrence Berkeley National Laboratory. (2013). THERM 6.3 / WINDOW 6.3 - NFRC Simulation Manual.

Mehling, H., & Cabeza, L. F. (2008). Heat and cold storage with PCM: An up to date introduction into basics and applications. (D. Mewes & F. Mayinger, Eds.). Berlin: Springer.

Pedersen, C. O. (2007). Advanced zone simulation in EnergyPlus: incorporation of variable properties and phase change material (PCM) capability. In Building Simulation (pp. 1341–1345). Beijing.

Phase change energy solutions. (2008). BioPCM longevity cycle testing. Retrieved from http://www.phasechange.com/index.php/en/contractor-library

Poulad, M. E., Fung, A. S., & Naylor, D. (2011). Effects of convective heat transfer coefficient on the ability of PCM to reduce building energy demand. In 12th Conference of International Building Performance Simulation Association (pp. 270–277). Sydney.

Recktenwald, G. W. (2011). Finite-Difference Approximations to the Heat Equation (Vol. 0). Portland, Oregon, USA. Retrieved from http://www.f.kth.se/~jjalap/numme/FDheat.pdf

Schranzhofer, H., Puschnig, P., Heinz, A., & Streicher, W. (2006). Validation of a TRNSYS simulation model for PCM energy storages and PCM wall construction elements. In 10th International Conference on Thermal Energy Storage. New Jersey.

Sharma, A., Tyagi, V. V, Chen, C. R., & Buddhi, D. (2009). Review on thermal energy storage with phase change materials and applications. Renewable and Sustainable Energy Reviews, 13(2), 318–345. doi:http://dx.doi.org/10.1016/j.rser.2007.10.005

Shrestha, S., Miller, W., Stovall, T., Desjarlais, A., Childs, K., Porter, W., Bhandary, M., Coley, S. (2011). Modeling PCM-enhanced insulation system and benchmarking EnergyPlus against controlled field data. In 12th Conference of International Building Performance Simulation Association (pp. 800–807). Sydney.

Solé, A., Miró, L., Barreneche, C., Martorell, I., & Cabeza, L. F. (2013). Review of the T-history method to determine thermophysical properties of phase change materials (PCM). Renewable and Sustainable Energy Reviews, 26, 425–436. doi:10.1016/j.rser.2013.05.066

Spakovszki, Z. S. (2014). 19.3 Radiation heat transfer between planar surfaces. Retrieved February 25, 2015, from http://web.mit.edu/16.unified/www/FALL/thermodynamics/notes/node136.html

Tabares-Velasco, P. C., Christensen, C., & Bianchi, M. (2012). Verification and validation of EnergyPlus phase change material model for opaque wall assemblies. Building and Environment, 54, 186–196.

The MathWorks Inc. (2014). GA - Find minimum of function using genetic algorithm. Retrieved July 2, 2014, from http://www.mathworks.com/help/gads/ga.html

Voller, V. R., & Cross, M. (1981). Accurate solutions of moving boundary problems using the enthalpy method. International Journal of Heat and Mass Transfer, 24(3), 545.

Yao, M., & Chait, A. (1993). An alternative formulation of the apparent heat capacity method for phase change problems. Numerical Heat Transfer, Part B, Fundamentals, 24(3), 279.

Zalba, B., Marín, J. M., Cabeza, L. F., & Mehling, H. (2003). Review on thermal energy storage with phase change: materials, heat transfer analysis and applications. Applied Thermal Engineering, 23(3), 251–283. doi:http://dx.doi.org/10.1016/S1359-4311(02)00192-8

# CHAPTER 7 ARTICLE 3: THERMAL BEHAVIOR MAPPING OF A PHASE CHANGE MATERIAL BETWEEN THE HEATING AND COOLING ENTHALPY-TEMPERATURE CURVES

Delcroix, B., Kummert, M., Daoud, A., (2015). Thermal behavior mapping of a phase change material between the heating and cooling enthalpy-temperature curves. 6th International Building Physics Conference. Torino, Italy.

## Abstract

This paper presents the results of experimental tests performed on a wall section equipped with phase change materials (PCM). The wall is quickly transferred between cold and warm enclosures to observe the PCM behavior when melting or solidification is interrupted. A 1-D model of the wall based on the enthalpy method is used to identify the enthalpy curves that provide the best fit to experimental data. Results show that the PCM experiences a quick transition between different enthalpy curves when the heat flow direction (heating or cooling) is reversed during phase-change. According to our experiments and to the comparison with the 1-D model, the PCM investigated here follows an enthalpy curve that is very close to the heating curve when a cooling process is interrupted during solidification. If a heating process is interrupted during melting, the PCM follows an enthalpy curve that is located between the heating and cooling curves. This information is important to develop models for PCM used in buildings and further work is required to assess the impact of different factors on the transitional behavior.

## Nomenclature

| | |
|---|---|
| $A$ | Area [m²] |
| Bi | Biot number [-] |
| Fo | Fourier number [-] |
| $h$ | Enthalpy [J/g] |
| $i$ | Node [-] |
| $l$ | Left [-] |

$m$ Mass [g]

$n$ Number of nodes [-]

$r$ Right [-]

$T$ Temperature [°C]

$U$ Heat transfer coefficient [W/m²-K]

$t$ Time [s]

## 7.1 Introduction

Using phase change materials (PCM) to increase the building thermal mass is a possible solution for peak shaving and shifting of heating and cooling loads (Farid, Khudhair, Razack, & Al-Hallaj, 2004; Sharma et al., 2009). Recent efforts focus on developing models (Al-Saadi & Zhai, 2013; Dutil, Rousse, Salah, Lassue, & Zalewski, 2011) which generally rely on enthalpy-temperature curve(s) which define the PCM thermal behavior during heating and cooling processes. The PCM behavior during its two-phase state (liquid-solid state) remains uncertain. For example, if a PCM is cooled down after a partial melting, different scenarios are possible, as shown in Figure 7-1. A first scenario suggested by Bony and Citherlet (2007) is a transition to the cooling curve using a slope equivalent to the solid or liquid specific heat (wT). Chandrasekharan et al. (2013) have suggested a second option (noT) which consists in staying on the heating curve.

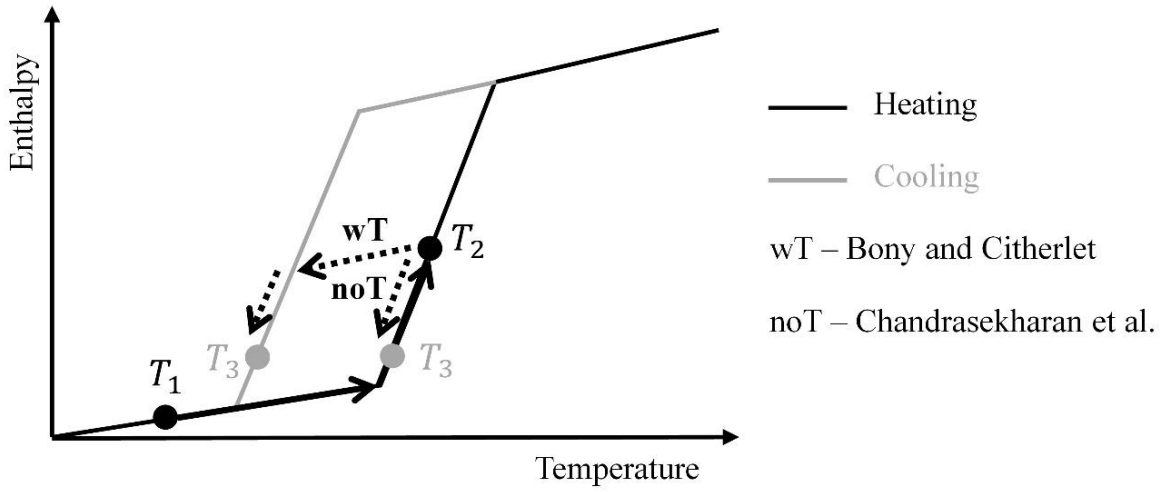


Figure 7-1: Possible behavior of a PCM cooled down after partial melting

The objective of this paper is to analyze the behavior of a commercially available PCM after partial melting or solidification. Specific experiments including partial heating and cooling cycles were performed on a PCM-equipped wall and two models were developed for both suggested scenarios. The comparison between experimental and simulated data will be used to identify the behavior of the tested PCM.

## 7.2 PCM modeling through an enthalpy method

Classical PCM models are based on the effective heat capacity (Goodrich, 1978) and enthalpy (Voller & Cross, 1981) methods. In this study, a 1-D enthalpy model is used for the PCM, expressed mathematically by the following differential equation:

$$\frac{dh_i}{dt} = \frac{U_{i,l}\,A}{m_i}\,(T_{i-1} - T_i) + \frac{U_{i,r}\,A}{m_i}\,(T_{i+1} - T_i) \qquad (7.1)$$

Equation ( 7.1 ) is developed for each node defined in the wall (Figure 7-2) and the entire system is then solved using a Forward Time and Central Space (FTCS) finite-difference method (Recktenwald, 2011). Temperatures are then related to enthalpy through the enthalpy-temperature curves. This method yields stable and reliable results if the Fourier number Fo and the expression Fo $(1 + \mathrm{Bi})$ are lower than or equal to 0.5 (Bergman et al., 2011), respectively for internal and surface nodes.

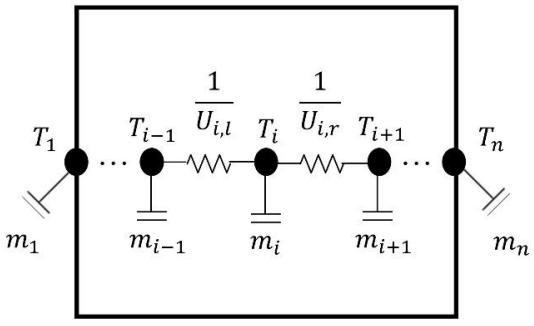


Figure 7-2: 1-D finite-difference model of a wall

## 7.3 Experimental set-up

The selected PCM is a bio-based product provided in a plastic film with PCM pouches (Phase change energy solutions, 2014). Additives (gelling agent and fire retardant) are included in the

product. Manufacturer data (Phase change energy solutions, 2014) on the PCM includes some properties for the pure PCM and some for the final product with additives. Table 7-1 summarizes the available data. The density and the thermal conductivity for the PCM with additives have been obtained through additional experimentations.

Table 7-1: PCM properties

| Without additives | | | With additives | | |
|---|---|---|---|---|---|
| Phase change temperature | °C | 23 | Phase change temperature | °C | 23 |
| Latent heat storage capacity | J/g | 203 | Latent heat storage capacity | J/g | 165-200 |
| Density | kg/m³ | 830 | | | |
| Specific heat (solid) | J/g-K | 1.84 | Weight per unit surface | kg/m² | 1.465 |
| Specific heat (liquid) | J/g-K | 1.99 | Density | kg/m³ | 883 * |
| Thermal conductivity (solid) | W/m-K | 0.207 | Thermal conductivity (solid and liquid) | W/m-K | 0.212 ^ |
| Thermal conductivity (liquid) | W/m-K | 0.171 | | | |
| * Experimental measurements (standard deviation: ± 10 kg/m³) – not from manufacturer | | | | | |
| ^ Experimental measurements (standard deviation: ± 0.022 W/m-K) – not from manufacturer | | | | | |

The tested wall consists of a double layer of plastic film with PCM pouches, sandwiched between two plywood boards. The wall has an area of 0.6 m² (1 m x 0.6 m) and is instrumented with thermocouples (accuracy: ± 0.5 °C) (Figure 7-3). The wall perimeter is insulated to avoid side-effects. The central layer composed of PCM, plastic film and air is modeled as an equivalent 1-D layer (Figure 7-4 (a)). The main properties of the wall are given in Table 7-2. Figure 7-4 (b) presents the enthalpy-temperature curves of the equivalent layer obtained from a model calibration performed on experimental data with complete heating/cooling cycles. Figure 7-4 (a) also shows the temperature values that are further presented and compared to experimental data. $T_{PCM}$ is compared to the mean value of $T_{in,pcm}$ and $T_{in}$ (Figure 7-3) weighted by the mass of each material in the equivalent layer (PCM (76 %) and others (24 %)). $T_{si}$ is compared to the mean value of $T_{si,1}$ and $T_{si,2}$. The same method as $T_{si}$ is applied for $T_{so}$.

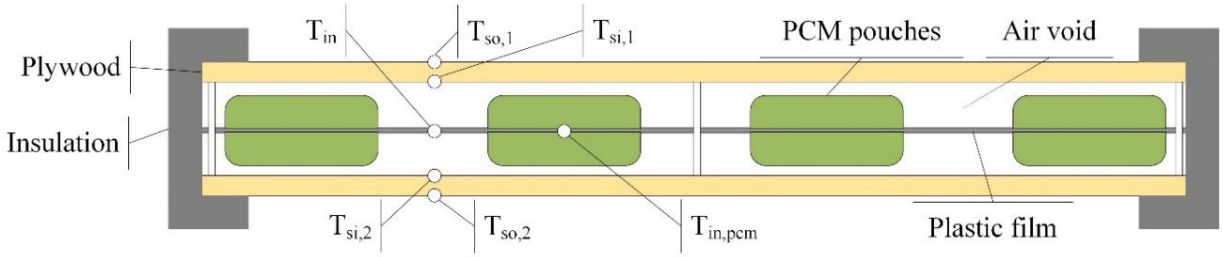


Figure 7-3: Instrumented PCM-equipped wall

Table 7-2: Layers properties

| Layer | Thickness [m] | Thermal conductivity [W/m-K] | Density [kg/m³] | Specific heat [J/g-K] |
|---|---|---|---|---|
| Plywood | 0.006 | 0.084 | 850 | 1.25 |
| Equivalent layer | 0.017 | 0.042* | 223 | See Figure 7-4 (b) |
| * Using THERM (Lawrence Berkeley National Laboratory, 2013) | | | | |

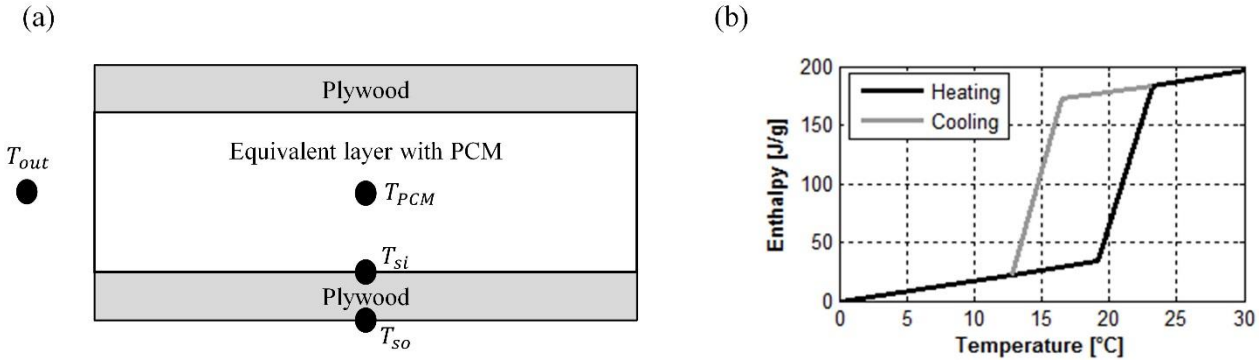


Figure 7-4: (a) PCM-equipped wall model; (b) Enthalpy-temperature curves of the equivalent layer

## 7.4 Results

### 7.4.1 Experimental data

Two series of experiments were performed on one PCM-equipped wall. Figure 7-5 (a) presents the interrupted heating scenario where the PCM-equipped wall, initially at a uniform cold temperature, is heated up by quickly transferring the wall into a warmer environment, until the PCM starts melting. Before the end of the phase change, the wall is quickly transferred back into the colder

environment. The interrupted cooling presented in Figure 7-5 (b) is the opposite scenario. Temperature results are given for the outside environment ($T_{out}$), outside surface ($T_{so}$), the interface between the plywood panel and the central equivalent layer ($T_{si}$) and the center of the equivalent layer ($T_{PCM}$). The most important observation is the steep PCM temperature change when heating is replaced by cooling (or conversely) during the phase change. It then reaches a new temperature plateau. This seems to agree with the idea that the PCM switches from the heating curve to the cooling one (or conversely).

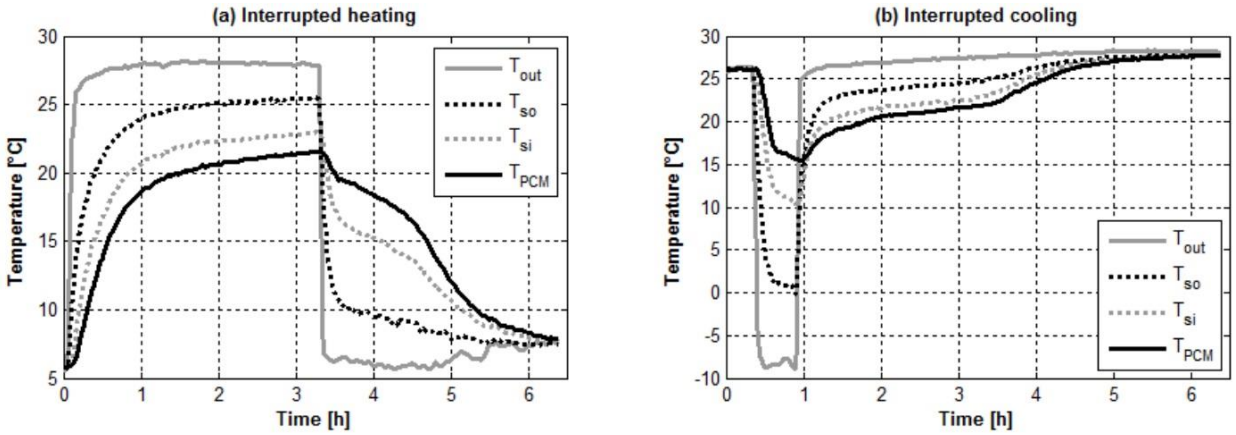


Figure 7-5: Experimental data for the interrupted heating (a) and cooling (b) scenarios

### 7.4.2 Comparison between experimentations and models

Simulations were performed using two models: first, a model which allows transition between the heating and cooling curves during phase change (Figure 7-1 – wT); secondly, a model which considers no transition during phase change (Figure 7-1 – noT). Both simulated scenarios are compared to experimental data in Figure 7-6. The model without transition does not agree with the experimental data. The model with transition is in good agreement with the experimental data of the interrupted cooling scenario with a root mean square deviation (RMSD) value of 0.37 °C (lower than the measurement accuracy of ± 0.5 °C). The agreement is not as good for the interrupted heating scenario: the "plateau" in the temperature curve associated with solidification starts earlier and is less pronounced in the experimental data than for the model with transition. The experimental results are enclosed between the two modeling options, with and without transition.

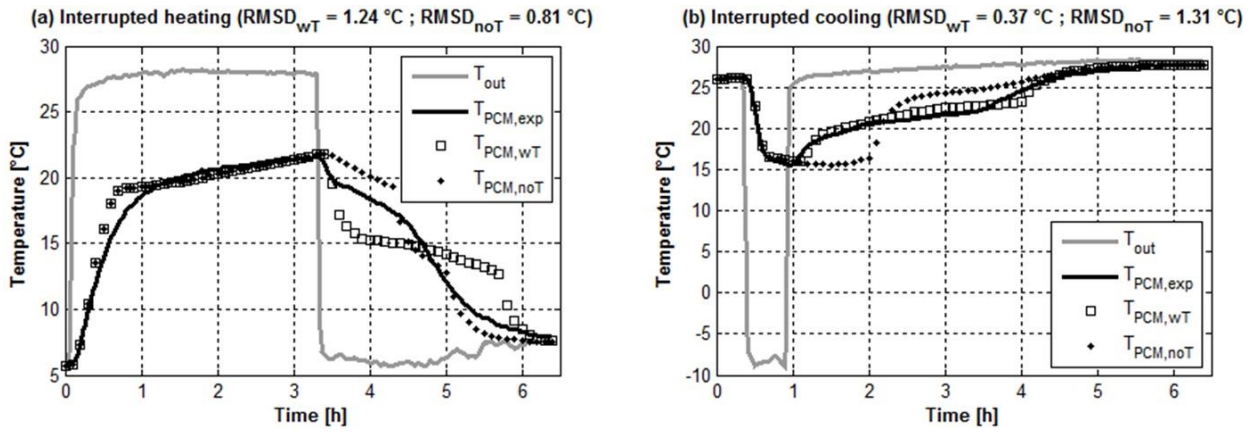


Figure 7-6: Comparison between experimental and simulated data for the interrupted heating (a) and cooling (b) scenarios

### 7.4.3 Mapping of a solution

An optimization algorithm was used in order to find the enthalpy-temperature curves that match the experimental and simulated data for both tests. The resulting temperature profiles are presented in Figure 7-7; they show a good agreement with experimental data, with RMSD values of 0.64 °C and 0.28 °C, respectively for the interrupted heating and cooling scenarios. Both values are close to the measurement accuracy of ± 0.5 °C.

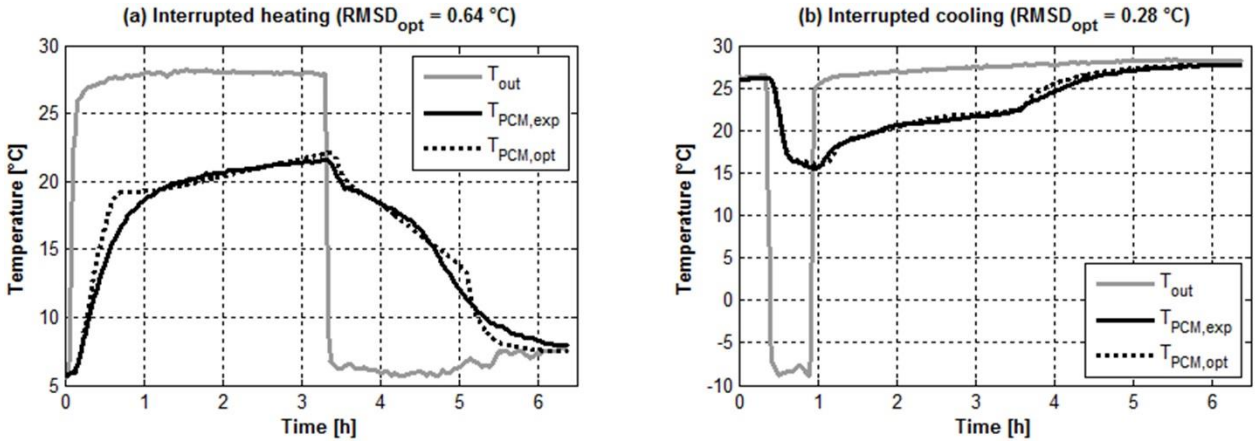


Figure 7-7: Comparison between experimental and optimized simulated data for the interrupted heating (a) and cooling (b) scenarios

Figure 7-8 shows the path followed by the PCM on the enthalpy-temperature curves for both scenarios according to the optimization results. Initial curves (solid lines) from Figure 7-4 (b) are preserved while the optimized curve (dotted lines) followed by the PCM after the transition is also

presented for each test. The PCM is first heated/cooled from $T_1$ to $T_2$, following the initial heating/cooling curve. A partial transition then occurs between $T_2$ and $T_3$ towards an intermediate cooling or heating curve. The assumption that the transition follows a line of constant specific heat close to the solid and liquid values is verified in our case. The PCM then follows this intermediate curve until the end of the phase change (between $T_3$ and $T_4$), and it finally returns to the initial enthalpy curve between $T_4$ and $T_5$.

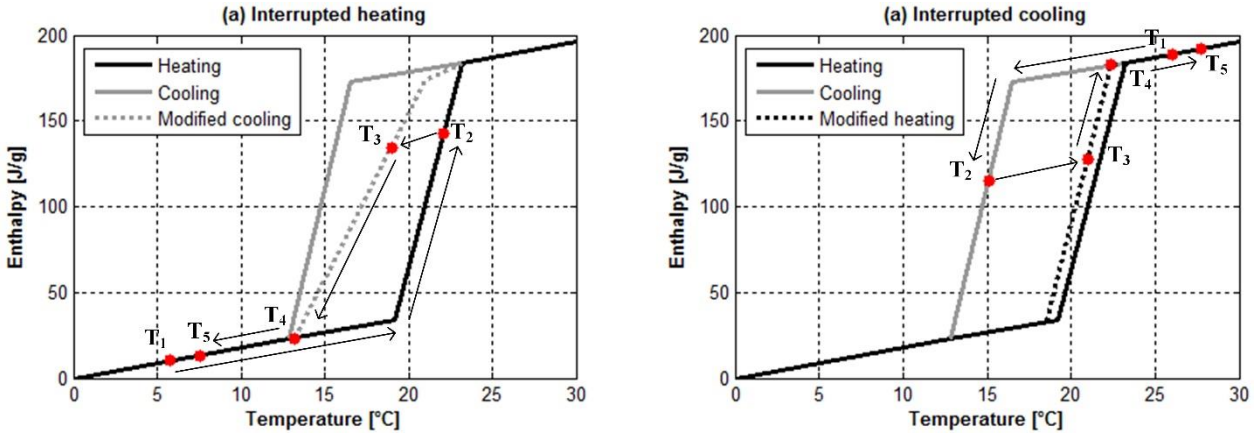


Figure 7-8: Thermal behavior mapping of the optimized solution

The location of the intermediate curve (Figure 7-8) between the heating and cooling curves is different in the interrupted heating and cooling scenarios. Experimental data (Figure 7-5) shows that the driving force to heat up or cool down the wall is different in both cases: the difference between the environment and PCM temperatures when the transition is initiated is about 15 °C in the interrupted heating scenario and 10 °C in the other scenario. This could play a role in the different transitional behavior.

## 7.5 Conclusions and further research

This paper presents a comparison between experimental and simulated data in order to evaluate the thermal behavior of a PCM when its phase change is interrupted. Experimentations were performed by quickly transferring a PCM-equipped wall section from a cold to a hot environment, and conversely. In parallel, two models were developed to simulate the thermal behavior of a PCM-equipped wall according to two scenarios to describe the behavior of the PCM after an interrupted melting or solidification process. The comparison between experimental and simulated data shows that the PCM studied in this paper is subject to a rapid transition between the heating and cooling

curves if the heating or cooling process is interrupted during phase change. For the interrupted heating process, the transition is partial and the PCM follows an enthalpy curve which is located between the heating and cooling curves. Further research will aim at assessing the impact of different factors such as the heat transfer rate on the transitional behavior.

# References

Al-Saadi, S. N., & Zhai, Z. (John). (2013). Modeling phase change materials embedded in building enclosure: A review. Renewable and Sustainable Energy Reviews, 21, 659–673. doi:10.1016/j.rser.2013.01.024

Bergman, T. L., Lavine, A. S., Incropera, F. P., & Dewitt, D. P. (2011). Fundamentals of heat and mass transfer. Wiley.

Bony, J., & Citherlet, S. (2007). Numerical model and experimental validation of heat storage with phase change materials. Energy and Buildings, 39, 1065–1072. Retrieved from http://www.sciencedirect.com/science/article/pii/S037877880600291X

Chandrasekharan, R., Lee, E. S., Fisher, D. E., & Deokar, P. S. (2013). An Enhanced Simulation Model for Building Envelopes with Phase Change Materials. ASHRAE Transactions, 119(2).

Dutil, Y., Rousse, D. R., Salah, N. Ben, Lassue, S., & Zalewski, L. (2011). A review on phase-change materials: Mathematical modeling and simulations. Renewable and Sustainable Energy Reviews, 15, 112–130. Retrieved from http://www.sciencedirect.com/science/article/pii/S1364032110001589

Farid, M. M., Khudhair, A. M., Razack, S. A. K., & Al-Hallaj, S. (2004). A review on phase change energy storage: materials and applications. Energy Conversion and Management, 45(9–10), 1597–1615. doi:http://dx.doi.org/10.1016/j.enconman.2003.09.015

Goodrich, L. E. (1978). Efficient numerical technique for one-dimensional thermal problems with phase-change. International Journal of Heat and Mass Transfer, 21(5), 615.

Lawrence Berkeley National Laboratory. (2013). THERM 6.3 / WINDOW 6.3 - NFRC Simulation Manual.

Phase change energy solutions. (2014). Manufacturing innovative thermal storage technologies for smart & sustainable buildings. Retrieved February 9, 2015, from http://www.phasechange.com/index.php

Recktenwald, G. W. (2011). Finite-Difference Approximations to the Heat Equation (Vol. 0). Portland, Oregon, USA. Retrieved from http://www.f.kth.se/~jjalap/numme/FDheat.pdf

Sharma, A., Tyagi, V. V, Chen, C. R., & Buddhi, D. (2009). Review on thermal energy storage with phase change materials and applications. Renewable and Sustainable Energy Reviews, 13(2), 318–345. doi:http://dx.doi.org/10.1016/j.rser.2007.10.005

Voller, V., & Cross, M. (1981). Accurate solutions of moving boundary problems using the enthalpy method. International Journal of Heat and Mass Transfer, 24(3), 545.

# CHAPTER 8 ARTICLE 4: MODELING OF A WALL WITH PHASE CHANGE MATERIALS. PART I: DEVELOPMENT AND NUMERICAL VALIDATION

Delcroix, B., Kummert, M., Daoud, A., (2015). Modeling of a wall with phase change materials. Part I: Development and numerical validation. Submitted to Journal of Building Performance Simulation on the 15th of July 2015.

## Abstract

This paper presents a new TRNSYS model of a wall with variable properties, named Type 3258 and dedicated to modeling phase change materials (PCMs) in the building envelope. The 1-D conduction heat transfer equation is solved using an explicit finite-difference method coupled with an enthalpy method to take into account the variable PCM thermal capacity. This model includes temperature-dependent thermal conductivity as well as PCM-specific effects such as hysteresis and subcooling. The stability conditions are discussed and the algorithm implemented in TRNSYS is described. A numerical validation performed on wall test cases proposed by the International Energy Agency (Annex 23) is presented, showing that the developed model is in agreement with reference models. The paper also discusses the impact of temporal and spatial discretization on the model performance. Modeling problems encountered when using an effective heat capacity method (compared to an enthalpy method) and subcooling modeling issues are also highlighted.

## Nomenclature

*Abbreviations*

| | |
|---|---|
| BPS | Building Performance Simulation |
| C-N | Crank-Nicolson |
| FD | Finite-Difference |
| PCM(s) | Phase Change Material(s) |
| RMSD | Root Mean Square Deviation |

*Variables*

| | |
|---|---|
| $A$ | Surface area [m²] |
| Bi | Biot number [-] |
| $C$ | Space discretization constant [-] |
| $C_p$ | Specific heat [J/kg-K or J/g-K] |
| Fo | Fourier number [-] |
| $H$ | Enthalpy [J/kg] |
| $h$ | Convective heat transfer coefficient [W/m²-K] |
| $h_g$ | Global heat transfer coefficient [W/m²-K] |
| $k$ | Thermal conductivity [W/m-K] |
| $L$ | Thickness of layer [m] |
| $m$ | Mass [kg] |
| $n$ | Number of nodes [-] |
| $\dot{Q}$ | Heat flow [W] |
| $R$ | Thermal resistance [m²K/W] |
| $T$ | Temperature [°C] |
| $t$ | Time [s] |
| $\alpha$ | Thermal diffusivity [m²/s] |
| $\Delta H$ | Enthalpy variation [J/kg] |
| $\Delta t$ | Time-step [s] |
| $\Delta x$ | Half-interval between 2 nodes [m] |
| $\rho$ | Density [kg/m³] |
| *Subscripts* | |
| $ext$ | Exterior |
| $f$ | Final (time-step) |

| | |
|---|---|
| $i$ | Initial (time-step) |
| $in$ | Inside |
| $int$ | Interior |
| $new$ | Final (internal time-step) |
| $norm$ | Normalized |
| $old$ | Initial (internal time-step) |
| $out$ | Outside |
| $si$ | Inside surface |
| $so$ | Outside surface |
| $s-s$ | Steady-state |

## 8.1 Introduction

Using phase change materials (PCMs) and their high energy storage capacity in building envelopes to increase thermal mass is an interesting option in order to mitigate inside temperature fluctuations. Increasing thermal inertia is an effective manner for maintaining thermal comfort and stabilizing space cooling and heating loads. Models have been developed for predicting their thermal behavior in several Building Performance Simulation (BPS) programs, such as TRNSYS (Klein et al., 2012), EnergyPlus (Crawley et al., 2001), ESP-r (Energy Systems Research Unit, 1998) or BSim (Danish Building Energy Institute, 2013). Most models rely on enthalpy-temperature or specific heat-temperature curves to represent the variable PCM thermal capacity. Different levels of modeling complexity can be found, from a simple one-curve model to a two-curve model with additional PCM specific effects (see Table 8-1). Figure 8-1 (a) shows the most complex case with a two-curve representation including hysteresis and subcooling. Hysteresis is the temperature difference between heating and cooling enthalpy-temperature curves during phase change. Subcooling is a process that occurs during cooling of a liquid PCM. The temperature decreases below the solidification temperature while the PCM remains liquid (Günther et al., 2007). It is followed by a nucleation process coupled with a steep temperature increase, leading to solidification. Kuznik and Virgone (2009) and Günther et al. (2007) have shown that both effects

(hysteresis and subcooling) can be significant. Figure 8-1 (b) shows another issue that is rarely addressed in PCM modeling, which is the material behavior when heating ($T_h$ in Figure 8-1 (b)) or cooling ($T_c$ in Figure 8-1 (b)) is interrupted before the phase change is complete. In the literature, different methods have been used. Bony and Citherlet (2007) suggested that a transition is performed between cooling and heating curves using a slope equal to the solid or liquid specific heat. A second scenario suggested by Rose et al. (2009) and implemented in BSim is an instantaneous transition. The third option, proposed by Chandrasekharan et al. (2013), suggests that there is no transition, i.e. that the PCM remains on the same enthalpy curve. This latter option is applied when using a one-curve method.

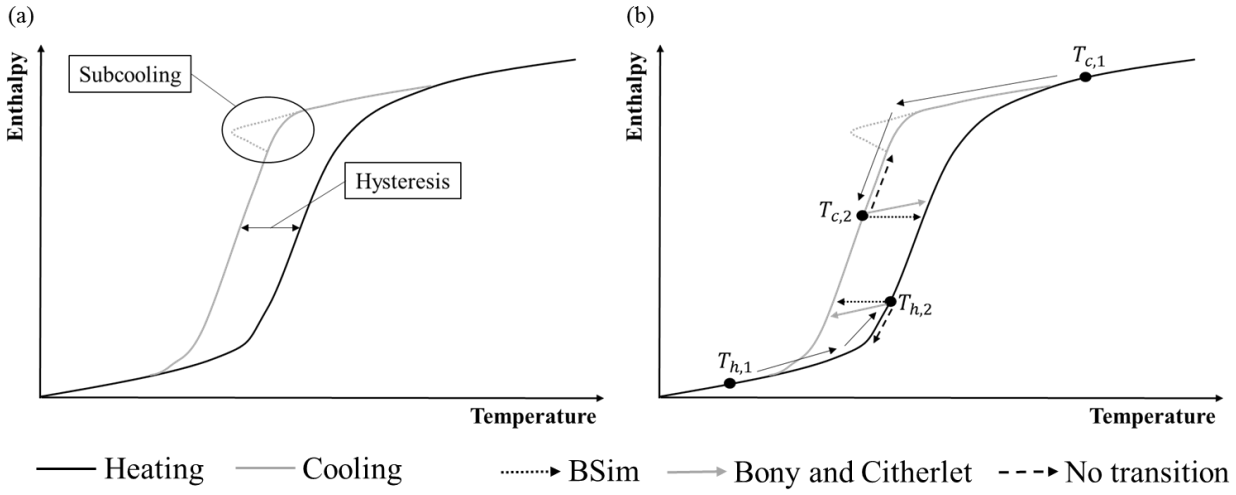


Figure 8-1: (a) PCM specific effects and (b) transitional PCM thermal behavior during phase change

In the majority of BPS programs, heat conduction through walls is considered unidimensional. In order to model the non-linear PCM thermal behavior, the effective heat capacity (Goodrich, 1978; Yao & Chait, 1993) and enthalpy methods (Voller & Cross, 1981) are often used. The starting point of both methods is the 1-D conduction heat transfer equation:

$$\rho\, C_p \frac{dT}{dt} = \frac{d\left(k \frac{dT}{dx}\right)}{dx} \qquad (8.1)$$

Using an effective heat capacity method means that the $C_p$ value in Equation ( 8.1 ) is adapted depending on temperature conditions.

An enthalpy formulation can be expressed, knowing that the variation of enthalpy $\Delta H$ of a material going from an initial temperature $T_i$ to a final temperature $T_f$ is given by the following equation:

$$\Delta H = \int_{T_i}^{T_f} C_p \, dT \qquad ( 8.2 )$$

Combining Equations ( 8.1 ) and ( 8.2 ), the governing conduction heat transfer equation can be reformulated using an enthalpy term:

$$\rho \frac{dH}{dt} = \frac{d\left(k \frac{dT}{dx}\right)}{dx} \qquad ( 8.3 )$$

Table 8-1 presents different models that can be used in TRNSYS to simulate a wall with PCM. These TRNSYS models are encapsulated in components called “Types”:

- Type 1270 (Thermal Energy Systems Specialists, 2012) is a very simple PCM model: it considers a constant-temperature phase change and a spatially uniform temperature inside the PCM layer. Type 1270 is only able to model a PCM layer and must be complemented with Type 56 (TRNSYS multizone building model) to model the other wall parts.
- Type 260 (Kuznik, Virgone, & Johannes, 2010) uses a fully implicit finite-difference method coupled with the effective heat capacity method to model PCM. Thermal conductivity can be defined as variable, depending on the PCM state. Thermal properties are based on the previous time-step. Hysteresis is not modeled.
- Type 399 (Arno Dentel & Stephan, 2013) also uses an effective heat capacity method but the conduction heat transfer governing equation is solved with a Crank-Nicolson finite-difference method. Thermal conductivity is constant, but two different $C_p(T)$ curves can be defined for both heating and cooling processes to take hysteresis into account. Like Type 260, thermal properties are based on the previous time-step. Type 399 also has the capability to model embedded tubes with fluid circulation for heating and cooling (known as “active layers” in TRNSYS). This capability is unique among the components listed in Table 8-1.

- Type 285 (Al-Saadi & Zhai, 2014) uses an iterative fully implicit finite-difference coupled with an enthalpy method for modeling PCMs. Defining temperature-dependent thermal conductivity, hysteresis or subcooling is not possible with this model.
- TRNSYS Type 3258 is the new model presented in the present paper. Unlike the other models, this type is able to model PCM with hysteresis, subcooling and temperature-dependent thermal conductivity. It uses an explicit finite-difference method coupled with an enthalpy method.

Table 8-1: TRNSYS PCM models for building walls and their possibilities

| Characteristics | Type 1270 | Type 260 | Type 399 | Type 285 | Type 3258 |
|---|---|---|---|---|---|
| PCM modeling method | Constant-temperature phase change | Effective heat capacity method | | Enthalpy method | |
| Numerical method | Lumped capacitance model | Implicit FD method | Semi-implicit FD method (C-N) | Iterative implicit FD method | Explicit FD method |
| Hysteresis | No | | Yes | No | Yes |
| Subcooling | No | | | | Yes |
| Transition between heating and cooling curves | Not possible (one-curve model) | | Instantaneous switch between $C_p(T)$ curves. | Not possible (one-curve model) | Optional: Bony and Citherlet, or no transition (see Figure 8-1 (b)) |
| Variable thermal conductivity | No | Yes | No | No | Yes |

Besides these TRNSYS components, other PCM models exist in common BPS programs such as EnergyPlus and ESP-r:

- EnergyPlus uses an enthalpy method combined with an iterative finite-difference method using a Crank-Nicolson or fully implicit scheme (Pedersen, 2007). This model uses a one-curve method, which is unable to represent hysteresis and subcooling. Temperature-dependent thermal conductivity can be defined.

- ESP-r also proposes a PCM model based on the effective heat capacity method (Heim & Clarke, 2004) and solved with a finite-difference method. The thermal conductivity can be defined for solid and liquid states. The original implementation cannot model hysteresis or subcooling. Geissler (2008) recently implemented in ESP-r a development version of a subroutine based on the work of Hoffman (2006) allowing to model hysteresis.

## 8.2 Objectives

This paper presents a newly developed TRNSYS component (Type) used for simulating a wall including layer(s) with temperature-dependent properties. It also presents its numerical validation using wall test cases proposed by the International Energy Agency and a discussion about its performance in terms of CPU time and the number of nodes implemented in the model. Practical examples are used to demonstrate the advantage of using an enthalpy method instead of an effective heat capacity method. Particular attention is given to instances in which some models can miss phase change episodes and to the PCM thermal behavior when phase change is interrupted (transitional behavior between heating and cooling curves). This paper ends with a discussion about subcooling modeling.

The experimental validation of the new model and the methodology to use it in conjunction with the TRNSYS multizone building model (Type 56) are discussed in Part II of this paper (Delcroix, Kummert, & Daoud, 2015b).

## 8.3 Model algorithm

The proposed model is intended to be used within whole building performance simulation. In line with the assumptions generally made when calculating the building heat balance, heat transfer through walls is assumed to be unidimensional. A wall model using a 1-D finite-difference method can be represented such as in Figure 8-2. The wall is spatially discretized in nodes with heat storage capacity. Two nodes are separated by a thermal resistance $R$. The length $\Delta x$ is the half-space represented by a node or the whole space represented by a half-node. Half-nodes are the first and last nodes of each layer.

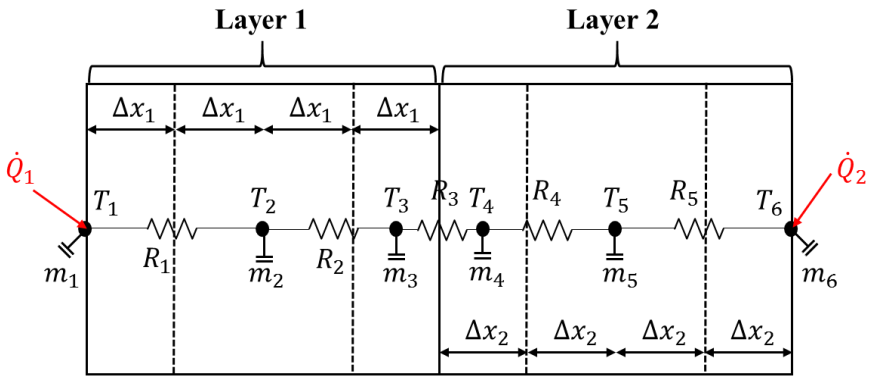


Figure 8-2: 1-D finite-difference model of a 2-layer wall with 6 nodes

Typical node distributions schemes in wall models include nodes at the interfaces between two layers. It is not the case in the proposed model to avoid having to combine two different enthalpy-temperature curves to define the node properties. If required, the interface temperature can be linearly interpolated at a later stage. For example, the interface temperature $T_{interf}$ between nodes 3 and 4 (Figure 8-2) is calculated such as:

$$T_{interf} = \frac{\frac{\Delta x_2}{k_2}}{\left(\frac{\Delta x_1}{k_1} + \frac{\Delta x_2}{k_2}\right)} T_3 + \frac{\frac{\Delta x_1}{k_1}}{\left(\frac{\Delta x_1}{k_1} + \frac{\Delta x_2}{k_2}\right)} T_4 \qquad ( 8.4 )$$

Equation ( 8.3 ) is differently expressed for surface and internal nodes. For surface nodes (e.g. node 1), it can be mathematically expressed as follows:

$$m_1 \frac{dH_1}{dt} = \frac{A}{R_1} (T_2 - T_1) + \dot{Q}_1 \qquad ( 8.5 )$$

Where $\dot{Q}_1$ is the heat transfer including radiative and convective heat exchange going into (+) or out (-) from the wall.

For internal nodes (e.g. node 2), only conductive heat transfer is considered:

$$m_2 \frac{dH_2}{dt} = \frac{A}{R_1} (T_1 - T_2) + \frac{A}{R_2} (T_3 - T_2) \qquad ( 8.6 )$$

Using a Forward Time and Central Space (FTCS) finite-difference method (Bergman et al., 2011), Equations ( 8.5 ) and ( 8.6 ) are discretized such as:

$$H_1^{t+1} = \frac{\Delta t\ A}{R_1\ m_1}(T_2^t - T_1^t) + \frac{\Delta t\ \dot{Q}_1}{m_1} + H_1^t \quad (8.7)$$

And:

$$H_2^{t+1} = \frac{\Delta t\ A}{R_1\ m_2}(T_1^t - T_2^t) + \frac{\Delta t\ A}{R_2\ m_2}(T_3^t - T_2^t) + H_1^t \quad (8.8)$$

Since the FTCS method is explicit, stability conditions (Bergman et al., 2011) must be met. For internal nodes, the Fourier number $Fo$ must be equal to or lower than 0.5:

$$\text{Fo} = \frac{\alpha\ \Delta t}{\Delta x^2} \leq \frac{1}{2} \quad (8.9)$$

The stability condition required for the surface nodes involves the Biot number and is often more restrictive:

$$\text{Fo}\ (1 + \text{Bi}) = \frac{\alpha\ \Delta t}{\Delta x^2}\left(1 + \frac{h_g\ \Delta x}{k}\right) \leq \frac{1}{2} \quad (8.10)$$

The choice of the number of nodes $n$ per layer depends on the thermal diffusivity $\alpha$, the time-step $\Delta t$, the thickness $L$ and the space discretization constant $C$ (Equation ( 8.11 )). This constant is in fact the inverse of the Fourier number that will result from the discretization, and it is traditionally set to a value of 3 in order to obtain a Fourier number of 1/3 which meets the stability criterion. This method is for example used in EnergyPlus (2014).

$$n = floor\left(\frac{L}{\sqrt{C\ \alpha\ \Delta t}}\right) \quad (8.11)$$

The minimum number of nodes per layer is set to 3. An uneven number of nodes is also imposed so that there is always one node for the center of the layer.

Figure 8-3 presents a diagram of the steps performed by the proposed model. A first initialization step deals with obtaining and checking input parameters and external files. The external files define the temperature-dependent thermal conductivity and the $H(T)$ curve(s) of each layer. This step also sets the number of nodes (as defined by Equation ( 8.11 )) and the internal time-step required to

meet the stability conditions (Equations ( 8.9 ) and ( 8.10 )). The worst case scenario is used to meet the stability conditions, i.e. using the most diffusive properties (the highest thermal conductivity and the lowest specific heat for layers with variable properties).

The next step stores variables that will be required the next time the same instance of the Type will be used (TRNSYS components can be used several times in the same simulation).

Once the simulation starts, two major loops are performed: one for each simulation time-step and one for internal time-steps. For each internal time-step, the first stage consists in calculating the new enthalpy values $H_{new}$ for each node, depending on initial conditions ($H_{old}$ and $T_{old}$) and boundary conditions (Equations ( 8.7 ) and ( 8.8 )). A second step consists in computing the new node temperatures $T_{new}$. For a layer without variable thermal capacity, the following equation is applied:

$$T_{new} = T_{old} + \frac{H_{new} - H_{old}}{C_p} \qquad (8.12)$$

For layers with variable thermal capacity, their new node temperatures depend on the $H(T)$ graph. Figure 8-4 takes the most complex case: the PCM thermal behavior is defined by two curves including subcooling. The graph is divided in five possible zones. Zones 1 and 2 are respectively the heating and cooling curves (excluding subcooling). Zone 3 is accessible only if transition between heating and cooling curves is allowed when phase change is interrupted (see Figure 8-1 (b)). The behavior during such an interrupted phase change is set by one of the Type's parameters. Zone 4 is the subcooling curve. It is accessible only if the entire PCM is initially totally liquid ($H \geq H_{liquid}$) and experiences a continuous cooling process. When subcooling occurs, it is assumed that the entire layer experiences this effect (as explained further in section 8.8). Finally, zone 5 is a transition phase if heating interrupts subcooling. In this case, new temperatures are computed using a $C_p$ value equivalent to the specific heat in the liquid state.

Once all node temperatures are determined, new finite-difference coefficients must be computed if one or more layers has a variable thermal conductivity (depending on the final temperature). If there is no variable thermal conductivity, the finite-difference coefficients remain constant during the whole simulation. These steps are repeated until the entire internal loop is completed.

The next step consists in setting output values. TRNSYS requires average values to be exchanged between Types, so average temperatures $T_{mean}$ are computed as follows:

$$T_{mean} = \frac{T_f + T_i}{2} \qquad (8.13)$$

The variation of the enthalpy inside the wall over a time-step is also set as output and is equal to the difference between initial and final enthalpy values $H_i$ and $H_f$.

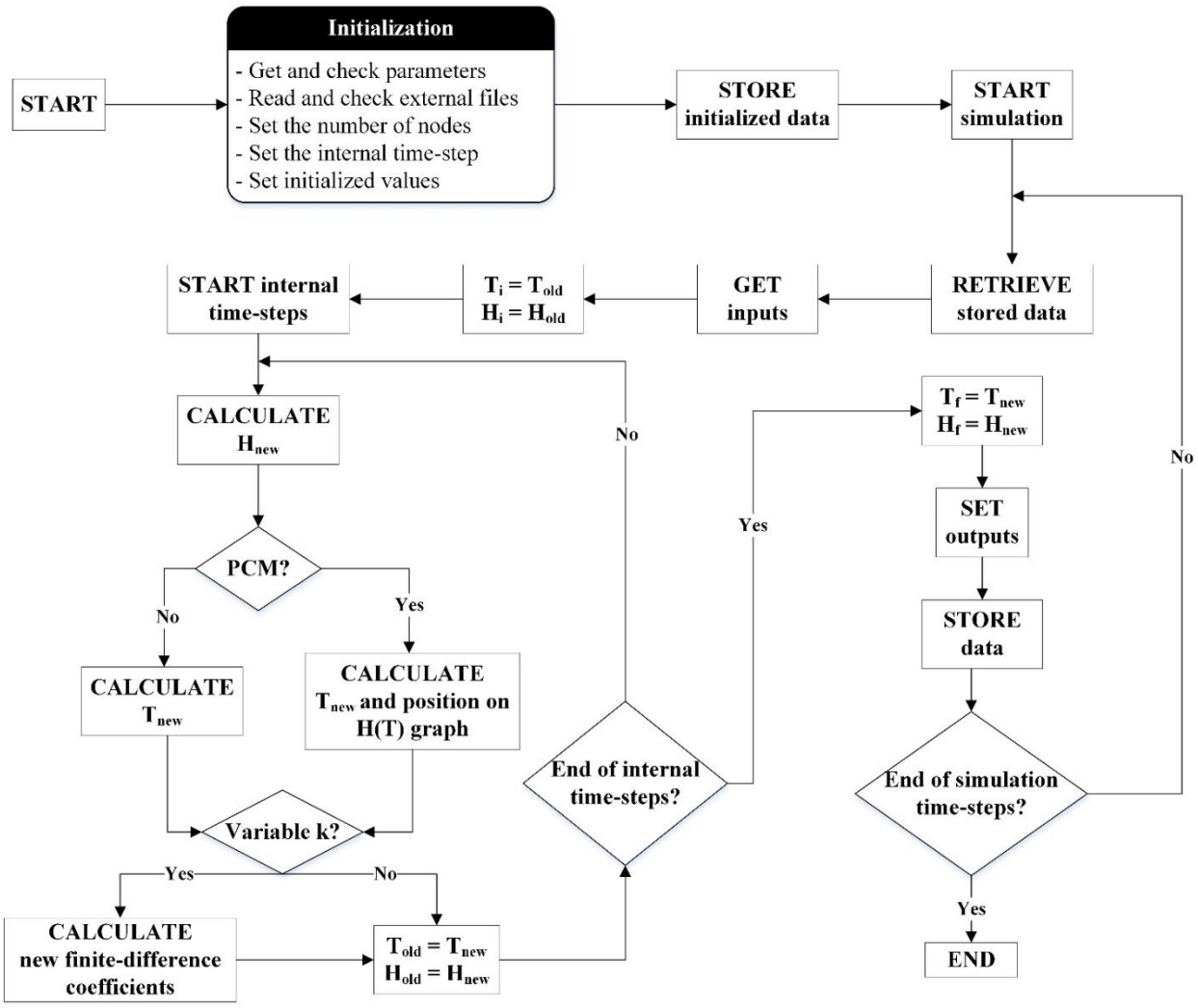


Figure 8-3: Process scheme of the algorithm

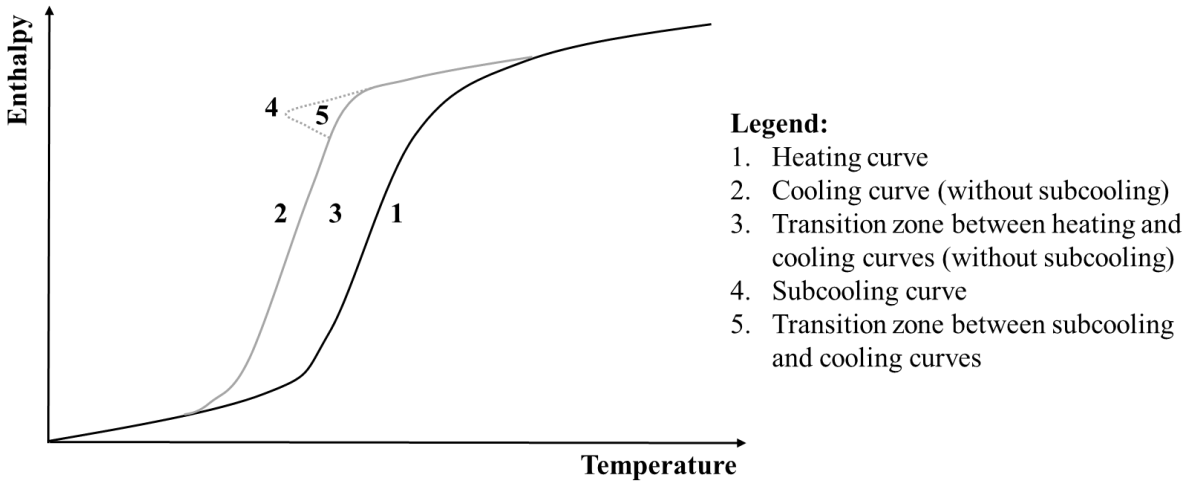


Figure 8-4: Schematic zones of an enthalpy-temperature graph used during simulation

## 8.4 Numerical validation

Numerical validation through model comparison performed on simple wall test cases is proposed by the International Energy Agency (IEA) (Haghighat et al., 2013; Johannes et al., 2011). Wall test cases are defined with materials described in Table 8-2. The PCM thermal capacity and conductivity depending on its temperature are given in Figure 8-5. As there is only one curve in Figure 8-5 (a), the PCM experiences no hysteresis or subcooling.

Table 8-2: Material properties

| Material | Thermal conductivity [W/m-K] | Density [kg/m³] | Specific heat [J/g-K] |
|---|---|---|---|
| Concrete | 1.20 | 2000 | 1.0 |
| Insulation | 0.04 | 50 | 1.0 |
| Gypsum | 0.14 | 800 | 1.5 |
| PCM | See Figure 8-5 (b) | 1100 | See Figure 8-5 (a) |

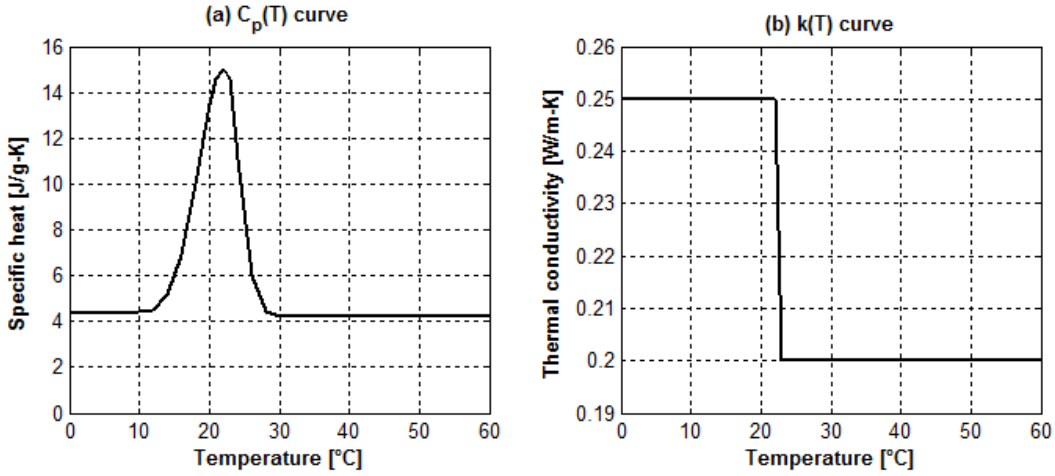


Figure 8-5: (a) Specific heat-temperature curve and (b) thermal conductivity-temperature curve of the PCM used in the test cases

The nine wall cases proposed by the IEA are defined in Table 8-3. The left part of the table presents the nomenclature of each layer while the right part gives the wall configuration for each case. The first three cases are only composed of a PCM layer while the six following others are 2-layer walls.

Table 8-3: Case studies

| Layer (nomenclature) | Material | Thickness [mm] | | Case | Wall configuration | |
|---|---|---|---|---|---|---|
| | | | | | External (layer 1) | Internal (layer 2) |
| C30 | Concrete | 30 | | 1 | P5 | - |
| C200 | Concrete | 200 | | 2 | P10 | - |
| I100 | Insulation | 100 | | 3 | P50 | - |
| G10 | Gypsum | 10 | | 4 | C30 | P10 |
| P5 | PCM | 5 | | 5 | P10 | C30 |
| P10 | PCM | 10 | | 6 | C200 | P10 |
| P50 | PCM | 50 | | 7 | P10 | C200 |
| | | | | 8 | I100 | P10 |
| | | | | 9 | P10 | I100 |

The boundary conditions are defined in Figure 8-6. They are the same for each case. The inside temperature is constant (20 °C). The outside temperature goes linearly from 12 °C initially to 32 °C during the first hour, and remains constant after that. The inside and outside convection coefficients remain constant at 2.5 W/m²-K and 8 W/m²-K, respectively. Radiative heat transfer is ignored. The

initial wall temperature is 12 °C. The results comparison focuses on the evolution of the inside and outside surface temperatures $T_{si}$ and $T_{so}$.

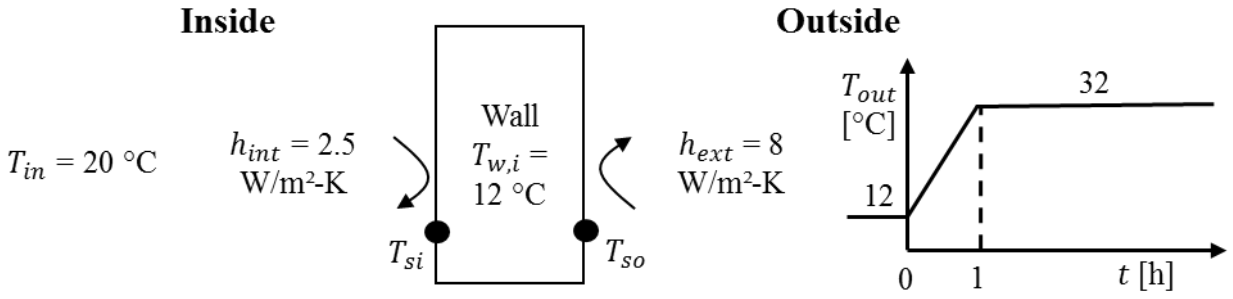


Figure 8-6: Initial and boundary conditions used for the test cases

These nine test cases have been initially simulated with six different models from France, China, Norway, Spain, Canada and Sweden (Haghighat et al., 2013). Detailed results are only available for France and Norway (Johannes et al., 2011). Our model results are compared to these two models. The French results are given using TRNSYS Type 260 developed by Kuznik et al. (2010). No details on the Norwegian model were found in the IEA report (Haghighat et al., 2013).

Figure 8-7 presents the results comparison for each case and Table 8-4 gives the corresponding Root Mean Square Deviation (RMSD) values between each model for both inside and outside surface temperatures $T_{si}$ and $T_{so}$. These results show that the developed model is closer to the Norwegian model for the two first cases and closer to the French model for the others. Steady-state conditions at the end of the simulation are nearly equivalent for all models. The greatest $RMSD$ values for both inside and outside surface temperatures are observed between the French and Norwegian models for the second case. For each case and both temperatures, lower $RMSD$ values between the developed model and a reference model than between reference models are observed. The only exception is the third case for the outside surface temperature. This shows that the proposed model is within the reference range provided by the IEA report.

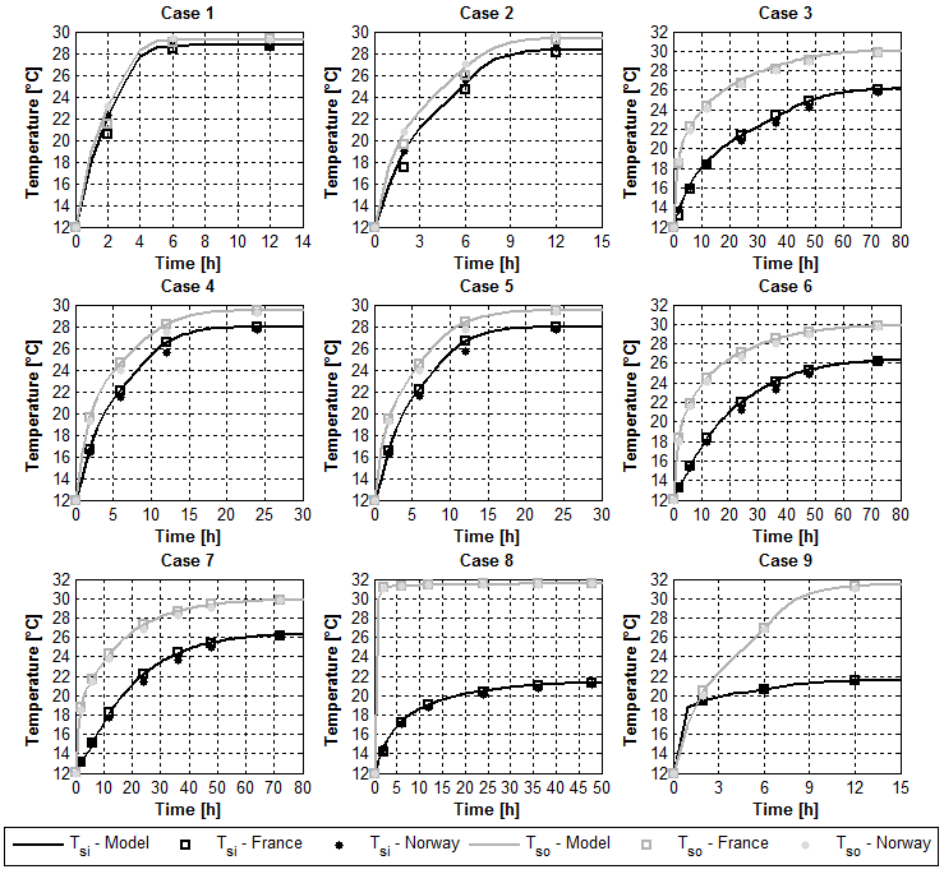


Figure 8-7: Comparison between reference models and the new model for each case

Table 8-4: Root mean square deviations [°C] for each case

| Case | $T_{si}$ – France VS Norway | $T_{si}$ – France VS Model | $T_{si}$ – Norway VS Model | $T_{so}$ – France VS Norway | $T_{so}$ – France VS Model | $T_{so}$ – Norway VS Model |
|---|---|---|---|---|---|---|
| 1 | 0.5980 | 0.5781 | 0.0511 | 0.5414 | 0.5328 | 0.0468 |
| 2 | 0.6293 | 0.6071 | 0.1285 | 0.5558 | 0.5174 | 0.1132 |
| 3 | 0.4645 | 0.2991 | 0.4001 | 0.2062 | 0.2502 | 0.3449 |
| 4 | 0.3957 | 0.0500 | 0.4325 | 0.3641 | 0.0416 | 0.3892 |
| 5 | 0.3825 | 0.0574 | 0.4040 | 0.3314 | 0.0431 | 0.3610 |
| 6 | 0.4037 | 0.0512 | 0.4195 | 0.3442 | 0.0522 | 0.3366 |
| 7 | 0.4167 | 0.0468 | 0.4003 | 0.3409 | 0.0456 | 0.3200 |
| 8 | 0.2198 | 0.1362 | 0.2162 | 0.0437 | 0.0219 | 0.0285 |
| 9 | 0.0386 | 0.0345 | 0.0379 | 0.2181 | 0.0226 | 0.2280 |

Surface heat-flows are also compared between all models. The inside and outside surface heat-flows $\dot{Q}_{si}$ and $\dot{Q}_{so}$ are computed as follows:

$$\dot{Q}_{si} = h_{int}(T_{in} - T_{si}) \quad (8.14)$$

$$\dot{Q}_{so} = h_{ext}(T_{out} - T_{so}) \quad (8.15)$$

Table 8-5 indicates the steady-state heat-flows (i.e. at the end of the 120-hour simulations) for all models and the maximum difference observed between the developed model and one of the reference models (France or Norway). The maximum difference of 3 % is acceptable given the other uncertainty sources in building simulation and is also within the range of the differences observed between the two reference models in the IEA test cases.

Table 8-5: Steady-state surface heat-flows [W/m²] (after 120 hours)

| Case | $\dot{Q}_{si}$ – France | $\dot{Q}_{si}$ – Norway | $\dot{Q}_{si}$ – Model | Max. diff. with reference [%] ($\dot{Q}_{si}$) | $\dot{Q}_{so}$ – France | $\dot{Q}_{so}$ – Norway | $\dot{Q}_{so}$ – Model | Max. diff. with reference [%] ($\dot{Q}_{so}$) |
|---|---|---|---|---|---|---|---|---|
| 1 | 21.75 | 21.83 | 21.83 | 0.34 | 21.60 | 21.84 | 21.84 | 1.11 |
| 2 | 20.75 | 20.88 | 20.88 | 0.60 | 20.80 | 20.88 | 20.88 | 0.38 |
| 3 | 15.75 | 15.50 | 15.48 | 1.75 | 16.00 | 15.44 | 15.52 | 3.00 |
| 4 | 20.00 | 20.00 | 20.00 | 0.00 | 20.00 | 20.00 | 20.00 | 0.00 |
| 5 | 20.00 | 20.00 | 20.00 | 0.00 | 20.00 | 20.00 | 20.00 | 0.00 |
| 6 | 16.25 | 16.13 | 16.15 | 0.62 | 16.00 | 16.32 | 16.24 | 1.50 |
| 7 | 16.25 | 16.18 | 16.15 | 0.62 | 16.00 | 16.16 | 16.24 | 1.50 |
| 8 | 4.00 | 3.88 | 3.90 | 2.50 | 4.00 | 3.92 | 3.92 | 2.00 |
| 9 | 4.00 | 3.90 | 3.90 | 2.50 | 4.00 | 3.92 | 3.92 | 2.00 |

Table 8-6 presents normalized $RMSD$ values computed on inside and outside surface heat-flows between the developed and reference models. Normalized $RMSD$ values are calculated as follows:

$$RMSD_{norm} = \frac{RMSD}{\dot{Q}_{s-s}} \times 100 \quad (8.16)$$

Where $\dot{Q}_{s-s}$ is the steady-state heat-flow obtained with the reference model.

All values presented in Table 8-6 are below 10 %, except in 2 cases (Case 8 - $\dot{Q}_{si}$, Case 9 - $\dot{Q}_{so}$, with the "Norway" reference model). Again, these normalized RMSD values are smaller than or similar to the differences observed between the two reference models (fourth and seventh columns).

Table 8-6: Normalized $RMSD$ for each case [%]

| Case | $\dot{Q}_{si}$ – France VS Model | $\dot{Q}_{si}$ – Norway VS Model | $\dot{Q}_{si}$ – France VS Norway | $\dot{Q}_{so}$ – France VS Model | $\dot{Q}_{so}$ – Norway VS Model | $\dot{Q}_{so}$ – France VS Norway |
|---|---|---|---|---|---|---|
| 1 | 6.65 | 0.59 | 6.85 | 6.17 | 0.54 | 6.27 |
| 2 | 7.31 | 1.54 | 7.54 | 6.22 | 1.36 | 6.68 |
| 3 | 4.75 | 6.45 | 7.37 | 3.91 | 5.58 | 3.34 |
| 4 | 0.63 | 5.41 | 4.95 | 0.52 | 4.86 | 4.55 |
| 5 | 0.72 | 5.05 | 4.78 | 0.54 | 4.51 | 4.14 |
| 6 | 0.79 | 6.50 | 6.21 | 0.82 | 5.16 | 5.38 |
| 7 | 0.72 | 6.19 | 6.41 | 0.71 | 4.95 | 5.33 |
| 8 | 8.51 | 13.95 | 13.74 | 1.37 | 1.82 | 2.79 |
| 9 | 2.16 | 2.43 | 2.41 | 1.41 | 14.54 | 13.91 |

## 8.5 Model performance – speed vs. accuracy trade-off

Model performance depends on the number of nodes and the internal time-step. Higher numbers of nodes and lower internal time-steps impact negatively on CPU time and positively on the model accuracy. Table 8-7 presents for 2 cases the evolution of CPU time depending on the number of nodes and the internal time-step, which are related through the stability conditions. Higher numbers of nodes lead to lower internal time-steps. Table 8-7 indicates that the CPU time significantly rises when the number of nodes increases and the internal time-step is reduced. Consequently an important consideration is the impact of the number of nodes on model precision. Using a minimal number of nodes can be used to avoid a longer computation time. It should be considered if the model precision is not impacted significantly by this low spatial resolution.

Figure 8-8 presents a simulation results comparison for both cases when using the minimum number of nodes and a very large number. Table 8-8 presents the corresponding $RMSD$ values between the simulations with the minimum and a very large number of nodes. Both the figure and the table show that no significant differences are observed, except for $T_{so}$ in the third case where a

significantly higher $RMSD$ value is observed. When a layer with a high thermal mass is modeled with a few nodes, the simulation accuracy decreases significantly. However, $RMSD$ values are all lower than or nearly equivalent to the $RMSD$ values between both reference models (France and Norway). Furthermore, Table 8-9 indicates that the steady-state inside and outside surfaces heat-flows are strictly identical for both number of nodes. Likewise, the normalized $RMSD$ values are lower than or nearly equivalent to the values observed between both reference models. Hence, using a minimal number of nodes (i.e. three nodes per layer) in the presented cases is satisfactory.

Table 8-7: CPU time depending on the number of nodes and the internal time-step for a 120-hour simulation

| Case 3 | | | Case 8 | | |
|---|---|---|---|---|---|
| Number of nodes | Internal time-step [s] | CPU time [s] | Number of nodes | Internal time-step [s] | CPU time [s] |
| 3 | 900 | 0.00 | 6 | 56.25 | 0.05 |
| 5 | 225 | 0.02 | 9 | 12.5 | 0.16 |
| 7 | 112.5 | 0.05 | 12 | 6.25 | 0.33 |
| 10 | 56.25 | 0.08 | 16 | 6.25 | 0.42 |
| 14 | 28.12 | 0.14 | 27 | 2.5 | 2.13 |
| 20 | 14.06 | 0.45 | 39 | 1.25 | 7.42 |
| 28 | 7.03 | 1.33 | 55 | 0.62 | 24.98 |
| 40 | 3.52 | 4.08 | 88 | 0.25 | 137.75 |

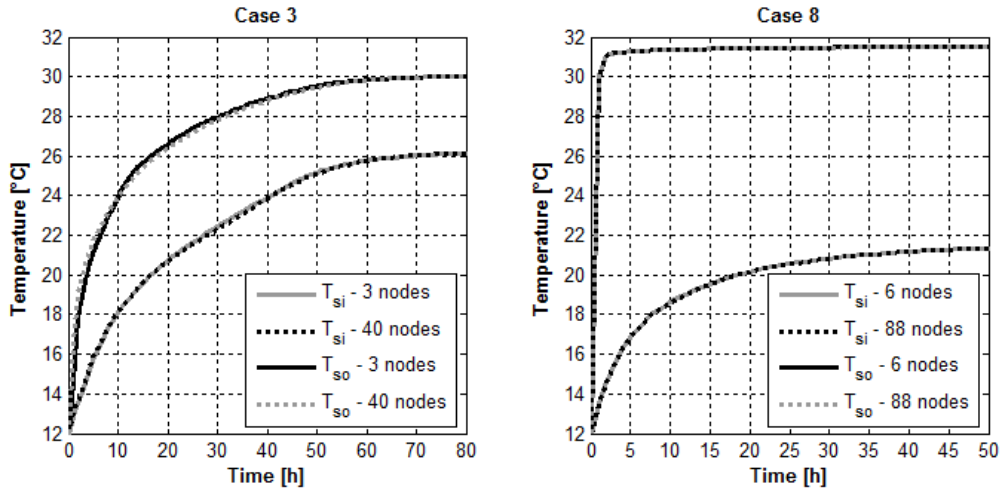


Figure 8-8: Results comparison between models with a different number of nodes for 2 cases

Table 8-8: $RMSD$ values for a variation of the number of nodes for cases 3 and 8

| Case | Minimum number of nodes | Large number of nodes | $RMSD$ for $T_{si}$ | $RMSD$ for $T_{so}$ |
|---|---|---|---|---|
| 3 | 3 | 40 | 0.0588 °C | 0.2704 °C |
| 8 | 6 | 88 | 0.0045 °C | 0.0119 °C |

Table 8-9: Surface heat-flows differences for cases 3 and 8

| | Case 3 | Case 8 |
|---|---|---|
| Minimum number of nodes | 3 | 6 |
| Large number of nodes | 40 | 88 |
| Steady-state heat-flow $\dot{Q}_{si}$ (minimum number of nodes) | 15.48 W/m² | 3.90 W/m² |
| Steady-state heat-flow $\dot{Q}_{si}$ (large number of nodes) | 15.48 W/m² | 3.90 W/m² |
| Steady-state heat-flow $\dot{Q}_{so}$ (minimum number of nodes) | 15.52 W/m² | 3.92 W/m² |
| Steady-state heat-flow $\dot{Q}_{so}$ (large number of nodes) | 15.52 W/m² | 3.92 W/m² |
| $RMSD_{norm}$ for $\dot{Q}_{si}$ | 0.95 % | 0.29 % |
| $RMSD_{norm}$ for $\dot{Q}_{so}$ | 13.94 % | 2.43 % |

## 8.6 Phase change detection issue

A usual problem of the effective heat capacity method used to model PCM thermal behavior is the likelihood for phase change events to be undetected if too large time-steps are used. This method is implemented in TRNSYS Type 399 and Type 260, which use a semi-implicit or implicit finite-difference method where it is assumed that initial and final state properties (thermal capacity) are similar. As illustrated in Figure 8-9, these models can then miss a phase change event since no iterative correction is implemented. For example, the calculation in Type 399 of the future temperature $T_{t0+1}$ depends on the initial and future temperature $T_{t0}$ and $T_{to+1}$ and the initial specific heat $C_{p,t0}$. As the new computed temperature $T_{t0+1}$ is beyond the phase change, the new specific heat $C_{p,t0+1}$ is located in the liquid state. In this case, the phase change has not been detected.

On the other hand, the model proposed in this paper is based on the enthalpy method (Equations ( 8.5 ) and ( 8.6 )) and uses an explicit finite-difference method. The applied enthalpy method has the benefit to remove from the equations the PCM thermal capacity property, which is highly

variable. Only the thermal conductivity can be variable in Equations ( 8.5 ) and ( 8.6 ), but its dependency on temperature is weaker for typical building materials (including PCM), and it is often assumed to be constant. The automatic adjustment of the internal time-step to meet stability conditions for the explicit finite-difference method also ensures relatively short time-step for which it is unlikely to "miss" phase-change events.

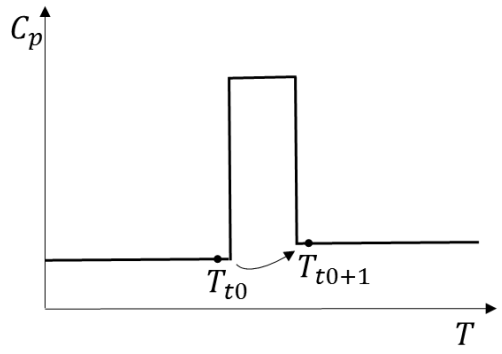


Figure 8-9: Phase change detection issue

In order to illustrate this phase change detection issue, the following example is proposed. A simple 1-layer wall composed of PCMs described in Table 8-10 is modeled. Initial and boundary conditions are described in Figure 8-10. The initial wall temperature is just below the phase change temperature range and strong heating is performed between the 23rd and 24th hours, leading to a fast phase change event.

Table 8-10: PCM properties for the phase change detection issue case

| Thickness [m] | Density [kg/m³] | Thermal conductivity [W/m-K] | Specific heat (solid) [J/g-K] | Specific heat (liquid) [J/g-K] | Latent heat [J/g] | Phase change temperature range [°C] |
|---|---|---|---|---|---|---|
| 0.005 | 1000 | 0.5 | 2 | 2 | 100 | 20 – 21 |

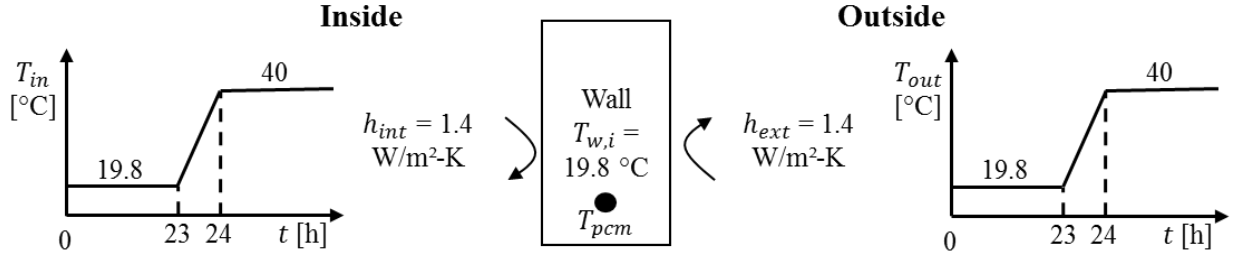


Figure 8-10: Initial and boundary conditions used for the phase change detection issue case

The scenario presented in Table 8-10 and Figure 8-10 is simulated in TRNSYS using Type 399 (effective heat capacity method) and Type 3258 (enthalpy method) with a 1-hour simulation time-step. A results comparison of both methods is presented in Figure 8-11. We can notice that results obtained with Type 399 are affected by the user-defined internal time-step. If the internal time-step is set to 1 hour (equivalent to the simulation time-step), the effective heat capacity model is unable to capture the phase change event. If the internal time-step is lowered to 6 minutes, just a part of the phase change is captured. The internal time-step must be reduced to 1 minute to model this event accurately. At the present stage this problem remains undetected by Type 399 and the simulation continues.

On the other hand, the enthalpy method implemented in Type 3258 is not affected by this issue. Moreover, the internal time-step is calculated directly in the model, based on the stability conditions.

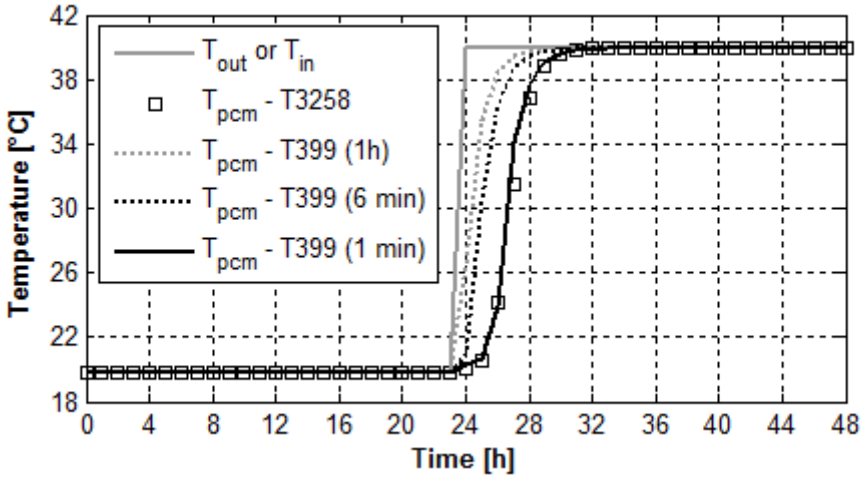


Figure 8-11: Results comparison between TRNSYS Type 399 and Type 3258 for the phase change detection issue case

## 8.7 Transitional behavior issues

In previous work (Delcroix, Kummert, & Daoud, 2015c), a bio-based PCM was implemented in a wall and tested experimentally to assess its behavior during a phase change interruption. The experiments consisted in placing a PCM-equipped wall successively in a warm and cold rooms.

It was shown that the PCM experienced a complete or partial switch from the heating to the cooling $H(T)$ curves, and conversely. This fact is in agreement with the suggestion of Bony and Citherlet (2007) illustrated in Figure 8-1 (b). This possibility is implemented in Type 3258, in addition with the one modeling no transition.

The effective heat capacity method implemented in Type 399 assumes an instantaneous switch between heating and cooling $C_p(T)$ curves. If the PCM is heated up / cooled down, the $C_p$ value is respectively chosen on the heating / cooling curve. Unfortunately this procedure can lead to the energy not being conserved. Figure 8-12 illustrates a case where the solidification of a PCM is interrupted. The PCM is initially liquid at a temperature $T_1$. It is then cooled down (step 1) at a temperature $T_2$, following the cooling $C_p(T)$ or $H(T)$ curve. Before the end of the solidification, the PCM is heated up (step 2) at a temperature $T_3$. In the effective capacity method implemented in Type 399, the $C_p$ value used is the one defined by the heating $C_p(T)$ curve. This is equivalent to assuming that the whole PCM is totally solid at the beginning of the heating process ($T_2'$ instead of $T_2$ in Figure 8-12). In reality, the PCM should be considered in a mushy state ($T_2$). These assumptions lead to an overestimation of the latent heat gained from $T_2$ to $T_3$ equivalent to the interval illustrated by the double-arrow.

Type 399 was used to simulate a case of an interrupted solidification, as previously presented by Delcroix et al. (2015). Figure 8-13 presents the experimental and simulated results and shows that the effective capacity method implemented in Type 399 overestimates the PCM latent heat, as initially illustrated in Figure 8-12.

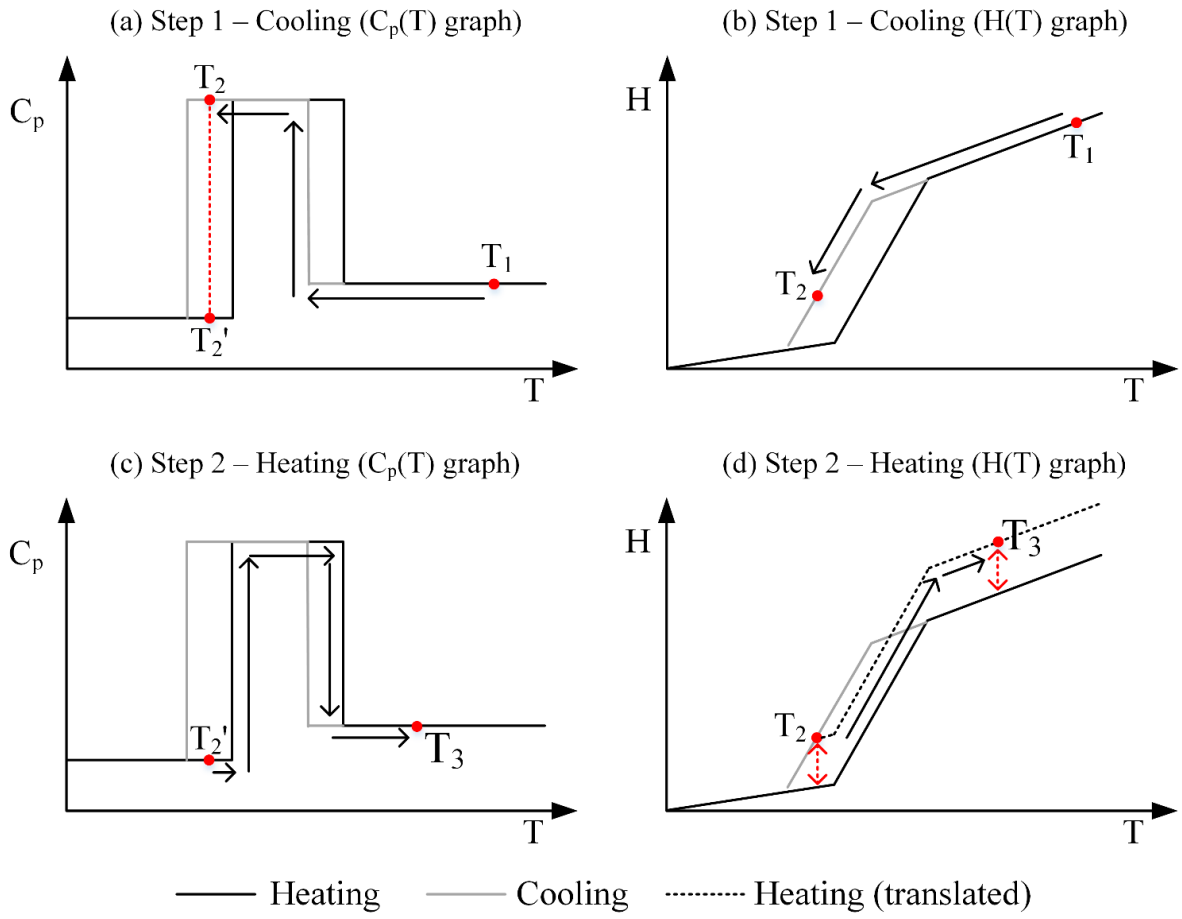


Figure 8-12: Illustration of the problem caused by an instantaneous switch between cooling and heating $C_p(T)$ curves

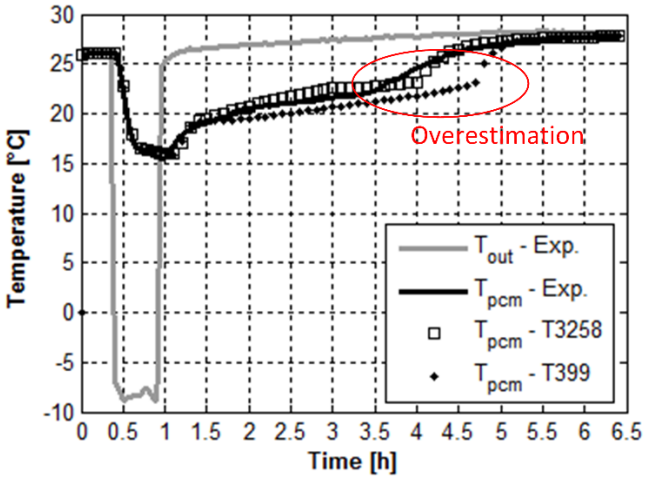


Figure 8-13: Practical consequence caused by an instantaneous switch between cooling and heating $H(T)$ curves

## 8.8 Subcooling issue

Subcooling occurs when a liquid is cooled down below its assumed solidification temperature. It is followed by a steep temperature increase caused by an abrupt nucleation process leading to solidification. This results in a paradox: an enthalpy decrease leads to a temperature rise. This anomaly causes a modeling difficulty, illustrated in Figure 8-14 with a 2-node example. A problem arises as soon as node $n_1$ nucleates and its temperature is higher than the other node $n_2$ (Figure 8-14 (b)). At that moment, heat transfer takes place from $n_1$ to $n_2$ and the modeled temperature of $n_2$ rises, leading to an enthalpy increase and to a higher distance to the nucleation zone. In a real PCM, nucleation normally expands to other nodes. The model is therefore modified to take this into account. The method adopted (Figure 8-14 (c)) consists in equalizing the temperature of $n_1$ and $n_2$ while keeping the enthalpy of $n_2$ constant ($H_2$). This solution is applied only if temperature $T_1$ is higher than $T_2$. Once node $n_1$ reaches the cooling curve without subcooling, this workaround is no more applied and the temperature for all nodes is computed based on the cooling curve without subcooling.

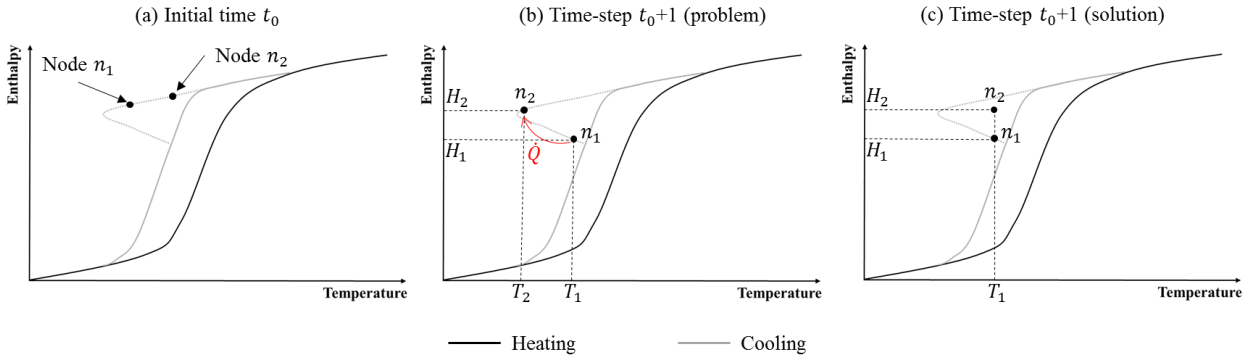


Figure 8-14: Subcooling modeling issue

Some PCMs (in particular most salt hydrates) exhibit a high degree of subcooling which can have an impact in whole building simulations.

An example with a 3-layer wall is discussed hereafter to illustrate the impact of subcooling modeling. The layers properties are given in Table 8-11. The PCM thermal conductivity $k(T)$ curve shown in Figure 8-5 (b) is assumed, and the $H(T)$ curve given in Figure 8-5 (a) is assumed for heating processes. Three cooling curves are added including a hysteresis and varying degrees of subcooling (Figure 8-15), i.e. one without subcooling and the two others with low and high

subcooling. The overall enthalpy change between solid and liquid states is assumed to be the same for all curves, with and without subcooling.

Table 8-11: Layers properties for the subcooling issue case (from outside to inside)

| Layer | Material | Thermal conductivity [W/m-K] | Density [kg/m³] | Specific heat [J/g-K] | Thickness [m] |
|---|---|---|---|---|---|
| I100 | Insulation | 0.04 | 50 | 1.0 | 0.1 |
| P10 | PCM | See Figure 8-5 (b) | 1100 | See Figure 8-15 | 0.01 |
| G10 | Gypsum | 0.14 | 800 | 1.5 | 0.01 |

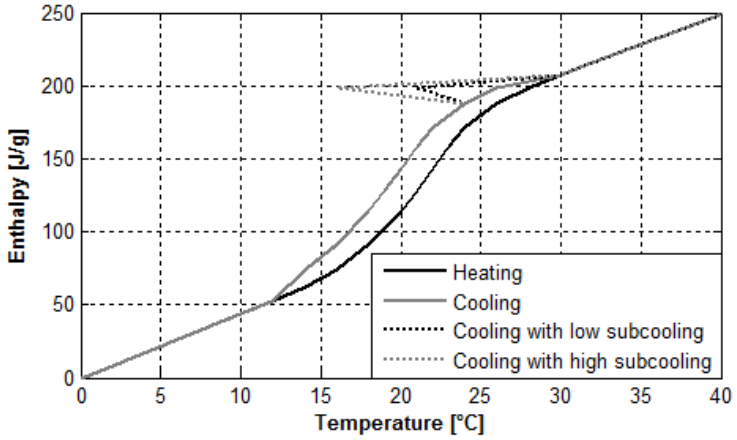


Figure 8-15: Enthalpy-temperature curves for the subcooling issue case

Initial and boundary conditions are presented in Figure 8-16. The initial wall temperature $T_{w,i}$ is 40 °C and the wall is submitted to constant boundary conditions on both sides with a temperature of 0 °C and a convection coefficient of 5 W/m²-K. Temperature results are presented for the PCM layer center $T_{pcm}$ and for the inside and outside surfaces $T_{si}$ and $T_{so}$.

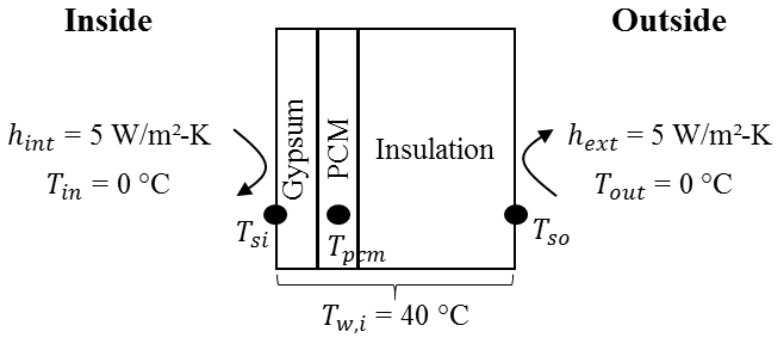


Figure 8-16: Initial and boundary conditions used for the subcooling issue case

Figure 8-17 and Figure 8-18 present all temperature results. Figure 8-17 shows that subcooling occurs approximately at the second hour of the simulation. It also indicates that the PCM temperature evolution is nearly equivalent for the 3 cases after subcooling.

No significant differences are observed in outside surface temperatures, the subcooling effect being mitigated by the thick insulation layer. On the other hand, a significant difference is observed on the inside surface for a short period of time (almost 2 h in the figure).

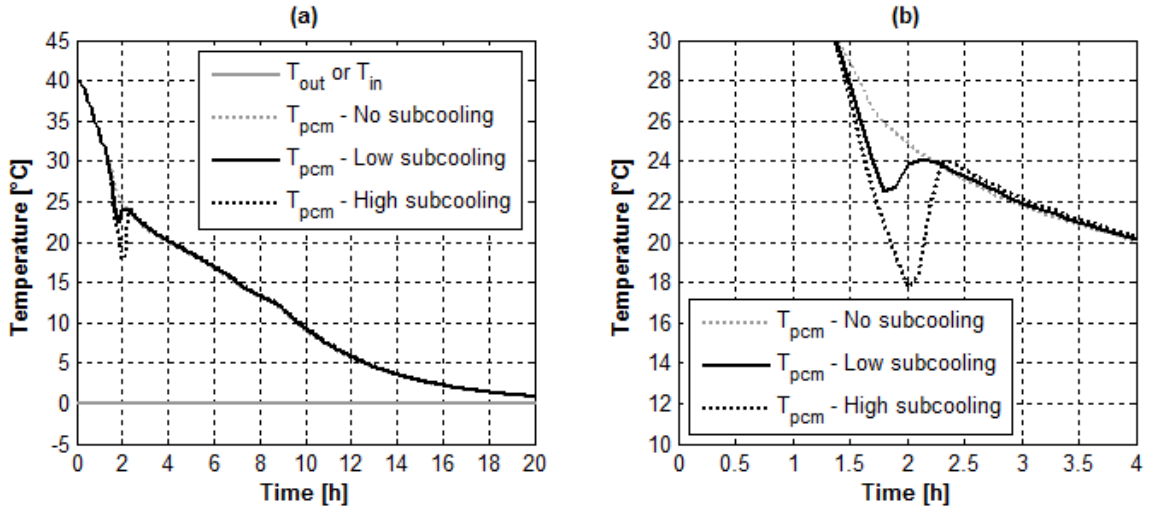


Figure 8-17: PCM temperature results for the subcooling issue case (zoom on subcooling (b))

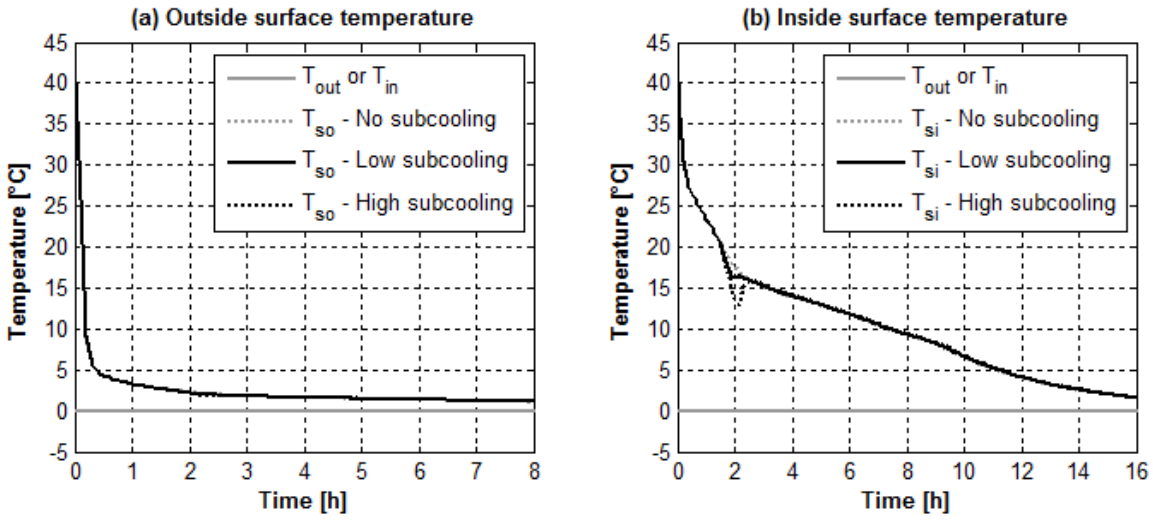


Figure 8-18: Outside (a) and inside (b) surface temperature results for the subcooling issue case

## 8.9 Conclusion

This paper presents a new model implemented in TRNSYS and named Type 3258, which is dedicated to simulate walls including layer(s) with temperature-dependent properties. This model uses a Forward Time and Central Space finite-difference method, combined with an enthalpy method to represent the PCM thermal behavior. Type 3258 has been compared to other reference models from France and Norway using wall test cases proposed by the International Energy Agency (Annex 23). The comparison has shown that the developed model is in good agreement with both reference models, showing differences that are smaller than or similar to the differences existing between the two reference models. Our work also shows that the model, which uses an enthalpy method, offers significant advantages over an effective capacity method to capture fast transient phase change events and to model transitional PCM thermal behavior when phase change is interrupted. The method implemented to model subcooling is also demonstrated.

The experimental validation of the new model and the methodology to use it in conjunction with the TRNSYS multizone building model (Type 56) are discussed in Part II of this paper (Delcroix, Kummert, & Daoud, 2015b).

## Acknowledgements

The research work presented in this paper is financially supported by Hydro-Québec, FRQNT (Fonds de Recherche du Québec en Nature et Technologies) and NSERC (Natural Sciences and Engineering Research Council of Canada). We also would like to thank Marion Hiller, of TRANSSOLAR, for providing TRNSYS Type 399.

## References

Al-Saadi, S. N., & Zhai, Z. J. (2014). TRNSYS Type 285 - Phase Change Materials Embedded in Wall System. Boulder, CO.

Bergman, T. L., Lavine, A. S., Incropera, F. P., & Dewitt, D. P. (2011). Fundamentals of heat and mass transfer. Wiley.

Bony, J., & Citherlet, S. (2007). Numerical model and experimental validation of heat storage with phase change materials. Energy and Buildings, 39, 1065–1072. Retrieved from http://www.sciencedirect.com/science/article/pii/S037877880600291X

Chandrasekharan, R., Lee, E. S., Fisher, D. E., & Deokar, P. S. (2013). An Enhanced Simulation Model for Building Envelopes with Phase Change Materials. ASHRAE Transactions, 119(2).

Crawley, D. B., Lawrie, L. K., Winkelmann, F. C., Buhl, W. F., Huang, Y. J., Pedersen, C. O., Strand, R. K., Liesen, R. J., Fischer, D. E., Witte, M. J., Glazer, J. (2001). EnergyPlus: creating a new-generation building energy simulation program. Energy and Buildings, 33(4), 319–331. doi:http://dx.doi.org/10.1016/S0378-7788(00)00114-6

Danish Building Energy Institute. (2013). BSim - Building Simulation. Retrieved February 24, 2015, from http://sbi.dk/en/bsim

Delcroix, B., Kummert, M., & Daoud, A. (2015a). Modeling of a wall with phase change materials. Part II: Experimental validation. Journal of Building Performance Simulation.

Delcroix, B., Kummert, M., & Daoud, A. (2015b). Thermal behavior mapping of a phase change material between the heating and cooling enthalpy-temperature curves. In 6th International Conference on Building Physics for a Sustainable Built Environment. Torino, Italy.

Dentel, A., & Stephan, W. (2013). TRNSYS TYPE 399 - Phase change materials in passive and active wall constructions. Nürnberg.

Energy Systems Research Unit. (1998). ESP-r User Guide: The ESP-r System for Building Energy Simulation. Glasgow.

EnergyPlus. (2014). EnergyPlus Engineering Reference.

Geissler, A. (2008). SPMCMP56 subroutine in ESP-r Source Standard Code.

Goodrich, L. E. (1978). Efficient numerical technique for one-dimensional thermal problems with phase-change. International Journal of Heat and Mass Transfer, 21(5), 615.

Günther, E., Mehling, H., & Hiebler, S. (2007). Modeling of subcooling and solidification of phase change materials. Modelling and Simulation in Materials Science and Engineering, 15, 879–892. doi:10.1088/0965-0393/15/8/005

Haghighat, F., Yu, Z., Inard, C., Michaux, G., Kuznik, F., Johannes, K., Virgone, J., Barzin, R., Farid, M., Bastani, A., Stathopoulos, N., El Mankibi, M., Nkwetta, D. N., Moreau, A., Vouillamoz, P-E., Castell, A., Adl-Zarrabi, B. (2013). Annex 23: Energy storage in buildings of the future - Applying Energy Storage in Ultra-low Energy Buildings.

Heim, D., & Clarke, J. A. (2004). Numerical modelling and thermal simulation of PCM–gypsum composites with ESP-r. Energy and Buildings, 36, 795–805. doi:10.1016/j.enbuild.2004.01.004

Hoffman, S. (2006). Numerische und experimentelle Untersuchung von Phasenübergangsmaterialien zur Reduktion hoher sommerlicher Raumtemperaturen. Bauhaus-Universität Weimar.

Johannes, K., Virgone, J., Kuznik, F., Wang, X., Haavi, T., & Fraisse, G. (2011). Annex 23: Applying Energy Storage in Buildings of the Future - Development of Sustainable Energy Storage Designs for a variety of Ultra-low energy building thermal, phase change materials and electrical storage options.

Klein, S. A., Beckman, W. A., Mitchell, J. W., Duffie, J. A., Duffie, N. A., & Freeman, T. L. (2012). TRNSYS 17: A Transient System Simulation Program. Madison, USA: Solar Energy Laboratory, University of Wisconsin. Retrieved from http://sel.me.wisc.edu/trnsys

Kuznik, F., & Virgone, J. (2009). Experimental investigation of wallboard containing phase change material: Data for validation of numerical modeling. Energy and Buildings, 41(5), 561–570. doi:10.1016/j.enbuild.2008.11.022

Kuznik, F., Virgone, J., & Johannes, K. (2010). Development and validation of a new TRNSYS type for the simulation of external building walls containing PCM. Energy and Buildings, 42, 1004–1009.

Pedersen, C. O. (2007). Advanced zone simulation in EnergyPlus: incorporation of variable properties and phase change material (PCM) capability. In Building Simulation (pp. 1341–1345). Beijing.

Rose, J., Lahme, A., Christensen, N. U., Heiselberg, P., Hansen, M., & Grau, K. (2009). Numerical method for calculating latent heat storage in constructions containing phase change material. In Eleventh International IBPSA Conference (pp. 400–407). Glasgow.

Thermal Energy Systems Specialists. (2012). TESSLibs3 - Type 1270: Phase Change Material (PCM) Wall Layer for Type 56.

Voller, V. R., & Cross, M. (1981). Accurate solutions of moving boundary problems using the enthalpy method. International Journal of Heat and Mass Transfer, 24(3), 545.

Yao, M., & Chait, A. (1993). An alternative formulation of the apparent heat capacity method for phase change problems. Numerical Heat Transfer, Part B, Fundamentals, 24(3), 279.

# CHAPTER 9 ARTICLE 5: MODELING OF A WALL WITH PHASE CHANGE MATERIALS. PART II: EXPERIMENTAL VALIDATION

Delcroix, B., Kummert, M., Daoud, A., (2015). Modeling of a wall with phase change materials. Part II: Experimental validation. Submitted to Journal of Building Performance Simulation on the 15th of July 2015.

## Abstract

In Part I of this paper, a new wall model with phase change materials (PCMs) implemented in TRNSYS is described and numerically validated. Part II focuses on its experimental validation and on how to use this model in TRNSYS. The experimental investigation is performed in two identical full-scale test-cells (only one with PCMs) exposed to the ambient environment. These experimental data are primarily used to benchmark a TRNSYS simulation model of the test-cell without PCMs. After calibration, this model is complemented with the PCM model for experimental validation. Compared to the benchmarking procedure (without PCMs), the root mean square deviation values between the experiments and the simulations (with PCMs) are lower or in the same order of magnitude. The simulations reproduce the same PCM effects as observed in the experiments, such as mitigation and time-shift effects. A discussion about computation time concludes this work.

## Nomenclature

| | |
|---|---|
| Bi | Biot number [-] |
| $C_p$ | Specific heat [J/g-K] |
| Fo | Fourier number [-] |
| $H$ | Enthalpy [J/kg] |
| $h$ | Coefficient of convection [W/m²-K] |
| $k$ | Thermal conductivity [W/m-K] |
| $m$ | Mass [g] |
| $n$ | Number of nodes [-] |
| $\dot{Q}$ | Heat flow [W] |

| | |
|---|---|
| $T$ | Temperature [°C] |
| $t$ | Time [s] |
| $U$ | Heat transfer coefficient [W/m²-K] |
| $\alpha$ | Thermal diffusivity [m²/s] or coefficient of absorption [-] |
| $\Delta t$ | Time-step [s] |
| $\Delta x$ | Half-interval between 2 nodes [m] |
| $\rho$ | Density [kg/m³] |

*Subscripts*

| | |
|---|---|
| $cw$ | Center of the wall |
| $i$ | i-node |
| $l$ | Left |
| $r$ | Right |
| $si$ | Inside surface |
| $so$ | Outside surface |

*Abbreviations*

| | |
|---|---|
| NW | North-west |
| SW | South-west |

## 9.1 Introduction

Part I of this paper documents a new explicit finite-difference wall model with phase change materials (PCM) implemented in TRNSYS (Delcroix, Kummert, & Daoud, 2015a). The developed model uses an enthalpy method for modeling PCM temperature-dependent thermal capacity. A numerical validation was successfully performed using test cases proposed by the International Energy Agency (Haghighat et al., 2013).

The algorithm implemented in the TRNSYS multizone building model, known as Type 56, to model transient conduction through walls is based on the Conduction Transfer Function (CTF)

method (TRANSSOLAR Energietechnik Gmbh, 2012). This method does not allow to model layers with temperature-dependent properties. Using an external type in TRNSYS is then needed to model a wall with phase change materials (PCMs). The CTF method was primarily developed by Mitalas and Stephenson (1971) and implemented in an algorithm later by Mitalas and Arseneault (1972). This method is based on constant CTF coefficients dedicated to model the wall thermal response. Barbour and Hittle (2005) have proposed to adapt the CTF method to phase change materials by generating multiple sets of CTF coefficients. During the simulation, a switching mechanism operates in order to choose the right set of CTF coefficients corresponding to the right properties. This method was implemented in a developer version of EnergyPlus but to the author's knowledge it has never been released publicly.

A more common method to model a wall including PCMs is the finite-difference method (Bergman et al., 2011), which is used to solve the 1-D conduction heat transfer equation, formulated as follows:

$$\rho\, C_p \frac{dT}{dt} = \frac{d\left(k \frac{dT}{dx}\right)}{dx} \qquad (9.1)$$

Where:

$$C_p = \frac{dH}{dT} \qquad (9.2)$$

Combining Equations ( 9.1 ) and ( 9.2 ), the 1-D conduction heat transfer equation can be reformulated with an enthalpy term:

$$\rho \frac{dH}{dt} = \frac{d\left(k \frac{dT}{dx}\right)}{dx} \qquad (9.3)$$

Two categories of models are commonly used for simulating walls with PCM. First, the effective heat capacity method (Goodrich, 1978; Yao & Chait, 1993) consists in solving Equation ( 9.1 ) while considering a temperature-dependent specific heat $C_p$. Second, the enthalpy method (Voller & Cross, 1981) is based on Equation ( 9.3 ) and needs enthalpy-temperature curves to relate temperatures to enthalpy values. Part I of the present paper describes a new model based on the

enthalpy method, which is named Type 3258 (Delcroix, Kummert, & Daoud, 2015a). This model uses a Forward Time Central Space scheme to solve Equation ( 9.3 ).

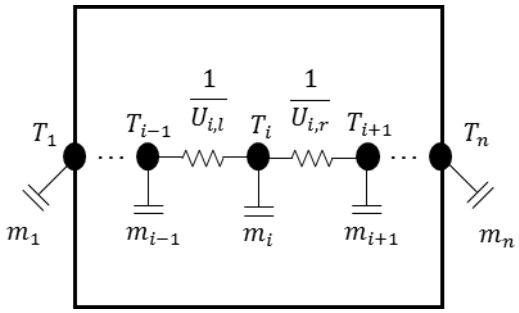


Figure 9-1: 1-D finite-difference of a 1-layer wall

For the case presented in Figure 9-1, Equation ( 9.3 ) is discretized as follows:

$$H_i^{t+1} = H_i^t + \frac{U_{i,l}\, A\, \Delta t}{m_i}\,(T_{i-1}^t - T_i^t) + \frac{U_{i,r}\, A\, \Delta t}{m_i}\,(T_{i+1}^t - T_i^t) \qquad (9.4)$$

Temperature $T_i^{t+1}$ is then found from enthalpy $H_i^{t+1}$ through user-defined enthalpy-temperature curves. This explicit method requires to meet two different stability conditions (Bergman et al., 2011). For internal nodes, the Fourier number Fo must be equal to or lower than 0.5:

$$\mathrm{Fo} = \frac{\alpha\, \Delta t}{\Delta x^2} \leq \frac{1}{2} \qquad (9.5)$$

For surface nodes, the stability condition is more constraining and involves the Biot number:

$$\mathrm{Fo}\,(1 + \mathrm{Bi}) = \frac{\alpha\, \Delta t}{\Delta x^2}\left(1 + \frac{h\, \Delta x}{k}\right) \leq \frac{1}{2} \qquad (9.6)$$

Besides Type 3258, other models exist in TRNSYS for simulating PCM walls, such as:

- Type 1270 (Thermal Energy Systems Specialists, 2012) is a simple PCM model based on a lumped heat balance method. It considers a constant-temperature phase change and a spatially uniform temperature inside the PCM layer.
- Type 260 (Kuznik et al., 2010) uses a fully implicit finite-difference method coupled with the effective heat capacity method. Thermal properties are based on the previous time-step. It was experimentally validated by Kuznik et al. (2010).

- Type 399 (Arno Dentel & Stephan, 2013) uses a Crank-Nicolson finite-difference method to solve the 1-D conduction heat equation, coupled with the effective heat capacity method for PCM modeling. Like Type 260, thermal properties are based on the previous time-step. It was experimentally validated by Dentel and Stephan (2010).
- Type 285 (Al-Saadi & Zhai, 2014) uses an iterative fully implicit finite-difference method and an enthalpy method for PCM modeling. It was experimentally validated by Al-Saadi (2014).

A PCM module also exists in other BPS programs such as EnergyPlus. The algorithm implemented in EnergyPlus is based on an iterative semi-implicit or fully implicit finite-difference method coupled with an enthalpy method (Pedersen, 2007). It was also numerically and experimentally validated by Tabares-Velasco et al. (2012).

## 9.2 Objectives

This paper aims at validating experimentally the proposed TRNSYS model named Type 3258, using the experimental data generated in the full-scale test-cells (equipped with PCMs or without). An in-depth description of this test-bench and the corresponding experimental results are presented. The experimental data of the test-cell without PCMs are primarily used to benchmark a TRNSYS building model. This model is then complemented with the developed PCM model in order to simulate the test-cell with PCMs. Simulations results are compared to experimental data to evaluate if the developed model simulates adequately the PCMs effects.

This paper also discusses the coupling methods used to link the external PCM wall model (such as Type 3258) to the TRNSYS building model (Type 56) and the resulting convergence considerations.

## 9.3 Coupling between Type 56 and the external type

TRNSYS PCM models (such as the ones described in the introduction) have not been integrated within the multizone building model (Type 56) at this time, so they must be connected to Type 56 by the TRNSYS solver. Two different methods have been proposed by TESS (Thermal Energy Systems Specialists, 2012) and by Dentel and Stephan (2013). Both methods involve defining a fictitious wall in Type 56 that will interact with the zone heat balance calculations (radiative and

convective heat transfer to and from the zone). This implies that for walls between thermal zones, one fictitious wall is defined in each zone, and boundary conditions for these two walls are imposed by the external wall model (see Figure 9-2 for an illustration of that principle). The coupling method applied in the experimental validation is slightly different to both methods proposed by TESS and by Dentel and Stephan since the surface temperatures are calculated only in Type 56. This alternative is explained in the Appendix.

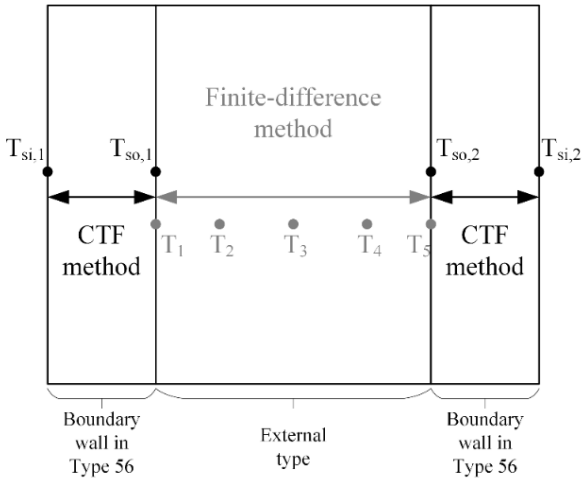


Figure 9-2: Principle of the coupling between Type 56 and the external PCM wall model

Since the external type and Type 56 are connected to each other and exchange consequently information, convergence considerations matter. When simulating a whole system, TRNSYS solves one component at a time and then performs iterations until convergence between all components is reached. Convergence is verified from the input values variation, such as illustrated in Figure 9-3. If inputs change more than the user-defined tolerance, new iterations are performed until convergence is reached. A maximum number of iterations is defined by the user to avoid infinite loops. If this limit is reached, TRNSYS proceeds to the next time-step with a “warning” message indicating that a specified type did not reach convergence. If an excessive number of warning is reached (defined by the user), the simulation stops and an error message is generated.

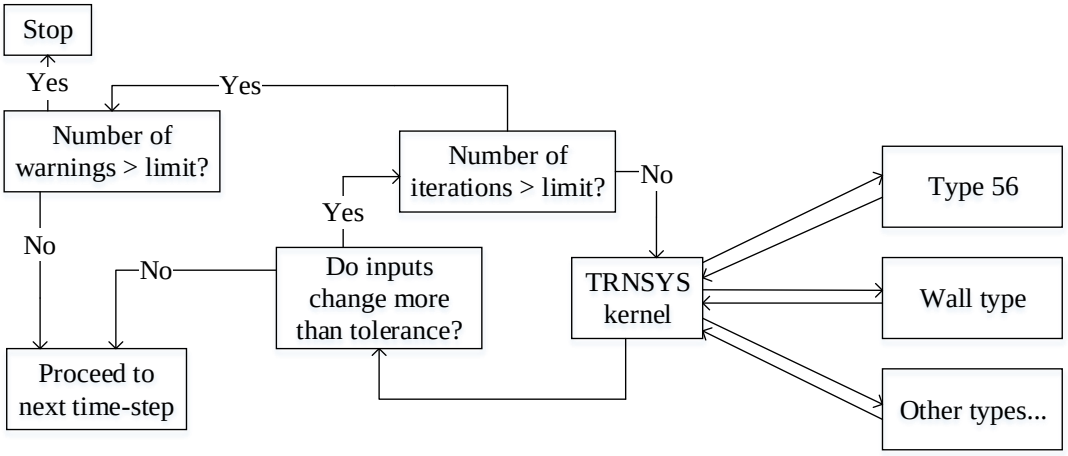


Figure 9-3: TRNSYS solution methodology (adapted from (Jost, 2012))

## 9.4 Experimental setup for PCM testing

In order to validate the new model for PCM-equipped walls, experimentations were performed in a test-bench composed of two similar test-cells. One is equipped with PCM while the other is not.

### 9.4.1 PCM description

The chosen material is a bio-based PCM composed of biodegradable soybean and palm oil, mixed with additives (gelling agent and fire retardant). It is commercially provided in pouches, as illustrated in Figure 9-4.

Figure 9-4: PCM pouches

The main properties are presented in Table 9-1. Most properties are known for the material without the additives (Entropy Solutions Inc., 2011). After mixing with additives (Phase change energy solutions, 2014), only a few properties are known. The density and thermal conductivity have been obtained through additional experimentations.

Table 9-1: PCM properties

| **Without additives** | | **With additives** | |
|---|---|---|---|
| Phase change temperature | 23 °C | Phase change temperature | 23 °C |
| Latent heat storage capacity | 203 J/g | Latent heat storage capacity | 165-200 J/g |
| Density | 830 kg/m³ | | |
| Specific heat (solid) | 1.84 J/g-K | Weight per unit surface | 1.465 kg/m² |
| Specific heat (liquid) | 1.99 J/g-K | Density | 883 kg/m³ * |
| Thermal conductivity (solid) | 0.207 W/m-K | Thermal conductivity (solid and liquid) | 0.212 W/m-K ** |
| Thermal conductivity (liquid) | 0.171 W/m-K | | |
| * Experimental measurements (standard deviation: ± 15 kg/m³) – not from manufacturer<br>** Experimental measurements (standard deviation: ± 0.022 W/m-K) – not from manufacturer | | | |

Figure 9-5 presents the results of a Differential Scanning Calorimetry (DSC) test performed by the manufacturer (with additives). Figure 9-5 (a) shows the variation of the heat flow depending on the material temperature. Positive and negative values correspond respectively to heat release and absorption. Figure 9-5 (b) gives the corresponding enthalpy-temperature curves. These graphs shows that the fusion and solidification occur over different temperature ranges: between 20 °C and 25 °C for fusion and between 15 °C and 20 °C for solidification. A resulting hysteresis of around 5 °C is then observed.

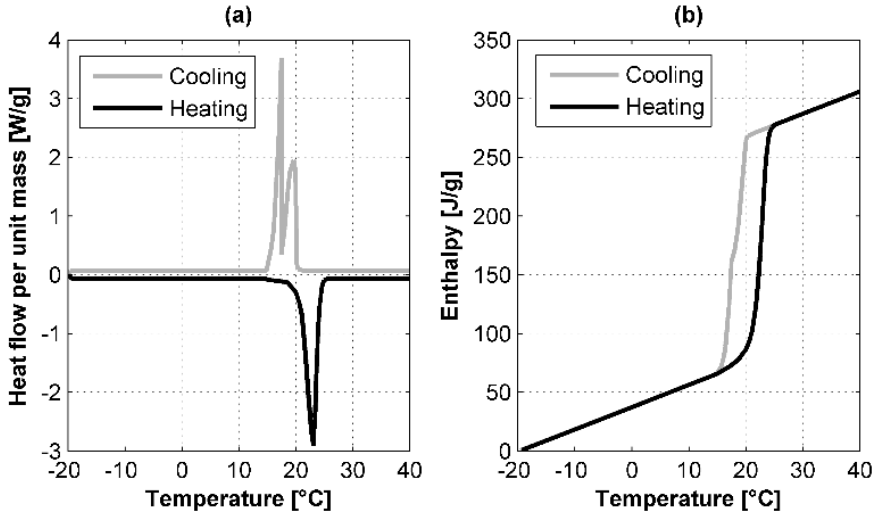


Figure 9-5: (a) DSC test and (b) resulting enthalpy-temperature curves (adapted from (Phase change energy solutions, 2008)).

### 9.4.2 PCM-equipped walls

The tested PCM-equipped wall consist of a double layer of plastic film with PCM pouches between two plywood boards, as illustrated in Figure 9-6. Equivalent walls were also built but without PCM, with air between both plywood boards. Both kind of walls are instrumented with thermocouples as shown in Figure 9-6. For walls without PCM, only three thermocouples were added (center, outside and inside surfaces). These walls are added to the inside surfaces of both test-cells (with and without PCM) and have approximately a length of 2.4 m and a width of 0.5 m.

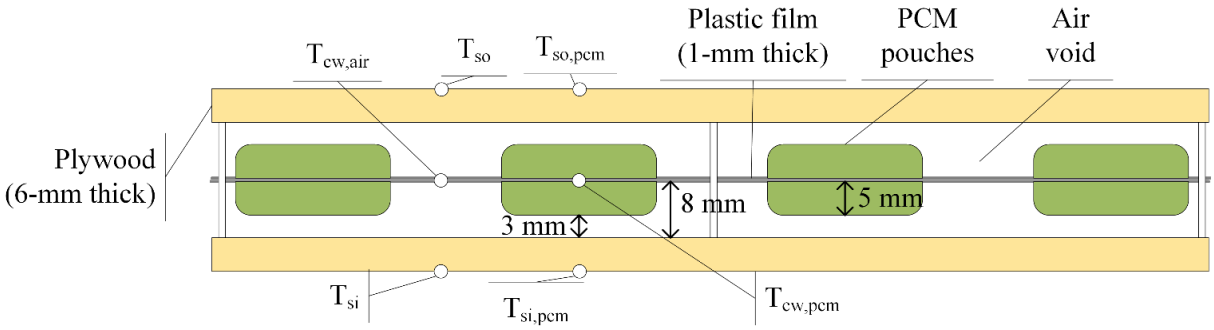


Figure 9-6: Instrumented PCM-equipped wall

### 9.4.3 Test-cells and instrumentation

The test bench is located at the energy technology laboratory (Hydro-Québec Research Institute) in Shawinigan (QC, Canada) and consists of two identical test-cells, which are wood-frame constructions. Newly built walls with and without PCM are fitted on the inside surfaces of the external walls oriented north-west and south-west, as illustrated in Figure 9-7. Both test-cells are heated with electric baseboards with a power of 1500 W. They are controlled by electronic thermostats whose the algorithm is not known.

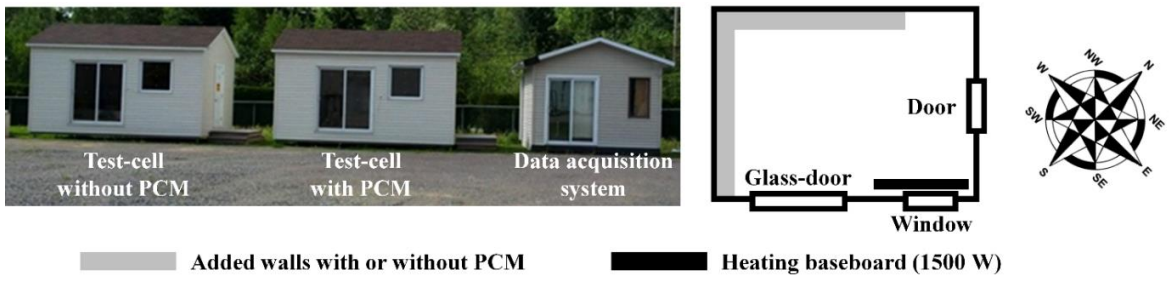


Figure 9-7: Test-bench description

Table 9-2 presents the U-values of each external surfaces, the infiltration and the dimensions of both test-cells.

Table 9-2: U-values, infiltration and dimensions of test-cells

| **U-values** | | **Infiltration** | **Dimensions** | |
|---|---|---|---|---|
| External wall | 0.28 W/m²-K | 0.1 $h^{-1}$ | Length | 5.49 m |
| Roof | 0.19 W/m²-K | | Width | 3.66 m |
| Slab | 0.14 W/m²-K | | Height | 2.44 m |
| Door | 1.25 W/m²-K | | Window area | 1.19 m² |
| Window | 1.6 W/m²-K | | Glass-door area | 3.91 m² |
| Glass-door | 1.6 W/m²-K | | | |

Both test-cells are similarly instrumented with sensors which measure electric energy use for heating, air dry bulb temperatures at different heights and inside surface temperatures (walls, ceiling, floor and windows). The added walls are also instrumented, as shown in Figure 9-6. A weather station is located next to the test-bench.

### 9.4.4 Tests description

Tests were carried out from the end of February to the end of July 2013. During the heating season, different temperature set-point scenarios were tested. On the other hand, the temperature in the test-cells during the cooling season was allowed to float. Table 9-3 presents the scenarios and their strategies. The extreme set-back scenario was tested in order to highlight the PCM effects, i.e. the PCM melting when the set-point is switched to 30 °C and the solidification after each set-point temperature fall.

### 9.4.5 Experimental results

Figure 9-8 (a) compares the evolution of the temperatures of the indoor room air and in the center of the added walls for the test-cell with PCM and without PCM for the residential scenario during two days (17-03 and 18-03). During the day, solar radiation overheats the test-cells and the indoor air temperature rises significantly. In the PCM-equipped test-cell, the PCMs allow mitigating the temperature increase by 2 °C by storing more energy in the walls. The temperature difference at the center of the added walls is significant, showing the impact of PCMs on the wall transient

response. The temperature at the center of the added wall in the reference test-cell (without PCMs) is stabilized around 19 °C during the night while it takes about 6 to 7 more hours for the temperature at the center of the PCM-equipped wall to decrease to 19 °C (in the PCM-equipped test-cell).

Table 9-3: Tested scenarios in 2013

| **Scenario** | **Date** | **Set-point** | | | |
|---|---|---|---|---|---|
| Constant temperature | 28-02 → 11-03 | 23 °C | | | |
| Residential workday | 11-03 → 22-03 | 6:00 AM | | 4:00 PM | |
| | | ↓ 19 °C | | ↑ 23 °C | |
| Commercial and institutional (CI) | 25-03 → 28-03 | 6:00 AM | | 6:00 PM | |
| | | ↑ 24 °C | | ↓ 18 °C | |
| Early morning preheating | 28-03 → 05-04 | 3:00 AM | 6:00 AM | 9:00 AM | 8:00 PM |
| | | ↑ 25 °C | ↓ 20 °C | ↑ 22 °C | ↓ 18 °C |
| Extreme set-back | 08-04 → 30-04 | 8:00 AM | | 8:00 PM | |
| | | ↑ 30 °C | | ↓ 5 °C | |
| Free-floating | 30-04 → 31-07 | - | | | |

Figure 9-8 (b) presents the evolution of the heating power (mean power over a 15-min time-step) in both test-cells. At 6 AM, when the set-point is reduced from 23 °C to 19 °C, the heating system is turned off during a few moments (the test-cells have very little thermal mass). Afterwards, it is turned on just to maintain the set-point of 19 °C. At this moment, the power demand is more important in the reference test-cell due to less stored heat in the walls (in comparison with the PCM-equipped test-cell). At the end of the day, when the set-point is set again to 23 °C, the heating system is turned on to match the set-point. Because of its higher thermal mass (and for charging energy in the PCMs), the PCM-equipped test-cell needs more power than the reference test-cell to reach the set-point, as shown at the end of the afternoon on Figure 9-8 (b). Finally, during the night, as the wall temperature in the PCM-equipped test-cell decreases more slowly, the heating power is less important than in the reference test-cell where the wall temperature has already reached a colder state.

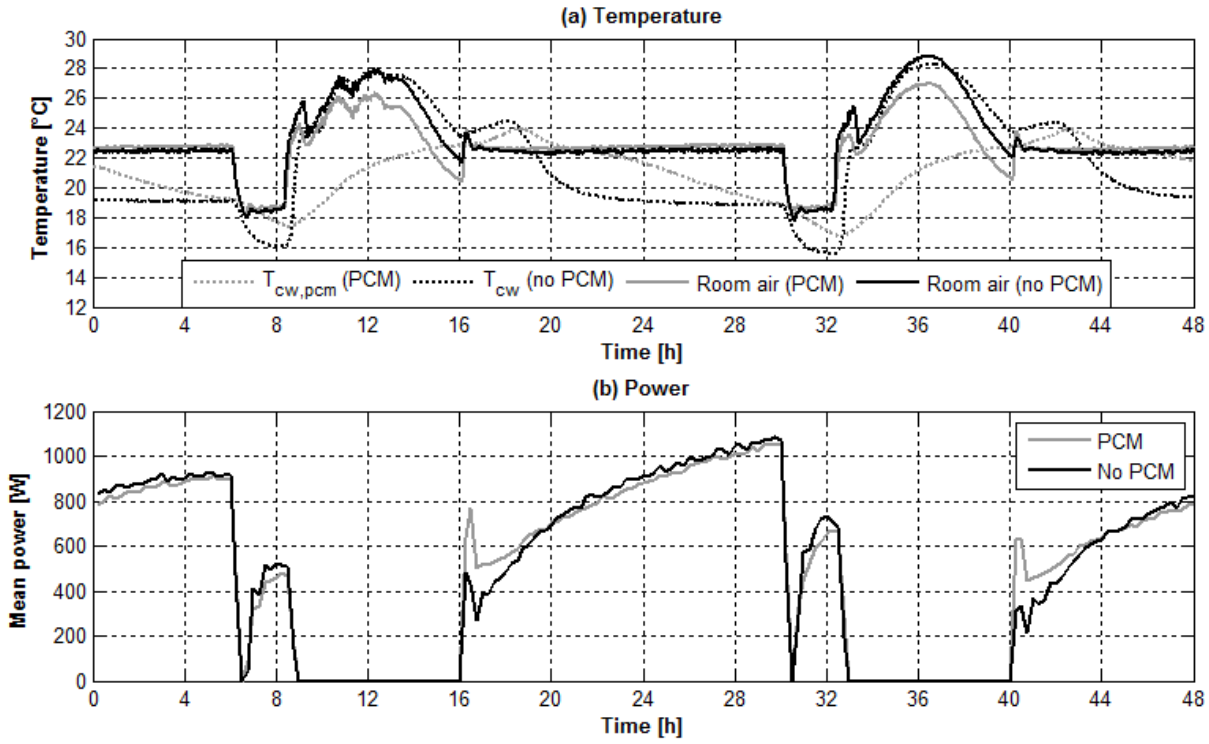


Figure 9-8: (a) Evolution of temperatures inside the test-cells and in the center of the added walls (with and without PCMs) and (b) evolution of the heating power during residential workday scenario (17-03 and 18-03)

Figure 9-9 presents the same results for the CI scenario. The effects of temperature peak mitigation and delay that were visible in Figure 9-8 (a) are also present in Figure 9-9 (a). The phase change effect appears here clearly at the end of the day, around 8 PM. The temperature slope decreases significantly at this moment.

The heating power demand (Figure 9-9 (b)) shows two main differences. First, the power demand during the night is different: in the PCM-equipped test-cell, the heating system turns on later and then delivers a lower heating power, which can be explained by the slow temperature decrease in the PCM-equipped walls at this moment (especially in comparison with the added walls without PCMs in the reference test-cell). On the other hand, the heating system needs to add a small amount of heat at the end of the afternoon in the PCM-equipped test-cell to maintain the set-point of 24 °C, which is not the case in the reference test-cell where the solar radiation has overheated the zone during the day.

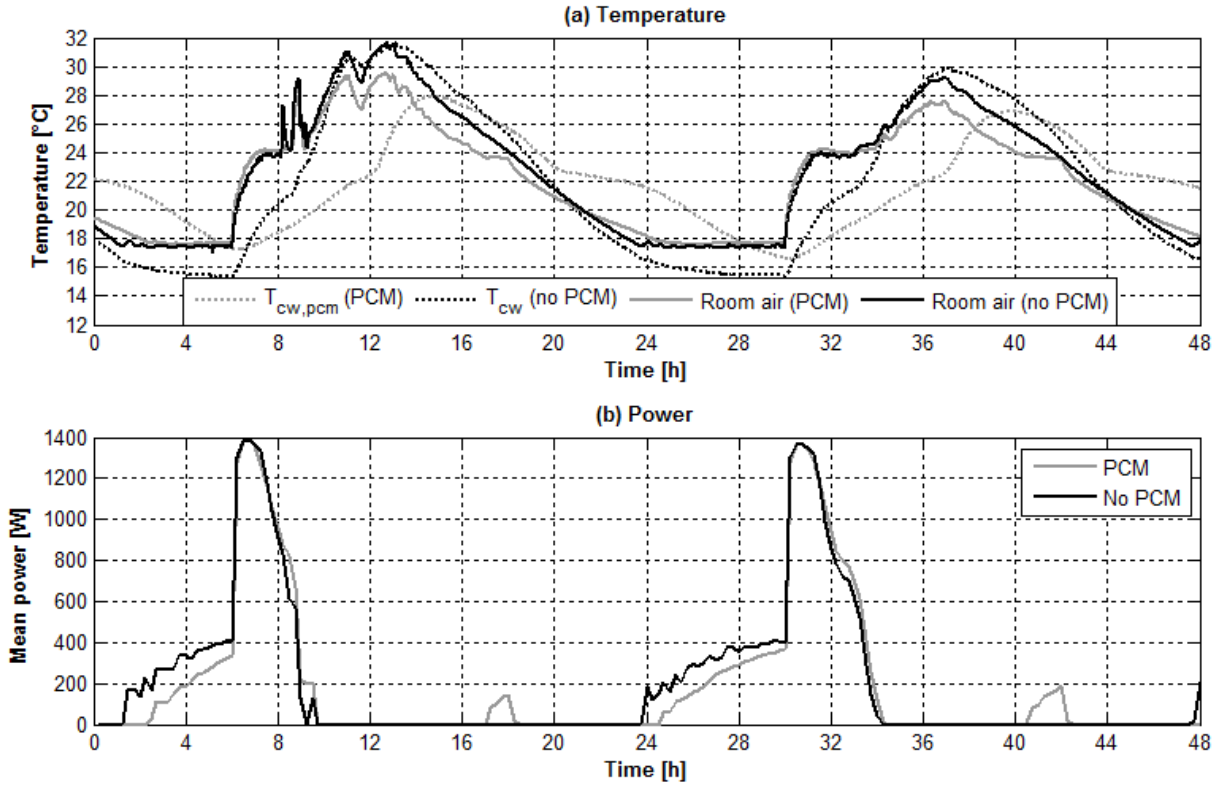


Figure 9-9: (a) Evolution of temperatures inside the test-cells and in the center of the added walls (with and without PCMs) and (b) evolution of the heating power during CI scenario (26-03 and 27-03)

The detailed temperature measurements within the walls showed two other interesting effects.

First, the temperature gradient inside a wall is strongly different, as shown in Figure 9-10. It presents the evolution of air and walls temperatures during the extreme set-back scenario (without (a) and with (b) PCMs). Figure 9-10 (a) shows moderate temperature gradients since all temperatures are relatively close. PCM-equipped walls (Figure 9-10 (b)) show a different dynamic response. The increased thermal mass makes the wall center the coldest spot (for a short time) during a temperature rise while it becomes the warmest point (for a longer period) during a temperature fall.

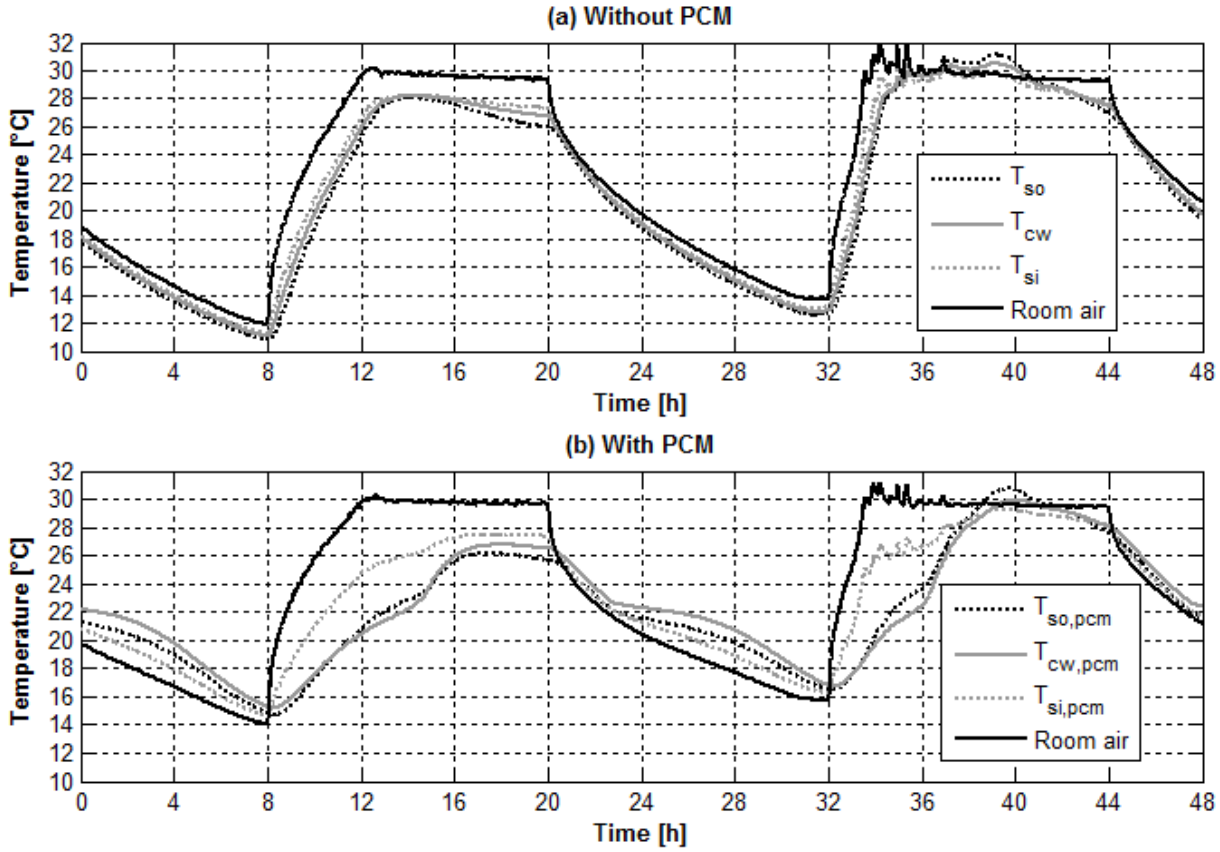


Figure 9-10: Evolution of the temperature gradient in the added walls without (a) and with (b) PCM during the extreme set-back scenario (13-04 and 14-04)

A second observable effect is the appearance of an inhomogeneous temperature pattern inside the center of the PCM-equipped wall ($T_{cw,air} \neq T_{cw,pcm}$), caused by the heterogeneity of the central layer composed of air, PCMs and a small amount of plastic film (Figure 9-11). During the test, measurements at the level of the PCMs pouches and in the air spaces besides the pouches were carried out as shown in Figure 9-6. Two measurement points were also placed at the level of the inside surface to evaluate if the thermal heterogeneity was extended to the inside surface. A significant difference is observed in the central layer (especially during the phase change (around 21 - 23 °C)). It seems that this thermal heterogeneity is mitigated at the level of the inside surface as no significant difference is visible ($T_{si} = T_{si,pcm}$).

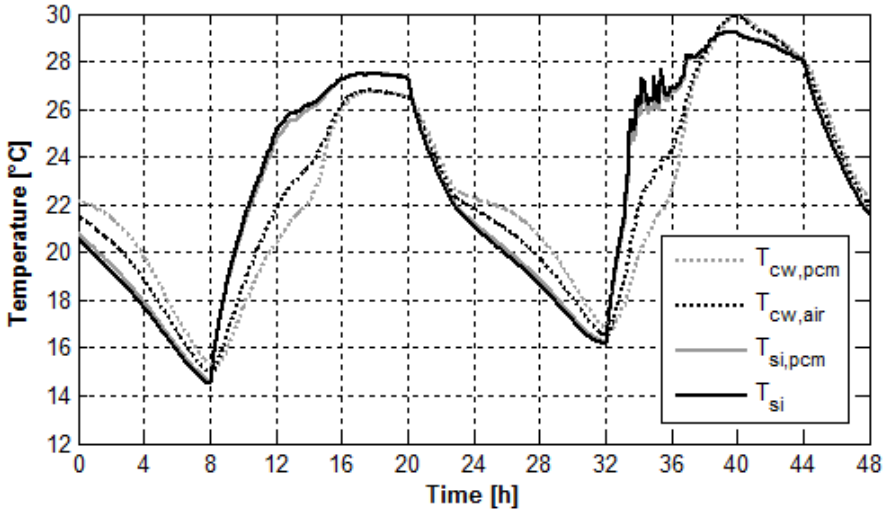


Figure 9-11: Illustration of the temperature heterogeneity in the PCM-equipped wall (13-04 and 14-04)

During the tests, heating consumption of both test-cells was recorded for each scenario. Figure 9-12 shows that the difference between test-cells with and without PCMs is relatively small (less than 3 %), except for the CI scenario. The combined effect of solar radiation and a higher set-point during the day allowed storing more energy, leading to a reduced heating use during the night.

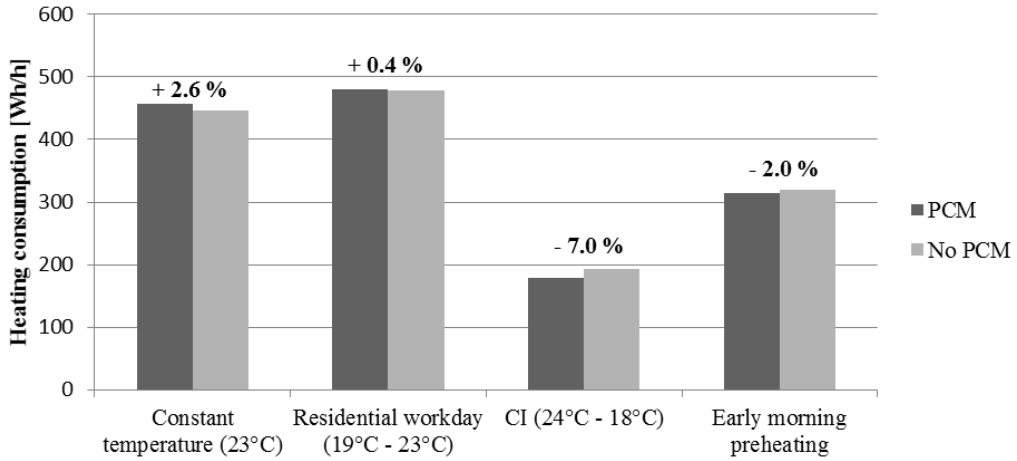


Figure 9-12: Heating consumption for different scenarios with and without PCM

## 9.5 Models

This section presents models developed for both test-cells without and with PCM. The model without PCM is considered as a benchmark. The way how the PCM layer is modeled is then

explained. A comparison between experimental and simulated results for the test-cell with PCM and computation times are finally discussed.

### 9.5.1 Reference test-cell model and benchmarking

The test-cell is modeled without PCM to fine-tune some parameters using the measured data. The test-cell is modeled as a wood-frame construction while considering the parameters given in Table 9-2. Among the parameters to be fine-tuned are the convection coefficients and the zone capacitance. The inside surface convection coefficients are internally computed in TRNSYS, according to empirical relationships (TRANSSOLAR Energietechnik Gmbh, 2012). The outside surface convection coefficients are set to the default value suggested in TRNSYS, i.e. 18 W/m²-K. The air capacitance in the zones is set to a value of 1.2 kJ/m³-K. The extreme set-back scenario (see Table 9-3) is chosen for the benchmarking procedure since step-changes tests are interesting for model calibration. The electric baseboards are not explicitly modeled in TRNSYS. Instead, Type 56's internal heating is used. This option calculates the amount of heat that must be added over a time-step to match the set-point. This explains the lack of oscillations in the simulated results.

Figure 9-13 presents a comparison between experimental and simulated results and their resulting Root Mean Square Deviation (RMSD):

(a) The heating power.

(b) The room air temperature (mid-height).

(c) The inside surface temperature of the south-west wall (mid-height).

(d) The inside surface temperature of the north-west wall (mid-height).

(e) The inside surface temperature of the ceiling.

(f) The inside surface temperature of the floor.

All graphs present clear similarities between experiments and simulations with reasonable RMSD values. During the presented period (from the 11$^{th}$ of April to the 17$^{th}$ of April 2013), the experimental and simulated energy consumption are respectively 59.3 kWh and 58.4 kWh, i.e. a low error of around 1.5 %. In Figure 9-13 (f), the presence of two peaks in the experimental temperature results is caused by direct solar radiation hitting the thermocouple during the morning

(the windows are oriented South-East). This calibrated model is used as a starting point for modeling the test-cell with PCM.

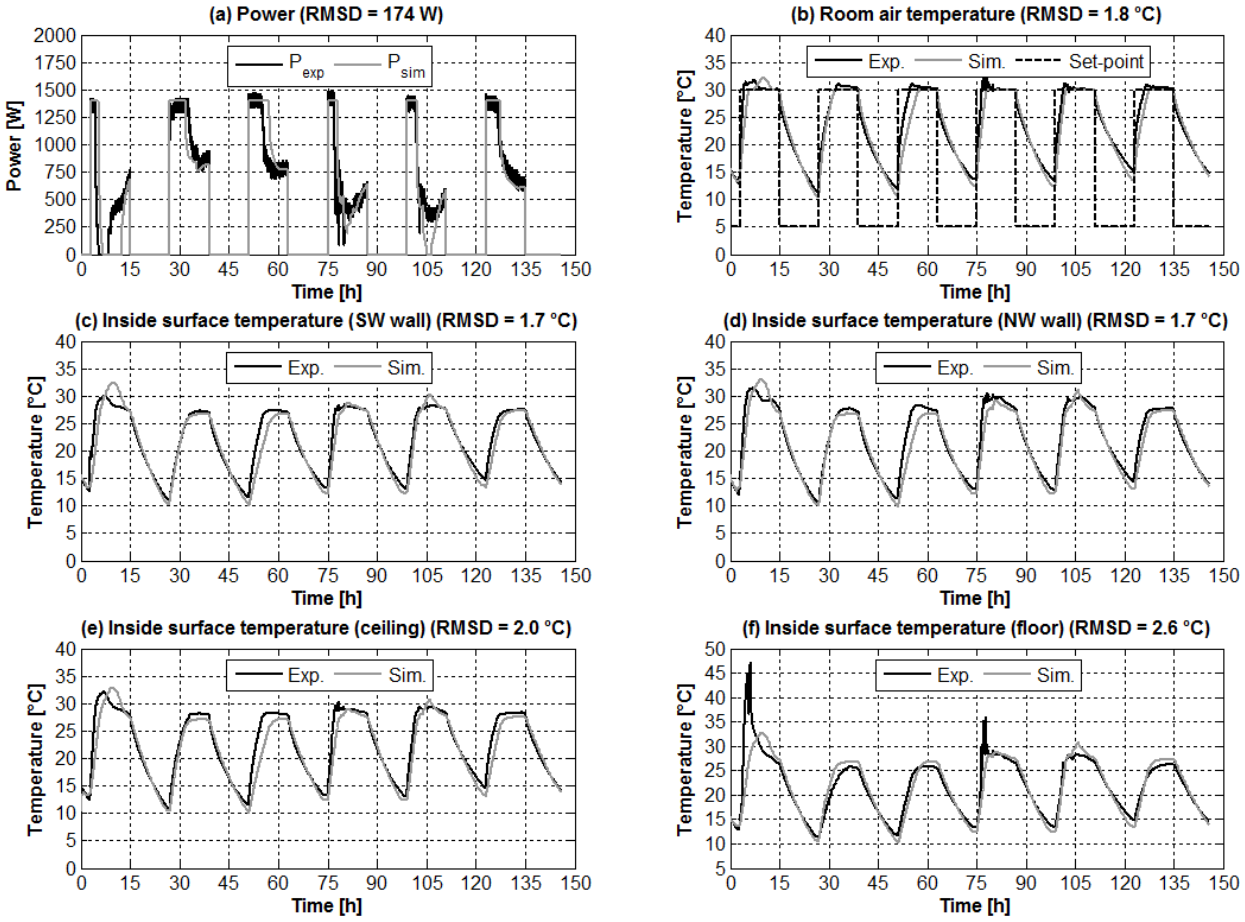


Figure 9-13: Comparison between experimental and simulated results for the test-cell without PCM during the extreme set-back scenario (from 11-04-2013 to 17-04-2013)

### 9.5.2 PCM modeling

As illustrated in Figure 9-6, the PCM layer is heterogeneous. In TRNSYS, conduction heat transfer through walls is modeled in 1-D. The PCM layer is then modeled as an equivalent layer. The properties of both layers (the plywood board and the equivalent layer with PCM) are presented in Table 9-4.

The equivalent density is calculated as the volumetric average of all materials included in the equivalent layer. The thermal conductivity has been computed using THERM (Lawrence Berkeley National Laboratory, 2011). The temperature-dependent specific-heat of the equivalent layer is

defined by enthalpy-temperature curves (Figure 9-14), determined through previous work (Delcroix, Kummert, Daoud, & Bouchard, 2015). This work based on inverse modeling technics concludes that:

- The specific-heat of the equivalent layer in the solid and liquid states are 1.76 J/g-K and 1.87 J/g-K, respectively.
- The latent heat of the equivalent layer is 150 J/g.
- The phase change temperature ranges during melting and solidification are between 16.5 °C and 24 °C and between 15.5 °C and 23 °C, respectively (including therefore a hysteresis of 1 °C).

Table 9-4: Layers properties of the PCM-equipped wall

| Layer | Thickness [m] | Thermal conductivity [W/m-K] | Density [kg/m³] | Specific heat [J/g-K] |
|---|---|---|---|---|
| Plywood | 0.006 | 0.084 | 850 | 1.25 |
| Equivalent layer | 0.017 | 0.042 | 223 | See Figure 9-14 |

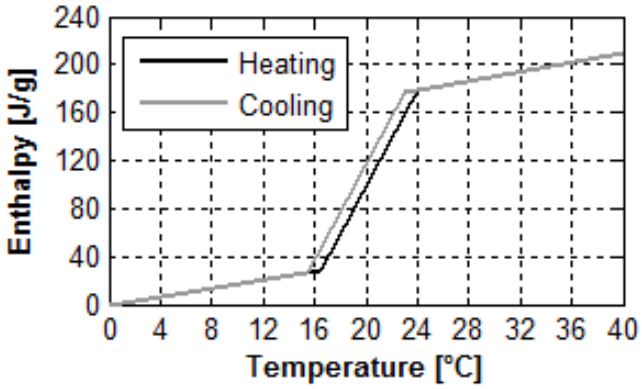


Figure 9-14: Enthalpy-temperature curves of the equivalent layer

If the melting or solidification is interrupted, a switch between both enthalpy-temperature curves is performed using a slope equivalent to the liquid or solid specific heat. This method is suggested by Bony and Citherlet (2007) and experimentally validated by Delcroix et al. (2015b).

The coupling method used to link Type 3258 (PCM wall model) to Type 56 (multizone building model) is the method explained in the Appendix. Only the PCM layer as equivalent layer is

modeled in Type 3258 (with an explicit finite-difference method) while the other part of the wall is modeled in Type 56 (with the CTF method).

### 9.5.3 Comparison between models and experiments

Figure 9-15 presents comparisons of different variables between experiments and simulations and their resulting RMSD values:

(a) The heating power.

(b) The room air temperature (mid-height).

(c) The inside surface temperature of the south-west wall (mid-height).

(d) The temperature at the center of the PCM layer for the south-west wall (mid-height).

(e) The inside surface temperature of the ceiling.

(f) The inside surface temperature of the floor.

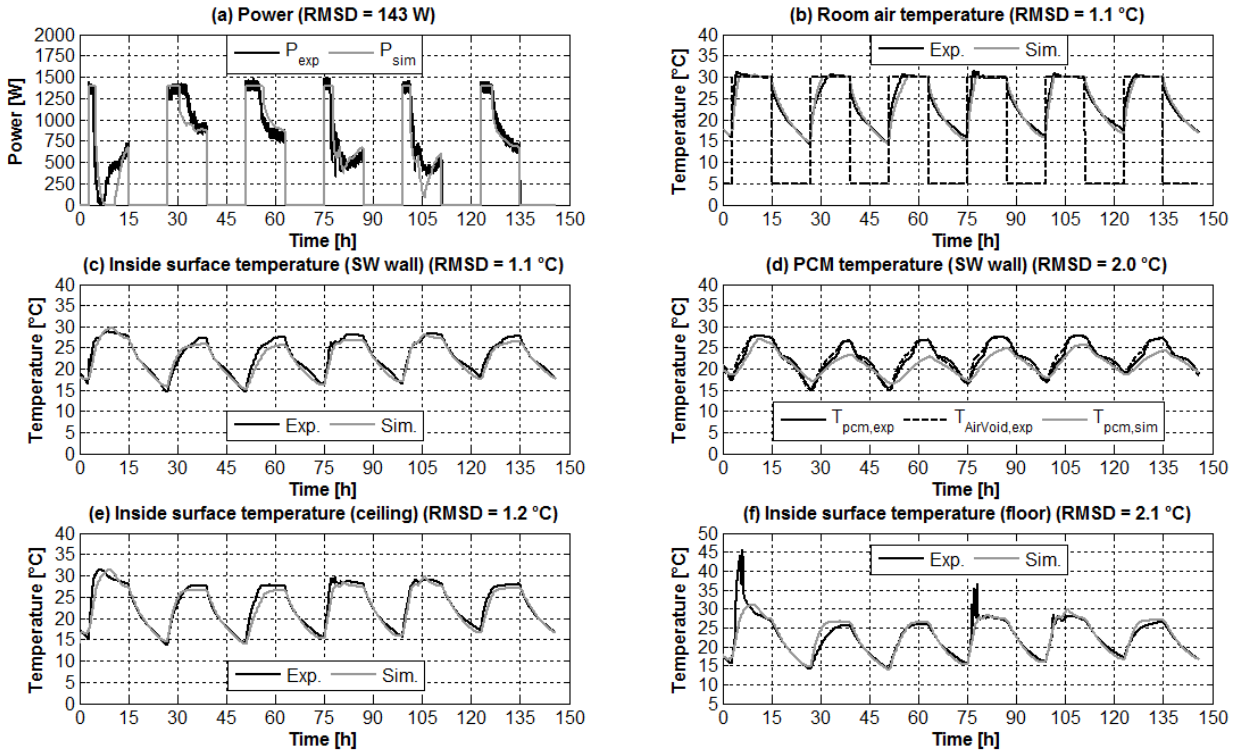


Figure 9-15: Comparison between experimental and simulated results for the test-cell with PCM during the extreme set-back scenario (from 11-04-2013 to 17-04-2013)

Such as in Figure 9-13 (f), Figure 9-15 (f) presents the same peaks in the experimental temperature results, which are caused by direct solar radiation hitting the thermocouple.

The RMSD values are generally lower than the ones measured for the test-cell without PCM. Experimental and simulated energy consumptions are also close with respective values of 62.7 kWh and 60.4 kWh, i.e. a low error of around 3.7 %.

A results comparison between the reference and PCM-equipped test-cells shows that both experiments and simulations indicate the same dissimilarities. Figure 9-16 presents the case of the residential workday scenario, in which the set-point is set to 19 °C during the working hours and to 23 °C otherwise. Experimental and simulated results show that adding PCMs mitigates temperature extremes, as illustrated in figures (c) and (d) (in the circles). Figures (a) and (b) indicate that the heating power presents the same dissimilarities (in the circles) between both test-cells (with and without PCMs) in the experiments and simulations.

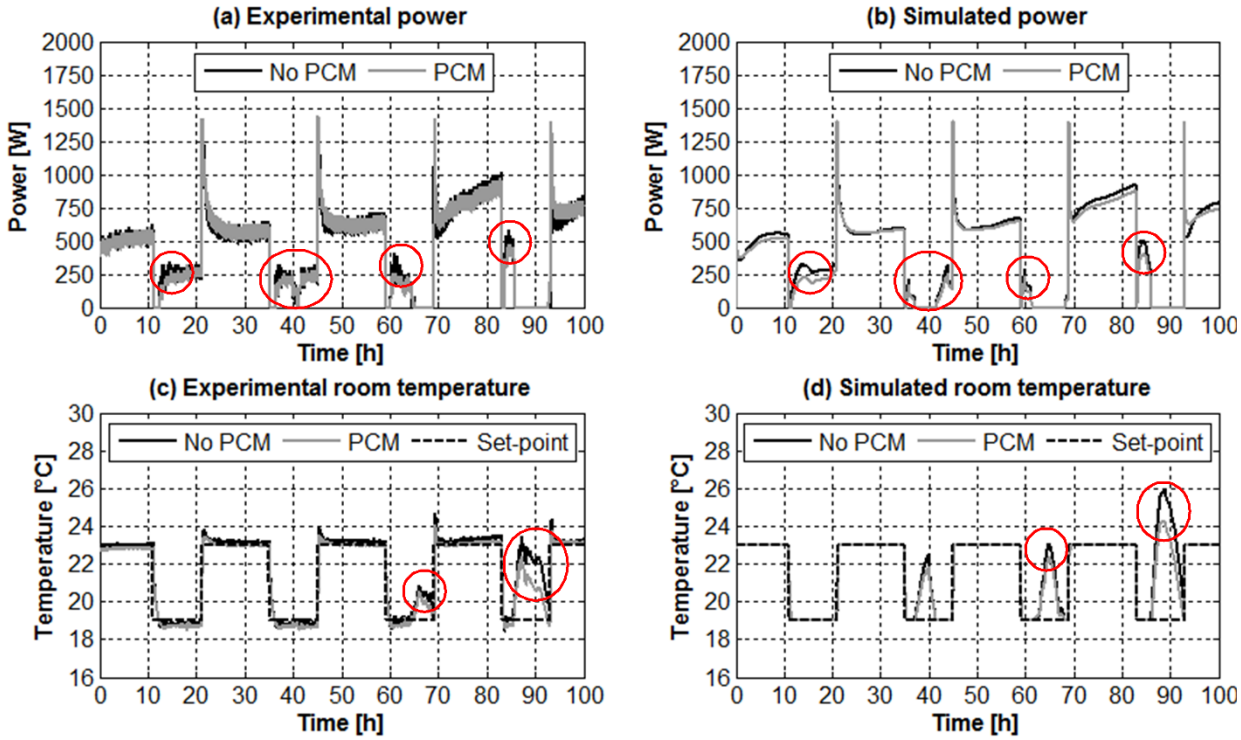


Figure 9-16: Results comparison between the test-cells equipped with and without PCMs during the residential workday scenario (from 11-03-2013 to 15-03-2013)

However, the comparison between Figure 9-16 (c) and (d) shows that the solar radiation during the last three days is overestimated. No shading is modeled and this can explain the overestimation of solar radiation in the simulations.

Figure 9-17 presents the case of the commercial and institutional scenario, in which the set-point is set to 24 °C during the working hours and to 18 °C otherwise. Such as the previous scenario, the experimentations and simulations show that adding PCMs mitigates temperature extremes, as illustrated in figures (c) and (d) (in the circles). Furthermore, the PCM-equipped test-cell experiences a slower temperature decrease after a set-point drop, as similarly indicated by the experiments and simulations. Figures (a) and (b) indicate that the heating power presents the same dissimilarities (in the circles) between both test-cells (with and without PCMs) in the experiments and simulations.

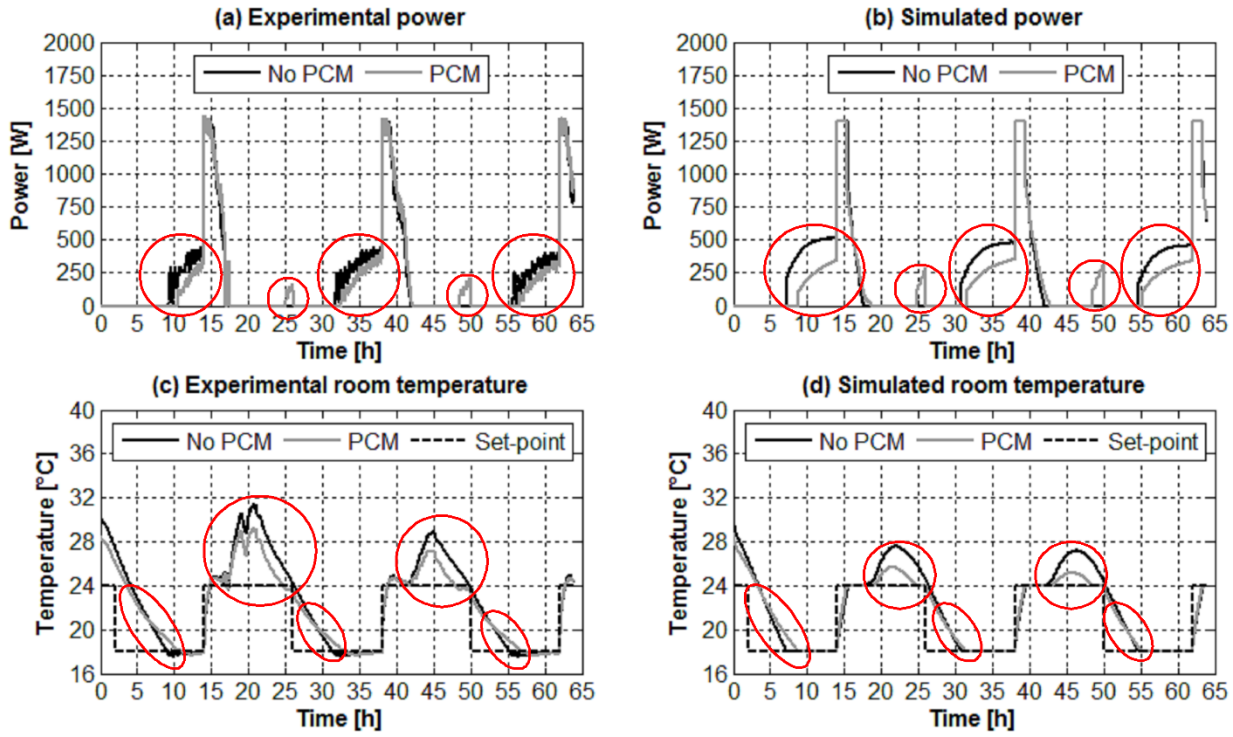


Figure 9-17: Results comparison between the test-cells equipped with and without PCMs during the commercial and institutional scenario (from 25-03-2013 to 28-03-2013)

Figure 9-16 and Figure 9-17 show that the simulations reproduce the same effects than the ones observed experimentally. Table 9-5 indicates moreover that the RMSD values between experiments and simulations for both test-cells (with or without PCMs) are all lower than the ones

measured during the benchmarking procedure. It shows then that the simulations are in good agreement with the experimentations.

Table 9-5: RMSD values between experiments and simulations for the scenarios illustrated in Figure 9-16 and Figure 9-17

| **Scenario** | **Power – RMSD** | | **Room temperature – RMSD** | |
|---|---|---|---|---|
| | No PCM | PCM | No PCM | PCM |
| Residential workday | 145 W | 139 W | 1.0 °C | 0.9 °C |
| Commercial and institutional (CI) | 133 W | 104 W | 1.4 °C | 1.1 °C |

### 9.5.4 Computation time

Table 9-6 shows computation times for simulations of the test-cell with and without PCM and 3-D geometry within Type 56. 3-D geometry in TRNSYS allows using a detailed calculation of radiative heat transfer in buildings (TRANSSOLAR Energietechnik Gmbh, 2012). Computation times are given for a 146-hour simulation using a 1-min time-step.

Table 9-6: Computation times for the test-cell simulations with the extreme set-back scenario (146-hour simulation with a 1-min time-step)

| | Computation time [s] | Normalized computation time |
|---|---|---|
| Test-cell without PCM (no 3-D) | 6 s | 1 |
| Test-cell without PCM (3-D) | 68 s | 12 |
| Test-cell with PCM (no 3-D) | 18 s | 3 |

As expected, simulating the test-cell without PCM and 3-D geometry requires the least computation time. Adding 3-D geometry makes the simulation largely more time-consuming (around 12 times). Finally, the simulation of the test-cell including PCM is around 3 times more time-consuming than the one without 3-D and PCM. The increase in computation time seems acceptable with regard to the new capability offered. In order to keep computation times low, it is recommended to use Type 3258 only for including PCMs.

## 9.6 Conclusion

Conduction heat transfer through walls is currently modeled in Type 56 (multizone building model in TRNSYS) with the CTF method. This method is unable to model layers with temperature-dependent properties. A model based on an explicit finite-difference method was developed and implemented in an external component, named Type 3258. This model is coupled with an enthalpy method for PCM modeling. Part I of the current paper describes with details this model and its numerical validation. This part presents the coupling methods to link Type 56 to the PCM wall model and the experimental validation of Type 3258. The experimental data comes from a full-scale test-bench composed of two identical test-cells (one equipped with PCMs and one without). Several scenarios are tested and clear differences are observed between both test-cells. The experimental data show that adding PCMs to building walls mitigates inside temperature variations and produces a time shift of wall temperature extremes. Differences in heating power are small, but temperature swings mitigation and time-shift effects are observed. A model benchmarking procedure is firstly performed on the test-cell without PCMs, leading to a calibrated model. A comparison between the experimental and simulated data (without PCMs) shows low RMSD values and an error of 1.5 % for the heating consumption during the selected 7-day period. The PCM layers are then added to this model using Type 3258 and the experimental data of the PCM-equipped test-cell are compared to the simulated results. Compared to the benchmarking results (without PCMs), the RMSD values between the experiments and the simulations (with PCMs) are lower or in the same order of magnitude (for both power and temperatures data). A further result comparison between both test-cells (with and without PCM) indicates that the simulations reproduce adequately the impact of PCMs, i.e. mitigation and time-shift effects. Finally, the increase in computation time caused by Type 3258 is less important than considering 3-D geometry and seems acceptable with regard to the capability offered. However, it is recommended to use Type 3258 only when it is needed.

## Acknowledgements

The research work presented in this paper is financially supported by Hydro-Québec, FRQNT (Fonds de Recherche du Québec en Nature et Technologies) and NSERC (Natural Sciences and

Engineering Research Council of Canada). We also would like to thank the energy technology laboratory (Hydro-Québec Research Institute) where the experimentations were achieved.

# Appendix - Applied coupling method between Type 56 and Type 3258

This coupling method is similar to the methods suggested by TESS and by Dentel and Stephan, which are illustrated in Figure 9-2. The main difference consists in modeling the wall without considering surface temperatures. The first and last nodes are modeled slightly inside the wall, as illustrated in Figure 9-18. The surface temperatures are only calculated in Type 56 where the boundary walls are modeled. Type 3258 is configured to model the wall without considering surface temperatures. Such as the methods suggested by TESS and by Dentel and Stephan, the coupling method is different for internal and external walls. As a boundary wall in Type 56 cannot receive solar radiation, a dummy zone must be defined to model a direct contact zone between the external and boundary walls (Figure 9-18 (b)).

The inputs from Type 56 to Type 3258 are the surface temperatures generated by Type 56. The outputs from Type 3258 to Type 56 are the temperatures calculated for the first and last nodes by the 1-D finite-difference model. The heat transfer coefficients between the surface temperatures and the first and last nodes of the 1-D finite-difference model must be defined in Type 56 and are the inverses of the thermal resistances between $T_{so,1}$ and $T_1$ and between $T_{so,2}$ and $T_n$ (see Figure 9-18). These coefficients are given as outputs in Type 3258 and can be directly connected to Type 56. Table 9-7 presents the connections that should be performed between Type 56 and Type 3258 for this coupling method. Variable names (e.g. TSO) and output numbers (e.g. NType 18) refer to the nomenclature used in the Type 56 manual (TRANSSOLAR Energietechnik Gmbh, 2012).

A positive side-effect of this method is the reduced constraint on the stability conditions (Equations ( 9.5 ) and ( 9.6 )). As no surface nodes are defined in the finite-difference model, the most constraining stability condition (Equation ( 9.6 )) does not apply. A simulation speed-up is then observed.

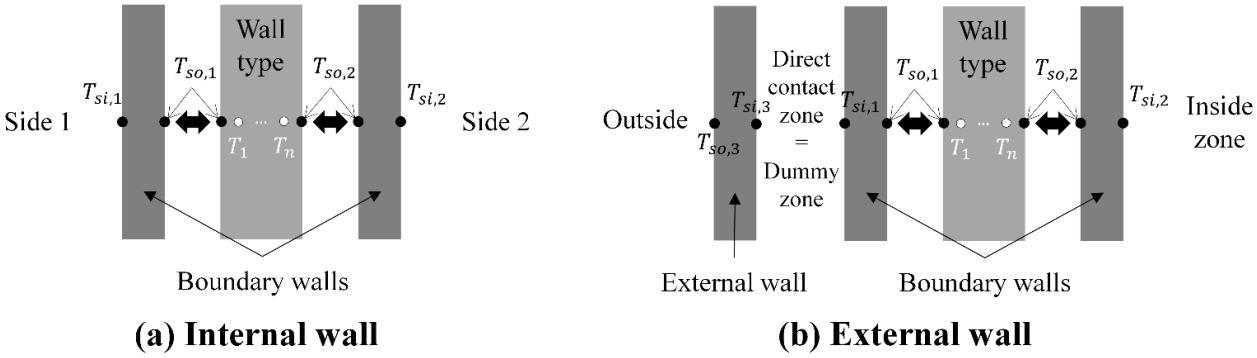


Figure 9-18: Proposed methodology to link an external wall type to Type 56

Table 9-7: Connections between Type 56 and the external wall type

| Inputs from Type 56 | Notes for inputs | Outputs toward Type 56 | Notes for outputs |
|---|---|---|---|
| TSO (NType 18) for side 1 | Outside surface temperatures from Type 56 are the boundary temperatures of the wall | Temperature at the first node (side 1) | Boundary temperatures must be connected to Type 56 |
| | | Temperature at the last node (side 2) | |
| TSO (NType 18) for side 2 | | Heat transfer coefficient between the first node and the surface temperature (side 1) | / |
| | | Heat transfer coefficient between the last node and the surface temperature (side 2) | |

# References

Al-Saadi, S. N. (2014). Modeling and simulation of PCM-enhanced façade systems. University of Colorado.

Al-Saadi, S. N., & Zhai, Z. J. (2014). TRNSYS Type 285 - Phase Change Materials Embedded in Wall System. Boulder, CO.

Barbour, J. P., & Hittle, D. C. (2005). Modeling Phase Change Materials With Conduction Transfer Functions for Passive Solar Applications. Journal of Solar Energy Engineering, 128(1), 58–68. Retrieved from http://dx.doi.org/10.1115/1.2000977

Bergman, T. L., Lavine, A. S., Incropera, F. P., & Dewitt, D. P. (2011). Fundamentals of heat and mass transfer. Wiley.

Bony, J., & Citherlet, S. (2007). Numerical model and experimental validation of heat storage with phase change materials. Energy and Buildings, 39, 1065–1072. Retrieved from http://www.sciencedirect.com/science/article/pii/S037877880600291X

Delcroix, B., Kummert, M., & Daoud, A. (2015a). Modeling of a wall with phase change materials. Part I: Developement and numerical validation. Journal of Building Performance Simulation.

Delcroix, B., Kummert, M., & Daoud, A. (2015b). Thermal behavior mapping of a phase change material between the heating and cooling enthalpy-temperature curves. In 6th International Conference on Building Physics for a Sustainable Built Environment. Torino, Italy.

Delcroix, B., Kummert, M., Daoud, A., & Bouchard, J. (2015). Influence of experimental conditions on measured thermal properties used to model phase change materials. Building Simulation: An International Journal.

Dentel, A., & Stephan, W. (2010). Thermal comfort in rooms with active PCM constructions. In 8th International Conference on System Simulation in Buildings. Liège, Belgium.

Dentel, A., & Stephan, W. (2013). TRNSYS TYPE 399 - Phase change materials in passive and active wall constructions. Nürnberg.

Entropy Solutions Inc. (2011). PureTemp: the world's only 100% renewable phase change material. Retrieved July 15, 2013, from http://www.puretemp.com/

Goodrich, L. E. (1978). Efficient numerical technique for one-dimensional thermal problems with phase-change. International Journal of Heat and Mass Transfer, 21(5), 615.

Haghighat, F., Yu, Z., Inard, C., Michaux, G., Kuznik, F., Johannes, K., Virgone, J., Barzin, R., Farid, M., Bastani, A., Stathopoulos, N., El Mankibi, M., Nkwetta, D. N., Moreau, A., Vouillamoz, P-E., Castell, A., Adl-Zarrabi, B. (2013). Annex 23: Energy storage in buildings of the future - Applying Energy Storage in Ultra-low Energy Buildings.

Jost, R. (2012). Developing a run-time coupling between ESP-r and TRNSYS. École Polytechnique de Montréal. Retrieved from http://publications.polymtl.ca/978/1/2012_RomainJost.pdf

Kuznik, F., Virgone, J., & Johannes, K. (2010). Development and validation of a new TRNSYS type for the simulation of external building walls containing PCM. Energy and Buildings, 42, 1004–1009.

Lawrence Berkeley National Laboratory. (2011). THERM 6.3 / WINDOW 6.3: NFRC Simulation Manual.

Mitalas, G. P., & Arseneault, J. G. (1972). Fortran IV program to calculate z-transfer functions for the calculation of transient heat transfer through walls and roofs. Division of Building research, National Research Council Canada. Retrieved from http://nparc.cisti-icist.nrc-cnrc.gc.ca/npsi/ctrl?action=shwart&index=an&req=5752842

Pedersen, C. O. (2007). Advanced zone simulation in EnergyPlus: incorporation of variable properties and phase change material (PCM) capability. In Building Simulation (pp. 1341–1345). Beijing.

Phase change energy solutions. (2008). BioPCM longevity cycle testing. Retrieved from http://www.phasechange.com/index.php/en/contractor-library

Phase change energy solutions. (2014). Manufacturing innovative thermal storage technologies for smart & sustainable buildings. Retrieved February 9, 2015, from http://www.phasechange.com/index.php

Stephenson, D. G., & Mitalas, G. P. (1971). Calculation of heat conduction transfer functions for multi-layer slabs. ASHRAE Transactions, 77(2), 117–126. Retrieved from http://nparc.cisti-icist.nrc-cnrc.gc.ca/npsi/ctrl?action=shwart&index=an&req=5757086&lang=en

Tabares-Velasco, P. C., Christensen, C., & Bianchi, M. (2012). Verification and validation of EnergyPlus phase change material model for opaque wall assemblies. Building and Environment, 54, 186–196.

Thermal Energy Systems Specialists. (2012). TESSLibs3 - Type 1270: Phase Change Material (PCM) Wall Layer for Type 56.

TRANSSOLAR Energietechnik Gmbh. (2012). TRNSYS 17 - Multizone building modeling with Type 56 and TRNBuild. Stuttgart, Germany.

Voller, V. R., & Cross, M. (1981). Accurate solutions of moving boundary problems using the enthalpy method. International Journal of Heat and Mass Transfer, 24(3), 545.

Yao, M., & Chait, A. (1993). An alternative formulation of the apparent heat capacity method for phase change problems. Numerical Heat Transfer, Part B, Fundamentals, 24(3), 279.

# CHAPTER 10 GENERAL DISCUSSION

The literature review highlights some limitations in common BPS programs such as TRNSYS, EnergyPlus and ESP-r with respect to modeling walls that include Phase Change Materials (PCMs). No current BPS program is capable of modeling a wall with PCMs including temperature-dependent thermal conductivity, hysteresis and subcooling. In particular, TRNSYS is not adapted for this purpose since conduction heat transfer through walls is modeled using the CTF method. This method is furthermore not appropriate for short-time-step simulations (< 5 minutes) of buildings with highly resistive and heavy walls, which is required for simulating power demand management strategies.

The literature review also highlights the complexity of measuring PCM thermophysical properties, and in particular the heat capacity. Measurement techniques can lead to different test results, depending on the experimental conditions.

These challenges were addressed in the present thesis, which resulted in the contributions detailed below.

The first main contribution is the improvement brought to the CTF method in TRNSYS multizone building model (Type 56). As shown in Chapter 4, the proposed method to generate CTF coefficients, based on a state-space method, can significantly reduce the gap between the simulation time-step and the timebase value used to generate the CTF coefficients, decreasing the stair-step effects and the corresponding inaccuracies. It is specifically useful for highly resistive and thermally heavy walls, i.e. walls with low Fourier numbers. Unfortunately, this method cannot ensure for all cases that the timebase value is equivalent to the simulation time-step. For extremely difficult cases, another solution is proposed in Chapter 5. It consists of a coupling in TRNSYS between Type 56 and another external type modeling a wall with a finite-difference method (such as Type 3258). Using a finite-difference model for modeling walls with low Fourier number and the CTF method for the other walls ensures that the timebase value is equivalent to the simulation time-step. Hence Chapter 5 highlights the complementarity of both modeling methods: the finite-difference method is appropriate for walls with low Fourier numbers while the CTF method is more suitable for walls with higher Fourier numbers. However, modeling PCM layers requires using a finite-difference model since the CTF method is only appropriate for walls with constant properties.

The second contribution of this thesis is the in-depth thermal characterization of the selected PCM and a critical assessment of current measurement techniques for the heat capacity. Chapter 6 highlights the inability of the traditional heat capacity measurement techniques such as DSC tests or the T-history method to obtain the effective heat capacity used for PCM modeling in building applications. This is caused by the inadequacy between the experimental measurement conditions (small samples and high heat transfer rates) and the actual PCM use in building applications, especially in building envelopes (large PCM quantity and low heat transfer rates). Using an inverse method for PCM characterization overcomes some limitations of the traditional measurement and data processing methods, and is adaptable to different situations. An inverse method is applied on PCM-equipped walls experimentations with varying heat transfer rates (50 cooling cases and 48 heating cases). Depending on heat transfer rates, the tested PCM behaves differently. Different heat transfer rates (0.01 – 0.18 °C/min) impact on the phase change temperature range and on the hysteresis between heating and cooling enthalpy-temperature curves. Results show that higher heat transfer rates lead to higher hysteresis and colder phase change temperature ranges. Hence this chapter highlights that a test method should be carefully chosen depending on the PCM application. Appendices A to B detail the experiments performed to measure the density and thermal conductivity of the tested PCM. Appendix C indicates how the thermal conductivity of the PCM layer composed of PCM, air and plastic film is computed.

Chapter 7 focuses on the PCM thermal behavior during partial melting or solidification, i.e. when melting or solidification is interrupted. The literature documents multiple scenarios for these cases. Until now, no experimental validation dedicated to this specific issue was available. Chapter 7 provides an original contribution by addressing this issue experimentally. Two scenarios are tested: first, a switch between heating and cooling enthalpy-temperature curves using a slope equivalent to the solid or liquid specific heat; the second option consists in staying on the same curve. Two models are developed for simulating both scenarios. A comparison between both models and the experimentations shows a good agreement with the scenario modeling a transition between heating and cooling curves. Hence the scenario without transition should be rejected. However, the model with transition does not show a good agreement with the interrupted heating. In this case, the transition between the enthalpy-temperature curves is partial. Further research should then be conducted on the impact of different factors on the transitional behavior.

The final original contribution is the development and validation of a TRNSYS type dedicated to PCM wall modeling able to simulate PCM with temperature-dependent thermal conductivity, hysteresis and subcooling. This model is also appropriate for simulating walls with constant properties, as illustrated in Chapter 5. Chapter 8 offers an in-depth description and a numerical validation of the developed model named Type 3258. Type 3258 uses an explicit finite-difference method (i.e. a Forward Time Central Space scheme) coupled with an enthalpy method for PCM modeling. Stability conditions and a detailed description of the algorithm are presented. The numerical validation proposed by the International Energy Agency on nine wall test cases shows that the developed model is in good agreement with other reference models from France and Norway. This chapter also highlights the relative superiority of the enthalpy method, compared to the effective heat capacity. It is namely illustrated by two issues related to phase change detection and energy conservation problems. Chapter 8 also proposes a methodology for modeling PCM subcooling. Chapter 9 presents a further validation of Type 3258 using experimental data from test-cells exposed to ambient environment. The experimental validation indicates that the developed model is in agreement with experimental data and reproduces the specific effects caused by the presence of PCMs in the test-cell. Chapter 9 also describes the possible coupling methods used to link Type 56 to the PCM wall model (i.e. Type 3258 in our case) and discusses the corresponding convergence considerations. An alternative method (in Chapter 9) is proposed and allows a reduction of the model stability constraints, resulting in faster computational times. Appendix D presents the proforma (parameters/inputs/outputs description) of Type 3258.

# CHAPTER 11 CONCLUSION

As mentioned in the previous chapter, several contributions are presented in this thesis, i.e.:

1) Improvement of the CTF method in TRNSYS multizone building model (Type 56) based on a state-space method. A coupling between the CTF method (Type 56) and a finite-difference method (external type) can be performed in TRNSYS, leading to a potentially complete resolution of the highly resistive and heavy walls problem.
2) In-depth characterization of the selected PCM, including its behavior under different experimental conditions and during partial melting/solidification events.
3) Development and validation of a new PCM wall model, able to simulate PCM layers with temperature-dependent thermal conductivity, hysteresis and subcooling.

Some recommendations for further research are formulated below.

The coupling between the CTF method and a finite-difference method requires a good knowledge of the TRNSYS program to link an external type (such as Type 3258) to Type 56, which can be seen as an unnecessarily cumbersome and error-prone process. Ideally, a finite-difference method should be integrated directly within Type 56 for modeling heat transfer through walls. Alternatively, a method coupling the CTF method with a finite-difference method could be worthy to be implemented directly in Type 56 in order to benefit the complementarity of both methods.

The PCM characterization highlights the influence of the experimental conditions on the PCM thermal behavior, in particular on the PCM hysteresis, the phase change temperature range and during interrupted melting/solidification events. However, clear mathematical relationships defining the impacts of experimental conditions on the PCM thermal behavior have not been identified. This issue should be integrated in a future model. Ideally, the enthalpy-temperature curve should be scalable, depending on the experimental conditions.

Finally, the developed and validated model uses a 1-D explicit finite-difference method for modeling walls including PCM layers. If a highly diffusive layer (e.g. air) is included in the wall, the explicit scheme requires very short time-steps to meet the stability conditions, leading to higher computation times. Coupling this method with the CTF method in Type 56 is the solution proposed in this thesis. However, a few difficulties were mentioned earlier. Ideally, an implicit method could be implemented to avoid constraining stability conditions while considering convergence

considerations. The model could then select one of the two solving approaches depending on their respective advantages.

# REFERENCES

Alexiades, V., & Solomon, A. D. (1992). Mathematical Modeling Of Melting And Freezing Processes. Taylor & Francis. Retrieved from http://books.google.ca/books?id=WfJ13xBpBNYC

Al-Saadi, S. N. (2014). Modeling and simulation of PCM-enhanced façade systems. University of Colorado.

Al-Saadi, S. N., & Zhai, Z. (John). (2013). Modeling phase change materials embedded in building enclosure: A review. Renewable and Sustainable Energy Reviews, 21, 659–673. doi:10.1016/j.rser.2013.01.024

Al-Saadi, S. N., & Zhai, Z. J. (2014). TRNSYS Type 285 - Phase Change Materials Embedded in Wall System. Boulder, CO.

Alvarado, S., Marín, E., Juárez, A. G., Calderón, A., & Ivanov, R. (2012). A hot-wire method based thermal conductivity measurement apparatus for teaching purposes. European Journal of Physics, 33, 897–906.

Ames, W. F. (1992). Numerical methods for partial differential equations (third edit.). Boston: Academic Press.

ASHRAE. (2013). Chapter 18 - Nonresidential Cooling and Heating Load Calculations. In ASHRAE handbook - Fundamentals (pp. 18.15–18.20).

ASTM International. (2000). Standard Test Method for Determination of Thermal Conductivity of Soil and Soft Rock by Thermal Needle Probe Procedure. West Conshohocken, PA, USA.

Atchonouglo, K., Banna, M., Vallée, C., & Dupré, J.-C. (2008). Inverse transient heat conduction problems and identification of thermal parameters. Heat and Mass Transfer, 45(1), 23–29. doi:10.1007/s00231-008-0383-7

Baetens, R., Jelle, B. P., & Gustavsen, A. (2010). Phase change materials for building applications: A state-of-the-art review. Energy and Buildings, 42(9), 1361–1368. doi:http://dx.doi.org/10.1016/j.enbuild.2010.03.026

Barbour, J. P., & Hittle, D. C. (2005). Modeling Phase Change Materials With Conduction Transfer Functions for Passive Solar Applications. Journal of Solar Energy Engineering, 128(1), 58–68. Retrieved from http://dx.doi.org/10.1115/1.2000977

Bergman, T. L., Lavine, A. S., Incropera, F. P., & Dewitt, D. P. (2011). Fundamentals of heat and mass transfer. Wiley.

Bony, J., & Citherlet, S. (2007). Numerical model and experimental validation of heat storage with phase change materials. Energy and Buildings, 39, 1065–1072. Retrieved from http://www.sciencedirect.com/science/article/pii/S037877880600291X

Braun, J. E., & Chaturvedi, N. (2002). An Inverse Gray-Box Model for Transient Building Load Prediction. HVAC&R Research, 8(1), 73–99. Retrieved from http://www.tandfonline.com/doi/abs/10.1080/10789669.2002.10391290

Cao, Y., & Faghri, A. (1990). A Numerical Analysis of Phase-Change Problems Including Natural Convection. Journal of Heat Transfer, 112(3), 812–816. Retrieved from http://dx.doi.org/10.1115/1.2910466

Carslaw, H. H., & Jaeger, J. C. (1959). Conduction of Heat in Solids (Second Edi.). Oxford University Press.

Castell, A., Medrano, M., Castellón, C., & Cabeza, L. F. (2009). Analysis of the simulation models for the use of PCM in buildings. In Effstock: Thermal Energy Storage for Efficiency and Sustainability. Stockholm.

Ceylan, H. T., & Myers, G. E. (1980). Long-time solutions to heat conduction transients with time-dependent inputs. ASME Journal of Heat Transfer, 102(1), 115–120.

Chandrasekharan, R., Lee, E. S., Fisher, D. E., & Deokar, P. S. (2013). An Enhanced Simulation Model for Building Envelopes with Phase Change Materials. ASHRAE Transactions, 119(2).

Cheng, R., Pomianowski, M., Wang, X., Heiselberg, P., & Zhang, Y. (2013). A new method to determine thermophysical properties of PCM-concrete brick. Applied Energy, 112, 988–998. doi:10.1016/j.apenergy.2013.01.046

Cooper, J. (1998). Introduction to partial differential equation with MATLAB. Boston: Birkhäuser.

Crank, J. (1987). Free and Moving Boundary Problems. Clarendon Press. Retrieved from http://books.google.ca/books?id=wTB4AsVvQDsC

Crawley, D. B., Lawrie, L. K., Winkelmann, F. C., Buhl, W. F., Huang, Y. J., Pedersen, C. O., Strand, R. K., Liesen, R. J., Fischer, D. E., Witte, M. J., Glazer, J. (2001). EnergyPlus: creating a new-generation building energy simulation program. Energy and Buildings, 33(4), 319–331. doi:http://dx.doi.org/10.1016/S0378-7788(00)00114-6

Danish Building Energy Institute. (2013). BSim - Building Simulation. Retrieved February 24, 2015, from http://sbi.dk/en/bsim

Delcroix, B., Kummert, M., & Daoud, A. (2015a). Modeling of a wall with phase change materials. Part I: Developement and numerical validation. Journal of Building Performance Simulation.

Delcroix, B., Kummert, M., & Daoud, A. (2015b). Modeling of a wall with phase change materials. Part II: Experimental validation. Journal of Building Performance Simulation.

Delcroix, B., Kummert, M., & Daoud, A. (2015c). Thermal behavior mapping of a phase change material between the heating and cooling enthalpy-temperature curves. In 6th International Conference on Building Physics for a Sustainable Built Environment. Torino, Italy.

Delcroix, B., Kummert, M., Daoud, A., & Bouchard, J. (2014). Experimental assessment of a phase change material in walls for heating and cooling applications. In eSim (pp. 1 – 13). Ottawa, ON, Canada.

Delcroix, B., Kummert, M., Daoud, A., & Bouchard, J. (2015). Influence of experimental conditions on measured thermal properties used to model phase change materials. Building Simulation: An International Journal. doi:10.1007/s12273-015-0241-8

Delcroix, B., Kummert, M., Daoud, A., & Hiller, M. (2012). Conduction transfer functions in TRNSYS multizone building model: current implementation, limitations and possible improvements. In Fifth National Conference of IBPSA-USA (pp. 219 – 226). Madison, Wisconsin.

Dentel, A., & Stephan, W. (2010). Thermal Comfort in Rooms with active PCM Constructions. In 8th International Conference on System Simulation in Buildings (pp. 1–16). Liège, Belgium.

Dentel, A., & Stephan, W. (2013). TRNSYS TYPE 399 - Phase change materials in passive and active wall constructions. Nürnberg.

DuPont. (2012). Votre réponse en masse thermique aux bâtiments à faible inertie. Retrieved October 22, 2012, from http://www.energain.fr/Energain/fr_FR/index.html

Dutil, Y., Rousse, D. R., Salah, N. Ben, Lassue, S., & Zalewski, L. (2011). A review on phase-change materials: Mathematical modeling and simulations. Renewable and Sustainable Energy Reviews, 15, 112–130. Retrieved from http://www.sciencedirect.com/science/article/pii/S1364032110001589

Elsbett, G., Hiebler, S., & Mehling, H. (2006). Determination of the heat storage capacity of PCM and PCM-objects as a function of temperature. In The Tenth International Conference on Thermal Energy Storage. Galloway, NJ, USA.

Energy Systems Research Unit. (1998). ESP-r User Guide: The ESP-r System for Building Energy Simulation. Glasgow.

EnergyPlus. (2014). EnergyPlus Engineering Reference.

Entropy Solutions Inc. (2011). PureTemp: the world's only 100% renewable phase change material. Retrieved July 15, 2013, from http://www.puretemp.com/

Farid, M. M., Khudhair, A. M., Razack, S. A. K., & Al-Hallaj, S. (2004). A review on phase change energy storage: materials and applications. Energy Conversion and Management, 45(9–10), 1597–1615. doi:http://dx.doi.org/10.1016/j.enconman.2003.09.015

Fletcher, C. A. J. (1988). Computational techniques for fluid dynamics. Berlin: Springer-Verlag.

Fourier, J. (1822). Théorie analytique de la chaleur (Firmin Did.). Paris.

Geissler, A. (2008). SPMCMP56 subroutine in ESP-r Source Standard Code.

German Institute for Quality Assurance and Certification. (2009). Phase change material. Berlin, Germany.

Giaconia, C., & Orioli, A. (2000). On the reliability of ASHRAE conduction transfer function coefficients of walls. Applied Thermal Engineering, 20, 21–47.

Gong, Z.-X., & Mujumdar, A. S. (1997). Non-convergence versus non-conservation in effective heat capacity methods for phase change problems. International Journal of Numerical Methods for Heat & Fluid Flow, 7(6), 565–579.

Goodrich, L. E. (1978). Efficient numerical technique for one-dimensional thermal problems with phase-change. International Journal of Heat and Mass Transfer, 21(5), 615.

Günther, E., Hiebler, S., Mehling, H., & Redlich, R. (2009). Enthalpy of Phase Change Materials as a Function of Temperature: Required Accuracy and Suitable Measurement Methods. International Journal of Thermophysics, 30(4), 1257.

Günther, E., Mehling, H., & Hiebler, S. (2007). Modeling of subcooling and solidification of phase change materials. Modelling and Simulation in Materials Science and Engineering, 15, 879–892. doi:10.1088/0965-0393/15/8/005

Haghighat, F., Yu, Z., Inard, C., Michaux, G., Kuznik, F., Johannes, K., Virgone, J., Barzin, R., Farid, M., Bastani, A., Stathopoulos, N., El Mankibi, M., Nkwetta, D. N., Moreau, A., Vouillamoz, P-E., Castell, A., Adl-Zarrabi, B. (2013). Annex 23: Energy storage in buildings of the future - Applying Energy Storage in Ultra-low Energy Buildings.

Heim, D., & Clarke, J. A. (2004). Numerical modelling and thermal simulation of PCM–gypsum composites with ESP-r. Energy and Buildings, 36, 795–805. doi:10.1016/j.enbuild.2004.01.004

Hittle, D. C., & Bishop, R. (1983). An improved root-finding procedure for use in calculating transient heat flow through multilayered slabs. International Journal of Heat and Mass Transfer, 26(11), 1685–1693.

Hoffman, S. (2006). Numerische und experimentelle Untersuchung von Phasenübergangsmaterialien zur Reduktion hoher sommerlicher Raumtemperaturen. Bauhaus-Universität Weimar.

Hu, H., & Argyropoulos, S. A. (1996). Mathematical modelling of solidification and melting: a review. Modelling and Simulation in Materials Science and Engineering, 4(4), 371.

Huang, C.-H., & Jan-Yuan, Y. (1995). An inverse problem in simultaneously measuring temperature-dependent thermal conductivity and heat capacity. International Journal of Heat and Mass Transfer, 38(18), 3433–3441. doi:10.1016/0017-9310(95)00059-I

Hukseflux Thermal Sensors. (2014). Hukseflux Thermal Sensors MTN01. Delft, The Netherlands. Retrieved from http://www.hukseflux.com/product/mtn01

Hydro-Québec. (2006). Réponses à la demande de renseignements no.2 de l'AQCIE/CIFQ.

Ibánez, M., Lázaro, A., Zalba, B., & Cabeza, L. F. (2005). An approach to the simulation of PCMs in building applications using TRNSYS. Applied Thermal Engineering, 25, 1796–1807.

Instructional Physics Laboratory. (2013). A Summary of Error Propagation. Cambridge, MA, USA.

Johannes, K., Virgone, J., Kuznik, F., Wang, X., Haavi, T., & Fraisse, G. (2011). Annex 23: Applying Energy Storage in Buildings of the Future - Development of Sustainable Energy Storage Designs for a variety of Ultra-low energy building thermal, phase change materials and electrical storage options.

Jost, R. (2012). Developing a run-time coupling between ESP-r and TRNSYS. École Polytechnique de Montréal. Retrieved from http://publications.polymtl.ca/978/1/2012_RomainJost.pdf

Klein, S. A., Beckman, W. A., Mitchell, J. W., Duffie, J. A., Duffie, N. A., & Freeman, T. L. (2012). TRNSYS 17: A Transient System Simulation Program. Madison, USA: Solar Energy Laboratory, University of Wisconsin. Retrieved from http://sel.me.wisc.edu/trnsys

Klimes, L., Charvat, P., & Ostry, M. (2012). Challenges in the computer modeling of phase change materials. Materials and Technology, 46(4), 335–338.

Kosny, J., Stovall, T., Shrestha, S., & Yarbrough, D. (2010). Theoretical and Experimental Thermal Performance Analysis of Complex Thermal Storage Membrane Containing Bio-Based Phase-Change Material (PCM). In Building XI (p. 11).

Kravvaritis, E. D., Antonopoulos, K. A., & Tzivanidis, C. (2010). Improvements to the measurement of the thermal properties of phase change materials. Measurement Science and Technology, 21, 1–9.

Kula, L. W., & Yovanovich, M. M. (1991). Characteristic length of complex bodies for transient conduction. ASME Thermal Engineering Proceedings, 1, 259–267.

Kuznik, F., & Virgone, J. (2009). Experimental investigation of wallboard containing phase change material: Data for validation of numerical modeling. Energy and Buildings, 41(5), 561–570. doi:10.1016/j.enbuild.2008.11.022

Kuznik, F., Virgone, J., & Johannes, K. (2010). Development and validation of a new TRNSYS type for the simulation of external building walls containing PCM. Energy and Buildings, 42, 1004–1009.

LAPACK. (2011). DGEEVX: computation of the eigenvalues of a general matrix. Retrieved from http://www.netlib.org/lapack/individualroutines.html

Lawrence Berkeley National Laboratory. (2013). THERM 6.3 / WINDOW 6.3 - NFRC Simulation Manual.

Leduc, M.-A., Daoud, A., & Le Bel, C. (2011). Developing winter residential demand response strategies for electric space heating. In 12th Conference of International Building Performance Simulation Association (2011) (pp. 1111–1118). Sydney.

Lemmon, E. C. (1981). Multidimensional integral phase change approximations for finite element conduction codes. In R. W. Lewis, K. Morgan, & O. C. Zienkiewicz (Eds.), Numerical methods in heat transfer (pp. 201–213). New-York.

Li, X. Q., Chen, Y., Spitler, J. D., & Fisher, D. (2009). Applicability of calculation methods for conduction transfer function of building constructions. International Journal of Thermal Sciences, 48(7), 1441–1451. doi:10.1016/j.ijthermalsci.2008.11.006

Maestre, I. R., Mena, J. D., Pérez-lombard, L., & Gallero, J. G. (2014). Fitting conduction transfer function method to low Fourier numbers: application to ground-coupled floors. Journal of Building Performance Simulation, 1–11. doi:10.1080/19401493.2014.974210

Marín, J. M., Zalba, B., Cabeza, L. F., & Mehling, H. (2003). Determination of enthalpy – temperature curves of phase change materials with the temperature-history method : improvement to temperature dependent properties. Measurement Science and Technology, 14, 184–189.

Mehling, H., & Cabeza, L. F. (2008). Heat and cold storage with PCM: An up to date introduction into basics and applications. (D. Mewes & F. Mayinger, Eds.). Berlin: Springer.

Ministère des Ressources naturelles et de la Faune. (2010). Statistiques énergétiques. Retrieved from http://www.mrn.gouv.qc.ca/energie/statistiques/statistiques-production-centrales.jsp

Mitalas, G. P. (1968). Calculation of transient heat flow through walls and roofs. ASHRAE Transactions, 74(2), 182–188. Retrieved from http://nparc.cisti-icist.nrc-cnrc.gc.ca/npsi/ctrl?action=shwart&index=an&req=5753857&lang=en

Mitalas, G. P., & Arseneault, J. G. (1972). Fortran IV program to calculate z-transfer functions for the calculation of transient heat transfer through walls and roofs. Division of Building research, National Research Council Canada. Retrieved from http://nparc.cisti-icist.nrc-cnrc.gc.ca/npsi/ctrl?action=shwart&index=an&req=5752842

Moler, C., & Van Loan, C. (2003). Nineteen Dubious Ways to Compute the Exponential of a Matrix, Twenty-Five Years Later. SIAM Review, 45(1), 3–49.

Morgan, K., Lewis, R. W., & Zienkiewicz, O. C. (1978). An improved algrorithm for heat conduction problems with phase change. International Journal for Numerical Methods in Engineering, 12(7), 1191–1195.

Morton, K. W., & Mayers, D. F. (1994). Numerical solution of partial differential equations: an introduction. Cambridge: Cambridge University Press.

Myers, G. E. (1971). Analytical methods in conduction heat transfer (McGraw-Hil.). New-York.

Pasupathy, A., & Velraj, R. (2006). Mathematical modeling and experimental study on building ceiling system incorporating phase change material (PCM) for energy conservation. In ASME Conference Proceedings (pp. 59–68).

Patankar, S. (1980). Numerical heat transfer and fluid flow. CRC Press.

Pedersen, C. O. (2007). Advanced zone simulation in EnergyPlus: incorporation of variable properties and phase change material (PCM) capability. In Building Simulation (pp. 1341–1345). Beijing.

Peeters, L., & Mols, R. (2012). Zero Energy House Renovation. Retrieved February 8, 2013, from http://www.zehr.be

Pham, Q. T. (1985). A fast, unconditionally stable finite-difference scheme for heat conduction with phase change. International Journal of Heat and Mass Transfer, 28(11), 2079–2084.

Phase change energy solutions. (2008). BioPCM longevity cycle testing. Retrieved from http://www.phasechange.com/index.php/en/contractor-library

Phase change energy solutions. (2014). Manufacturing innovative thermal storage technologies for smart & sustainable buildings. Retrieved February 9, 2015, from http://www.phasechange.com/index.php

Pipes, L. A. (1957). Matrix analysis of heat transfer problems. Journal of the Franklin Institute, 263(3), 195–206.

Poirier, D. J. (1986). On numerical methods used in mathematical modelling of phase change in liquid metals. University of Ottawa.

Poulad, M. E., Fung, A. S., & Naylor, D. (2011). Effects of convective heat transfer coefficient on the ability of PCM to reduce building energy demand. In 12th Conference of International Building Performance Simulation Association (pp. 270–277). Sydney.

Recktenwald, G. W. (2011). Finite-Difference Approximations to the Heat Equation (Vol. 0). Portland, Oregon, USA. Retrieved from http://www.f.kth.se/~jjalap/numme/FDheat.pdf

Rose, J., Lahme, A., Christensen, N. U., Heiselberg, P., Hansen, M., & Grau, K. (2009). Numerical method for calculating latent heat storage in constructions containing phase change material. In Eleventh International IBPSA Conference (pp. 400–407). Glasgow.

Schranzhofer, H., Puschnig, P., Heinz, A., & Streicher, W. (2006). Validation of a TRNSYS simulation model for PCM energy storages and PCM wall construction elements. In 10th International Conference on Thermal Energy Storage. New Jersey.

Seem, J. E. (1987). Modeling of heat transfer in buildings. University of Wisconsin, Madison.

Shamsundar, N., & Rooz, E. (1988). Numerical methods for moving boundary problems. In W. J. Minkowycz, E. M. Sparrow, G. E. Schneider, & R. H. Pletcher (Eds.), Handbook of numerical heat transfer. New-York: Wiley-Interscience.

Shamsundar, N., & Sparrow, E. M. (1975). Analysis of Multidimensional Conduction Phase Change Via the Enthalpy Model. Journal of Heat Transfer, 97(3), 333–340. Retrieved from http://dx.doi.org/10.1115/1.3450375

Sharma, A., Tyagi, V. V, Chen, C. R., & Buddhi, D. (2009). Review on thermal energy storage with phase change materials and applications. Renewable and Sustainable Energy Reviews, 13(2), 318–345. doi:http://dx.doi.org/10.1016/j.rser.2007.10.005

Shrestha, S., Miller, W., Stovall, T., Desjarlais, A., Childs, K., Porter, W., Bhandary, M., Coley, S. (2011). Modeling PCM-enhanced insulation system and benchmarking EnergyPlus against controlled field data. In 12th Conference of International Building Performance Simulation Association (pp. 800–807). Sydney.

Sidje, R. B. (1998). Expokit: a software package for computing matrix exponentials. ACM Transactions on Mathematical Software, 24(1), 130–156.

Solé, A., Miró, L., Barreneche, C., Martorell, I., & Cabeza, L. F. (2013). Review of the T-history method to determine thermophysical properties of phase change materials (PCM). Renewable and Sustainable Energy Reviews, 26, 425–436. doi:10.1016/j.rser.2013.05.066

Spakovszki, Z. S. (2014). 19.3 Radiation heat transfer between planar surfaces. Retrieved February 25, 2015, from http://web.mit.edu/16.unified/www/FALL/thermodynamics/notes/node136.html

Stephenson, D. G., & Mitalas, G. P. (1971). Calculation of heat conduction transfer functions for multi-layer slabs. ASHRAE Transactions, 77(2), 117–126. Retrieved from http://nparc.cisti-icist.nrc-cnrc.gc.ca/npsi/ctrl?action=shwart&index=an&req=5757086&lang=en

Swaminathan, C. R., & Voller, V. R. (1992). A general enthalpy method for modeling solidification processes. Metallurgical Transactions B, 23(5), 651–664.

Swaminathan, C. R., & Voller, V. R. (1993). On the enthalpy method. International Journal of Numerical Methods for Heat & Fluid Flow, 3(3), 233–244. doi:10.1108/eb017528

Tabares-Velasco, P. C., Christensen, C., & Bianchi, M. (2012). Verification and validation of EnergyPlus phase change material model for opaque wall assemblies. Building and Environment, 54, 186–196.

Tabares-Velasco, P. C., Christensen, C., Bianchi, M., & Booten, C. (2012). Verification and Validation of EnergyPlus Conduction Finite Difference and Phase Change Material Models for Opaque Wall Assemblies. Contract, 303, 275–3000.

Tavakoli, R., & Davami, P. (2007). Unconditionally stable fully explicit finite difference solution of solidification problems. Metallurgical and Materials Transactions B, 38(1), 121–142.

The MathWorks Inc. (2010). Matlab help. Natick, MA, USA.

The MathWorks Inc. (2014). GA - Find minimum of function using genetic algorithm. Retrieved July 2, 2014, from http://www.mathworks.com/help/gads/ga.html

Thermal Energy Systems Specialists. (2012). TESSLibs3 - Type 1270: Phase Change Material (PCM) Wall Layer for Type 56.

TRANSSOLAR Energietechnik Gmbh. (2012). TRNSYS 17 - Multizone building modeling with Type 56 and TRNBuild. Stuttgart, Germany.

Voller, V. R. (1996). An overview of numerical methods for solving phase change problems. In W. J. Minkowycz & E. M. Sparrow (Eds.), Advances in numerical heat transfer - Volume 1 (pp. 341 – 375). CRC Press.

Voller, V. R., & Cross, M. (1981). Accurate solutions of moving boundary problems using the enthalpy method. International Journal of Heat and Mass Transfer, 24(3), 545.

Voller, V. R., Swaminathan, C. R., & Thomas, B. G. (1990). Fixed grid techniques for phase change problems: a review. International Journal for Numerical Methods in Engineering, 30(4), 875–898. doi:10.1002/nme.1620300419

Waters, J. R., & Wright, A. J. (1985). Criteria for the distribution of nodes in multilayer walls in finite-difference thermal modelling. Building and Environment, 20(3), 151–162.

Watson, E. S., O'Neill, M. J., Justin, J., & Brenner, N. (1964). A Differential Scanning Calorimeter for Quantitative Differential Thermal Analysis. Analytical Chemistry, 36(7), 1233–1238. doi:10.1021/ac60213a019

Yao, M., & Chait, A. (1993). An alternative formulation of the apparent heat capacity method for phase change problems. Numerical Heat Transfer, Part B, Fundamentals, 24(3), 279.

Zalba, B., Marín, J. M., Cabeza, L. F., & Mehling, H. (2003). Review on thermal energy storage with phase change: materials, heat transfer analysis and applications. Applied Thermal Engineering, 23(3), 251–283. doi:http://dx.doi.org/10.1016/S1359-4311(02)00192-8

Zhang, Y., Jiang, Y., & Jiang, Y. (1999). A simple method , the T -history method , of determining the heat of fusion , specific heat and thermal conductivity of phase-change materials. Measurement Science and Technology, 10, 201–205.

# APPENDIX A – EXPERIMENTS ON PCM DENSITY

The PCM density is measured on ten different samples. A precision balance (resolution: 0.001 gram) and a container with a known volume and mass of 32 milliliters and 3.055 grams is used to perform the density test measurements (Figure A-1). The PCM is in the liquid state during the whole experimentation. Additives included in the PCM are considered in these experimentations (contrary to the measurement performed by the manufacturer).

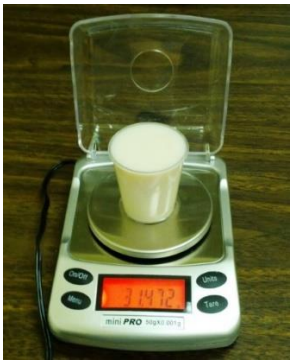

Figure A-1: Density test proceedings

A syringe of 10 milliliters, graduated every 0.1 mL, is used to measure the container volume. For doing so, four draws (3 draws of 10 mL and one of 2 mL) are necessary. An uncertainty of 0.1 mL per draw is assumed, i.e. a total uncertainty $\delta V$ of 0.4 mL (for a volume V of 32 mL).

Table A-1 presents the results for each test. The average PCM mass $\bar{m}$ is 28.261 grams and its corresponding standard deviation $\sigma_m$ is 0.316 grams. The uncertainty on mass measurement $\delta m$ is assumed to be the standard deviation $\sigma_m$. The average density is given in Table A-1 and is equal to 883.163 kg/m³. In order to obtain the uncertainty on density $\delta\rho$, the following equation is applied (Instructional Physics Laboratory, 2013):

$$\delta\rho = \bar{\rho}\sqrt{\left(\frac{\delta m}{\bar{m}}\right)^2 + \left(\frac{\delta V}{V}\right)^2} \qquad (A.1)$$

Using the actual values, Equation ( A.1 ) becomes:

$$\delta\rho = 883.163\sqrt{\left(\frac{0.316}{28.261}\right)^2 + \left(\frac{0.4}{32}\right)^2} = 14.812\ kg/m^3 \qquad (A.2)$$

The average measured density is around 883 kg/m³ and is significantly higher than the value given by the manufacturer (830 kg/m³ (without additives)). Considering the uncertainty, the underestimation is between 4.4 % and 7.6 %.

Table A-1: Density measurements of 10 PCM samples

| Test | Mass of fulfilled container [g] | PCM mass [g] | Density [kg/m³] |
|---|---|---|---|
| 1 | 31.643 | 28.588 | 893.375 |
| 2 | 31.469 | 28.414 | 887.938 |
| 3 | 31.421 | 28.366 | 886.438 |
| 4 | 31.315 | 28.260 | 883.125 |
| 5 | 30.843 | 27.788 | 868.375 |
| 6 | 31.060 | 28.005 | 875.156 |
| 7 | 31.833 | 28.778 | 899.313 |
| 8 | 30.993 | 27.938 | 873.063 |
| 9 | 31.509 | 28.454 | 889.188 |
| 10 | 31.076 | 28.021 | 875.656 |
| Mean | 31.316 ± 0.316 | 28.261 ± 0.316 | 883.163 ± 14.812 |
| Density given by the manufacturer (without additives) | | | 830 |

By cooling down the samples of liquid PCM, it would have been possible to evaluate the density in solid state indicated by the volume variation. However, the solidification creates gaps (Figure A-2) in the samples while taking the same volume. The solid density is apparently higher than the liquid density, but it was not possible to estimate a precise value from these samples. In short, the density given by the manufacturer is underestimated by around 6 % (if the average is

considered) in the liquid state and the underestimation becomes still more important when considering the solid state. The additives probably change significantly this property.

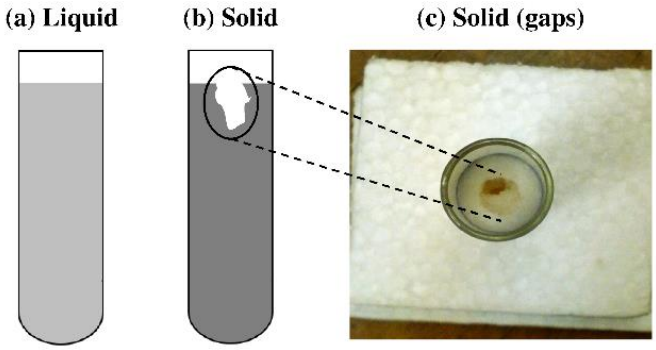


Figure A-2: Gaps in the sample during solidification

# APPENDIX B – EXPERIMENTS ON PCM THERMAL CONDUCTIVITY

The hot-wire method was used to evaluate experimentally the thermal conductivity of the PCM in liquid and solid states. The principle of the hot-wire method is to heat the sample locally in its center and to measure over the time the temperature rise at the heat injection point. Lower temperature rises lead to higher thermal conductivities. The hot-wire method is well documented, e.g. in (Alvarado et al., 2012; ASTM International, 2000). The volume of the PCM sample is around 5 liters and a cylindrical container was used. Additives included in the PCM are considered in these experimentations (contrary to the measurement performed by the manufacturer). The needle from the hot-wire equipment was immersed in the center of the sample, as illustrated in Figure B-1. The needle is a constant linear heating source and the heat flow is assumed to be radial. A temperature sensor is integrated within the needle to record the evolution of temperature over time.

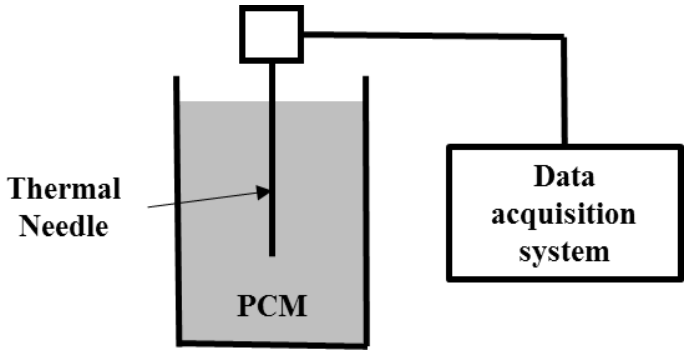


Figure B-1: Hot-wire equipment scheme

The experimentations were performed in liquid (3 times) and solid (4 times) states using Hukseflux MTN01 (Hukseflux Thermal Sensors, 2014). Figure B-2 summarizes the results of the experimental measurements in grey compared to the values provided by the manufacturer in black (without additives). Values from 0.184 W/m-K to 0.255 W/m-K were measured during experimentations with an average of 0.212 W/m-K and a standard deviation of 0.022 W/m-K. Experimental results in liquid state are very stable around 0.209 W/m-K (with a standard deviation of 0.001 W/m-K) while the values for solid state are more variable, which is probably due to the perturbation caused by the solidification process creating air gaps in the PCM sample. The average value for the solid state is 0.214 W/m-K with a standard deviation of 0.030 W/m-K. The

measurement accuracy for the hot wire method is estimated at ± (6 % + 0.04 W/m-K), as illustrated by the error bars in Figure B-2.

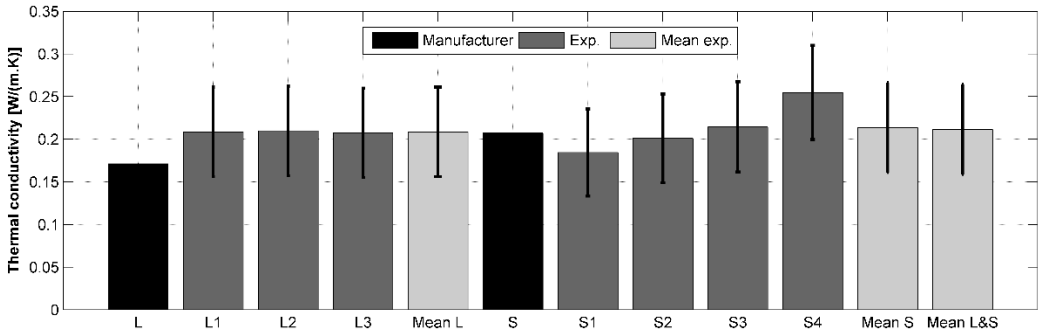


Figure B-2: Comparison between the manufacturer values and the experimental values of thermal conductivity in liquid (L) and solid (S) states

In summary, the thermal conductivity in liquid obtained experimentally (0.209 W/m-K) is significantly different from the value given by the manufacturer without the additives (0.171 W/m-K), i.e. an underestimation of around 18 %. On the other hand, the measurements for the solid state show a significant variability. The average value for the solid state (0.214 W/m-K) is slightly higher than the liquid, which is consistent with manufacturer data. As both average values are very close given the uncertainty, the global experimental average (0.212 W/m-K) is deemed to be a representative value for both states.

# APPENDIX C – EQUIVALENT LAYER THERMAL CONDUCTIVITY

As most building energy performance simulation programs only model 1-D heat conduction through walls, each layer should be homogeneous. The PCM-equipped wall illustrated in Figure C-1 has a central heterogeneous layer. The thermal conductivity of this layer can be obtained using a computational tool such as THERM (Lawrence Berkeley National Laboratory, 2013). Figure C-1 focuses on the thicknesses of each material. PCM pouches occupy 35 % of the surface. The remainder is occupied by air voids.

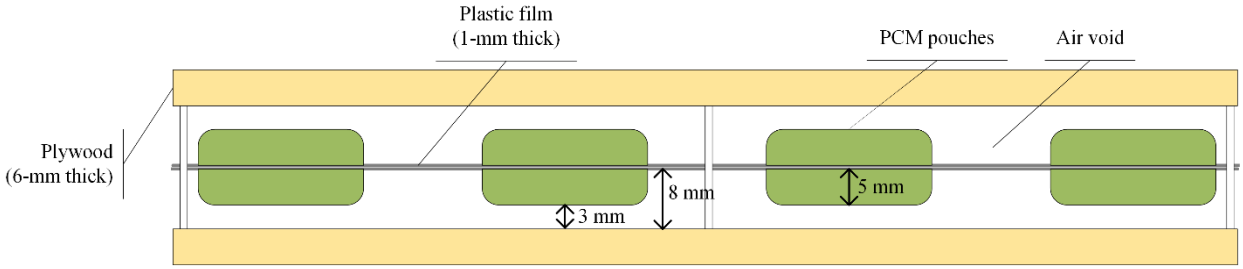


Figure C-1: Scheme of the PCM-equipped wall

Table C-1 presents the thickness and thermal conductivity of each material in the PCM-equipped wall.

Table C-1: Thickness and thermal conductivity of each material in the PCM-equipped wall

| | Air | | PCM | Plastic film | Plywood |
|---|---|---|---|---|---|
| Thickness $L$ [m] | 0.003 | 0.008 | 0.005 | 0.001 | 0.006 |
| Thermal conductivity $k$ [W/m-K] | 0.040 | 0.063 | 0.212 | 0.150 | 0.084 |

The equivalent air thermal conductivity is calculated by assuming negligible convection (thin layers), a "pure" thermal conductivity of 0.0256 W/m-K, and calculating the radiative heat transfer with Kirchoff's law (Bergman et al., 2011). The radiation heat transfer between planar surfaces (Spakovszki, 2014) is given by the following equation:

$$\dot{Q}_{1\ to\ 2} = \frac{\sigma(T_1^4 - T_2^4)}{\frac{1}{\varepsilon_1} + \frac{1}{\varepsilon_2} - 1} \qquad (C.1)$$

Where $\dot{Q}_{1\ to\ 2}$ is the net radiation heat transfer between surfaces 1 and 2; $\sigma$ is the Stefan-Boltzmann constant ($5.67 \times 10^{-8}$ W/m²-K⁴); $T_1$ and $T_2$ are the surface temperatures; $\varepsilon_1$ and $\varepsilon_2$ are the surface emissivity's.

Assuming a temperature difference of 1 K between $T_1$ (294 K or 21 °C) and $T_2$ (293 K or 20 °C) and surface emissivity's of 0.9, the resulting net radiation heat transfer from surface 1 to 2 is around 4.7 W/m². Considering a temperature difference of 1 K, the corresponding radiation heat transfer coefficient is 4.7 W/m²-K.

From these assumptions, the air thermal conductivity including radiative and conductive heat transfer can be computed as follows:

$$k_{air} = \left(\frac{0.0256}{L} + 4.7\right) \times L \qquad (C.2)$$

Equation ( C.2 ) gives air thermal conductivity values of 0.040 W/m-K ($L$ = 0.003 m) and 0.063 W/m-K ($L$ = 0.008 m).

The heat transfer coefficient of the configuration presented in Figure C-1 and Table C-1 has been computed using THERM. A U-value of 1.818 W/m²-K (R = 0.550 m²K/W) is obtained for the whole PCM-equipped wall. Removing the thermal resistance of both plywood boards (2 × 0.071 m²K/W), the thermal resistance of the equivalent layer is 0.408 m²K/W. Considering a thickness of 17 millimeters, the equivalent layer has a thermal conductivity of 0.042 W/m-K.

# APPENDIX D – PROFORMA OF TRNSYS TYPE 3258

This appendix describes the external files used in Type 3258 to define temperature-dependent thermal conductivities and capacities. It also presents a list of the parameters, inputs and outputs implemented in Type 3258 and a brief description for each element.

**External files**

- Data file defining temperature-dependent thermal conductivities

The first line of this file gives the number of rows and columns defined in the file. The first column gives the temperature values in °C in ascending order. Each following column gives the temperature-dependant thermal conductivities in W/m-K for each layer with variable thermal conductivity. The number of rows is the same for all layers. The order of definition follows the order of appearance from side 1 to side 2. If a layer does not have temperature-dependent thermal conductivity, there is no need to define a column in the data file and the value given in the parameters is used. For example, a 3-layer wall have 2 layers with temperature-dependent thermal conductivities (layer 1 and 3). The data file can have the following template:

```
4     3              ! Number of rows (m) and columns (n)
0     0.25   0.20    ! (m) temperature-thermal conductivity pairs for (n-1) layers
22    0.25   0.20
23    0.20   0.18
60    0.20   0.18
```

The first line indicates the number of rows and columns. The first column below the first line gives the temperatures. The two following columns indicate the temperature-dependent thermal conductivities, respectively for layer 1 and 3. The thermal conductivity of layer 2 is constant and defined in the parameters.

- Temperature-dependent thermal capacity

The first line of this file gives the number of rows and columns defined in the file. The first column is the enthalpies in J/g given in ascending order. Each following column gives the enthalpy-dependent temperatures in °C for each layer with variable thermal capacity. The number of rows is equivalent for all layers. The order of definition follows the order of appearance from side 1 to

side 2. If a layer is modeled using 2 enthalpy-temperature curves for heating and cooling processes, both columns must be defined for each process before dealing with the next layer. The values for heating are defined first. If a layer does not have temperature-dependent thermal capacity, there is no need to define a column in this data file. In the example below, a 3-layer wall has 2 layers with temperature-dependent thermal capacities (layer 1 and 3). Layer 1 has 2 enthalpy-temperature curves while layer 3 has only one. The data file can have the following template:

| | | | | |
|---|---|---|---|---|
| 6 | 4 | | | ! Number of rows (m) and columns (n) |
| 0 | 0 | 0 | 0 | ! (m) enthalpy-temperature pairs for (n-1) layers |
| 36 | 18 | 18 | 18 | |
| 38 | 19 | 18.1 | 19 | |
| 136 | 22.9 | 22 | 22.9 | |
| 138 | 23 | 23 | 23 | |
| 172 | 40 | 40 | 40 | |

The first line indicates the number of rows and columns. The first column below the first line gives the enthalpies. The next two columns indicate the enthalpy-dependent temperatures for layer 1, respectively for heating and cooling. The fourth column presents the enthalpy-dependent temperatures for layer 3 (only one enthalpy-temperature curve). The thermal capacity of layer 2 is constant and defined in the parameters.

The following pages presents tables of the parameters, inputs and outputs used in Type 3258. The tables are presented in landscape orientation.

Table D-1: List of parameters (1/6)

| Name | Unit | Description |
|---|---|---|
| Mode | [-] | The model can be used to model the entire wall (mode = 0). In this case, the boundary conditions on both sides include convection and radiation heat transfer.<br>If mode = 1, the modeled layer(s) is/are part of a wall modeled in Type 56. Boundary conditions are the surface temperatures of the other parts of the wall modeled in Type 56.<br>If mode = 2, the modeled layer(s) is/are part of a wall modeled in Type 56. The boundary condition on side 1 is the surface temperature of the other part of the wall modeled in Type 56. The boundary condition on side 2 includes convection and radiation heat transfer.<br>If mode = 3, the modeled layer(s) is/are part of a wall modeled in Type 56. The boundary condition on side 2 is the surface temperature of the other part of the wall modeled in Type 56. The boundary condition on side 1 include convection and radiation heat transfer. |
| Space discretization constant | [-] | Constant defining the number of nodes per layer. The default value is 3. If you want to set the number of nodes to the minimum (3 nodes per layer), set this parameter to 9999. It allows to decrease the computation time. |
| Minimum internal time-step | [s] | A minimum internal time-step should be set in order to avoid time-consuming simulations. For layer with very high diffusivity (e.g. air layer), the stability of the explicit method is insured with a very low internal time-step which can be lower than 1 second. |

Table D-1: List of parameters (2/6)

| Name | Unit | Description |
|---|---|---|
| Wall area | [m²] | Wall area in m². |
| Initial wall temperature | [°C] | Initial temperature of the whole wall. |
| Maximum global heat transfer coefficient on surfaces | [W/m²-K] | This value is used to evaluate the stability condition of the explicit method used in this type. It is an important parameter to insure the calculation stability. If the entire wall is modeled in Type 3258, this parameter should be equal to the maximum global heat transfer coefficient on both surfaces (not used if mode = 1). |
| Number of layer(s) | [-] | Total number of layer(s). |
| Number of layer(s) without variable thermal capacity | [-] | The number of layer without temperature-dependent specific heat, i.e. layer(s) with constant properties or with only temperature-dependent thermal conductivity. |
| Number of layer(s) with variable thermal capacity | [-] | Number of layer(s) with variable specific heat such as PCM. |
| Number of interface(s) | [-] | Number of layers interface(s). It is equal to the total number of layer(s) - 1. |

Table D-1: List of parameters (3/6)

| Name | Unit | Description |
|---|---|---|
| Logical unit for file k(T) | [-] | Logical unit of the data file defining the evolution of the thermal conductivity as a function of the temperature. |
| Logical unit for file T(h) | [-] | Logical unit of the data file defining the evolution of the temperature as a function of the enthalpy. |
| Position of the layer “x” without variable thermal capacity | [-] | Number of the layer inside the wall. If the layer is the first from side 1, the number is then 1. |
| Thickness of the layer “x” without variable thermal capacity | [m] | Thickness of the layer in m. |
| Thermal conductivity of the layer “x” without variable thermal capacity | [W/m-K] | Thermal conductivity of the layer. If this parameter is equal to -1, a variable thermal conductivity must be defined in the file defining the variable thermal conductivity for all the layers. |

Table D-1: List of parameters (4/6)

| Name | Unit | Description |
|---|---|---|
| Density of the layer “x” without variable thermal capacity | [kg/m³] | Density of the layer in kg/m³. |
| Specific heat of the layer “x” without variable thermal capacity | [J/kg-K] | Specific heat of the layer (no variable specific heat) |
| Position of the layer “y” with variable thermal capacity | [-] | Number of the layer inside the wall. If the layer is the first from side 1, the number is then 1. |
| Thickness of the layer “y” with variable thermal capacity | [m] | Thickness of the layer in m. |
| Thermal conductivity of the layer “y” with variable thermal capacity | [W/m-K] | Thermal conductivity of the layer. If this parameter is equal to -1, a variable thermal conductivity must be defined in the file defining the variable thermal conductivity for all the layers. |
| Density of the layer “y” with variable thermal capacity | [kg/m³] | Density of the layer in kg/m³. |

Table D-1: List of parameters (5/6)

| Name | Unit | Description |
|---|---|---|
| Variable specific heat of the layer “y” | [J/kg-K] | In this case, a variable specific heat as a function of the temperature must be used. If this parameter is set to -1, there is only one enthalpy-temperature curve defining the variable specific heat. If set to -2, 2 enthalpy-temperature curves are defined (one for heating and cooling processes). |
| Low phase change temperature (solid) of the layer “y” | [°C] | Temperature at and below which the PCM is solid. If there are 2 enthalpy-temperature curves, the low phase change temperature is the temperature where both curves meet each other. |
| High phase change temperature (liquid) of the layer “y” | [°C] | Temperature at and above which the PCM is liquid. If there are 2 enthalpy-temperature curves, the high phase change temperature is the temperature where both curves meet each other. |
| Transition type during phase change (heating) for the layer “y” | [-] | If this parameter is set to 1 (no transition (Chandrasekharan et al., 2013)), the PCM always follows the heating curve when there is a cooling after a heating period and during phase change. To switch from the heating curve to the cooling one, the PCM temperature must reach or overcome the liquid temperature.<br>If this parameter is set to 2 (Bony & Citherlet, 2007), a switch between curves during the phase change is possible. |

Table D-1: List of parameters (6/6)

| Name | Unit | Description |
|---|---|---|
| Transition type during phase change (cooling) for the layer "y" | [-] | If this parameter is set to 1 (no transition (Chandrasekharan et al., 2013)), the PCM always follows the cooling curve when there is a heating after a cooling period during phase change. To switch from the cooling curve to the heating one, the PCM temperature must reach or overcome the solid temperature.<br>If this parameter is set to 2 (Bony & Citherlet, 2007), a switch during the phase change is possible. |

Table D-2: List of inputs (1/2)

| Name | Unit | Description |
|---|---|---|
| Wall gain on side 1 | [kJ/h] | Heat flow coming in (+) or out (-) the wall. This information comes from Type 56 and depends on the type of implementation used to connect Type 3258 to Type 56 (see Chapter 9).<br>This input is not connected to Type 56 if the used mode (first parameter) is 1 or 3. |
| Wall gain on side 2 | [kJ/h] | Heat flow coming in (+) or out (-) the wall. This information comes from Type 56 and depends on the type of implementation used to connect Type 3258 to Type 56 (see Chapter 9).<br>This input is not connected to Type 56 if the used mode (first parameter) is 1 or 2. |

Table D-2: List of inputs (2/2)

| Name | Unit | Description |
|---|---|---|
| Coefficient of convection on side 1 | [kJ/h-m²-K] | Coefficient of convection on side 1.<br>This input is not used if the used mode (first parameter) is 1 or 3. |
| Coefficient of convection on side 2 | [kJ/h-m²-K] | Coefficient of convection on side 2.<br>This input is not used if the used mode (first parameter) is 1 or 2. |
| Boundary temperature on side 1 | [°C] | Boundary temperature on side 1. |
| Boundary temperature on side 2 | [°C] | Boundary temperature on side 2. |

Table D-3: List of outputs (1/3)

| Name | Unit | Description |
|---|---|---|
| Surface temperature on side 1 | [°C] | Surface temperature of the wall on side 1.<br>If mode = 1 or 3, it is not the surface temperature but the first node which is slightly inside the wall. |

Table D-3: List of outputs (2/3)

| Name | Unit | Description |
|---|---|---|
| Surface temperature on side 2 | [°C] | Surface temperature of the wall on side 2.<br>If mode = 1 or 2, it is not the surface temperature but the last node which is slightly inside the wall. |
| Surface heat flow on side 1 | [kJ/h] | Surface heat flow going out (+) the wall or in (-) the wall on side 1. |
| Surface heat flow on side 2 | [kJ/h] | Surface heat flow going out (+) the wall or in (-) the wall on side 2. |
| Internal energy change | [kJ] | Variation of the enthalpy of the wall over the time-step. A positive value means an increase of the enthalpy of the entire wall. |
| Energy change residue | [kJ] | Comparison between the heat flow going in or out the wall and the variation of enthalpy in the entire wall. It should be equal to or very close to zero. |
| Heat transfer coefficient between the 1$^{st}$ node and the boundary condition on side 1 | [kJ/h-m$^2$-K] | This value is the heat transfer coefficient between the first node of the modeled wall and the boundary condition on side 1. |
| Heat transfer coefficient between the last node and the boundary condition on side 2 | [kJ/h-m$^2$-K] | This value is the heat transfer coefficient between the last node of the modeled wall and the boundary condition on side 2. |

Table D-3: List of outputs (3/3)

| Name | Unit | Description |
|---|---|---|
| Temperature at the center of layer “x” | [°C] | Temperature at the center of each layer (from side 1 to 2). |
| Temperature at the layers interface “y” | [°C] | Temperature at the interface between 2 layers (from side 1 to 2). |
| Mean liquid fraction of layer “x” | [-] | Mean liquid fraction of each layer (from side 1 to 2). If equal to 0, it is solid. If equal to 1, it is liquid. |